# Synthesis elaboration of fragments that potentially inhibit the HOP-HSP90 protein-protein interaction.

*Submitted in fulfilment of the academic requirements for the degree of*

**Doctor of Philosophy**


*Faculty of Agriculture, Engineering and Science*

*School of Chemistry and Physics*

*(Pietermaritzburg)*

*South Africa*

By

**Patience Snenhlanhla Sthembile Molefe**

February 2024

# Thesis declaration

I declare that all that the work in this thesis represents the original work that was carried out for my research investigation; it has not been submitted for any degree.

This work was carried out under the supervision of Dr S. Sithebe and Prof. C.G.L Veale.

Signed [redacted] ……..……. Date.02/02/24……..

Patience Snenhlanhla Sthembile Molefe (**Candidate**)

I hereby certify that the statement is correct:

Signed… [redacted] …… Date…05/02/24…….

Dr. Siphamandla Sithebe (**Supervisor**)

I hereby certify that the statement is correct:

Signed…….. Date…….

Professor Clinton G.L. Veale (**Co-supervisor**)

# Publication and conference contribution

## Publication

Patience S.S Molefe, Sinothando Mtolo, Siphamandla Sithebe, Clinton Veale. The synthesis of valsartan through a late-stage DMF-free tetrazole cyclisation. *J. Med. Chem,* manuscript in preparation.

## Flash oral presentation

Patience S.S Molefe, Synthesis elaboration of fragments that inhibit the HOP-HSP90 protein-protein interaction. Postgraduate Research and Innovation Symposium (PRIS) 2023 – Coastlands Musgrave, Durban- South Africa, 02$^{nd}$ – 03$^{rd}$ November 2023.

# Abstract

Heat Shock Protein 90 (HSP90) is a molecular chaperone that mediates the stability and maturation of many important proteins for oncogenesis. There is an overexpression of the Heat Shock Protein 70/Heat Shock Protein 90 Organising Protein- HSP90 (HOP-HSP90) protein-protein interaction (PPI) complex in tumour tissues unlike in healthy cells. This PPI complex of HSP90 displayed a potential druggable target because of the crucial role it plays in cancer development. However, the challenge is the development of HOP-HSP90 PPI inhibitors. The literature showed the activity of valsartan **(27)** for the inhibition of HOP-HSP90 PPI as it entails the features of *ortho*-biphenyl tetrazole fragments that were obtained from the Structural-Binding Relationship (SBR) of the active fragments using fragment-based drug discovery (FBDD). These fragments bound to the tetratricopeptide repeat 2A (TPR2A) domain of HOP and inhibited the PPI of HOP-HSP90. As a result, this study aimed to synthesise and assay *ortho*-biphenyl tetrazole fragments as inhibitors of HOP-HSP90 for novel anticancer inhibitors, triple-negative breast cancer (TNBC).

Valsartan **(27)** and its analogues were synthesised following reported procedures and modified methods. A series of 13 *ortho*-biphenyl tetrazole desired fragments were successfully synthesised using a Suzuki-Miyaura cross-coupling reaction and [3 + 2] cycloaddition of nitrile with sodium azide. The cross-coupling of 2-iodobenzonitrile or 2-(2-bromophenyl) acetonitrile with *para*-substituted phenylboronic acid was conducted using different substrates including Cl, Br, F, $CH_3$, $CF_3$, H, and $OCH_3$. Cycloaddition was done after the cross-coupling to skip the protection step of the tetrazole.

With the desired *ortho*-biphenyl tetrazole fragments in hand, the PPI inhibition activity was evaluated at different concentrations from 0 mM to 2.0 mM. It is interesting to observe that some of these fragments showed PPI activity at different concentrations including compounds **76**, **80**, **82**, **83** and **84**. No activity was observed following the incorporation of the benzylic carbon. The data presents the successful lead optimisation for the development of HOP-HSP90 novel PPI inhibitors for the treatment of TNBC.

# Acknowledgements

I want to pass my gratitude to Dr Siphamandla Sithebe for his supervision, encouragement, mentorship, support, and motivation during my postgraduate studies and most importantly during my doctoral journey that had many obstacles, may God bless you.

To Associate Prof Clinton Veale, thank you so much for believing in me and giving me a chance to conduct a study that has given me many research skills; your patience, your guidance, and your supervision have helped me to reach a finish line, “PhD”.

Much appreciation to:

- Prof. Adrienne Edkins from Rhodes University for conducting biological studies for my synthesised fragments.
- UKZN technical team for the assistance in making my research easy: Mr Craig Grimmer, Mr Shaun Balls, Mrs Caryl Janse Van Rensburg, Ms Saideshnee Naidoo, and Mr Leigh Hunter.
- Chemistry family at PMB: postgraduates, technical staff, and academic staff for a great working environment.
- NRF and UKZN FLAGSHIP for financial assistance.

To my family, thank you for the love and support you have given me it gave me strength to thrive. Thanks to my friends for keeping this journey enjoyable even on bad days.

To my mother Primrose Jabu Molefe, thank you so much for the love, support, and patience; this journey has been peaceful and easy.

To Bonga and Nkanyezi, may this be the light that shines, giving you hope and strength. May it be a constant reminder that anything you want to achieve, you have the power to make it work.

GLORY BE TO GOD!!!

# Table of contents

# List of abbreviations

| | |
|---|---|
| ATP | Adenosine triphosphate |
| $NH_4OH$ | Ammonium hydroxide |
| $NH_4Cl$ | Ammonium chloride |
| $CH_3COOH$ | Acetic acid |
| $^{13}C$ NMR | Carbon nuclear magnetic resonance |
| $CDCl_3$ | Deuterated chloroform |
| MeOH | Deuterated methanol |
| *d* | Doublet |
| dd | Doublet of doublet |
| DNA | Deoxyribonucleic acid |
| Da | Dalton |
| DMA | Dimethylacetamide |
| DCM | Dichloromethane |
| DMF | Dimethylformamide |
| DMSO | Dimethylsulfoxide |
| $^oC$ | Degree Celsius |
| eq | Equivalent |
| EtOH | Ethanol |
| FDA | Food and drug administration |
| HRMS | High-resolution mass spectroscopy |
| $NH_2OSO_3H$ | Hydroxylamine-O-sulfonic acid |
| Hr/hrs | Hour (s) |
| Hz | Hertz |
| IR | Infrared |
| mRNA | Messenger ribonucleic acid |
| mmol | Millimoles |
| mL | Millilitre |
| mM | Millimolar |
| MHz | Megahertz |

| | |
|---|---|
| *m* | Multiplet |
| *m/z* | Mass to charge ratio |
| M | Molar |
| mol | Moles |
| $^{1}$H NMR | Proton nuclear magnetic resonance |
| ppm | Part per million |
| $POCl_3$ | Phosphoryl chloride |
| $Pd(OAc)_2$ | Palladium acetate |
| $P_2O_5$ | Phosphorus pentoxide |
| $K_2CO_3$ | Potassium carbonate |
| $cm^{-1}$ | Per centimetre |
| % | Percentage |
| $R_f$ | Retention factor |
| rt | Room temperature |
| *s* | Singlet |
| NaOH | Sodium hydroxide |
| $Na_2CO_3$ | Sodium carbonate |
| TOF-MS | Time-of-flight mass spectrometer |
| TPR | Tetratricopeptide repeat |
| $SOCl_2$ | Thionyl chloride |
| $PPh_3$ | Triphenyl phosphine |
| $Et_3N$ | Triethylamine |
| TLC | Thin layer chromatography |
| THF | Tetrahydrofuran |
| $Pd(PPh_3)_4$ | Tetrakis(triphenylphosphine)palladium |
| *t* | Triplet |
| $ZnBr_2$ | Zinc bromide |

# List of tables

# List of figures

# List of schemes

# Chapter 1

# Introduction

## 1.1 Cancer *versus* Triple Negative Breast Cancer (TNBC)

Cancer is the abnormal growth of cells that spreads uncontrollably throughout the body [1]. It is recognised as having the second highest global mortality rate after cardiovascular disease [2]. Every year, several cancer types are diagnosed, including breast, lung, prostate, and skin, to name a few [3]. Among these, lung cancer is the most diagnosed in both males and females and breast cancer is the second most diagnosed among females [3].

The classification of breast cancer is based on immunohistochemical strains according to the expression of estrogen receptor (ER), the progesterone receptor (PR), and human epidermal growth factor 2 (HER2) [4, 5]. The breast cancer treatment plan depends on the molecular subtypes. The treatment plan includes radiation and surgery therapy, and systematic therapy. Systematic therapy includes chemotherapy, immunotherapy, hormone therapy for hormone-positive disease, and anti-HER2-positive disease. Tamoxifen **(1)** was the first cancer chemopreventive drug approved by the Food and Drug Administration (FDA) targeting estrogen receptor-positive patients whereas testuzumab **(2)**, margetuximab and pertuzumab were for HER2-positive patients **(Figure 1.1)** [6, 7].

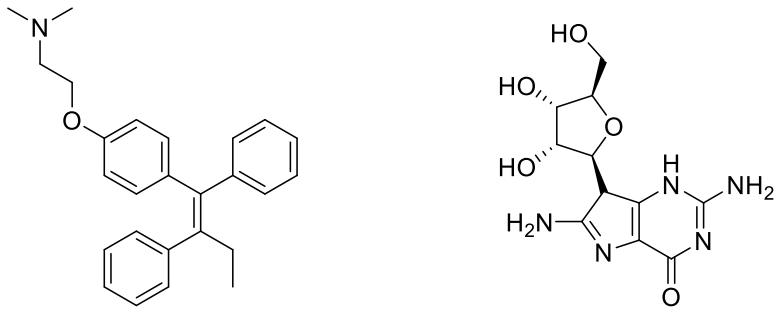


**1** **2**

**Figure 1.1**: Cancer therapies.

Triple-negative breast cancer (TNBC) is defined by the absence of estrogen receptor (ER), progesterone receptor (PR), and human epidermal growth factor 2 (HER2). About 15-20% accounts for TNBC of all breast cancer and it presents a therapeutic challenge due to low response

to the mentioned systematic therapies. It affects about 10-15% of women across the globe with aggressive behaviour, associated with early metastatic spread to the lungs, liver, central nervous system, and brain with fewer chances for survival [8]. In addition, women from Sub-Saharan Africa are more likely to die from TNBC before 75 compared to high-income countries in Europe and North America [9]. While the rate of cancer deaths is predicted to remain unchanged in the next 20 years, the numerical burden will double in Sub-Saharan Africa because of population growth [10]. TNBC is classified as a heterogeneous disease due to its diversity associated with gene expression that is studied to find a therapeutic target. Each subtype responds differently to chemotherapy because each displays a unique oncology. Different authors report different subtypes which shows that TNBC is a difficult disease to treat [11]. However, the recurrence of this disease and the lack of the target make this subtype have a poor prognosis.

Early cancer detection can improve the effectiveness of treatments, reduce side effects, and increase long-term survival. It can be challenging to distinguish between insignificant changes and lesions that will develop into life-threatening cancer, even though screening techniques are becoming more sensitive. Progress depends on a thorough comprehension of individual risk, a precise classification of the stages of cancer development, a variety of testing techniques with the best performance characteristics, and a thorough analysis of the implications for individuals and society. Future developments in sensors, contrast agents, molecular techniques, and artificial intelligence will make it easier to identify signals associated with cancer quickly. Risk-based detection and prevention must be affordable and widely available to lessen the financial and social toll that cancer takes on society [12].

A significant clinical challenge continues to be the survival of cancer cells resistant to treatment. The highest probability of recurrence among breast cancer subtypes is found in triple-negative breast cancer due to treatment resistance. Although nongenetic characteristics appear to be substantially responsible for the drug-tolerant state, the underlying mechanisms are not well known [13].

Due to its limited response to treatment and extremely invasive nature, it provides a therapeutic challenge and is therefore of considerable study interest. Based on cancer biology and early patient response to therapy, future therapeutic approaches for breast cancer seek to individualise treatment, de-escalate the situation, and intensify the situation [14].

TNBC has six different subtypes which were reported by Lehman *et al*. in 2011 including basal-like 1 and 2, immunomodulatory, mesenchymal, mesenchymal stem-like, and luminal androgen receptor [15]. In 2016, Lehman then regrouped these tumours into 4 groups, including, basal-like 1, basal-like 2, mesenchymal, and luminal androgen receptor [11] whereas Burstein *et al.* reported a different classification of TNBC including luminal androgen, mesenchymal, basal-like immune-suppressed and basal-like immune-activated [16]. Classification of TNBC subtypes of tumours is done by investigating DNA profiling and *m*RNA expression to identify a target. To date, there is no FDA-approved therapeutic target for TNBC. Therefore, treatment requires generalised chemotherapy and subsequently has a poor prognosis [11].

TNBC provides a challenge for patients and physicians since it has a worse prognosis, fewer available treatments, and a lack of targeted therapy utilisation, all of which are reflected in its high incidences compared to other breast cancer subtypes' mortality. Although TNBC is a more aggressive illness, the decision to operate is likely based on more conventional clinicopathological factors (such as patient age, tumour size, and tumour grade) and personal preference [17].

The luminal androgen receptor (LAR) expresses the androgen receptor which is a potential target for the treatment of TNBC. Clinical results display that this subtype has a better prognosis and responds poorly to chemotherapies. Therefore, anti-androgen therapies including bicalutamide **(3),** enzalutamide **(4)** and abiraterone **(5)** (**Figure 1.2**) are chemo-free and are used in patients that are unresponsive to chemotherapies [18].

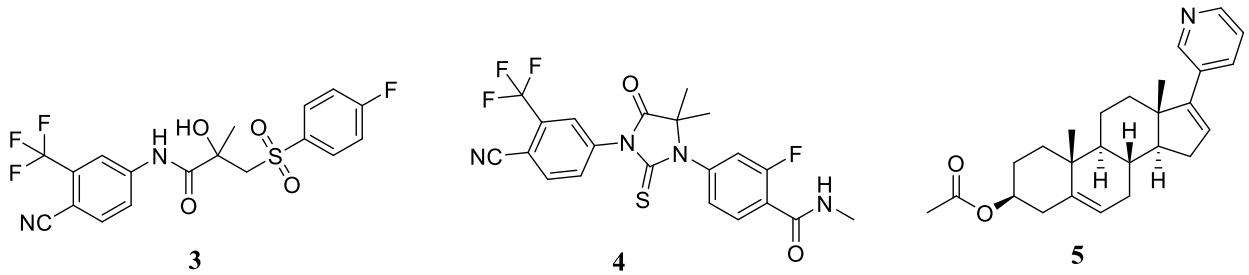


**Figure 1.2:** Anti-androgen therapy drugs that are used in patients who are not responsive to chemotherapies.

It has been pointed out that there is no target for small molecule TNBC therapy and treatment is generalised. However, recently, immunotherapy drugs have had a positive response. Atezolizumab

and pembrolizumab are the immune checkpoint inhibitors that have been approved for phase 3 clinical trials, but they are used in combination with frontline chemotherapy [19-21].

Targeting regulated cell death (RCD) is another strategy that has been explored to overcome this heterogeneous breast cancer with a poor prognosis. RCD is divided into many subroutines, such as apoptosis, pyroptosis, necroptosis, ferroptosis, mitotic catastrophe, anoikis, and autophagy dependent. This strategy involves the use of small-molecule compounds to achieve a therapeutic potential for TNBC. Moreover, to regulate the RCD subroutines, drugs are used as combined or as singular to achieve a great therapeutic capacity [22]. The combination of curcumin (Cur) **(6)** and gallic acid (GA) **(7)** was investigated by Moghtaderi in 2018 and the findings imply that GA combined with Cur may have potential as a chemopreventive medication for triple-negative breast cancer because they decrease the human cancer cell line MDA-MB-231 growth vigorously [23]. The use of artesunate **(8)** not only caused apoptosis but also resulted in an *in vitro* suppression of Heat Shock Protein 70 (HSP70) ATPase activity (P 0.001). With rising artesunate M concentrations, the degree of HSP70 refolding inhibition grew [24]. The above-mentioned are a few drugs that are active against TNBC but are still under clinical trials and they display the power of utilising fragment-based drug discovery (FBDD) (**Figure 1.3**).

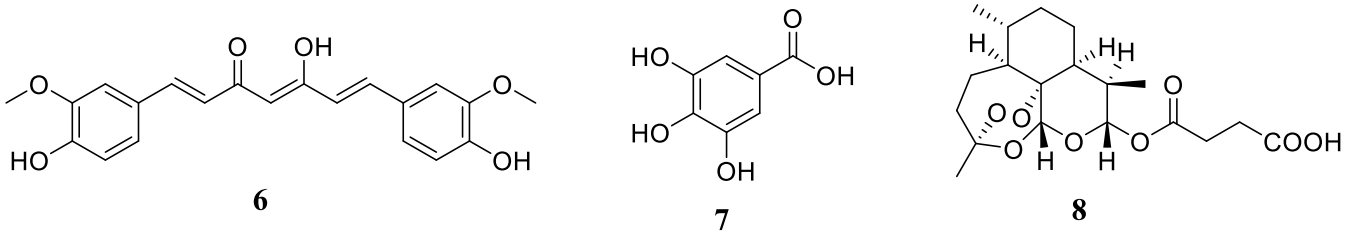


**Figure 1.3:** Small-molecule compounds that are in clinical trials for targeting regulated cell death for TNBC.

With the available therapies for the treatment of breast cancer, the challenge for the treatment of TNBC patients is the absence of expression of the three receptors which define the tumour subtype that is the target for the FDA-approved drugs e.g., tamoxifen **(1)**, testuzumab **(2)**, margetuximab, and pertuzumab; and they are designed to inhibit them. In addition, these therapies have low efficacy for the treatment of TNBC since it is defined as the absence of these three hormonal drug targets, therefore, they generalise chemotherapies. However, PPI has shown to be a possible target for the treatment of TNBC [6, 7].

## 1.2 Drug Discovery

Drug discovery is the process where new medicines are discovered by firstly understanding the biological process in which the disease operates in a human cell and therefore being able to find a drug that will inhibit that process [25]. Some stages need to be followed for a drug to be taken to a clinical trial/tested in humans. The process begins with target identification and verification, new molecule development, molecule screening, hit identification, drug-lead optimisation, and lastly the selection of the perfect lead for a clinical trial (**Figure 1.4**).


**Figure 1.4:** The flow chart of drug discovery.

The target identification process involves the examination of a target which can be a gene, RNA, enzyme, receptor, or protein that can be druggable [26]. Data mining is one of the techniques used for target identification, in which biomedical data is used to study the disease and be able to study and prioritise a potential disease target [27]. A good source for target identification is relevant literature from different scientists around the world because they reveal the pathway of genes and proteins. Merging three strategies which are: the basic understanding of molecular mechanisms, the understanding of the disease, and the ability to access technologies and models, helps succeed in identifying novel drug targets [28]. Hints of finding a target could also be the evaluation of data studied from protein or RNA expressed in the targeted tissue of the disease versus health tissue. Activity-based protein profiling (ABPP) is a focused proteomics strategy that does target identification by analysing the difference in enzymic activity of healthy and infected tissue, widening the target space [29]. This approach demonstrates the mechanism between the protein and the compound [30].

Although each step is vital in its confidence, each step allows one to proceed with relevant data that has been verified in the following step. Target verification is to assess a biological target whether it's druggable or not. Verification of the target is crucial because it helps in eliminating false data. Different methods are used to validate a target, including antisense technology that uses antisense agents to study the function of genes thereby extracting specific data of what causes that disease. The successful use of this technique was demonstrated by Honore and co-workers when

they examined the $P2X_3$ receptor in rats using the antisense probes they developed [31]. Cell-based mechanistic studies are done *in vitro* to interpret the pathways in which targets are involved as well as their regulative characteristics. Lastly, it could be necessary to validate the importance of a chosen target for a disease in a suitable animal model [28].

The hit development stage involves different screening processes that confirm the activity against the validated target of a disease [26]. The hit identification step in drug discovery involves the identification of compounds that interact with a validated target. To get good hits, different strategies are used with high-quality and diverse potential libraries coupled with either of these two techniques, visual screening, and fragment-based screening.

Visual screening is one of the hit identification techniques that uses computational techniques to select molecules that are likely to bind to a target using different methods, including ligand-based and structural-based visual screening. This technique typically applies different analytical models to create libraries. Ligand-bases use a pharmacophore model scanning the database of two-dimensional (2D) and three-dimensional (3D) molecular structures to obtain new hits and help to optimise lead compounds [32, 33]. Whereas structural-based visual screening investigates hits through docking and scoring large compounds if the 3D structure of a target is available. X-ray or NMR are techniques used for 3D structures for receptors, and as for a protein, if the structure is not available other techniques such as protein-structure prediction could be used so that docking could commence [34].

High Throughput Screening (HTS) is an experimental method to identify whether a molecule is biologically active or not. HTS is a method used to screen multiple samples of about 100,000 per day rather than one compound at a time method because it has an automated robot system, therefore, it is highly efficient, simple, and cost-effective [35]. Due to the high rate of compound screening using HTS, this maximises the searching of hits although it does not guarantee lead compounds. An example of the approved drug that was discovered using HTS is eltrombopag **(9)** (**Figure 1.5**) which was approved by FDA in 2008 for chronic idiopathic thrombocytopaenic purpura. The success of this journey was achieved by the collaboration of SmithKline Beecham and Ligand Pharmaceuticals in screening that was done in 1997 which led to the discovery of eltrombopag **(9)** [36]. Large compounds screened from combinatorial chemistry libraries are difficult to optimise especially during the lead optimisation stage because they violate the Lipinski

rule of five parameters of drug-like characteristics [37] [38]. Regardless of the advantages HTS possesses there are drawbacks such as the use of high molecular weight compounds that are more likely to be hydrophobic and, hence, difficult to infiltrate into a cell membrane [39].

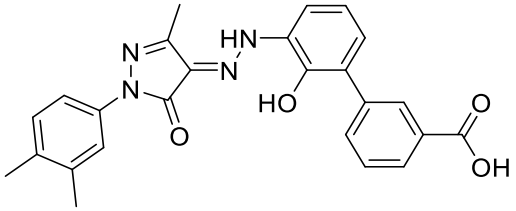


**9**

**Figure 1.5:** Eltrombopag **(9)** is the approved drug that was discovered through HTS.

## 1.3 Fragment-Based Drug Discovery

A complementary strategy to high-throughput screening (HTS) is already well-established and is known as FBDD) While huge libraries of drug-like molecules are screened in HTS, smaller, less complicated molecules are used in FBDD screening because they exhibit more 'atom-efficient' binding interactions than larger molecules, despite having a lower affinity for protein targets. Therefore, fragment hits can act as a more effective starting point for future optimisation, especially for targets that are difficult to drug [40].

With a lot fewer molecules, fragment libraries can sample a far larger chemical region than HTS libraries. Contrary to fragments, which are more likely to generate atom-efficient binding contacts, complex molecules have a higher likelihood of forming ineffective interactions and/or collisions with the desired target [41, 42].

Considering that HTS fails in some cases to generate hits, alternatively, FBDD is another screening method defined as a method that uses small molecules (fragments) to find hits. This is done by screening molecules that have a low molecular weight of less than 300 Da, called fragments. Fragment libraries are generated based on the concepts called ‘Lipinski rule’, stating that the fragment must have a maximum molecular weight of 300 Da, the number of hydrogen bond donors and acceptors must be equal or less than three, and a calculated log*P* less or equal to three [43]. Since fragments have low potency, they are screened with biophysical techniques including NMR [44], SPR (Surface Plasmon Resonance), thermal shift, X-ray [45], and native mass spectrometer [46]. This method has brought a powerful shift in medicinal chemistry/drug discovery because fragments exhibit high ligand binding affinity and, therefore, are drug-led. This technique

originated in the early 1980s, gained momentum, and became practical in the mid-1990s [47]. FBDD has shown to be very effective in drug discovery because of the high hit rate compared to HTS. Previously, it had been concluded that PPIs are undruggable but FBDD has proven to overcome that by developing potent inhibitors for PPI targets [48]. The first drug that was successfully discovered using FBDD is vemurafenib **(10)** which was approved in 2012 by the FDA for BRAF-mutant cancer [49, 50]. There are other five drugs found utilizing FBDD that are currently on the market, namely, erdafitinib **(11)** [51], asciminib **(12)** [52], venetoclax **(13)** [53], pexidartinib **(14)** [54], sotorasib **(15)** [55] (**Figure 1.6**) and a large number of clinical candidates. In 1976, Beddell used protein crystal structures that were available to demonstrate the importance of modifying and elaborating compounds that inhibited the targeted protein [56]. The above knowledge was supported by the detailed study of protein-ligand interaction that was done to get the target renin for anti-hypertensives [57, 58], and the target for AIDS [59, 60] is HIV protease. Furthermore, FBDD technologies have been shown to overcome the difficulties that scientists face through powerful outcomes of finding lead compounds that inhibit PPI [40].

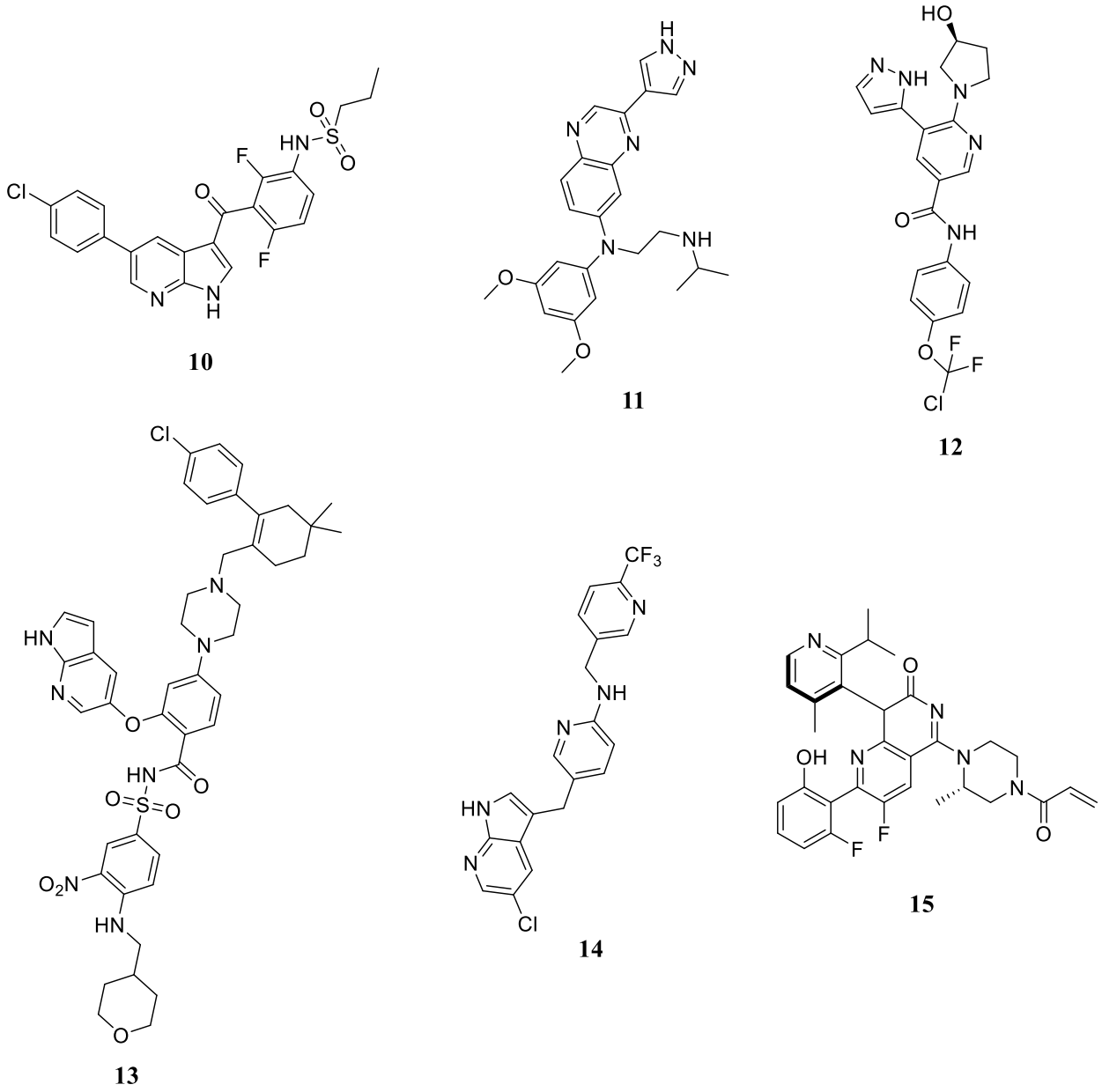


**Figure 1.6:** Examples of drugs that were discovered through FBDD.

The discovery of vemurafenib **(10)** as the BRAF inhibitor was done by screening 20,000 compounds and the compounds that inhibited the enzymic activity were identified. The co-crystallography was used to analyse the ligand-protein binding selectivity. A high binding affinity was observed on the compounds that contained 7-azaindole **(16)** moiety (**Scheme 1.1**) [61].

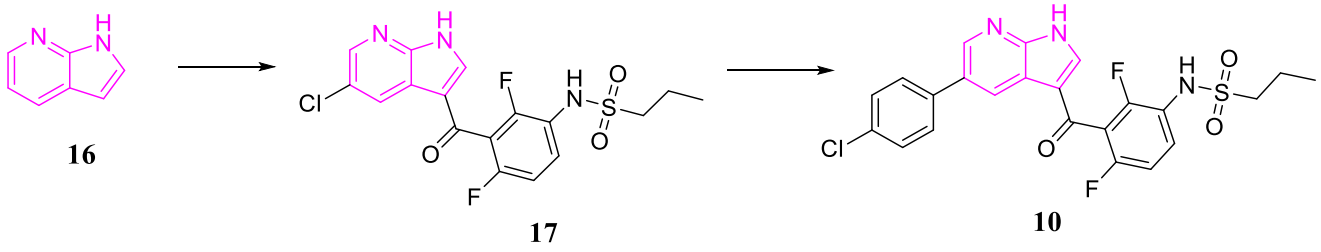

**Scheme 1.1:** The discovery of vemurafenib **(10)** from 7-aziandole **(16)** as a hit compound to lead optimisation compound PLX4720 **(17)**.

The power of FBDD has brought a positive shift in medicinal chemistry, especially for undruggable targets such as PPI. In addition, erdafitinib **(11)** is another drug that was approved as a fibroblast growth factor receptor (FGFR) inhibitor in 2019. It targets cancer cell lines that consist of FGFR alterations. The journey of this drug began with the fragment-based screening which produced imidazopyridine series **(19-21)**, (**11**); that were active through oral intake *in vivo*. However, these compounds show a lack of action against FGFR-independent xenograft models, proving the drugs' FGFR selectivity. Therefore, further investigation was done resulting in quinoline fragments that were further optimised until erdafitinib **(11)** was discovered (**Scheme 1.2**) [51]. The FBDD path has many steps and techniques that are used to validate the data until the drug is tested *in vivo*.

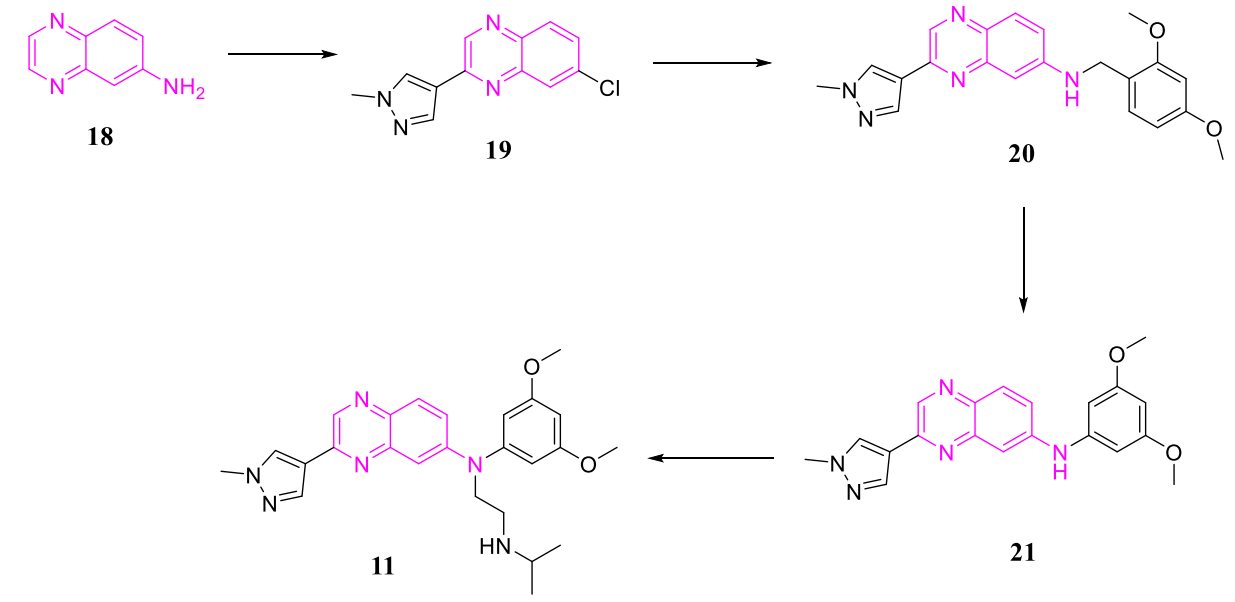

**Scheme 1.2:** The summary discovery of erdafitinib **(11)** from fragment imidazopyridine **(18)**.

One of the hit identification processes used in FBDD is the DOCK model used to screen commercially available molecules with a selected target. This computational method was used by Shoichet and co-worker to find inhibitors of Thymidylate Synthase (TS) screening molecules from Fine Chemical Directory, solisobenzone **(22)**, and phenolphthalein **(23)** (**Figure 1.7**) were one of the fragments that showed inhibition which led to the screening of their respective derivatives [62]. Other docking algorithm methods other than DOCK include FlexX, GOLD, and CDOCKER [63]. There are other computational approaches for finding fragments including fragment-based which was reported by Dean in 1992 [64], linked-fragment reported by Verlinde [65], and dynamic ligand design suggested by Kurplus [66]. All of the mentioned approaches help in pre-screening fragments and also optimise their linkage [67].

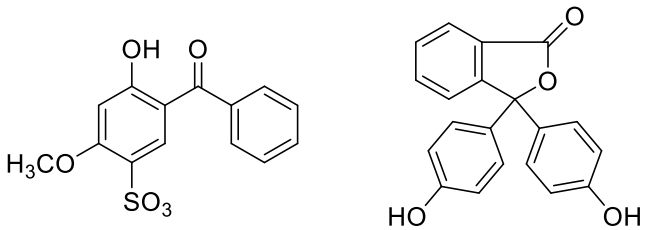


**22** **23**

**Figure 1.7:** Thymidylate Synthase (TS) inhibitors

After hit compounds have been identified through screening, their safety properties are assessed. Absorption, Distribution, Metabolism, Excretion, and Toxicology (ADME/Tox) properties are examined in each lead molecule to prioritise a promising hit. Researchers perform ADME/Tox studies *via* computational models, in animals as well as in living cells. Scientists investigate the absorption of each lead into the bloodstream, correct distribution to a desired target in the body, and effective and efficient metabolism. One of the important requirements for the lead compound is to get excreted completely from the body and a successful drug must be non-toxic [68].

## 1.4 Protein-Protein Interactions

Protein-protein interactions (PPIs) are the physical connections between two or more proteins and are important for the execution and regulation of most biological processes [69, 70]. PPIs involves many biological pathways including bonding that regulate protein folding [71]. Some challenges make a target difficult to be druggable, namely, the deficiency of hydrogen-bond acceptor and donor, featureless binding sites, the conformation instability, the metal ion existence, and the

residues' lipophilicity at the protein-ligand interaction. Protein-protein interfaces of multiprotein assemblies have many of these unfavourable characteristics. However, those that entail concerted binding and folding in their construction have better-defined grooves or pockets, and these can present chances for hit identification and lead optimisation [72].

Heat shock proteins (HSP) are proteins that are expressed in response to stress with a molecular weight ranging between 14 to 120 kDa present in all living organisms [73]. Almost all living things contain HSPs, and they express more of them in reaction to a variety of cellular insults, such as oxidative stress, high temperatures, and heavy metal presence [74]. In addition to heat shock, several other conditions result in the induction of heat shock proteins. Most heat shock proteins are big oligomeric proteins, and several cofactors and cochaperones often control how they operate. Heat shock proteins are a component of the cellular chaperone network and do not work in isolation. The main heat shock protein families' overall structural and functional characteristics are described, along with their functions in human disease. Due to increased cellular stress, their role is particularly crucial in diseases [75]. On the other hand, HSPs, especially HSP90 are frequently overexpressed and found in activated multichaperone complexes in neoplastic cells, which are linked to a worse prognosis [76]. The increase in the expression of HSP tends to stabilise the proteins that are crucial for oncogenesis. Therefore, HSPs promote the independence of proliferation, tumour-cell survival, growth factors, immortalisation, neovascularisation, and metastasis [76-79]. Lastly, cancerous cells seem to be more dependent on HSPs compared to normal cells and they are sensitive to HSP inhibition [80].

HSP90 is a chaperone that clients about 300 cellular proteins that are important for cellular function. This molecular chaperone plays a huge part in stabilising the activity of oncogenic proteins and tumour biology, also HSP90 is found as a complex in cancer cells with its client proteins and co-chaperones. Therefore, the inhibition of HSP90 is considered a drug target because many of its client proteins depend on this chaperone for the essential cellular processes and are regarded as hosts for viruses. At present, there are ongoing studies to find suitable HSP90 inhibitors for the treatment of cancer [81-83]. However, the HSP90 inhibitors have shown demonstrated resistance, hence they induce the pro-survival heat shock response [84].

The initial development of direct HSP90 inhibitors was encouraged by the discovery that natural annamycin antibiotic geldanamycin (GA) possessed anticancer activity by inhibiting HSP90 [85].

This was through the binding competition of GA with ATP to the *N*-terminal domain of HSP90. These positive outcomes led to the development of GA derivatives that were to target the *N*-terminal of HSP90 as its first inhibitors. However, the promising compounds ((17-AAG (tanespimycin) **(24)** and 17-DMAG (alvespimycin)) **(25)** (**Figure 1.8**) in the clinical trials stage showed poor results with the side effect of hepatotoxicity [86]. The direct inhibition of the *N*-terminal was not a good target because of the stress response that was observed which led to the over-expression of other heat shock proteins (HSP70 and HSP27) [87]. The over-expression of HSP arrays and the increase of chaperone lead to the cytoprotection resulting in the resistance of *N*-terminal inhibitors. These are unwanted outcomes for cancer therapy, therefore, scientists had to look for alternatives [88].

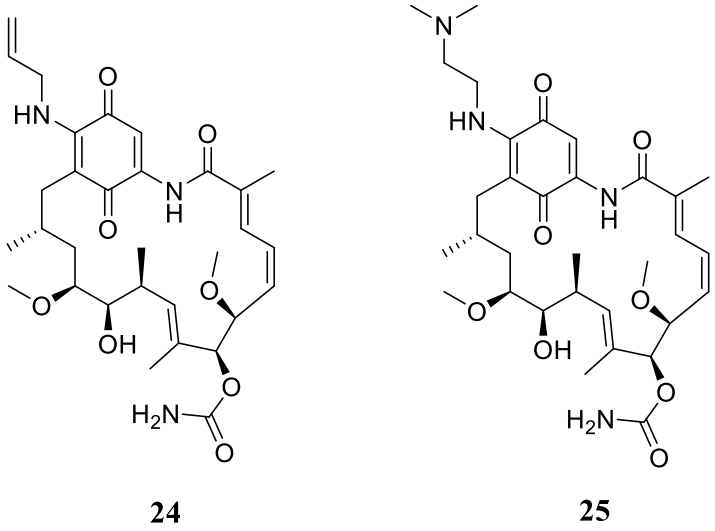


**24** **25**

**Figure 1.8:** 17-AGG **(24)** and 17-DMAG **(25)** are the *N*-terminal inhibitors for HSP90 to HOP [86].

HSP70/HSP90 Organising Protein (HOP) is a co-chaperone that forms PPI simultaneously between HSP90 and HSP70 molecular chaperones and regulates their chaperone activities [89]. Kubota and co-workers [90] investigated the level expression of co-chaperone HOP with HSP90 and complex formation in colonic carcinoma, the results showed an expression of HOP-HSP90 complex in cancerous tissue compared to normal tissue. Being able to regulate the protein folding, opens a potential druggable space for the treatment of many diseases. However, the challenge is finding new protein-protein interaction inhibitors [91]. Since some PPIs including HOP-HSP90 are crucial for oncogenic signal transduction and rely on HSP90 for stability and maturation, it is

worth noticing the role HSP90 plays, therefore, its inhibition will result in the disruption of HSP90 activity. Furthermore, the understanding of the HOP-HSP90 complex interaction presents an opportunity to develop PPI inhibitors.

A sequence of salt bridges between a C-terminal MEEVD pentapeptide motif of HSP90 and the carboxylate clamp region of the tetratricopeptide repeat 2A (TPR2A) domain of HOP serves as the key mediators of the PPI interaction between HSP90 (**Figure 1.9**) and HOP [92, 93]. HOP optimises HSP70 and HSP90's functional collaboration without acting as a molecular chaperone but by acting as an adaptor protein for them [94-96].

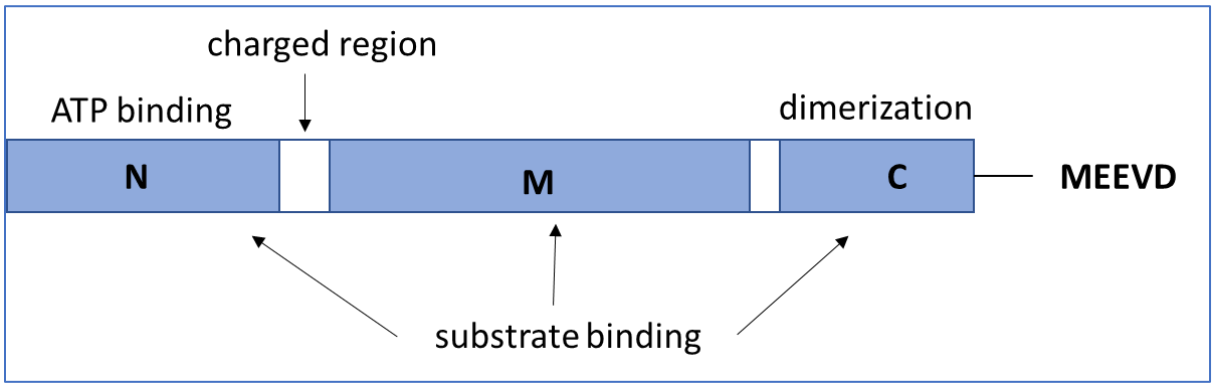


**Figure 1.9:** Schematic diagram of HSP90 consisting of three domains: an *N*-terminal ATP-binding domain (N); a middle domain (M); and a C-terminal dimerisation domain (C) with the MEEVD sequence. Between the N and M domains is a charged region. All three domains interact with a substrate protein [97].

In addition to being involved in the course of disease and malignant transformation in normal cells, HSP90 is also important for a variety of cellular functions (**Figure 1.10**) [89].

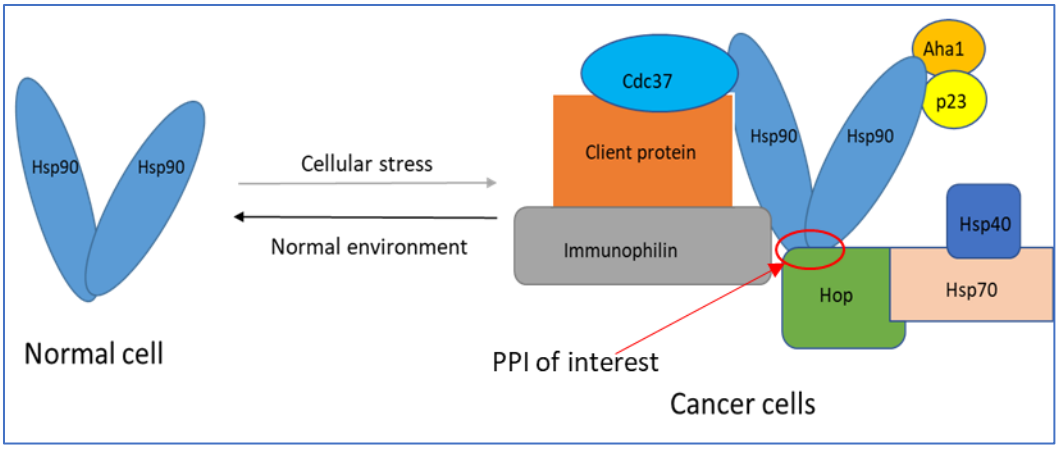


**Figure 1.10:** HOP makes high molecular weight complexes under a cancerous environment as it complexes with HSP90 and HSP70 unlike in normal cells.

Researchers validated the role of HOP as a drug target in cancer cells since it is found in the cancer cell as a complex along with HSP90 and is an oncogenic co-chaperone. This has widened the research space to find a drug target and given hope that these aggressive illness therapies can still be found [98]. Beraldo *et al*. demonstrated that the inhibition of HOP is another alternative anticancer drug target because HOP modulates the important cellular processes for cancer biology [99]. The strategy to inhibit HOP with HSP90 or HSP70 is currently underway with a different approach. Fragment-based drug discovery is the main common approach that is used to find small molecule analogues that will block the interaction of HOP TPR domains with HSP90 or HSP70 so that the chaperone cycle will be disrupted (**Figure 1.11**) [100-104].

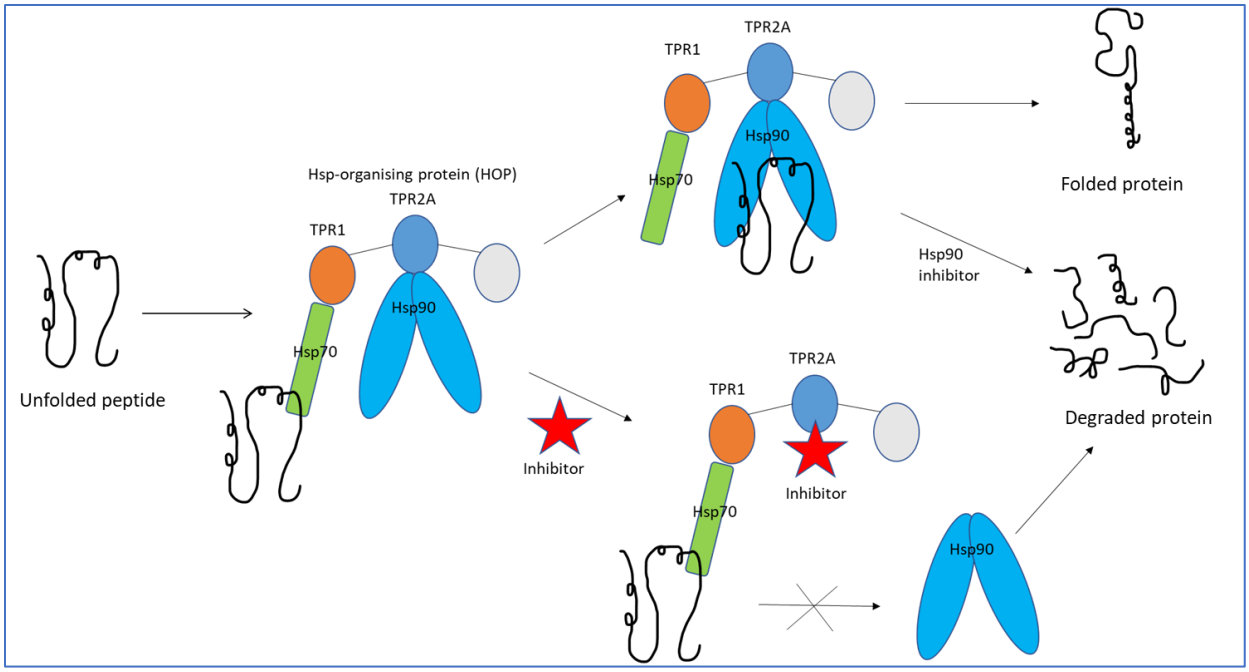


**Figure 1.11:** The schematic diagram illustrating the role of HOP-HSP90 PPI inhibitors in preventing the activity of HSP90 that leads to oncogenic protein degradation [89].

Given the challenges faced in targeting the HSP90 *N*-terminal domain with GA derivatives, Kawakami *et al*. investigated the hybrid TPR peptides to interact with the acidic MEEVD region of HSP90, therefore blocking its pro-oncogenic interaction with TPR2A of HOP [102]. McAlpine and Rahimi expanded the idea by reporting the cyclic TPR peptides that bound to the C-terminal MEEVD motif of HSP90 that disrupts PPI [105]. The other face of the PPI was investigated by Pimienta *et al*. [104] and Derby *et al*. [83], where they independently reported small molecules that bound to TPR2A, disrupting the binding of the MEEVD region of HSP90 without investigating the PPI inhibition.

The great potential of this target had been enlightened, therefore Veale and co-workers reported the tetrazole peptides that bound to TPR2A disrupting the PPI of HSP90 to HOP [46]. Tetrazoles are a group of five-membered heterocyclic compounds having planar structural characteristics rich in polynitrogen electrons. Tetrazole derivatives are valuable as medications, explosives, and other functional compounds with a variety of uses in many industries, including medicine, agriculture, material science, etc. thanks to their unique structure [106]. In addition to having a similar *pKa* to carboxylic acid, the tetrazolyl functional group was frequently regarded as a bioisoster for carboxylic acids since it offered pharmaceutical formulations with the highest nitrogen

concentration of any heterocyclic molecule making them metabolically stable with higher lipophilicity [107]. The reported study by Veale *et al.* of PPI inhibitors was conducted using a native mass spectrometer (MS) that had many advantages compared to other traditional methods [46].

The fragment strategy elaboration was built from the results reported by Vaaltyn *et al.* [108]. The Structural-Binding Relationship (SBR) was developed and showed that the six-membered ring, tetrazole, *ortho*-substituted with a benzene ring or halogen and benzoic acid analogues were binding to TPR2A. In addition, losartan **(26)** showed inhibition to the target since it entails the features that were described by the structural overlay of the fragments that were binders to TPR2A. The fragment strategy found was further confirmed by the other sartan family [valsartan **(27)** and irbesartan **(28)**] which inhibited the PPI although they were dose dependent. These features encouraged us to use valsartan **(27)** (**Figure 1.12**) as the proof of concept since it entails some of these features. *Ortho*-substituted phenyl tetrazole derivatives were therefore synthesised and then investigated for the inhibition of HOP-HSP90 PPI for the present study.

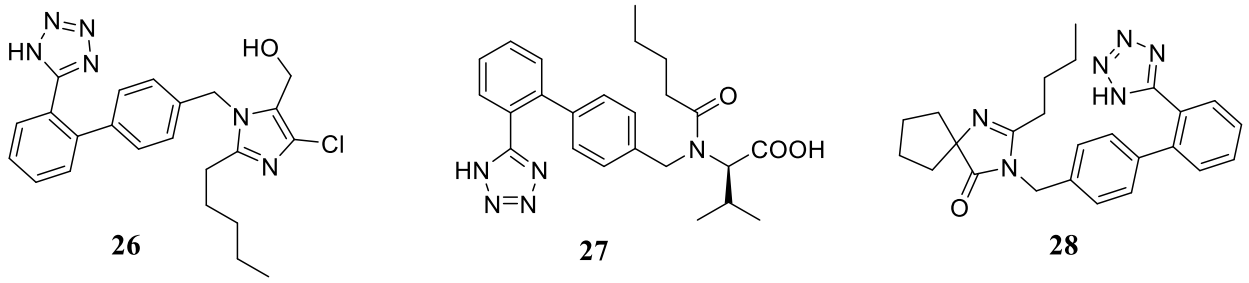


**Figure 1.12:** Losartan **(26)**, valsartan **(27)** and irbesartan **(28)**.

## 1.5 Aims and Objectives

The fight to find both effective and efficient therapies for TNBC has long been a losing battle for researchers over the years. Since TNBC does not contain hormones that are expressed in other cancers it does not respond to hormonal treatment or trastuzumab-based treatments [17], hence these therapies are ineffective for the treatment of TNBC. With all the techniques that have been used to come up with therapies for TNBC, none of them have been successful. It has been mentioned that the HOP-HSP90 PPI inhibition seemed to be a promising era for the development of TNBC therapies. Different authors have reported different approaches that intend to inhibit HOP-HSP90 PPI. Hybrid TPR peptides [102] and cyclic peptides [105] were investigated to interact with the HSP90 motif to inhibit HOP-HSP90 PPI. Alternatively, different authors reported fragments that interacted with the TPR2A domain without demonstrating PPI inhibition activity [83, 104]. Whereas Veale *et al*. investigated tetrazole peptides that disrupted HOP-HSP90 PPI [46]. With the aid of FBDD techniques, Vaaltyn *et al*. [108] investigated fragments hit that inhibited HOP-HSP90 PPI, with structural overlap resulting in *ortho*-phenyl tetrazole having valsartan **(27)** as one of the active compounds. Building from the knowledge that had been mentioned about the potential of *ortho*-phenyl tetrazole motifs, this project aimed at developing and elaborating valsartan derivatives to inhibit HOP-HSP90 PPI. This will provide a novel strategy for the development of TNBC therapies.

i. The objective was to synthesise the valsartan derivatives and then fully characterise them using NMR, IR, and TOF-MS.
ii. Elaborate their anti-cancer activity inhibitors *in vitro*.

# Chapter 2

## Results and Discussion

Breast cancer is caused as the overexpression of genes that are drug targets, including the expression of estrogen receptor (EP), human epidermal receptor 2 (HER2), and progesterone receptor (PR). Whereas triple-negative breast cancer (TNBC) is the absence of these genes that are the drug targets and that complicates the treatment plan for patients with this heterogeneous subtype of breast cancer. Chemotherapy is the backbone for the treatment of TNBC since it is resistant to HER2-targeted medicines e.g. trastuzumab and hormonal therapies include tamoxifen and aromatase inhibitors [109]. Although chemotherapy is currently the cornerstone of systemic medical care, triple-negative illness patients, when viewed as a group, have a worse prognosis following chemotherapy than patients with breast cancers of other subtypes, a result that underscores the disease's inherently poor prognosis [110, 111]. For TNBC, there isn't yet a recognised standard form of chemotherapy; instead, the course of treatment should be decided as it does for other cancer subtypes. The dearth of effective targeted treatments has increased interest in this patient population and is currently being researched [112]. Even though the pool of knowledge is wide, it is never enough; therefore, room for improvement is always available. However, TNBC targeted therapies still have a long way and scientists are working tirelessly to find suitable drugs to circumvent this heterogeneous disease.

Among the drug targets that have been mentioned in **Chapter 1**, protein-protein interaction (PPI) is regarded as the difficult target to drug, but fragment-based drug discovery (FBDD) has been shown to overcome that gap with its technologies since there are drugs available in the markets that were discovered using this technique. Over the past 20 years, the development of HSP90 inhibitors has gained a focus, especially the *N*-terminal inhibitors, and none of them have succeeded to date [5-7]. However, the *N*-terminal inhibitors lead to heat shock response (HSR) that causes drug resistance. Therefore, this has shifted the focus to C-terminal domain inhibitors whether they could potentially prevent induction of the pro-survival HSR while effectively suppressing oncogenic signalling [8-11].

The study that was conducted by Scheufler and co-workers [113] showed the interaction interface of HOP-HSP90 between peptides which then made it easy for researchers to have a starter point

for the development of protein-protein interaction (PPI) inhibitor for HOP-HSP90. Kawakami *et al*. [102] developed the hybrid TPR peptides and McAlpine *et al*. [13] developed cyclic peptides that bound to the C-terminal domain of HSP90 to inhibit the interaction with TPR2A of HOP. However, Pimienta *et al*. [14], and Darby *et al*. [15] reported the opposite phase to investigate the small molecules that bound to TPR2A disrupting the binding of the C-terminal to HOP. Veale *et al*. [16] studied the tetrazole peptides that bound to TPR2A disrupting the interaction with HSP90. With FBDD in hand as a new technique to use for hit identification, Vaaltyn and co-workers [108] identified different fragments that showed PPI inhibitory activity by binding to the TPR2A domain. They discovered binding and non-binding fragments which helped in illustrating their binding mode and structural binding relationship (SBP) pattern where the structural overlaps of fragments resulted in features like losartan **(26)**. Coupling the knowledge that has been reported by the above-mentioned authors, this project was aimed at synthesising and elaborating *ortho*-substituted biphenyl tetrazole scaffolds **(Figure 2.1)** that would bind to the TPR2A domain to inhibit HOP-HSP90 protein-protein interaction (PPI) for the treatment of TNBC. To begin the investigation, valsartan **(27)** was used as the proof of concept since it contains the features that were reported by Vaaltyn's findings, it was also demonstrated that valsartan **(27)** along with losartan **(26)** and irbesartan **(28)** also inhibited the HOP-HSP90 PPI [108].

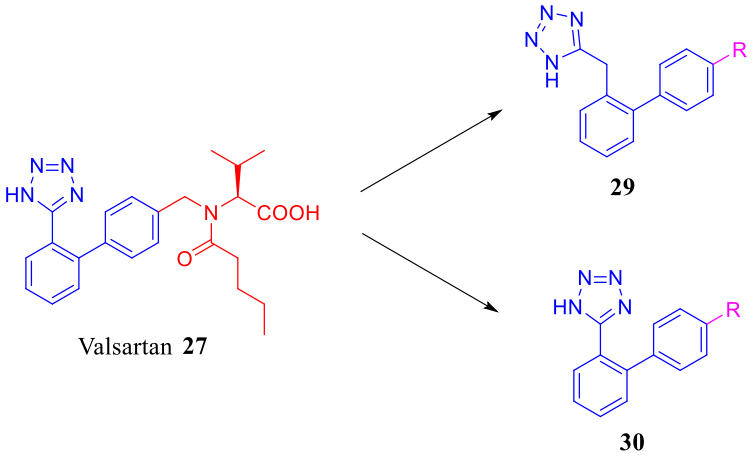


**R = H, $OCH_3$, $CH_3$, F, Cl, Br, $CF_3$**

**Figure 2.1:** Valsartan **(27)** and its derivatives desired for the HOP-HSP90 PPI inhibition.

The investigation started by looking at the retrosynthesis of valsartan **(27)** in **Scheme 2.1** which helped with the method to synthesise its derivatives. Retrosynthesis for *ortho*-substituted phenyl

tetrazole scaffolds pointed out the important functional groups that were converted to get the desired product. Both routes firstly demonstrate the based-catalysed hydrolysis of a methyl ester in **Step A** compared to the debenzylation that use large amount of Pd/C under high pressure of $H_2$ gas and produce a benzyl alcohol as a byproduct [114]. As indicated by **Route A** and **Route B**, the cycloaddition of tetrazoles could be done from the [3 + 2] cycloaddition of sodium azide **(33)** with nitrile in the presence of a Lewis acid in **Step B** [115].

As it showed from **Scheme 2.1** that compound **32** was the crucial intermediate since it could be achieved *via* two different routes, we envisioned that the difficulties associated with the purity in the acylation **Step D$^1$** because of the polarity of compound **37** and **38** being very close that could make purification step difficult. The cyclisation reaction was presented as the last step to avoid triphenylmethylation step and the deprotection. Acylation reactions are sensitive to moisture especially when an acyl chloride is used because it decomposes to an unreactive carboxylic acid, leading to an uncomplete reaction. For that reason, we decided to do an acylation reaction before **(Step D$^1$, Route B)** or after **(Step C, Route A)** the cross-coupling reaction to assess the best method. Suzuki-Miyara cross-coupling reaction in **Step D$^1$** seemed to be a smooth but the side reaction of homocoupling could reduce the yield of the desired product **(32)**, whereas the unreactive compound **38** along with excess of compound **37** could result to high impurities **(Route B)**. The cross-coupling reaction of compound **36** was predicted to be produced in **Route B** as the side product, therefore, we thought if we coupled directly, that could reduce the number of side product because alkylation of compound **40** is simple without any impurities.

In designing alternative synthetic route for valsartan **(27)**, our goal was to explore chemical space in developing a safe, robust, industrial applicable route for the synthesis valsartan **(27)** which will then be applied for the synthesis of valsartan derivatives **(29 & 30)**.

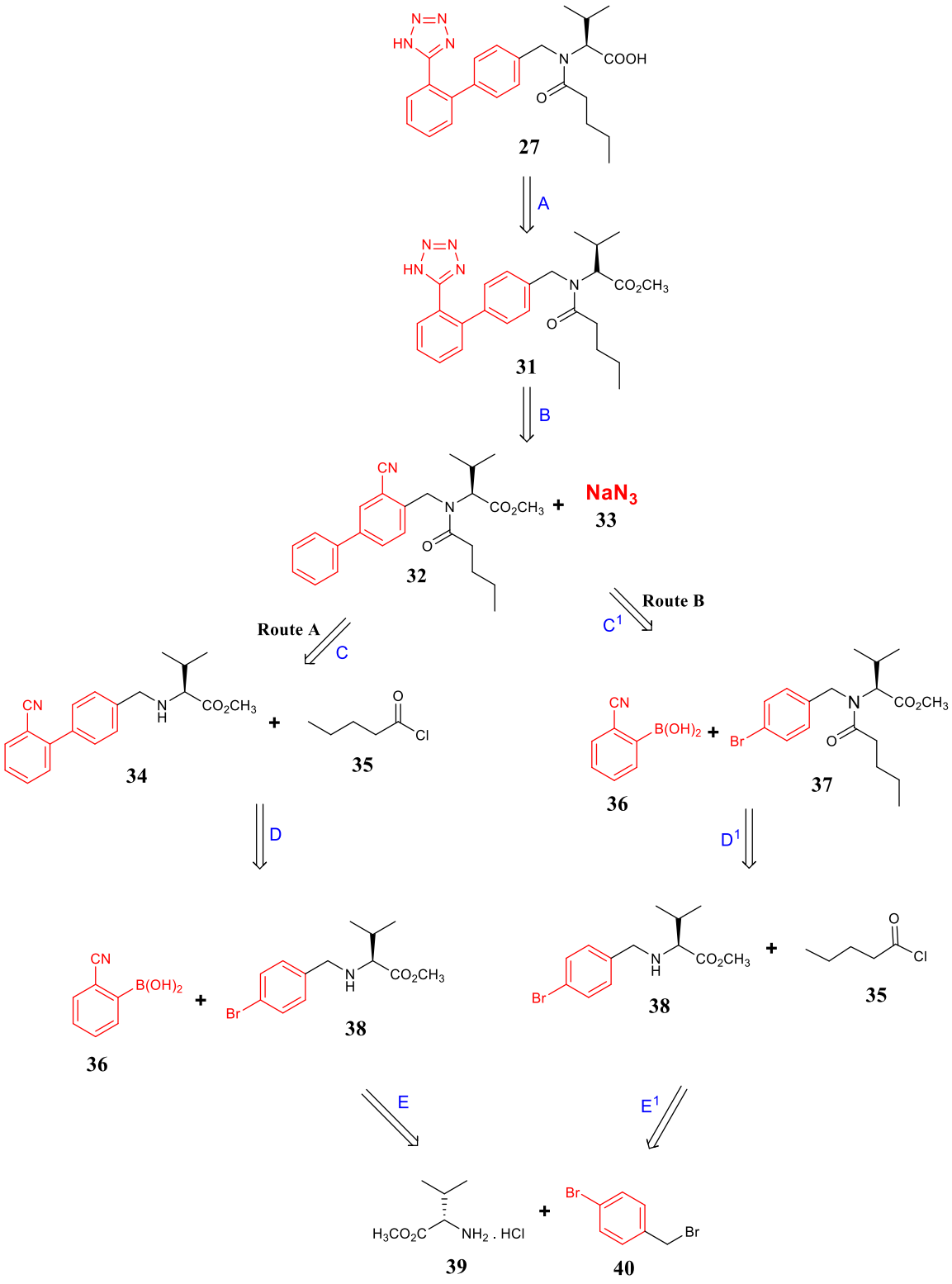


**Scheme 2.1:** Valsartan **(27)** retrosynthesis following two different routes.

## 2.1. Functional Group Conversion Optimisation

### 2.1.1 The synthesis of benzonitrile (42)

The retrosynthesis of valsartan **(27)** above **(Scheme 2.1)** indicated the important steps: the cycloaddition reaction for the conversion of nitrile to tetrazole as well as the formation of C-C bond using the Suzuki-Miyaura cross-coupling reaction. Since benzonitrile was not available in our lab, therefore, the first step was to synthesise a benzonitrile **(42)** to be cyclised with sodium azide **(33)** to form a tetrazole as illustrated in the retrosynthesis **(Scheme 2.1)**. With the aim of synthesising benzonitrile, readily available benzaldehyde **(40)** was reacted with sodium azide **(33)** in the presence of phosphoryl chloride under inert conditions as reported by Sribalan *et al*. However, the reaction was not successful because benzaldehyde was not dry enough making phosphoryl chloride to react with water leading to an explosion. An alternative safer method, using hydroxylamine-*O*-sulfonic acid reported by Quinns was adopted **(Scheme 2.2B)**. Even with the direct synthesis using hydroxylamine-*O*-sulfonic acid following Quinns's method, the reaction was unsuccessful which might be due to the autoxidation of benzaldehyde **(40)** to benzoic acid given the fact that benzoic acid is unreactive unless activated with thionyl chloride **(Scheme 2.2)** [116].

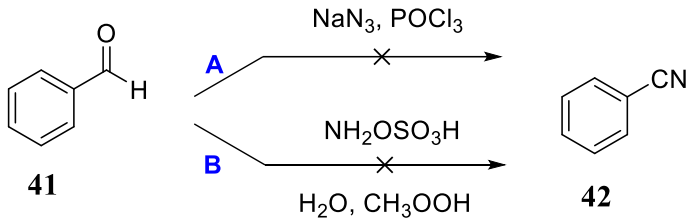


**Scheme 2.2:** Optimisation reaction for the synthesis of benzonitrile **(42)**.

With the attempted conversion above using benzaldehyde as a starting material being unsuccessful, we thought of using a more stable benzamide [compared to benzaldehyde **(41)**] as a starting material might yield different outcome. In literature, we came across the conversion of primary amide from the dehydration of primary amide to nitrile functional group using $POCl_3$, $P_2O_5$, and $SOCl_2$ reported by Rickborn and Jensen [117]. With the above information at hand three different methods to dehydrate amides using $POCl_3$ and $P_2O_5$ under different reaction conditions were attempted **(Scheme 2.3)**. The solvent free dehydration reaction of benzamide **(43)** with $POCl_3$ **(Scheme 2.3 A**) and the use of $P_2O_5$ in dry solvent **(Scheme 2.3 B)**, did not give the desired

benzonitrile **(42)** product because of the less contact between starting materials in solvent free reaction and $P_2O_5$ reacted with the solvent, respectively. The desired product was formed when DMF was used as a solvent along with $POCl_3$ as a dehydrating agent following Kusurkar and co-workers' procedure **(Scheme 2.3 C)** [118].

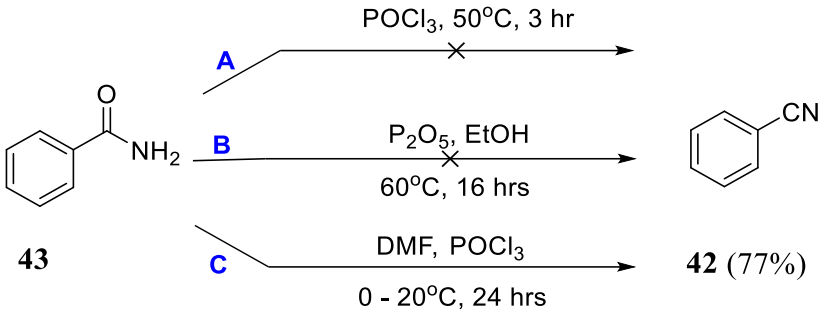


**Scheme 2.3:** Optimisation reaction for the dehydration of benzamide **(43)**.

The successful synthesis of benzonitrile **(43)** from benzamide **(43)** was confirmed using the IR spectrum in **Figure 2.2** by the appearance of the -CN stretching band at 2224 $cm^{-1}$. Nuclear Magnetic Resonance (NMR) spectroscopy further confirmed the formation of the desired product especially the $^{13}C$ NMR spectrum **(Figure 2.4)** with the appearance of a carbon signal at 118.8 ppm indicating the presence of nitrile functionality [119].

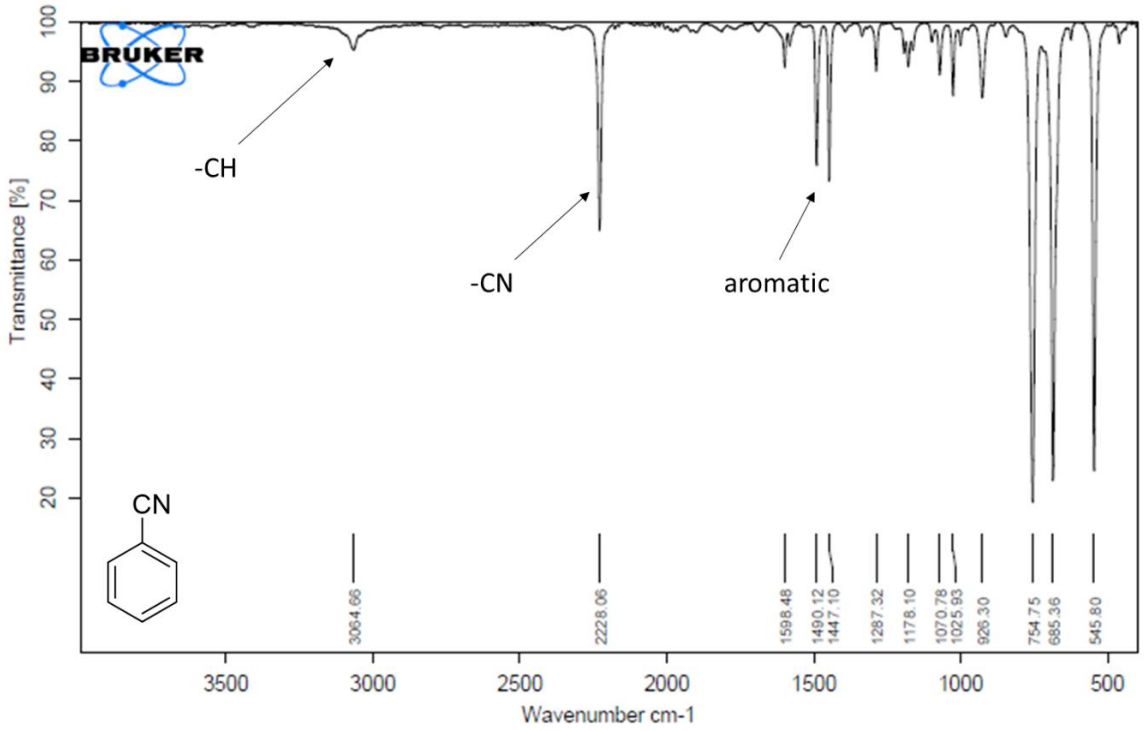


**Figure 2.2:** IR spectrum for benzonitrile **(42)** with the nitrile peak indicating the successful dehydration.

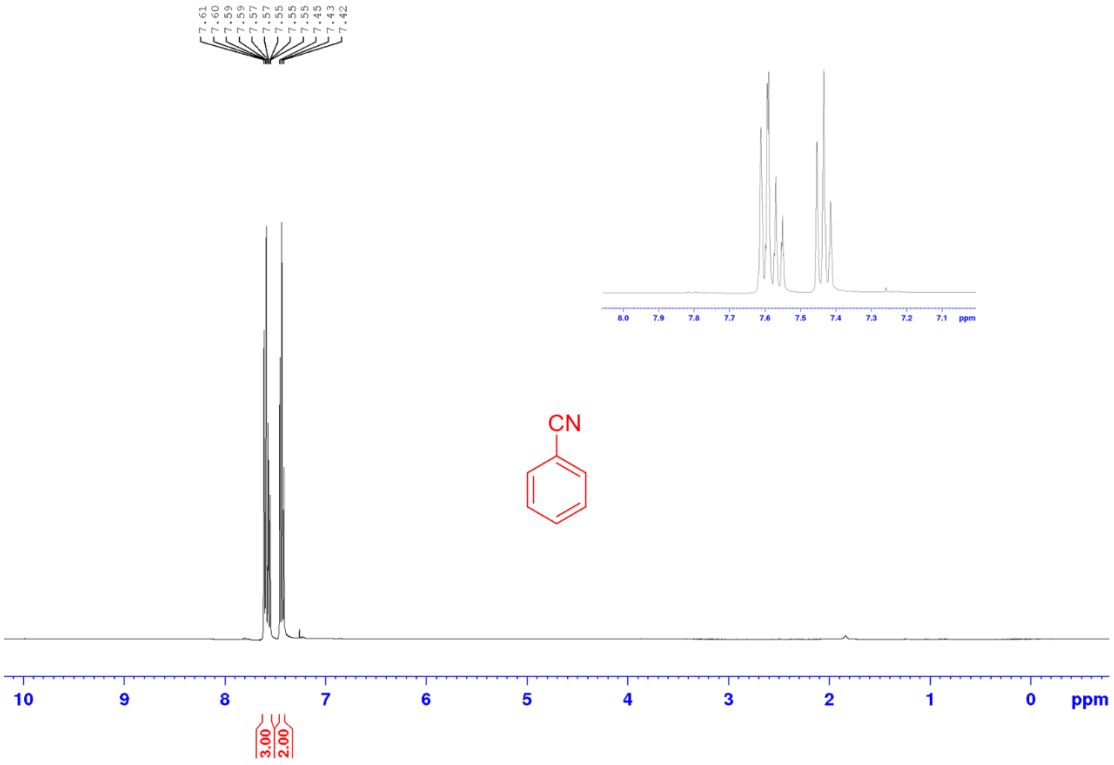


**Figure 2.3:** $^{1}$H NMR spectrum for benzonitrile **(42)**.

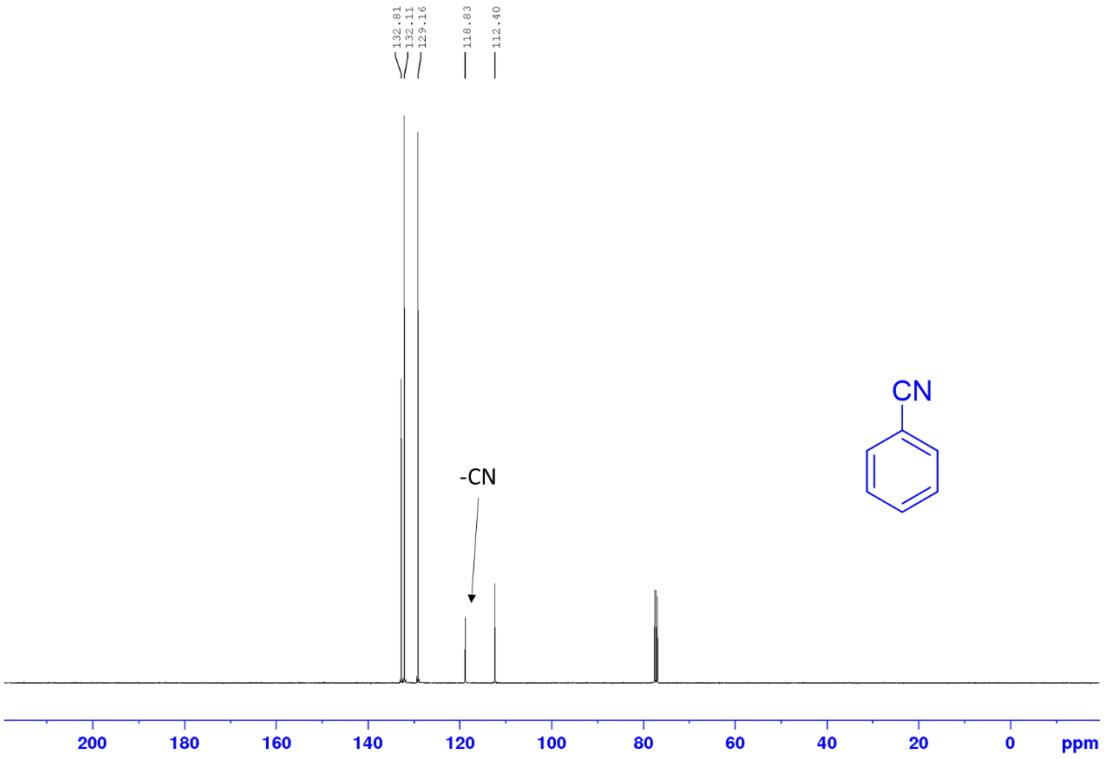


**Figure 2.4**: $^{13}$C NMR spectrum for benzonitrile **(42)**.

Now that we have successfully found a method that produces benzonitrile, our next step was to convert the benzonitrile to tetrazole. Tetrazoles are unsaturated five-membered heterocyclic compounds that contain four nitrogen atoms and one carbon atom **(Figure 2.5)** [120]. Because of the tetrazole structural features of being polynitrogen electron-rich planar ring, they give important application to their derivatives in medicine, explosives, agriculture, and material science [121]. In medicinal chemistry, tetrazoles are used as bioisosters of carboxylic acids because they are metabolic stable to the biological transformations present in the liver that decomposes carboxylic acids [122, 123]. In some prodrug procedures, the use of tetrazole moieties as bioisosters has been shown to improve bioavailability and lipophilicity [124, 125]. The reason behind tetrazoles being bioisoster of carboxylic acids is because their *pKa* values are close to each other and they almost have the same delocalised planar system [126]. Furthermore, tetrazoles can form noncovalent bonds with the target in the biological system since their moieties have different pharmacological properties such as anticancer [127], antibacterial [128], antimalarial [129], antifungal [130], antitubercular [131], antiviral [132], anti-Alzheimer's diseases [133], and antiangiogenic [134] activities. With all the different synthetic routes reported in the literature for the preparation of tetrazole functional group from different precursors, the conversion of aryl nitriles to tetrazole

moieties was the chosen method since it is easy to work with aryl nitrile including their preparation **(Figure 2.5)** [135].

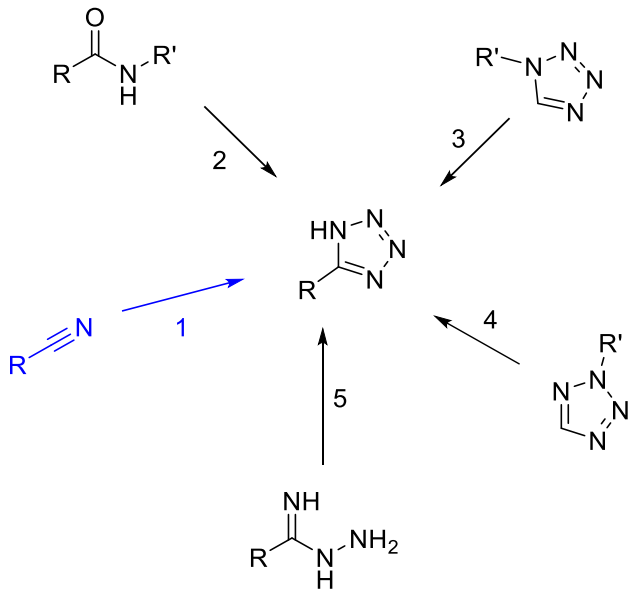

**Figure 2.5:** Different procedures for the synthesis of tetrazole.

### 2.1.2 The synthesis of 5-phenyl-1*H*-tetrazole (44)

With the above-mentioned methods for the synthesis of tetrazole, in our group we discovered that the addition of both zinc bromide and ammonium chloride as additives affords the [3 + 2] cycloaddition of tetrazole. Following the same method, 5-phenyl-1*H*-tetrazole **(44)** was produced in 61% yield as a white solid **Scheme 2.4**.

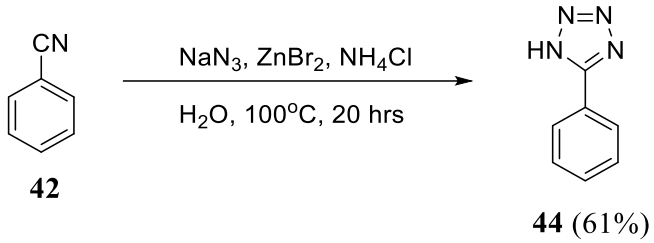


**42** **44** (61%)

**Scheme 2.4:** [3 + 2] Cycloaddition of benzonitrile **(42)** with sodium azide **(33)**.

The successful synthesis of 5-phenyl-1*H*-tetrazole **(44)** was confirmed using the $^{1}$H NMR spectrum which corresponded with the structure **(Figure 2.6)**. The disappearance of a nitrile peak at 119 ppm from the $^{13}$C NMR spectrum confirmed the full conversion of the nitrile to tetrazole after 20 hours of reflux **(Figure 2.7)** [136].

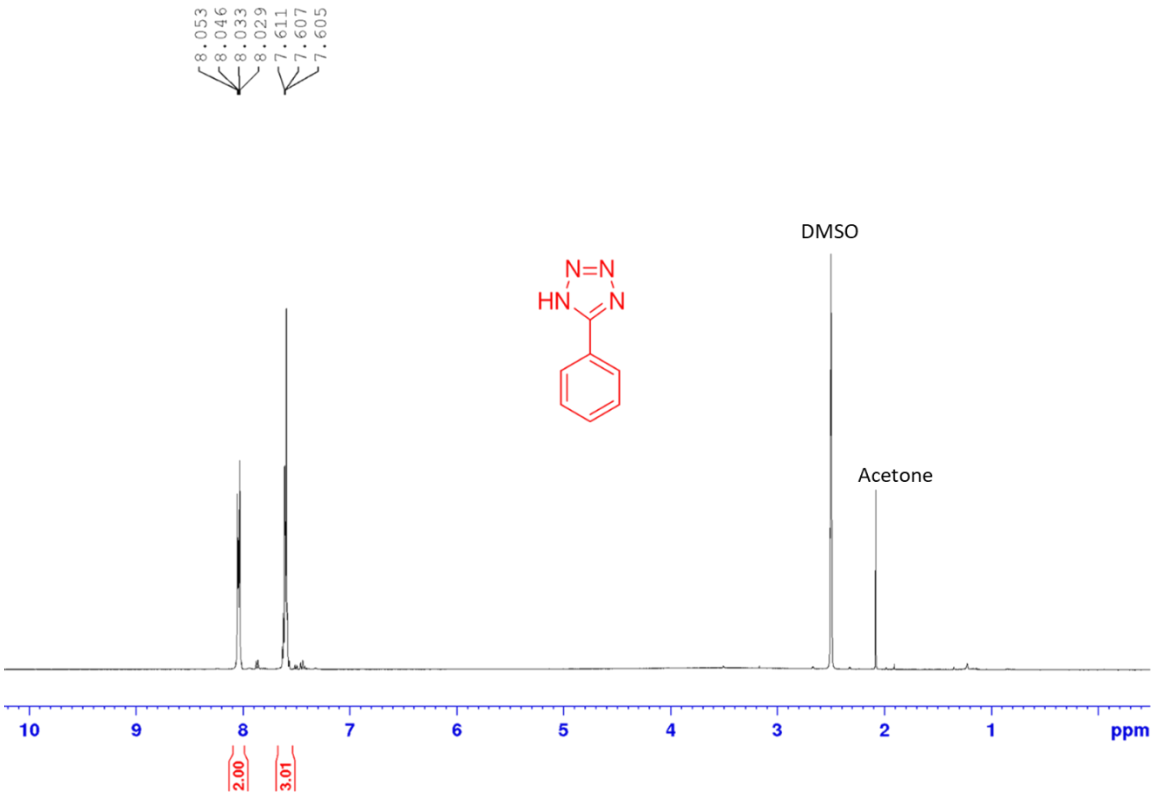


**Figure 2.6**: $^{1}$H NMR spectrum for 5-phenyl-1*H*-tetrazole **(44)**.

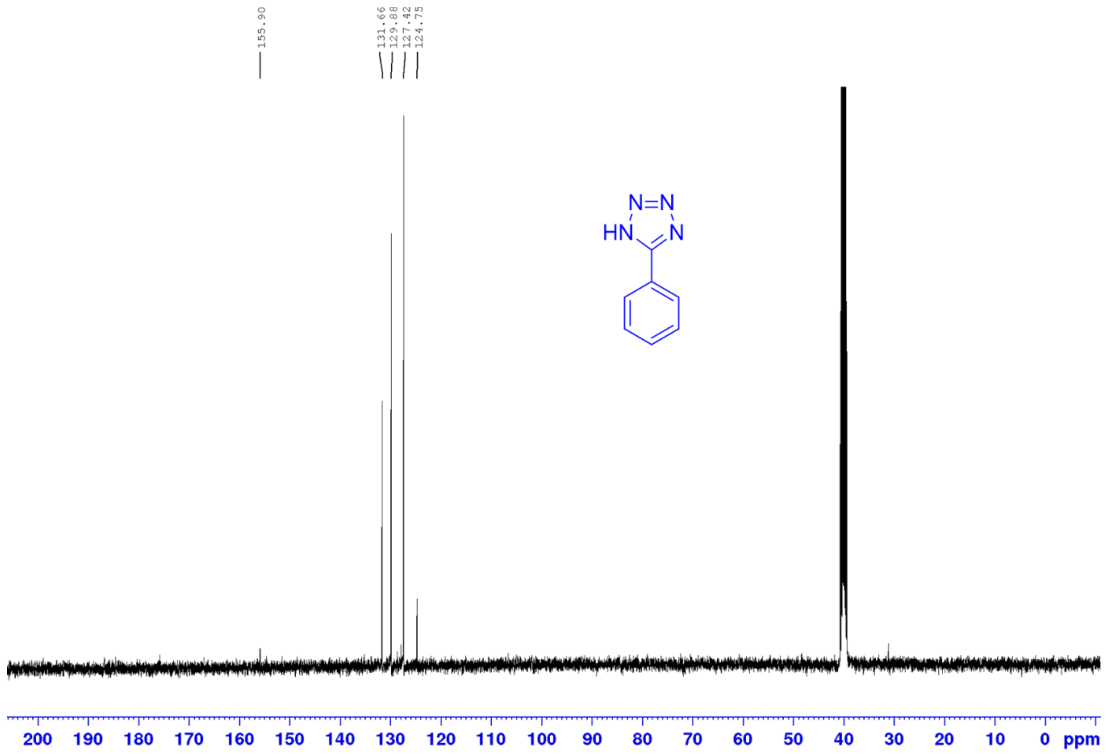


**Figure 2.7**: $^{13}$C NMR spectrum for 5-phenyl-1*H*-tetrazole **(44)**.

Since we have mastered the conversion of the benzamide to benzonitrile as well as its conversion to a tetrazole, this model method was further used for the substituted benzonitrile.

### 2.1.3 The synthesis of 2-iodobenzonitrile (47)

The preparation of tetrazole form benzamide was treated as a model reaction. With the model reaction successfully achieved, we then turn our attention in converting 2-iodobenzoic acid **(45)** to 2-iodobenzonitrile **(47)**. 2-Iodobenzonitrile was prepared following the method reported by Al-Huniti *et al.* [137] and Kusurkar *et al.* [118] in an isolated yield of 93% as a cream solid from the conversion of 2-iodobenzoic acid **(45)** to 2-iodobenzamide **(46)** which was later dehydrated to the desired product **(47) (Scheme 2.5)**.

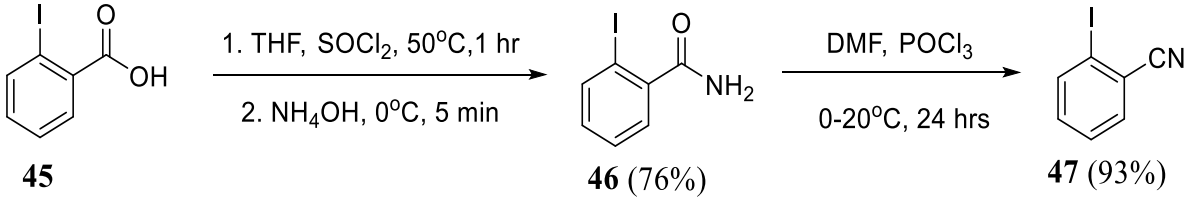


**45** **46** (76%) **47** (93%)

**Scheme 2.5**: Synthesis of 2-iodobenzonitrile **(47)**.

The conversion of carboxylic acid to nitrile functionality has been afforded and was confirmed using $^{1}$H NMR and $^{13}$C NMR spectra. All four signals orientate in the aromatic region between 7.26-7.93 ppm, and they all integrate for one proton each and the multiplicity corresponds to the neighbouring protons **(Figure 2.8)**. $^{13}$C NMR **(Figure 2.9)** has a nitrile peak at 119.3 ppm with a minimal intensity because the carbon is not attached to any hydrogen atom, which therefore confirms the dehydration of an amide [138, 139]. The IR spectrum **(Appendix A1.1)** confirmed the dehydration reaction with the nitrile peak at 2224 cm$^{-1}$ and the absence of a strong carbonyl peak around 1670-1780 cm$^{-1}$ and a medium peak of -NH group for a primary amide around 3300-3500 cm$^{-1}$ [140].

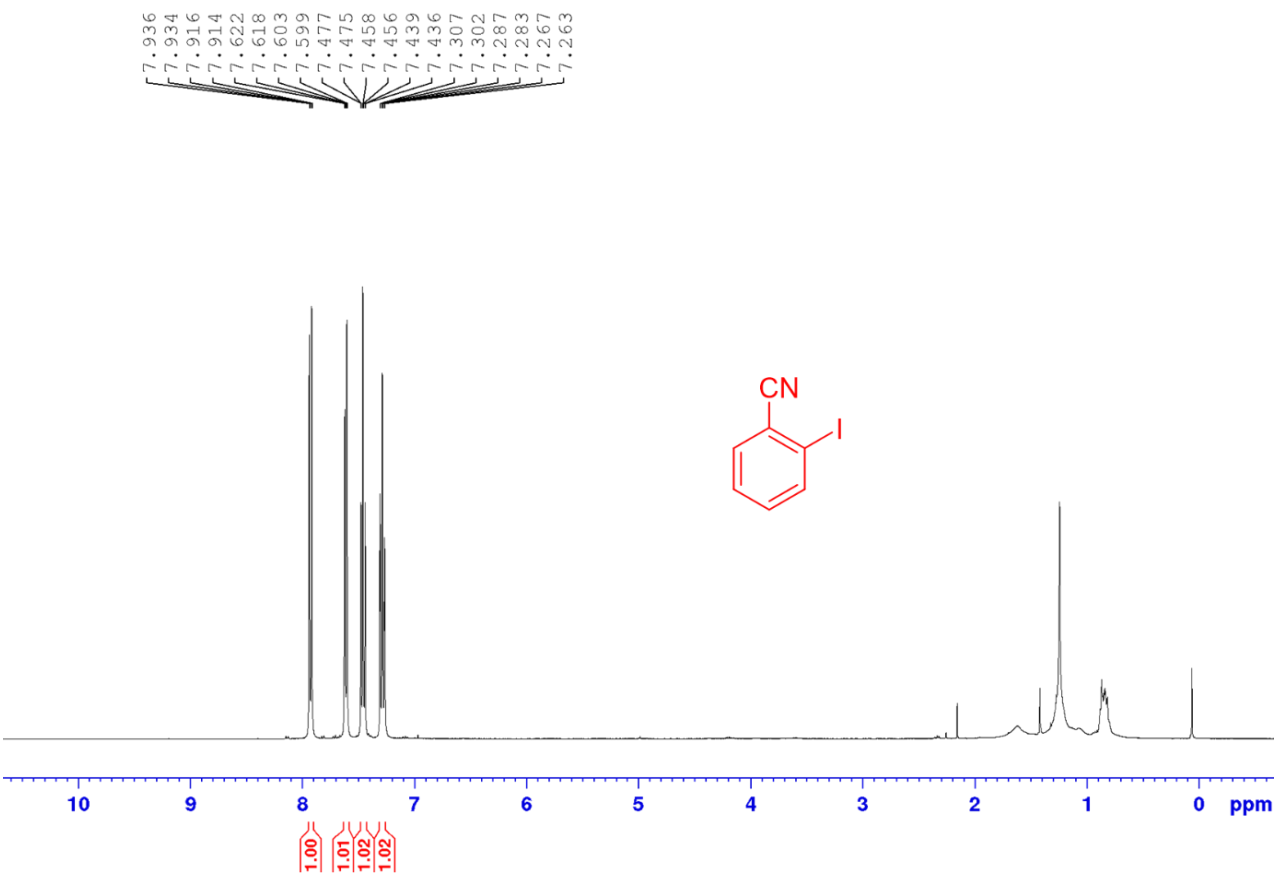


**Figure 2.8**: $^{1}$H NMR spectrum for 2-iodobenzonitrile **(47)**.

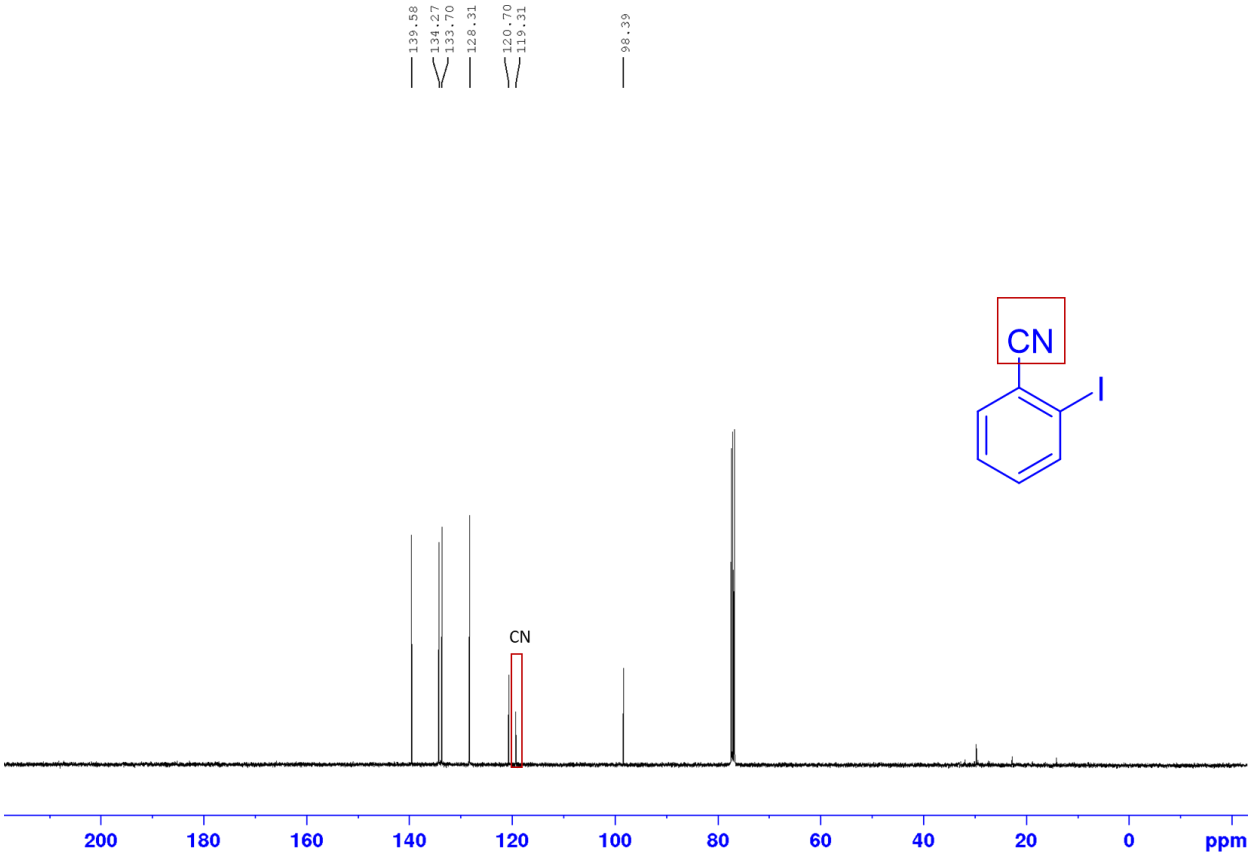


**Figure 2. 9**: $^{13}C$ NMR spectrum for 2-iodobenzonitrile **(47)**. The peak of interest at 119.3 ppm indicates the presence of the nitrile group, confirming the successful dehydration of the primary amide.

## 2.2. Suzuki-Miyaura Cross-coupling Optimisation

With the ortho-substituted benzonitrile at hand, our next step on the preparation of valsartan derivatives **(48)** was to perform a carbon-carbon bond forming reaction using a Suzuki -Miyaura cross-coupling reaction highlighted in **Scheme 2.6**.

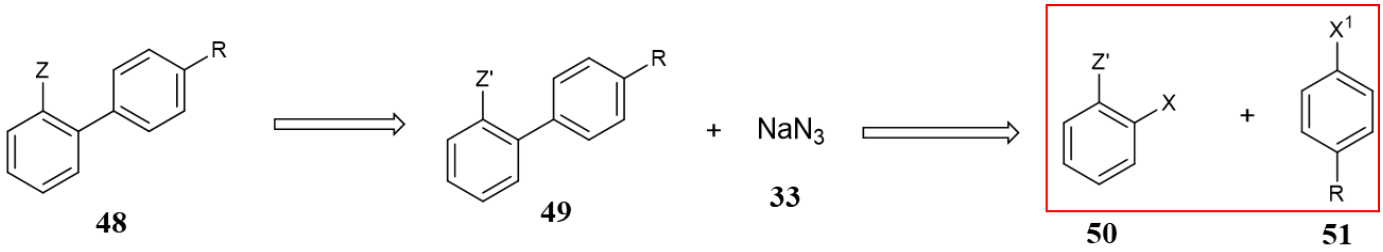


X = I or Br or $B(OH)_2$, $X^1$ = I or Br or $B(OH)_2$ :(*Note: X and $X^1$ will never be the same at the same time.)*

Z = tetrazole or benzylic tetrazole, Z' = nitrile or benzylic nitrile

**Scheme 2.6**: Retrosynthesis for the synthesis of valsartan derivatives **(48)**.

### 2.2.1 The synthesis of [1, 1'-biphenyl]-2-carbonitrile (53)

An optimisation reaction of phenylboronic acid **(52)** and 2-iodobenzonitrile **(47)** was performed using Suzuki-Miyaura cross-coupling reaction with the aim to achieve the best method to perform carbon-carbon bond **(Scheme 2.7)**.

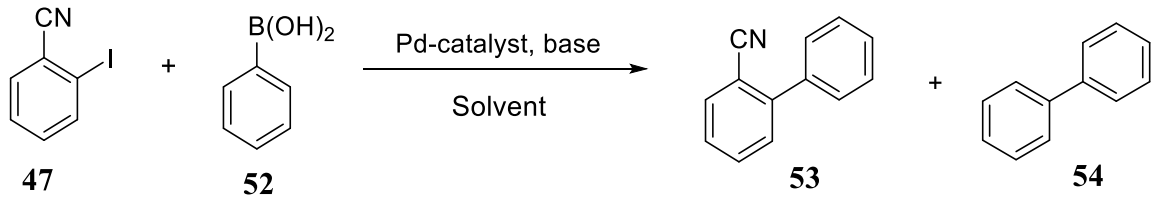


**Scheme 2.7:** General Suzuki-Miyaura cross-coupling optimisation reaction.

**Table 2.1**: Optimisation reactions for Suzuki cross-coupling [a].

| Entry | Catalyst | Solvent | Base | Conditions | Yield (%)[b] |
|---|---|---|---|---|---|
| 1 | $Pd(PPh_3)_2Cl_2$ | Toluene | $Na_2CO_3$ | 60°C | 22 |
| **2** | **$Pd(PPh_3)_4$** | **Toluene/ $H_2O$** | **$K_2CO_3$** | **80°C** | **86** |
| **3** | **$Pd(OAc)_2/PPh_3$** | **THF** | **$K_2CO_3$** | **80°C** | **81** |

**Entry 2 and 3** are optimised reaction conditions (bold text). [a]Reaction conditions: 2-iodobenzonitrile (1 mmol), phenylboronic acid (1.2 mmol), Pd catalyst (5 mol%), ligand (10 mol%), 24 hours. [b]Isolated yields after purification.

The cross-coupling was observed between phenylboronic acid **(52)** and 2-iodobenzonitrile **(47)** across the table in the presence of a palladium catalyst **(Table 2.1)**. Hussain and co-workers emphasised that the ligand plays a significant role in cross-coupling because of their binding ability

to the metal centre which is influenced by their electronic structure [141]. The Suzuki-Miyaura cross-coupling reaction between phenylboronic acid **(52)** and 2-iodobenzonitrile **(47)** proceeded smoothly producing predominantly the homo-coupling product **(54)**, and the reaction was not complete even after 24 hours **(Table 2.1, entry 1**). Li and co-workers argued that as much as the excess amount of a base in Suzuki-Miyaura cross-coupling reaction is necessary but adding too much of a base promote side reaction i.e. protodeboronation of arylboronic acid, homo-coupling and it suppresses the formation of the cross-coupling desired product [142]. The use of a freshly prepared $Pd(PPh_3)_4$ as well as $Pd(OAc)_2/PPh_3$ catalysts produced excellent yield, and both of these methods were adopted for the synthesis of valsartan derivatives **(Table 2.1, entry 2 and entry 3)**. A slight decrease in yields was observed when $Pd(OAc)_2$ was used along with the phosphine ligands but good separation and high purity was observed which made these conditions also be considered optimal conditions **(Table 2.1, entry 3)**.

With the optimised tetrazole cyclisation reaction conditions and cross-coupling reaction conditions at our disposal, the retrosynthesis **(Scheme 2.1)** of valsartan **(27)** suggested that we could do a cross-coupling reaction of compound **36** & **34** or **36** & **37** before the formation of tetrazole. The next section presents the preparation of valsartan **(27)** employing the optimised reaction conditions explored above.

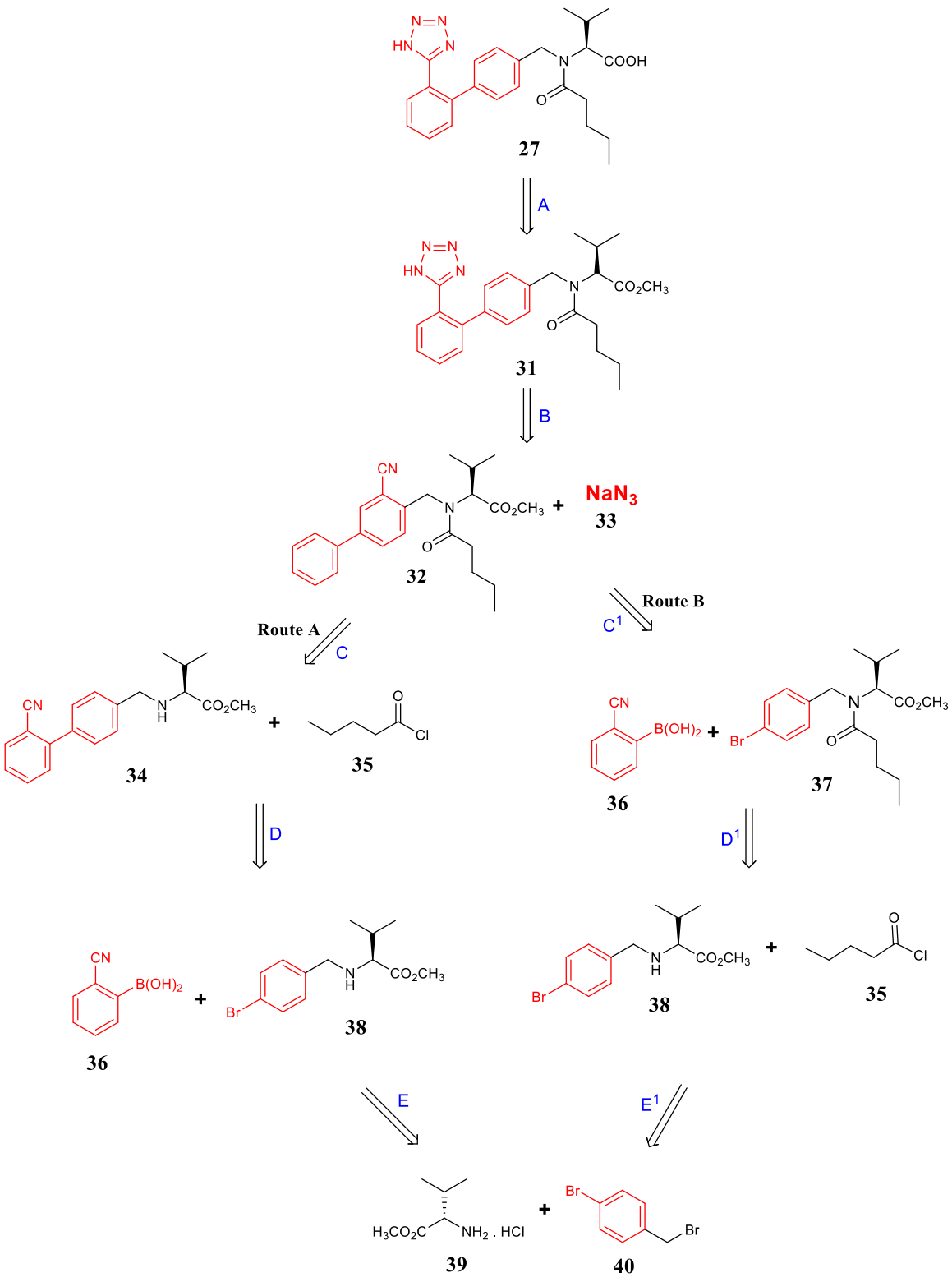


**Scheme 2.1:** Valsartan **(27)** retrosynthesis following two different routes.

## 2.3 The Synthesis of Valsartan

### 2.3.1 The synthesis of methyl (4-bromobenzyl)-*L*-valinate (38)

To begin the synthesis of valsartan **(27)**, the initial step was the synthesis of methyl (4-bromobenzyl)-*L*-valinate **(38)** from the alkylation reaction of 4-bromobenzyl bromide **(40)** and *L*-valine methyl ester **(39) (Scheme 2.8)**. The desired product was obtained as a colourless liquid with 93% yield [143].

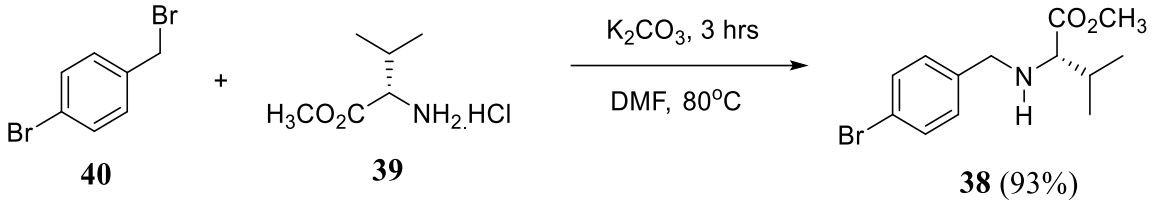


**40** **39** **38** (93%)

**Scheme 2.8:** Alkylation reaction of methyl (4-bromobenzyl)-*L*-valinate **(38)**.

The structure of the desired product corresponds to the $^{1}$H NMR and $^{13}$C NMR spectra obtained. All signals integrate for all the protons on the structure, which indicates that the alkylation reaction was a success. There are two doublets in the downfield region in $^{1}$H NMR with the chemical shift in the range 7.18-7.40 ppm integrating for two protons each. They indicate protons from the ring and both their coupling constants were 8.17 Hz which indicate that these protons are in the adjacent carbons (*para*). In the upfield region, the triplet at 0.89 ppm indicates the two methyls as it integrates for six protons since they are in the same chemical environment **(Figure 2.10)**. $^{13}$C NMR spectrum has a peak at 175.4 ppm that corresponds to an ester functionality in the structure which is within the expected range from the literature and all the signals correspond to the carbons in the structure **(Figure 2.11)**.

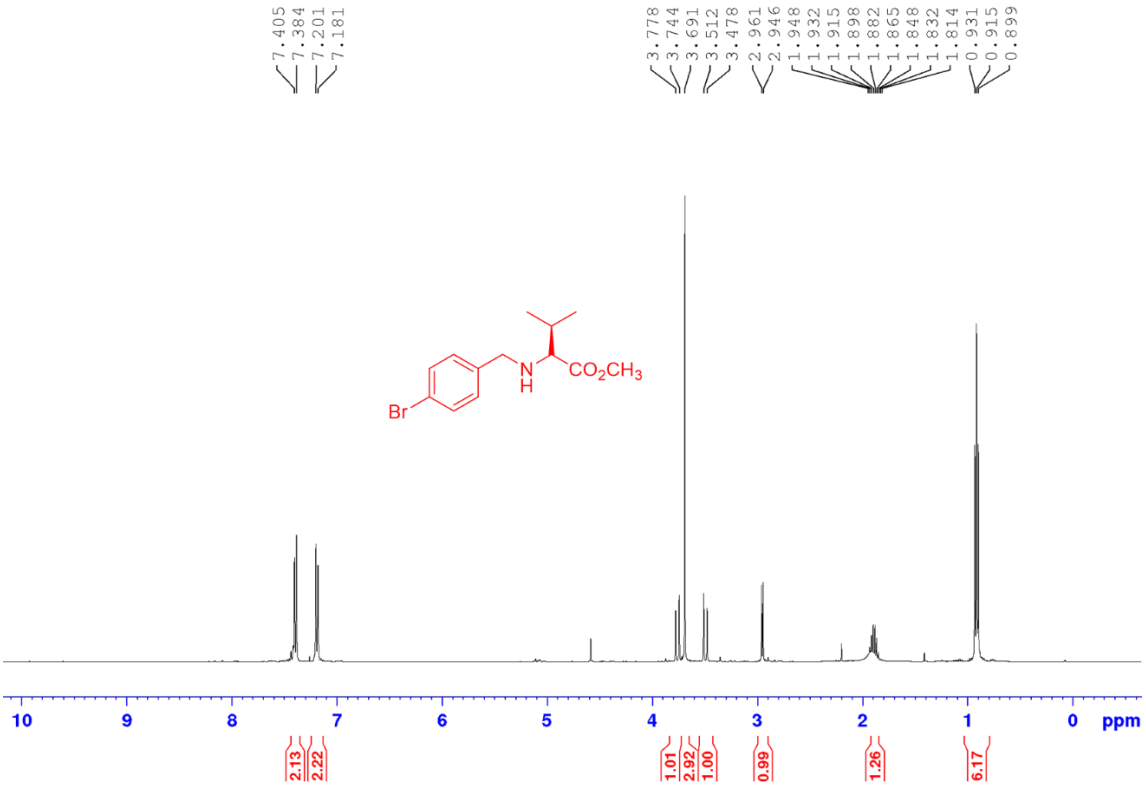


**Figure 2.10:** $^{1}$H NMR spectrum for methyl (4-bromobenzyl)-D-valinate **(38)**.

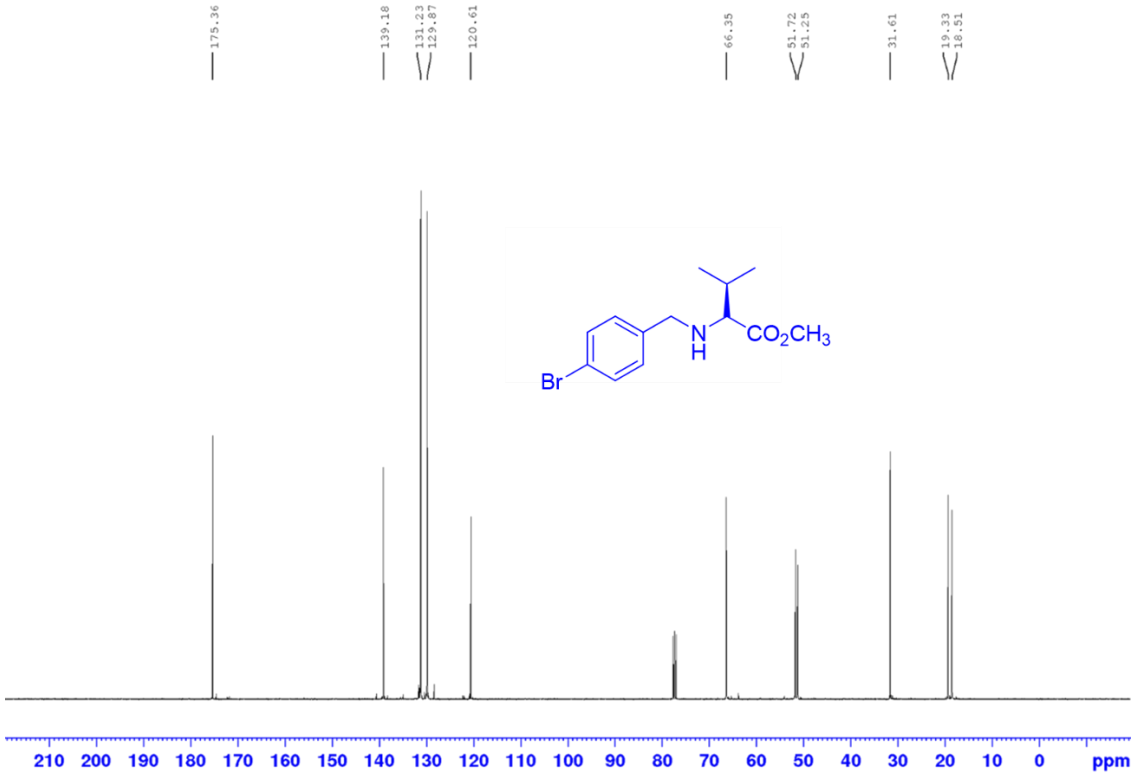


**Figure 2.11:** $^{13}$C NMR spectrum for methyl (4-bromobenzyl)-D-valinate **(38)**.

### 2.3.2 The synthesis of methyl *N*-(4-bromobenzyl)-*N*-pentanoyl-*L*-valinate (37)

To introduce the acyl group on the secondary amine, the acylation of methyl (4-bromobenzyl)-*L*-valinate **(38)** with valeroyl chloride **(35)** was initiated. The reaction was conducted in the presence of triethylamine base in dichloromethane at 0°C, producing methyl *N*-(4-bromobenzyl)-*N*-pentanoyl-*L*-valinate **(37)** with 73% yield as a yellow liquid **(Scheme 2.9)**.

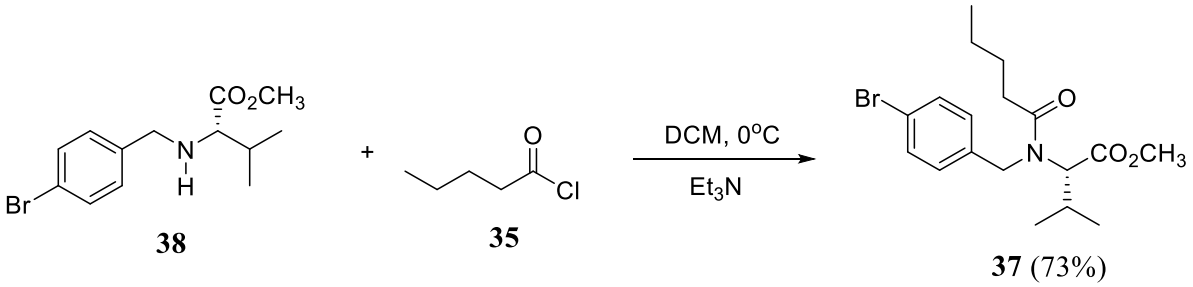


**Scheme 2.9:** Acylation reaction of methyl (4-bromobenzyl)-*L*-valinate **(37)**.

The $^{1}$H NMR spectrum elucidation of the furnished methyl *N*-(4-bromobenzyl)-*N*-pentanoyl-*L*-valinate **(37)** confirmed that indeed the acylation reaction step was a success evidenced by the appearance of aliphatic peaks of pentanoyl moiety **(Figure 2.12)** [144]. IR spectrum gives evidence that the structure has two carbonyl groups that are indicated by the signals at 1651 and 1732 cm $^{-1}$ **(Figure 2.13)**.

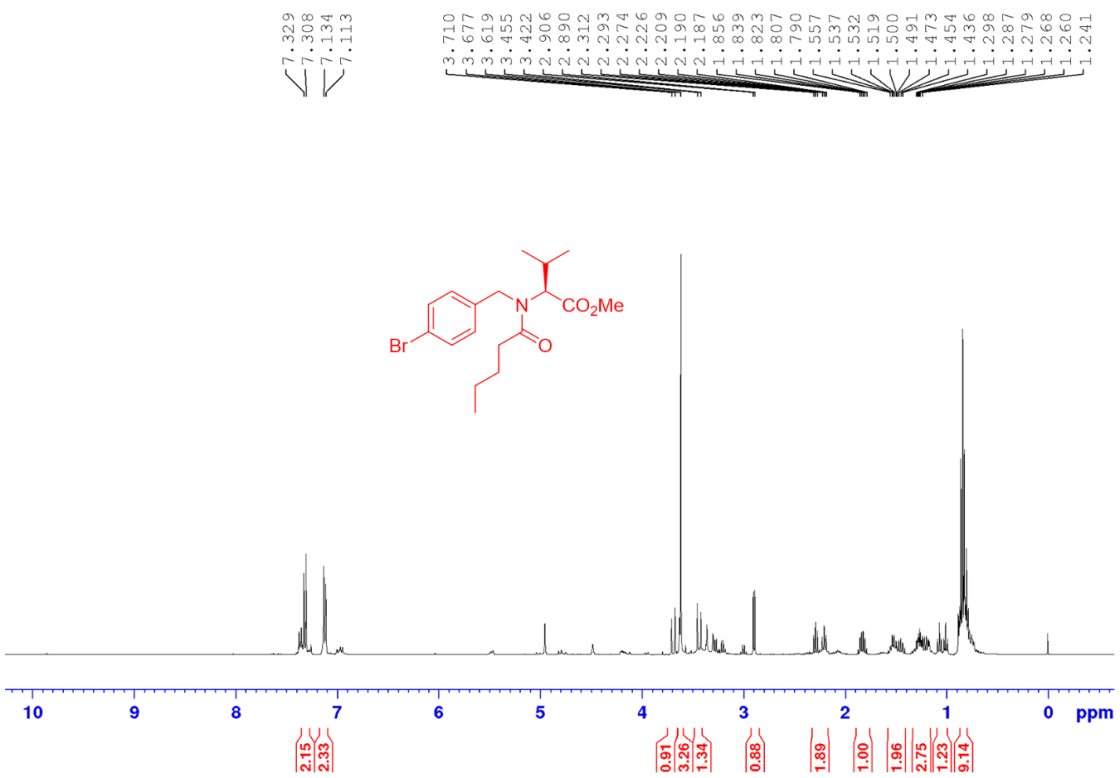


**Figure 2.12:** $^{1}$H NMR spectrum for methyl *N*-(4-bromobenzyl)-*N*-pentanoyl-*D*-valinate **(37)**.

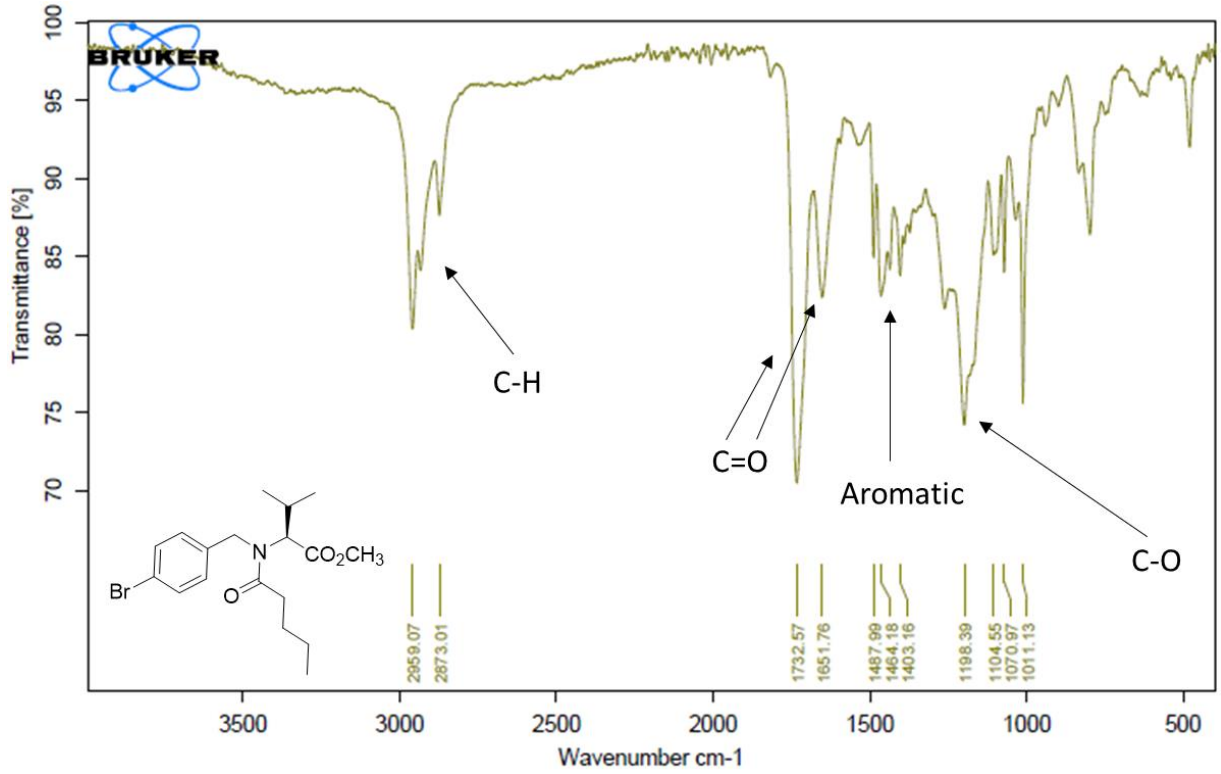


**Figure 2.13:** IR spectrum for methyl *N*-(4-bromobenzyl)-*N*-pentanoyl-*D*-valinate **(37)**.

### 2.3.3 The synthesis of methyl ((2'-cyano-[1, 1'-biphenyl]-4-yl)methyl)-*L*-valinate (34)

Retrosynthesis showed two possible routes that could lead to the synthesis of valsartan **(27)**. Compound **38** can also undergo Suzuki-Miyaura cross-coupling before acylation. **Scheme 2.10** shows the successful cross-coupling of 2-cyanophenylboronic acid **(36)** with methyl (4-bromobenzyl)-*D*-valinate **(38)** producing methyl ((2'-cyano-[1, 1'-biphenyl]-4-yl)methyl)-*L*-valinate **(34)** as a colourless liquid in 26% yield.

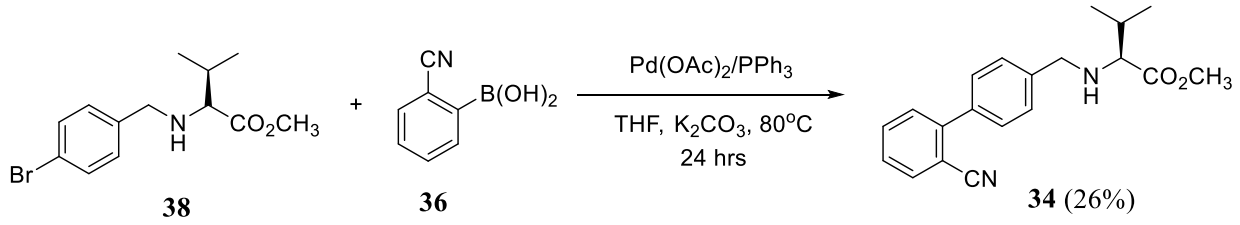


**Scheme 2.10**: The Suzuki-Miyaura cross-coupling reaction to produce a compound **(34)**.

The successful synthesis of methyl ((2'-cyano-[1, 1'-biphenyl]-4-yl) methyl)-*L*-valinate **(34)** was confirmed using spectroscopic techniques. $^{1}$H NMR spectrum had signals integrating for eight protons in the downfield region between 7.39-7.75 ppm indicating the successful carbon-carbon bond formation of biaryl moiety. The alkyl wing of the structure was still connected to the structure since all the signals' integration corresponded with all the protons in the structure **(Figure 3.14)**. $^{13}$C NMR spectrum in **Figure 3.15** had the number of signals corresponding to the number of carbons in the structure. The peak at 118.6 ppm corresponds to the nitrile functional group and the peak at 175.7 ppm corresponds to the carbonyl ester functional group [145].

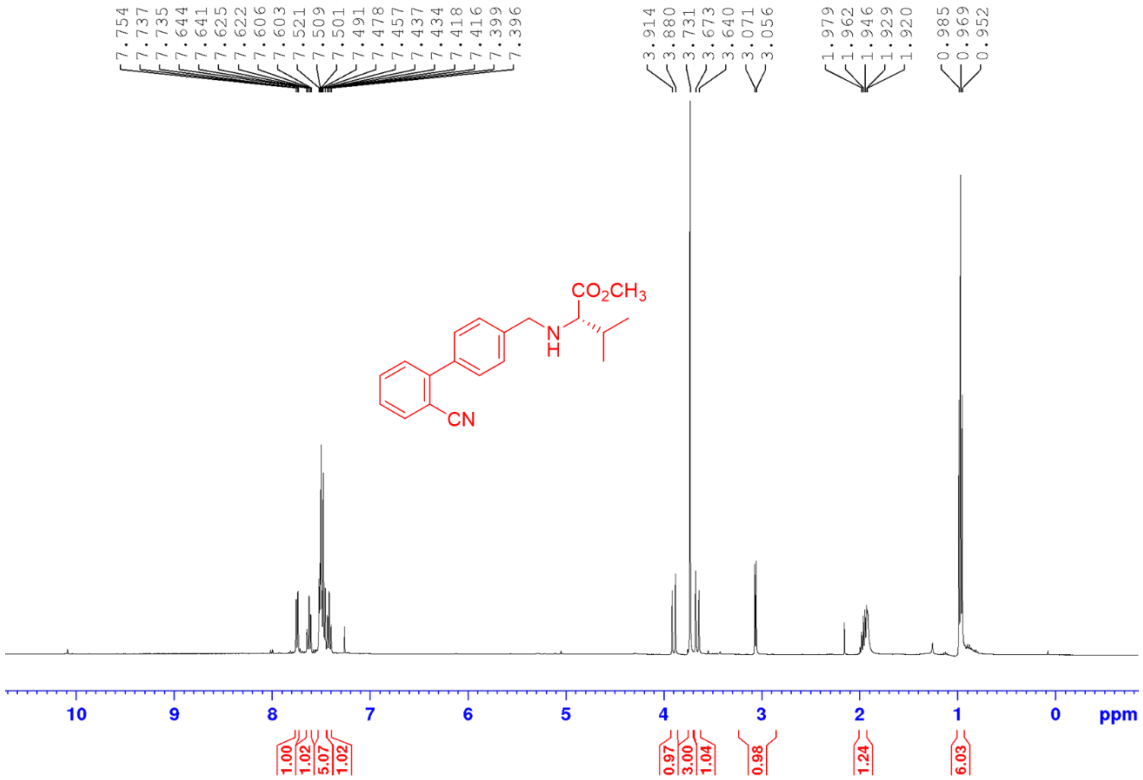


**Figure 2.14**: $^{1}$H NMR for methyl ((2'-cyano-[1, 1'-biphenyl]-4-yl)methyl)-*L*-valinate **(34)**.

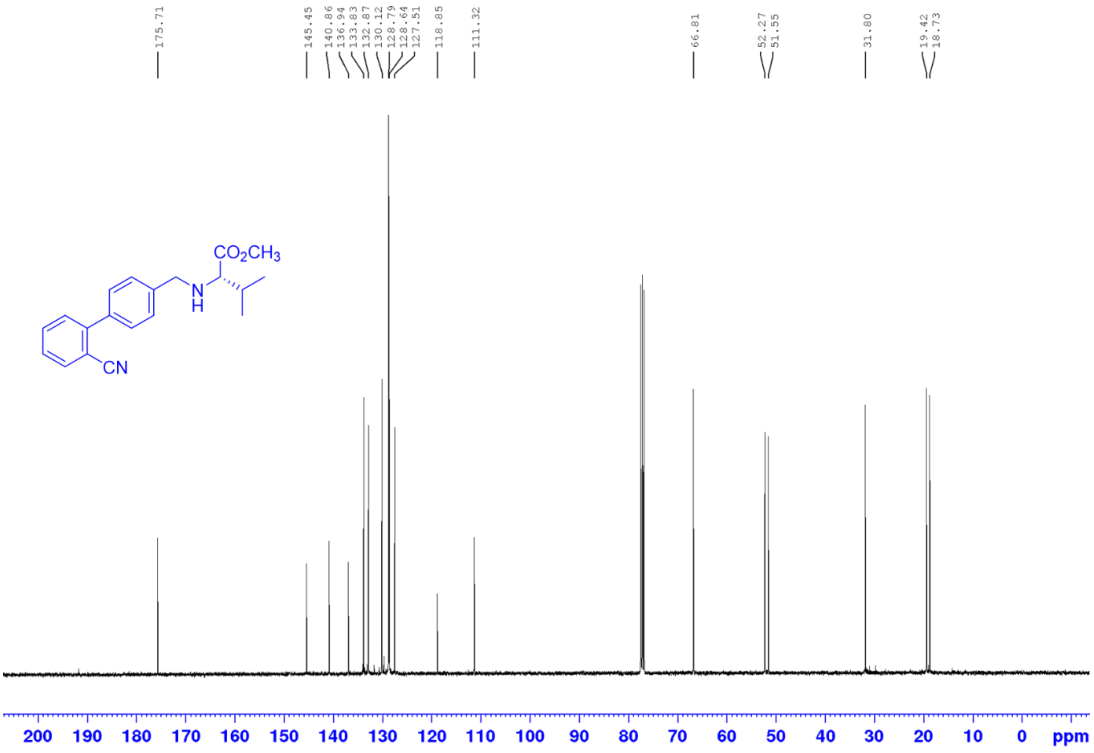


**Figure 2.15**: $^{13}$C NMR for methyl ((2'-cyano-[1, 1'-biphenyl]-4-yl)methyl)-*L*-valinate **(34)**.

### 2.3.4 The synthesis of methyl *N*-((2'-cyano-[1, 1'-biphenyl]-4-yl)methyl-*N*-pentanoyl-*L*-valinate (32)

The cross-coupling reaction of 2-cyanophenylboronic acid **(36)** and methyl *N*-(4-bromobenzyl)-*N*-pentanoyl-*D*-valinate **(37)** afforded methyl *N*-((2'-cyano-[1, 1'-biphenyl]-4-yl)methyl-*N*-pentanoyl-*L*-valinate **(32)** as a yellow liquid in 11% yield after 24 hours **(Scheme 2.11)**. The low yield was attributed by the side reactions including the homo-coupling of 2-cyanophenyl boronic acid **(36)** to produce compound **(55)** and the Suzuki-Miyaura cross-coupling reaction of methyl (4-bromobenzyl)-*D*-valinate **(38)** with 2-cyanophenyl boronic acid **(36)**. This indicates that the acylation reaction did not go to completion perhaps because the pentanoyl chloride **(35)** could have been hydrolysed. The challenge with the isolation of the acylated product was its close polarity with the starting material methyl *N*-(4-bromobenzyl)-*N*-pentanoyl-*D*-valinate **(37)** which led to almost equal $R_f$ values, therefore, making it difficult to purify using a column chromatographic technique.

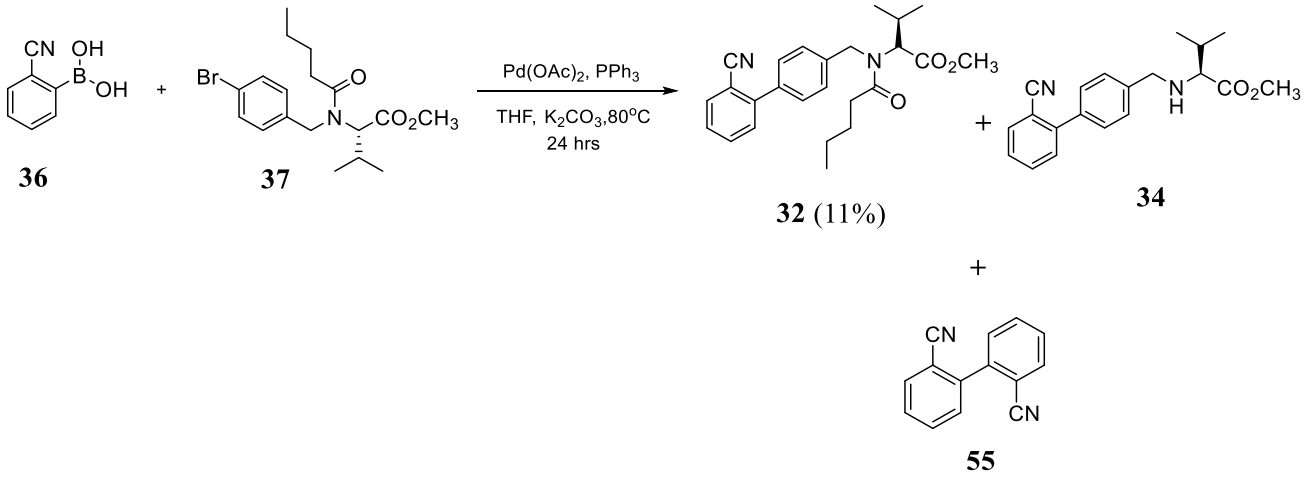


**36** **37** **32** (11%) **34** **55**

**Scheme 2.11**: The Suzuki-Miyaura cross-coupling reaction to produce compound **(32)**.

The acylation reaction of methyl ((2'-cyano-[1, 1'-biphenyl]-4-yl)methyl)-*L*-valinate **(34)** with valeroyl chloride **(35)** has afforded compound **32** in 86% yields as a yellow liquid after purification using column chromatographic technique **(Scheme 2.12)**.

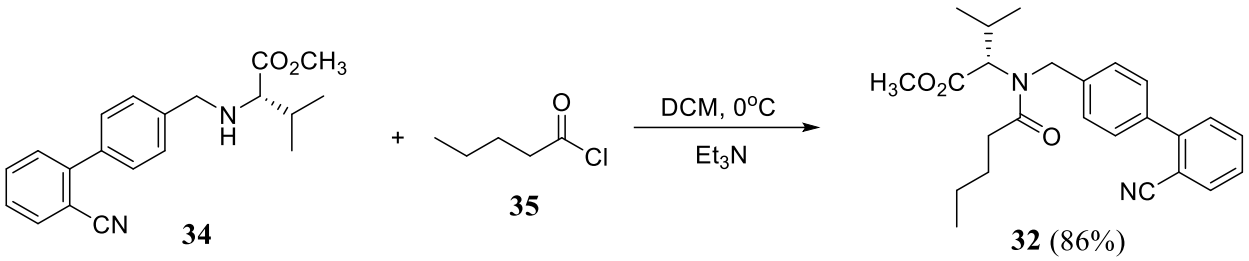


**Scheme 2.12**: Acylation reaction of compound **(32)**.

The appearance of the nitrile group stretching frequency at 2224 $cm^{-1}$, in an IR spectrum, as well as the presence of two carbonyl stretching frequencies at 1642 $cm^{-1}$ and 1735 $cm^{-1}$ confirmed the successful synthesis of methyl *N*-((2'-cyano-[1, 1'-biphenyl]-4-yl)methyl-*N*-pentanoyl-*L*-valinate **(32) (Figure 2.16)**.

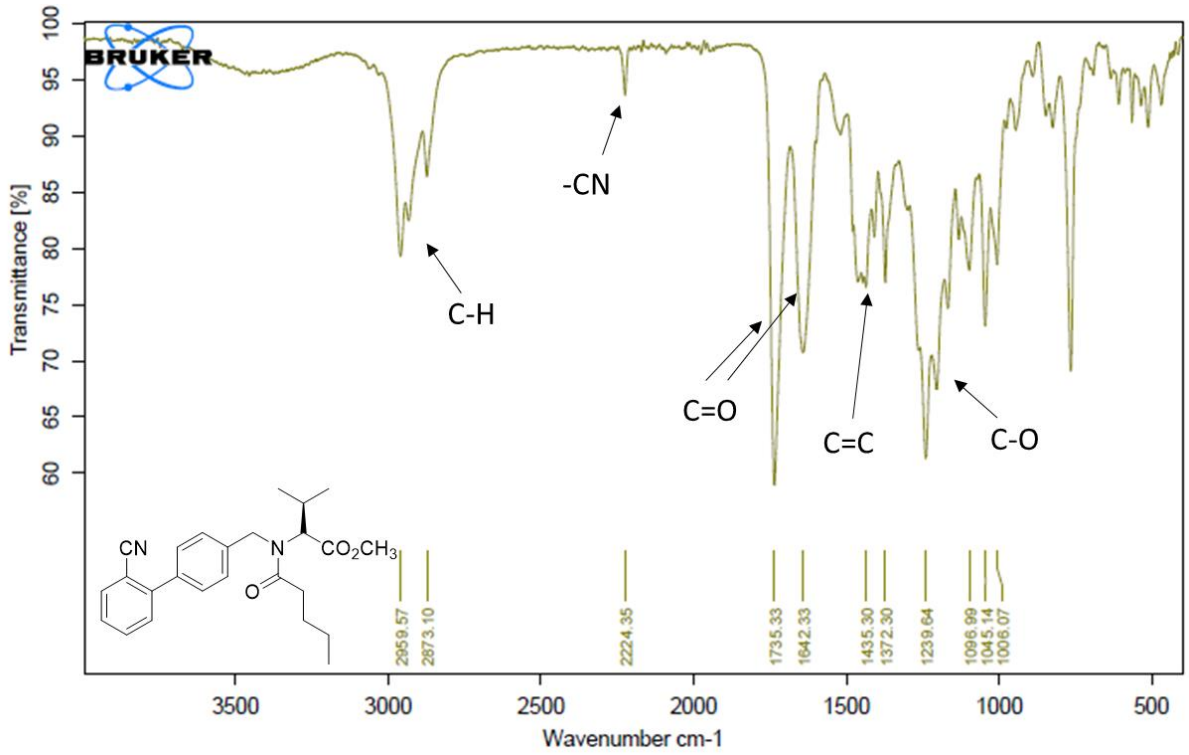


**Figure 2. 16**: $^{1}H$ NMR spectrum for methyl *N*-((2'-cyano-[1, 1'-biphenyl]-4-yl)methyl-*N*-pentanoyl-*L*-valinate **(32)**.

Methyl *N*-((2'-cyano-[1, 1'-biphenyl]-4-yl)methyl-*N*-pentanoyl-*L*-valinate **(32)** was the key intermediate for the synthesis of valsartan **(27)**. The $^{1}H$ NMR spectrum of the two routes showed the expected peaks corresponding with the structure **(Figure 2.17)**. $^{13}C$ NMR spectrum for **Route**

**A** was clean and had all the expected peaks especially the highlighted peaks indicate the terminal methyl group at 13.8 ppm, the methoxy peak at 51.8 ppm and the nitrile peak at 118.7 ppm indicating the successful acylation reaction **Scheme 2.12 (Figure 2.18)** [144].

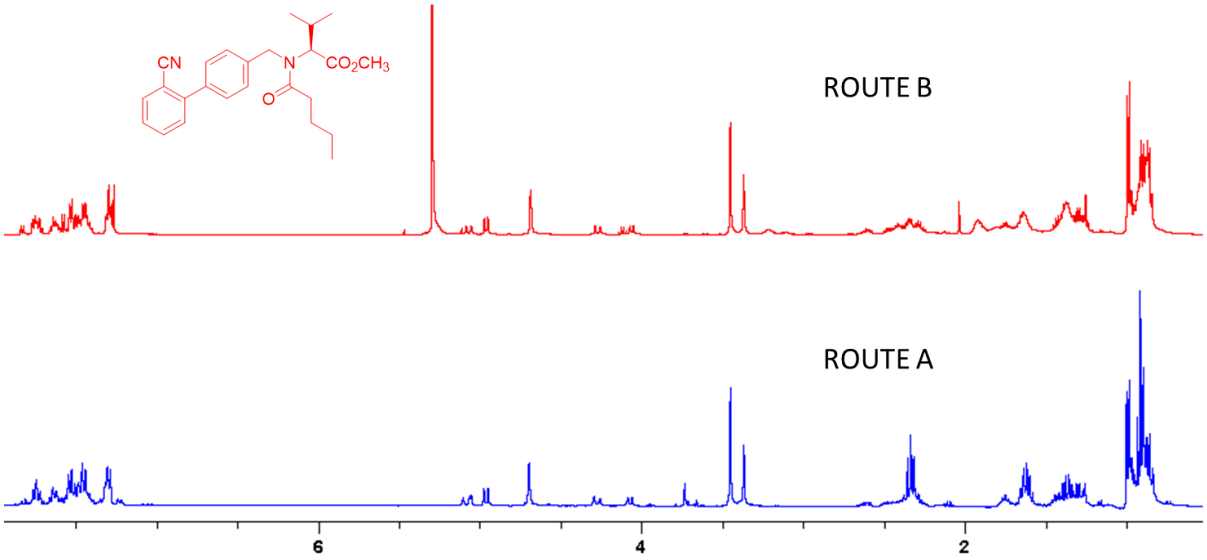


**Figure 2.17**: Comparative $^{1}$H NMR spectrum for methyl *N*-((2'-cyano-[1, 1'-biphenyl]-4-yl)methyl-*N*-pentanoyl-*L*-valinate **(32)** following **Route B** (top) with impurities from the side reaction and the cleaner spectrum (bottom) following **Route A**.

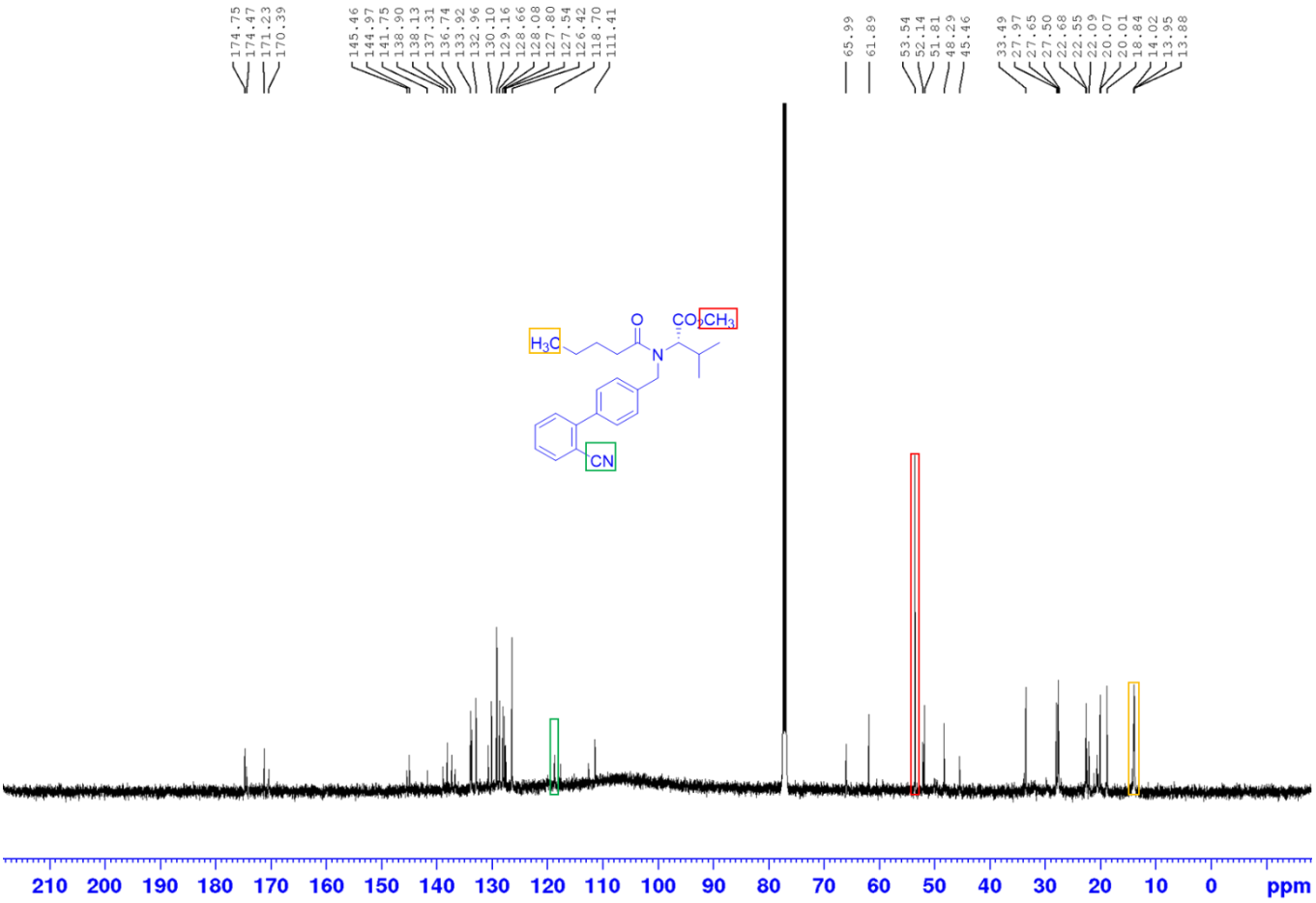


**Figure 2.18:** $^{13}C$ NMR spectrum for methyl *N*-((2'-cyano-[1, 1'-biphenyl]-4-yl)methyl-*N*-pentanoyl-*L*-valinate **(32)** showing the presence of the terminal peak at 13.8 ppm, the methoxy peak at 51.8 ppm and the nitrile peak at 118.7 ppm.

### 2.3.5 The synthesis of methyl *N*-((2'-(1*H*-tetrazol-5-yl)-[1, 1'-biphenyl]-4-yl)methyl)-*N*-pentanoyl-*D*-valinate (31)

[3 + 2] Cycloaddition reaction of nitrile to afford tetrazole scaffold has shown to be a useful method since tetrazoles are widely used in medicinal chemistry as bioisosters of carboxylic acids. Having successfully synthesise compound **(30)**, the next step was the transformation of a nitrile to a tetrazole. The cyclisation reaction of methyl *N*-((2'-cyano-[1, 1'-biphenyl]-4-yl)methyl-*N*-pentanoyl-*L*-valinate **(32)** with sodium azide **(33)** afforded the desired product **(31)** with 90% yield as a yellow liquid **(Scheme 2.13)**.

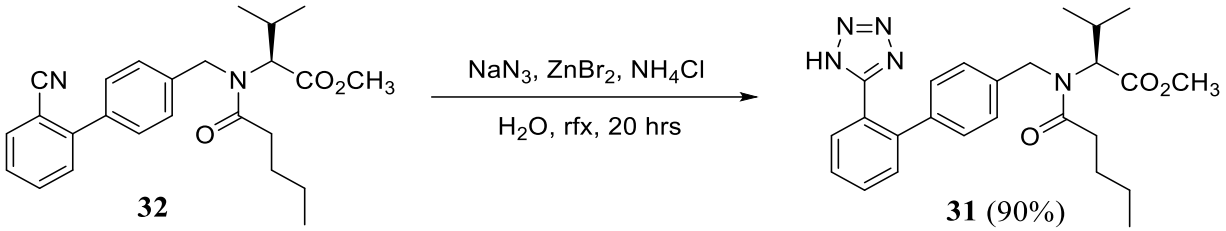


**Scheme 2.13**: Cyclisation of tetrazole reaction.

The $^{1}H$ NMR and $^{13}C$ NMR spectroscopic techniques were consistent with the structure of the desired product **(31) (Appendix A1.4)**. The IR spectrum indicate the disappearance of the nitrile peak at 2224.35 $cm^{-1}$ as it undergoes cycloaddition with sodium azide **(33)** to produce the tetrazole ring **(Figure 2.19)** [144].

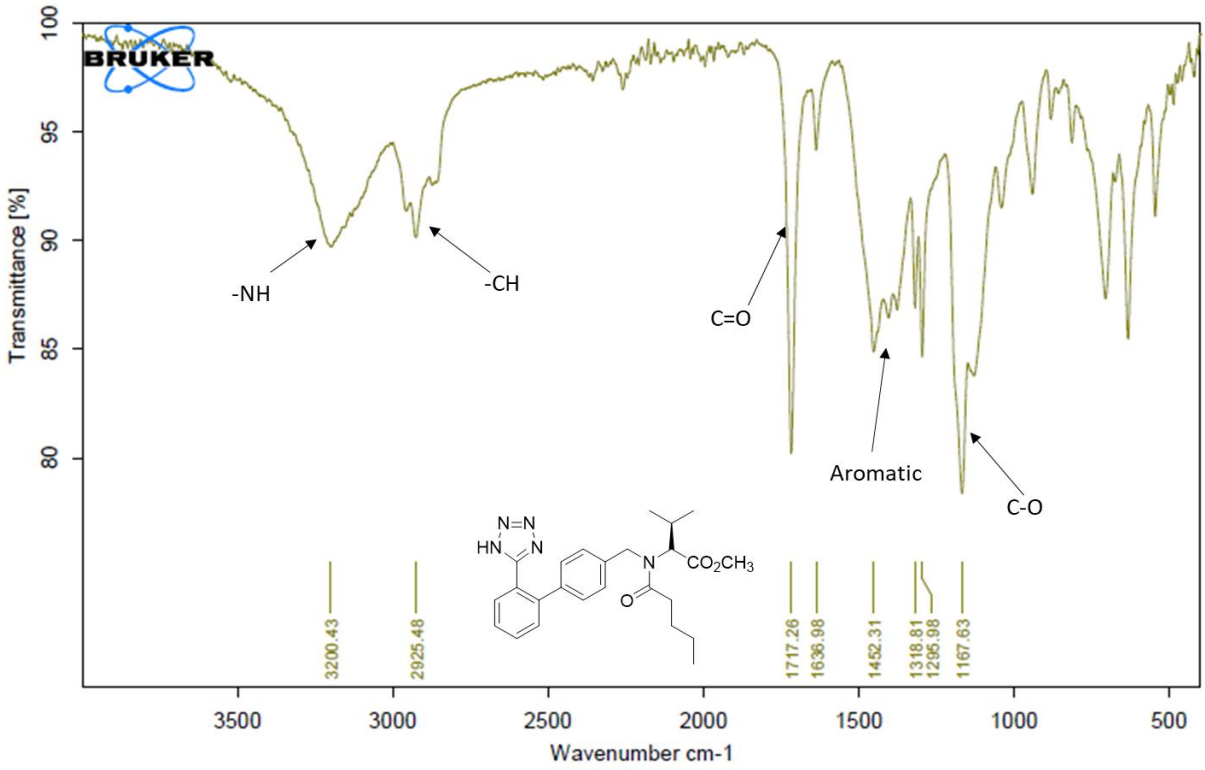


**Figure 2.19:** IR spectrum for methyl *N*-((2'-(1*H*-tetrazol-5-yl)-[1, 1'-biphenyl]-4-yl)methyl)-*N*-pentanoyl-*D*-valinate **(31)** that proves the successful cyclisation the tetrazole by the absence of the nitrile peak around 2224 $cm^{-1}$ and the appearance of the NH peak at 3415 $cm^{-1}$ of the tetrazole.

### 2.3.6 The synthesis of *N*-((2'-(1*H*-tetrazol-5-yl)-[1, 1'-biphenyl]-4-yl)-*N*-pentanoyl-*L*-valine (Valsartan) (27)

The hydrolysis of methyl *N*-((2'-(1*H*-tetrazol-5-yl)-[1, 1'-biphenyl]-4-yl)methyl)-*N*-pentanoyl-*D*-valinate **(31)** to produce *N*-((2'-(1*H*-tetrazol-5-yl)-[1, 1'-biphenyl]-4-yl)-*N*-pentanoyl-*L*-valine **(27)** was a success yielding the expected carboxylic acid derivative with 95% yield as a yellow solid **(Scheme 2.14)**.

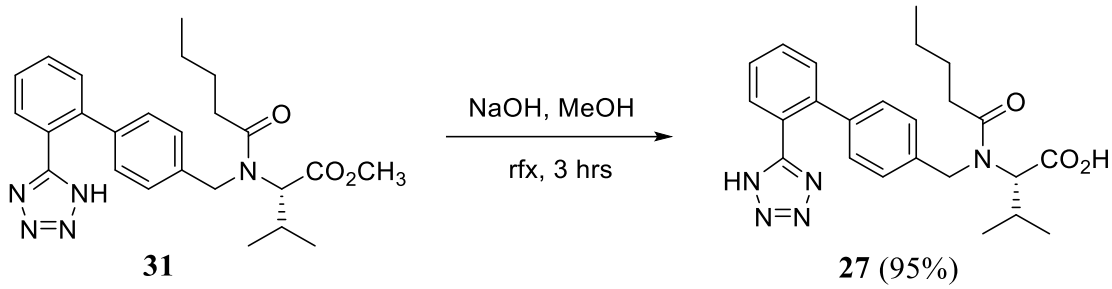


**Scheme 2.14**: Base catalysed hydrolysis of ester.

The successful synthesis of valsartan **(27)** was confirmed with HRMS showing the expected base peak at 434.2191 in the negative mode ($M^+ - H^+$) corresponding with the calculated molar mass of 434.2148 **(Figure 2.20)**. The disappearance of a singlet methoxy peak around 3.5 ppm on the $^1$H NMR spectrum of the desired carboxylic acid product **27** compared to the proton $^1$H NMR of valsartan ester **(31)** was evidence of a successful hydrolysis **(Figure 2.21)** [144].

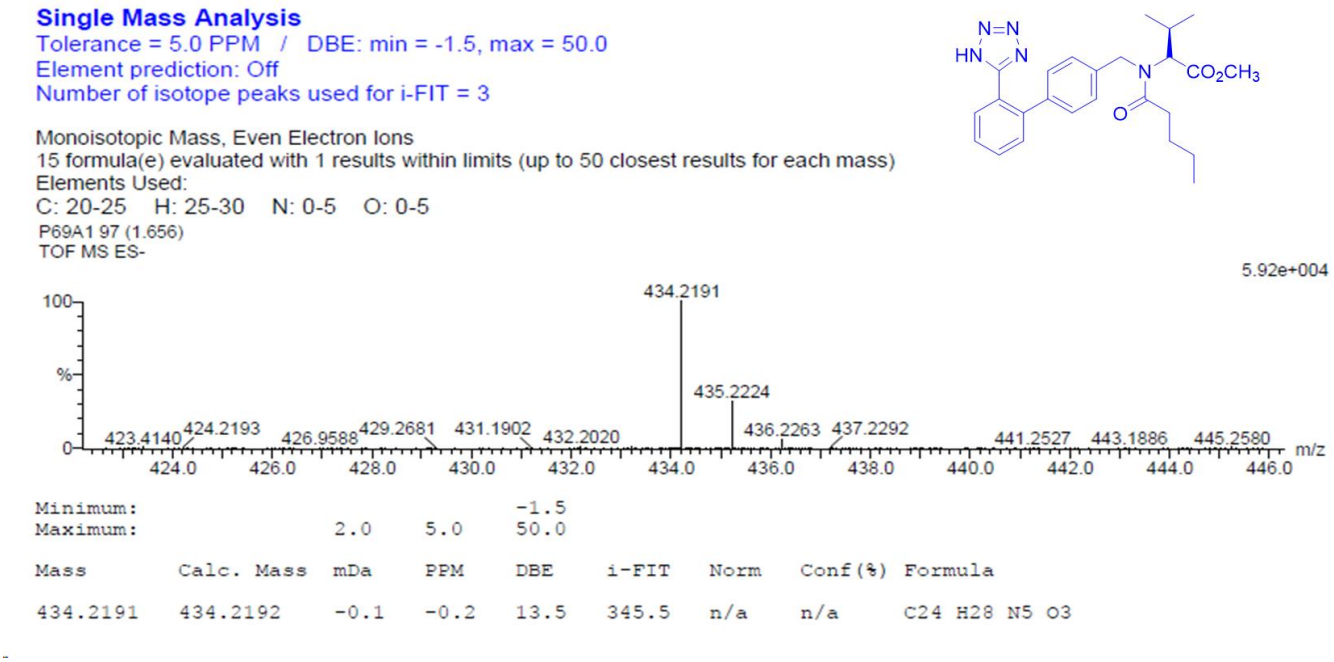


**Figure 2.20**: HRMS for valsartan **(27)** with the expected base peak at the negative mode.

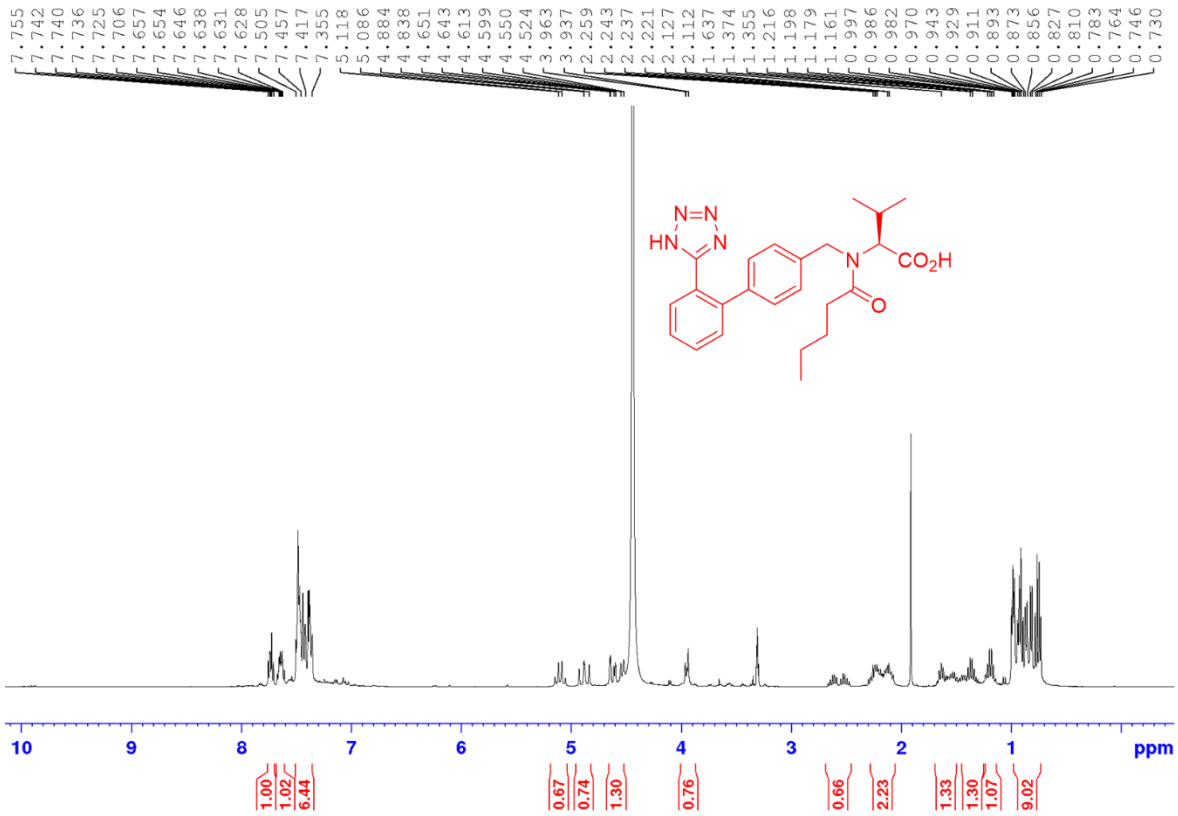


**Figure 2.21**: $^{1}$H NMR spectrum for valsartan **(27)** suggest the successful hydrolysis of the valsartan ester **(31)**.

## 2.4 Valsartan Derivatives

Having successful synthesised valsartan **(27)**, our next focus was to apply the synthetic knowledge we gathered from the previous section to the preparation of valsartan derivatives. In the synthesis of valsartan, we have learned that the sequence between cyclisation and the C-C bond forming is crucial. We have realised that starting with Suzuki-Miyaura cross-coupling reaction followed by the cyclisation reaction has some advantages such as high yields, cleaner product, easy purification, and fewer steps.

Reviewing the synthetic methods followed, the biphenyl backbone moiety optimised procedure was able to accommodate a sensitive amine functional group and the substituted phenylboronic acid. Therefore, this indicates that this method could accommodate a wide range of functional groups under mild reaction conditions. The developed method for the synthesis of valsartan **(27)** displayed high efficacy and would be industrial viable following **Route A** with low impurities and the use of environmentally friendly solvent, water for the [3 + 2] cycloaddition reaction.

The cross-coupling reaction was conducted between synthesised 2-iodobenzonitrile and different commercially available substituted phenylboronic acids.

### 2.4.1 The synthesis of [1, 1'-biphenyl]-2-carbonitrile (53)

The cross-coupling reaction of 2-iodobenzonitrile **(47)** with phenylboronic acid **(52)** afforded [1, 1'-biphenyl]-2-carbonitrile **(53)** successfully in 86% yield as a white solid **(Scheme 2.15) (Table 2, entry 1)**.

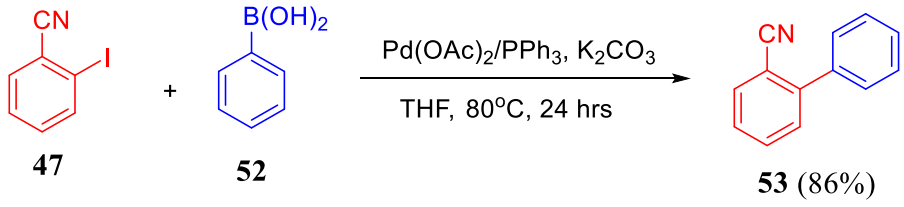


**47** **52** **53** (86%)

**Scheme 2.15:** Synthesis of compound **(53)**.

The successful preparation titled compound **(53)** was confirmed using $^{1}$H NMR and $^{13}$C NMR spectra that correspond to the structure. All signals resonate downfield between the aromatic region range and the integration counts for all nine protons present in the structure **(Figure 2.22)**. The number of signals on $^{13}$C NMR corresponded to the number of carbons in the structure **(Figure 2.23)** [146].

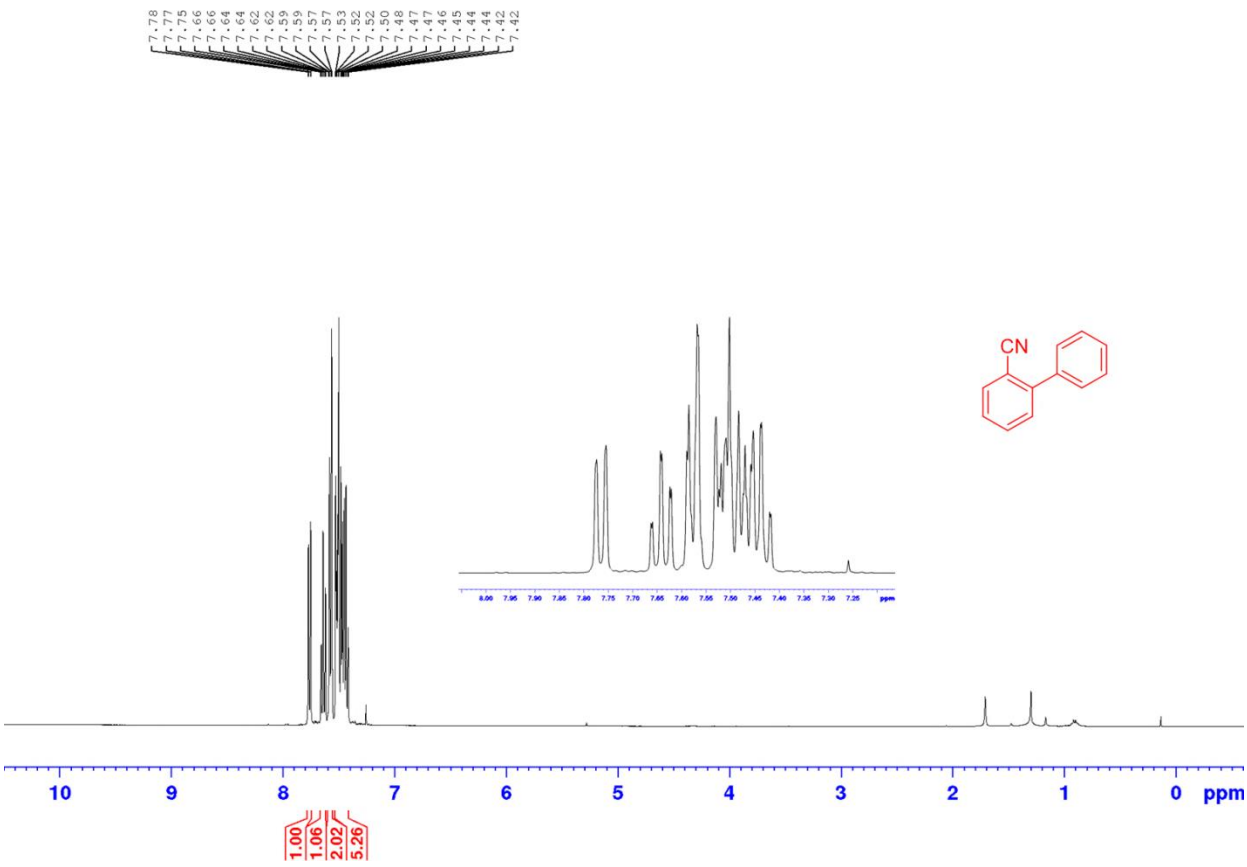


**Figure 2.22:** $^{1}$H NMR spectrum for [1, 1'-biphenyl]-2-carbonitrile **(53)**.

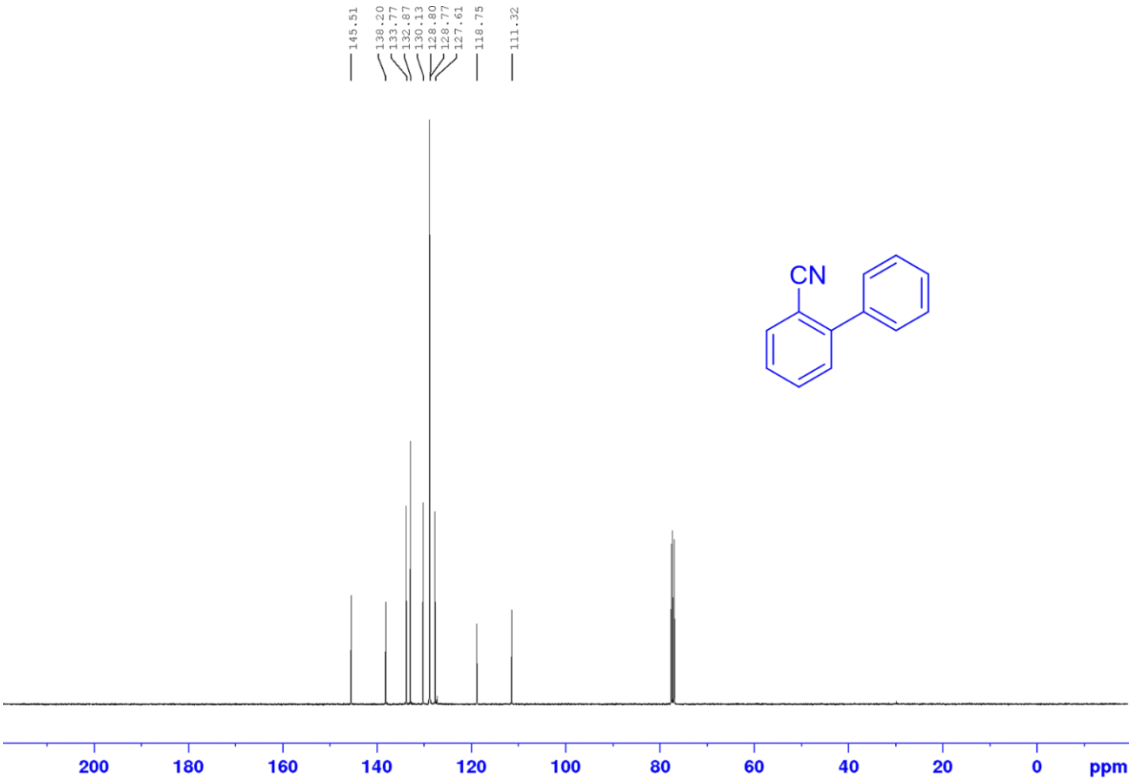


**Figure 2.23:** $^{13}$C NMR spectrum for [1, 1'-biphenyl]-2-carbonitrile **(53)**.

### 2.4.2 The synthesis of 4'-(trifluoromethyl)-[1, 1'-biphenyl]-2-carbonitrile (57)

(4-(Trifluoromethyl)phenyl)boronic acid **(56)** was reacted with 2-iodobenzonitrile **(47)** to afford the titled compound **(57)** in a yield of 65% **(Scheme 2.16)**.

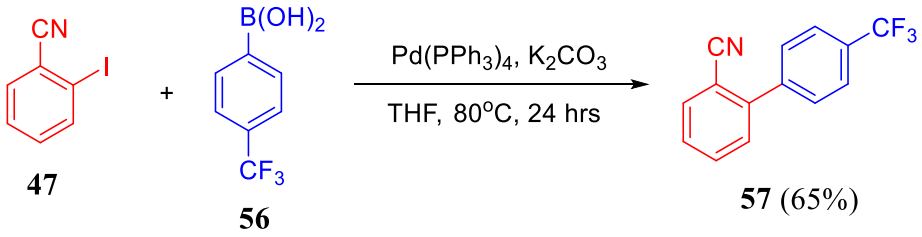


**Scheme 2.16:** Synthesis of compound **(57)**.

The obtained product **(57)** was afforded as a white solid and $^{1}$H NMR and $^{13}$C NMR spectra were in good agreement with the structure **(Figure 2.24 & 2.25)** [147].

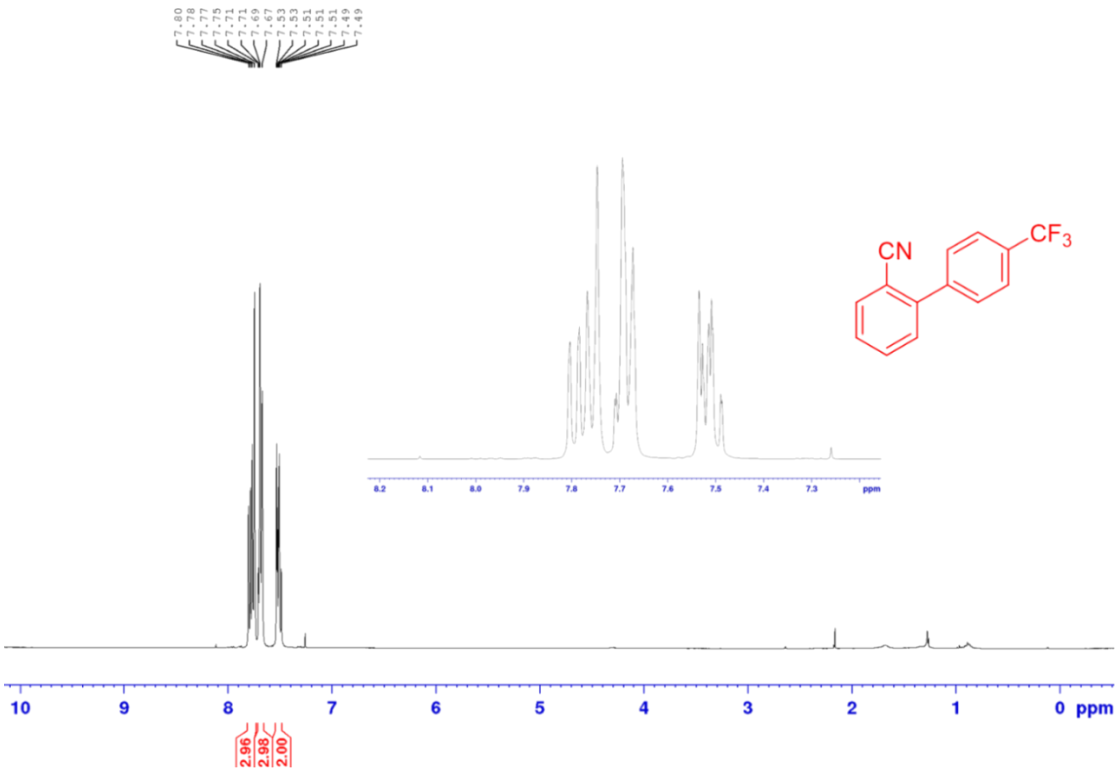


**Figure 2.24:** $^{1}$H NMR spectrum for 4'-(trifluoromethyl)-[1, 1'-biphenyl]-2-cabonitrile **(57)**.

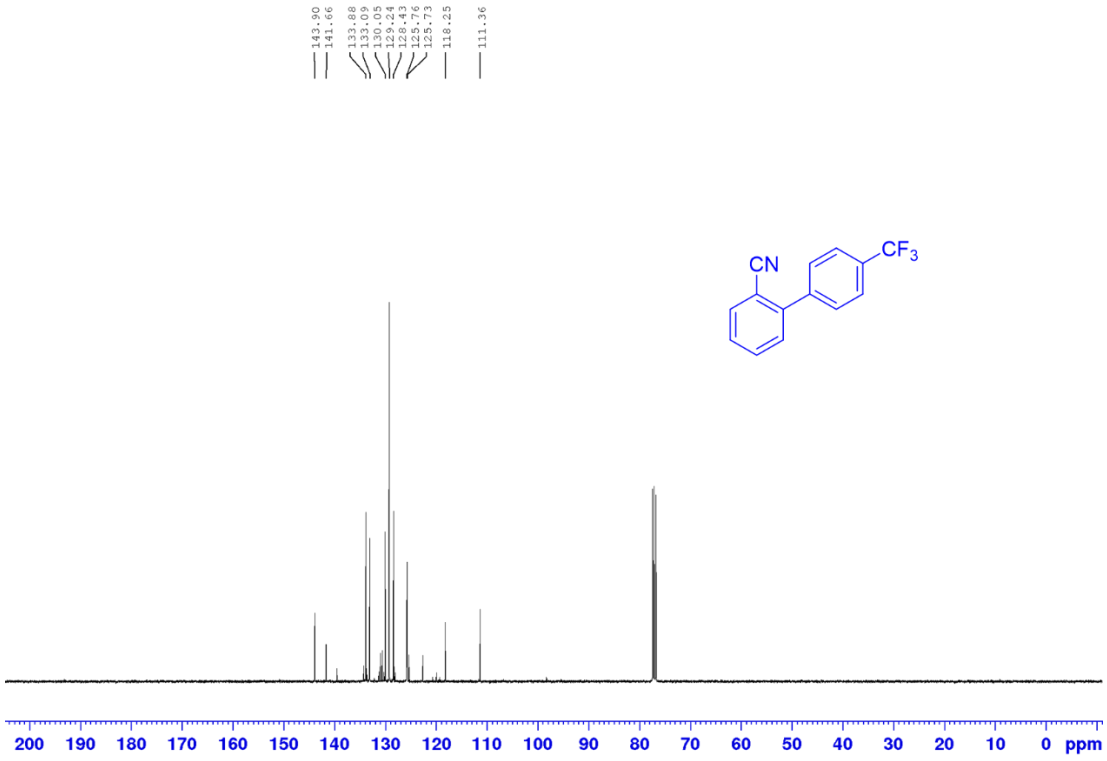


**Figure 2.25:** $^{13}$C NMR spectrum for 4'-(trifluoromethyl)-[1, 1'-biphenyl]-2-cabonitrile **(57)**.

**Table 2.2**: Suzuki-Miyaura cross-coupling of 2-iodobenzonitrile **(45)** with aryl boronic acids [c].

| Entry | Benzonitrile | Boronic acid | Product | Yield (%) |
|---|---|---|---|---|
| 1 | 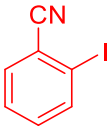 **47** | 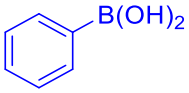 **52** | 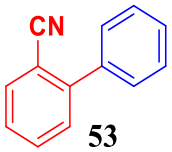 **53** | 86[a] |
| 2 | 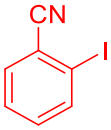 **47** | 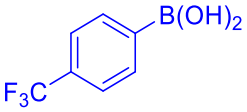 **56** | 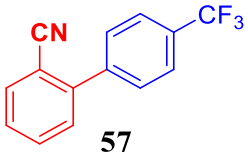 **57** | 65[b] |
| 3 | 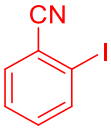 **47** | 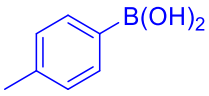 **58** | 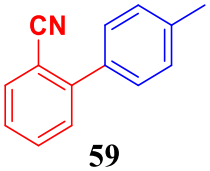 **59** | 81[a] |
| 4 | 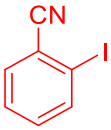 **47** | 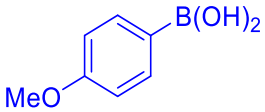 **60** | 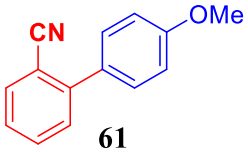 **61** | 28[b] |
| 5 | 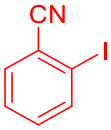 **47** | 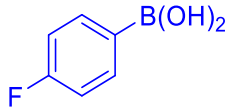 **62** | 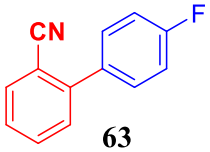 **63** | 73[b] |
| 6 | 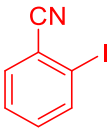 **47** | 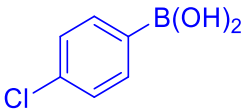 **64** | 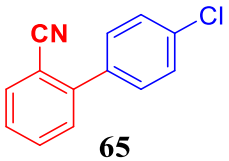 **65** | 44[a] |
| 7 | 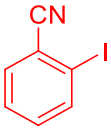 **47** | 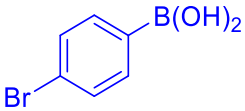 **66** | 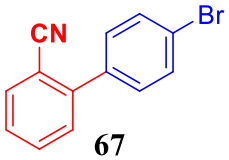 **67** | 79[a] |

[a]Reaction conditions: 2-iodobenzonitrile (1 eq), nucleophile (1.2 eq), $Pd(OAc)_2$ (5 mol%), $PPh_3$ (10 mol%), $K_2CO_3$ (3eq), THF (10 mL). [b]Reaction conditions: 2-iodobenzonitrile (1 eq), nucleophile (1.2 eq), $Pd(PPh_3)_4$ (5 mol%), $K_2CO_3$ (3eq), toluene (10 mL),

water (1 mL). [c]All reactions were conducted for 24 hours under an argon or nitrogen atmosphere at 80°C. All yields were isolated using flash column chromatography.

### 2.4.3 The synthesis of 2-([1, 1'-biphenyl]-2-yl)acetonitrile (65)

Part of our work was to investigate the influence of the addition of the benzylic carbon between the phenyl and the nitrile functional group. For this reason, we opted to synthesise benzylated biphenyl from the coupling reaction of 2-bromophenylacetonitrile and different substituted phenyl boronic acids. The cross-coupling reaction of compound **(68)** and phenyl boronic acid **(52)** furnished 2-([1, 1'-biphenyl]-2-yl)acetonitrile **(69)** in moderate 74% yield in 24 hours **(Scheme 2.17)**.

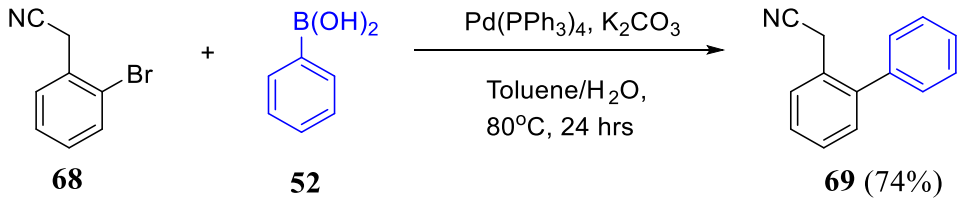


**Scheme 2.17:** Synthesis of compound **(69)**.

The formation of the desired coupled product was confirmed using spectroscopic techniques that were consistent with the structure **(69).** $^{1}$H NMR spectrum has proton peaks which integrate eight protons in the aromatic region and two protons upfield for alkyl protons in the structure **(Figure 2.26)**. The $^{13}$C NMR spectrum has the number of signals equal to the number of non-equivalent carbons in the structure **(Figure 2.27)** [148].

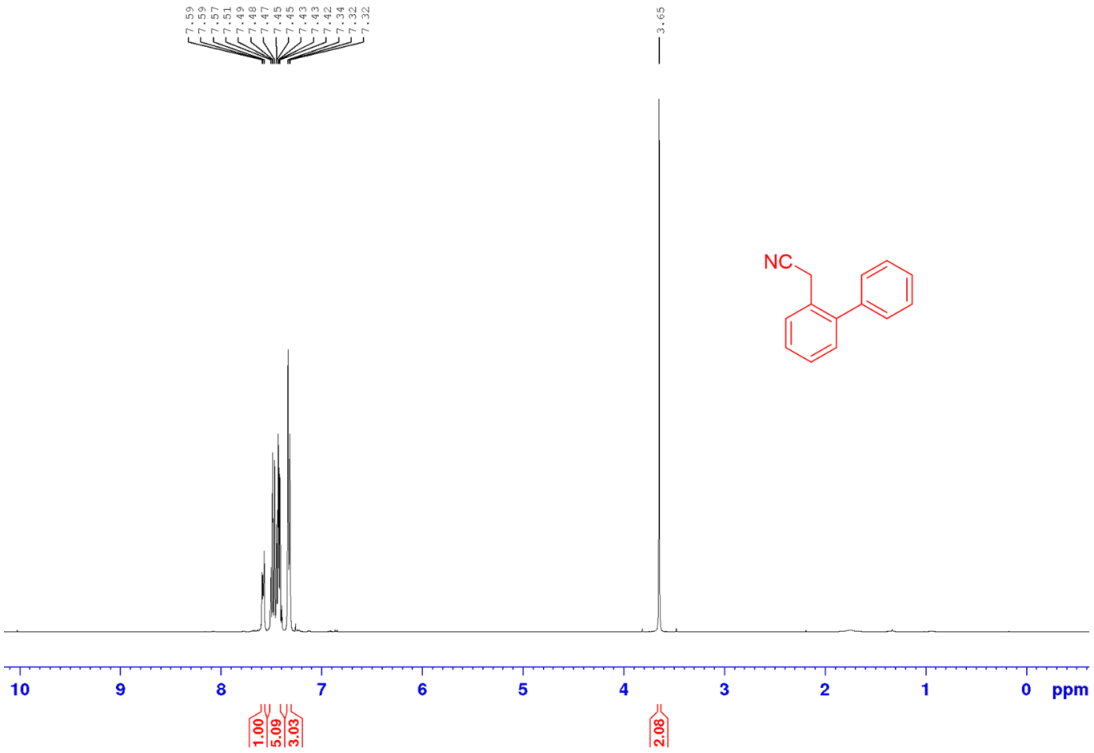


**Figure 2.26:** $^{1}$H NMR spectrum for 2-([1, 1'-biphenyl]-2-yl)acetonitrile **(69)**.

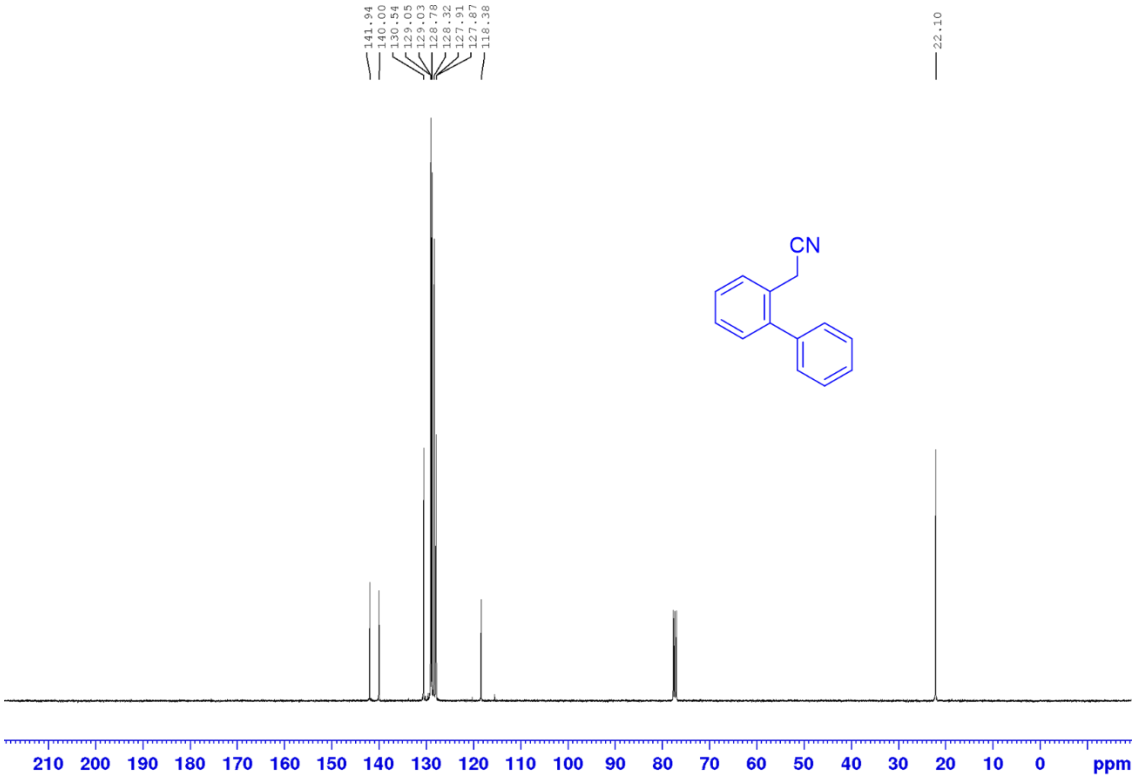


**Figure 2.27:** $^{13}$C NMR spectrum for 2-([1, 1'-biphenyl]-2-yl)acetonitrile **(69)**.

### 2.4.4 The synthesis of 2-(4'-methoxy-[1, 1'-biphenyl]-2-yl)acetonitrile (70)

The preparation of 2-(4'-methoxy-[1, 1'-biphenyl]-2-yl)acetonitrile **(70)** was successfully achieved through the cross-coupling reaction of 2-bromophenylacetonitrile **(68)** with 4-methoxyphenylboronic acid **(60)** following the optimised reaction condition **(Scheme 2.18)**. The desired product **(70)** was produced as a yellow liquid with an excellent yield of 96% in 24 hours.

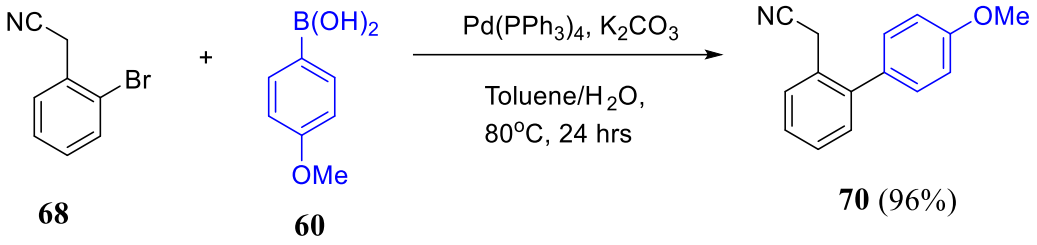


**Scheme 2.18:** Synthesis of compound **(70)**.

The purity and the structure of the product **(70)** were confirmed using $^{1}H$ NMR and $^{13}C$ NMR spectra. The $^{1}H$ NMR spectrum showed two different singlets, one resonating at 3.46 ppm integrating to two protons indicating a methylene proton, and the other singlet resonating at 3.87 ppm integrating to three protons indicating a methoxy group. The other signals resonating between 7.00-7.56 ppm indicates the protons in the aromatic rings and their integration correspond to the number of protons in the structure **(Figure 2.28)**. The $^{13}C$ NMR spectrum also showed the expected number of signals that correspond to the structure, especially the methylene, methoxy, and nitrile signals resonating at 22.1, 55.4, and 118.4 ppm, respectively **(Figure 2.29)**.

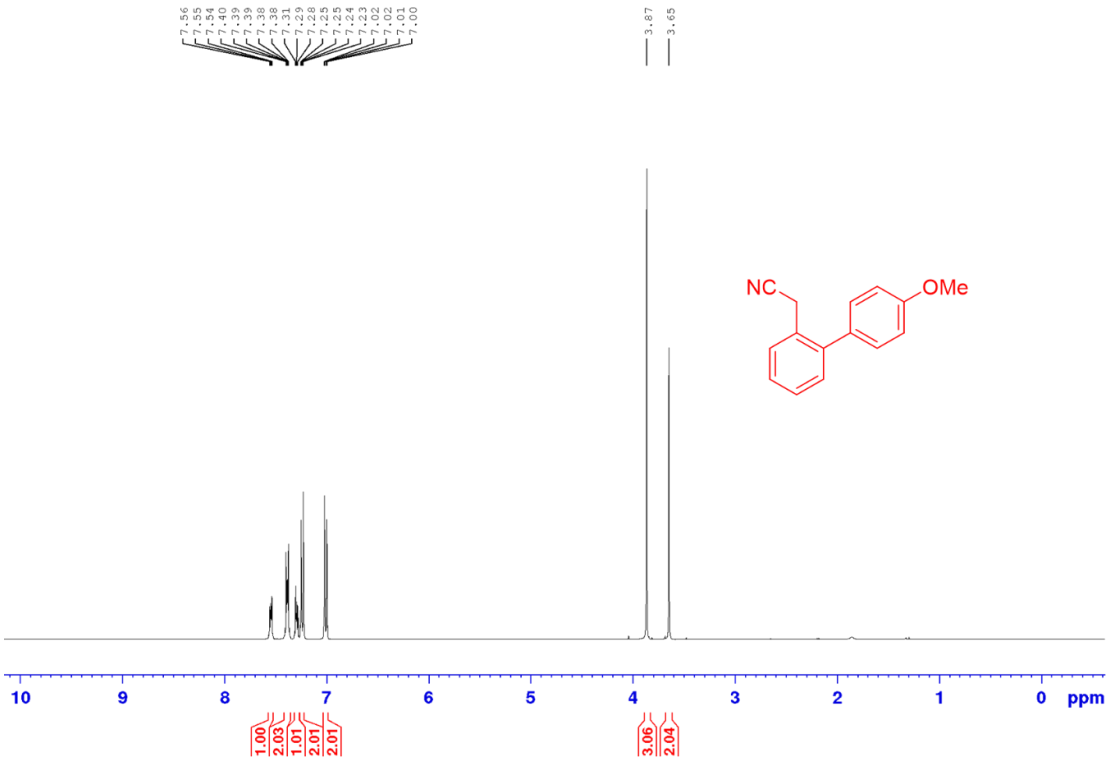


**Figure 2.28:** $^{1}$H NMR spectrum for 2-(4'-methoxy-[1, 1'-biphenyl]-2-yl)acetonitrile **(70)**.

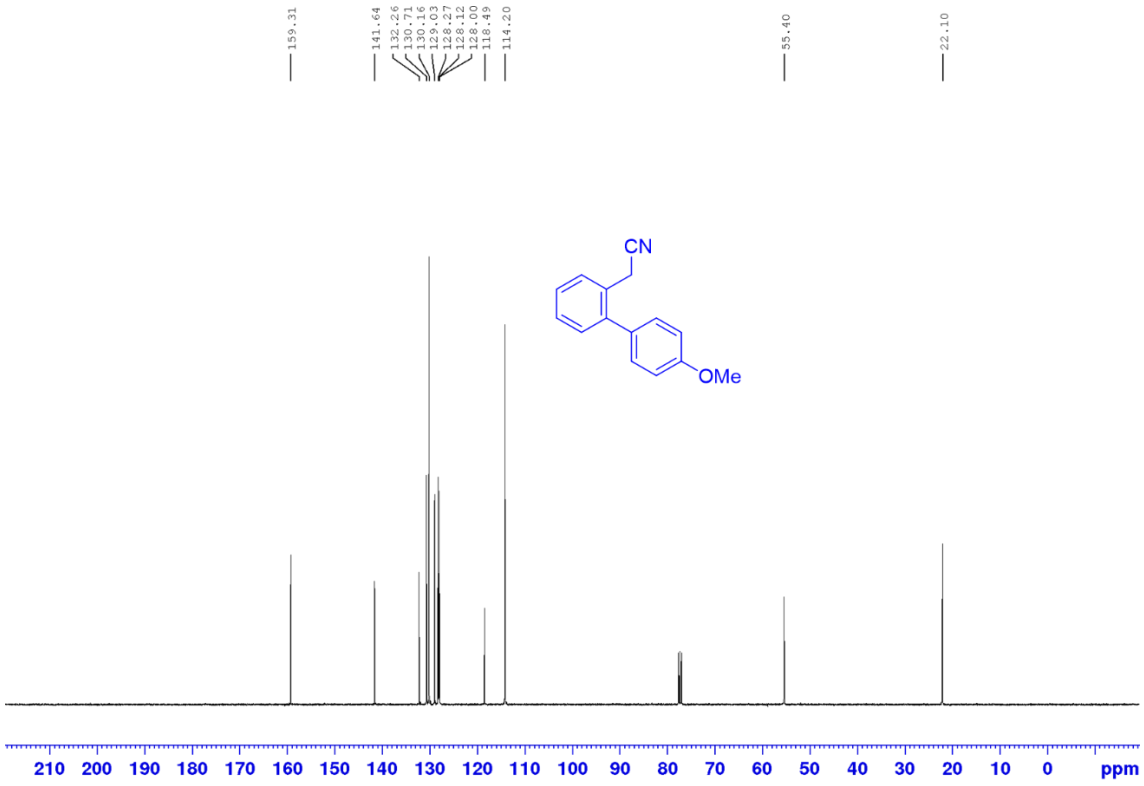


**Figure 2.29:** $^{13}$C NMR spectrum for 2-(4'-methoxy-[1, 1'-biphenyl]-2-yl)acetonitrile **(70)**.

**Table 2.3**: Suzuki cross-coupling of 2-bromophenylacetonitrile **(68)** with arylboronic acids [a]

| Entry | Benzyl nitrile | Boronic acid | Product | Yield (%) |
|---|---|---|---|---|
| 1 | 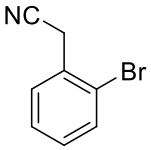 **68** | 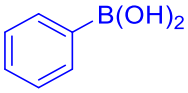 **52** | 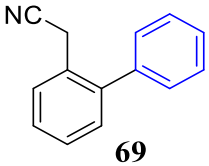 **69** | 74 |
| 2 | 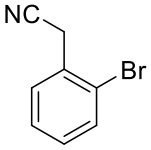 **68** | 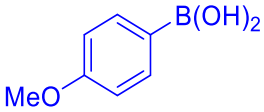 **60** | 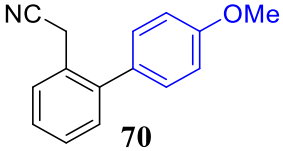 **70** | 92 |
| 3 | 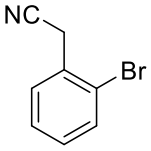 **68** | 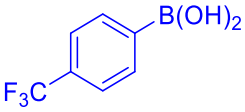 **56** | 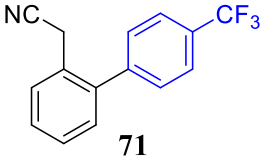 **71** | 64 |
| 4 | 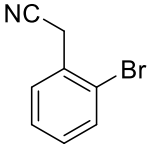 **68** | 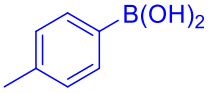 **58** | 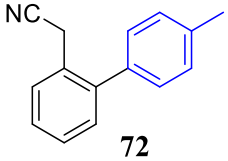 **72** | 96 |
| 5 | 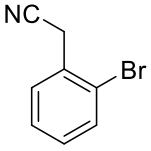 **68** | 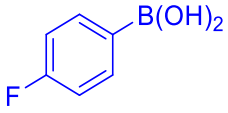 **62** | 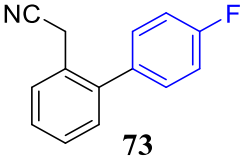 **73** | 84 |
| 6 | 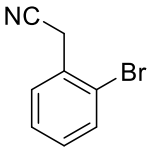 **68** | 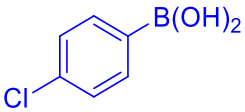 **64** | 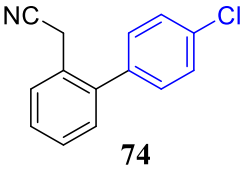 **74** | 55 |

| Entry | Benzyl nitrile | Boronic acid | Product | Yield (%) |
|---|---|---|---|---|
| 7 | 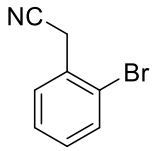 **68** | 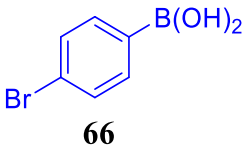 **66** | 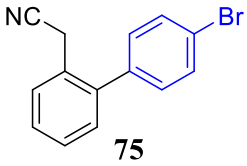 **75** | 0 |

[a]Reaction conditions: (2-bromophenyl)acetonitrile (1 eq.), nucleophile (1.2 eq.), $Pd(PPh_3)_4$ (5 mol%), $K_2CO_3$ (3 eq.), toluene (10 mL), water (1 mL). All reactions were conducted for 24 hours under an argon or nitrogen atmosphere at 80°C. All yields were isolated using flash column chromatography.

## 2.5 Cyclisation Reaction of Biaryls

Now that we have managed to synthesise the library of both benzonitriles and benzylic nitriles in moderate to excellent yields, our next step was to perform a cyclisation of our nitriles with sodium azides to form tetrazole. It is worth noticing the high yields that were obtained from the optimised Suzuki-Miyaura cross-coupling reactions that also accommodated the *ortho*-benzylic nitrile. Since a tetrazole pharmacophore is important in novel drug discovery it has the capacity to interact *via* noncovalent interaction with biological targets and it is a bioisoster of carboxylic acid [120].

### 2.5.1 The synthesis of 5-([1, 1'-biphenyl]-2-yl)-1*H*-tetrazole (76)

The preparation of 5-([1, 1'-biphenyl]-2-yl)-1*H*-tetrazole **(76)** was achieved by reacting [1, 1'-biphenyl]-2-carbonitrile **(53)** with sodium azide **(33)** for 20 hours to afford. The titled compound **(72)** was produced as a white solid with a 33% yield **(Scheme 2.19)**.

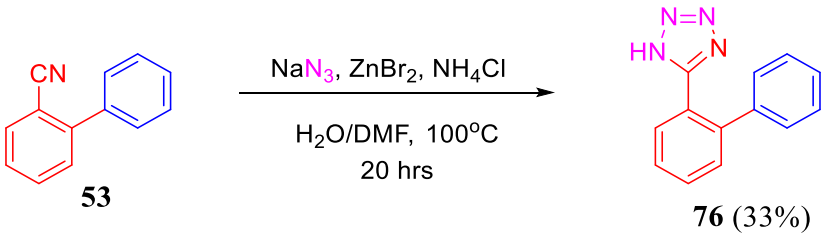


**53** **76** (33%)

**Scheme 2.19:** Synthesis of compound **(76)**.

The $^1$H NMR spectrum of the desired product **(76)** confirmed the structure of the product, showing the signals resonating in the aromatic region and they integrate for eight protons that are in the structure **(Figure 2.30)**. To confirm a conversion of a nitrile functional group to a tetrazole was illustrated by the disappearance of the nitrile peak at $^{13}$C NMR spectrum **(Figure 2.31)** [149].

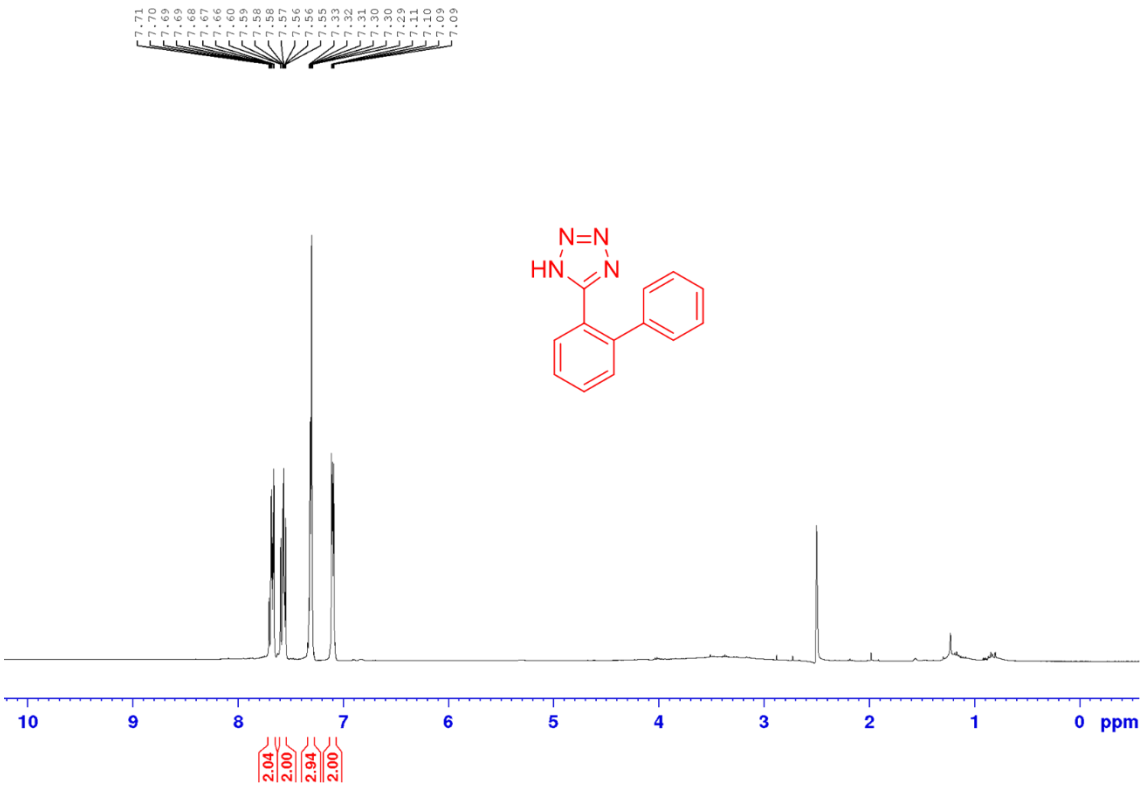


**Figure 2.30:** $^{1}$H NMR spectrum for 5-([1, 1'-biphenyl]-2-yl)-1H-tetrazole **(76)**.

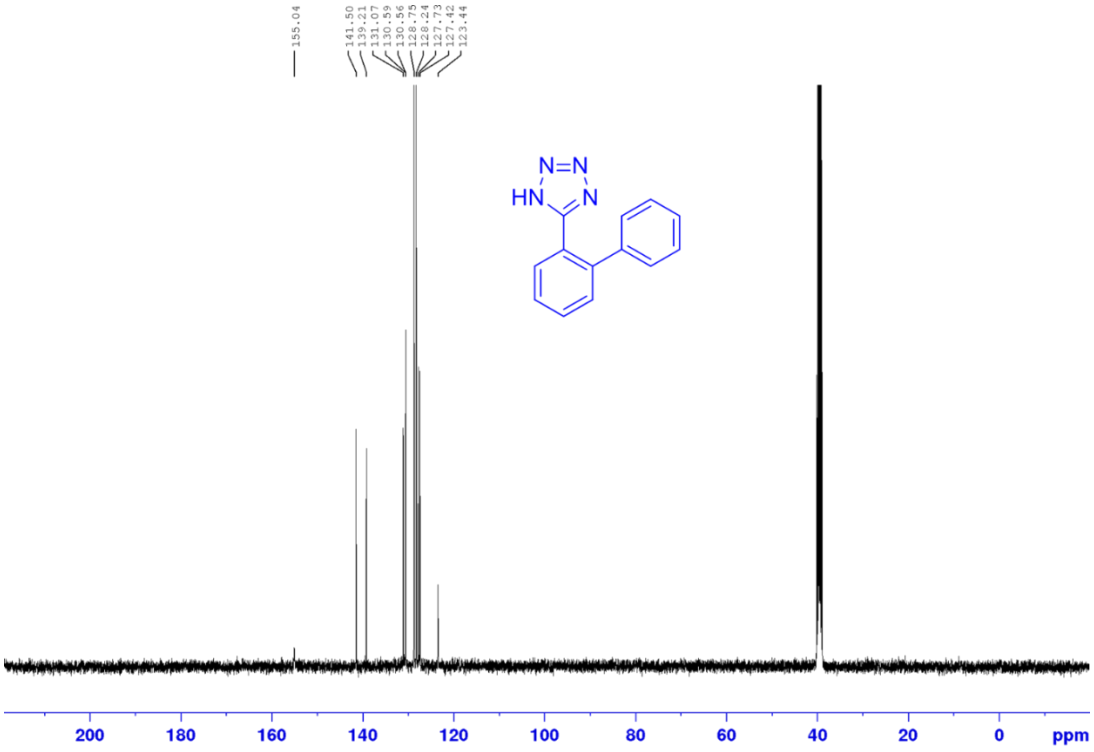


**Figure 2.31:** $^{13}$C NMR spectrum for 5-([1, 1'-biphenyl]-2-yl)-1*H*-tetrazole **(76)**.

### 2.5.2 The synthesis of 5-(bromobenzyl)-1*H*-tetrazole (77)

Utilising the model procedure discovered in **Scheme 2.4**, it was worth practising whether it will be applicable for the benzylic nitriles. Indeed, the synthesis of 5-(bromobenzyl)-1*H*-tetrazole **(77)** was achieved through the cyclisation of 2-bromophenylacetonitrile **(68)** with sodium azide **(33)** under reflux in water for 20 hours **(Scheme 2.20)**.

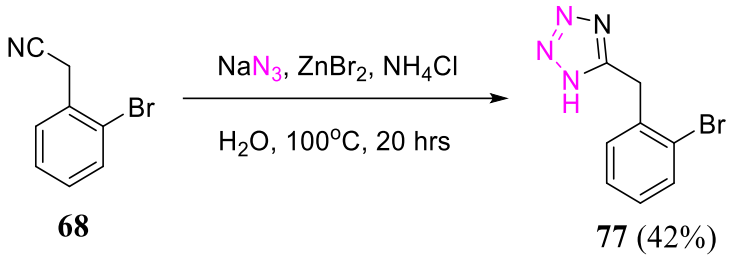


**Scheme 2.20:** Synthesis of compound **(77)**.

The successful synthesis of the compound **(77)** was confirmed using $^{1}$H NMR and $^{13}$C NMR spectroscopic techniques that corresponded to the structure **(Appendix A1.16)** [150]. The X-ray structure also confirmed that the desired product was obtained **(Figure 2.32)**.

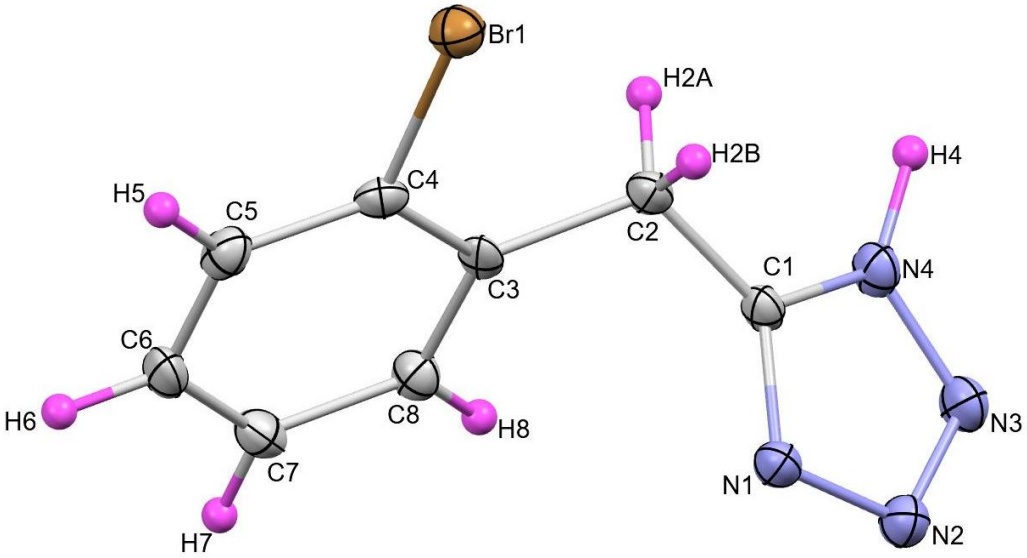


**Figure 2.32:** X-ray structure for 5-(bromobenzyl)-1*H*-tetrazole **(77)**.

### 2.5.3 The synthesis of 5-((4'-methyl-[1, 1'-biphenyl]-2-yl)methyl)-1*H*-tetrazole (78)

5-((4'-Methyl-[1, 1'-Biphenyl]-2-yl)methyl)-1*H*-tetrazole **(78)** was prepared in an isolated yield of 14% as white solid from the reaction of 2-(4'-methyl-[1, 1'-biphenyl]-2-yl)acetonitrile **(72)** and sodium azide **(33) (Scheme 2.21)**.

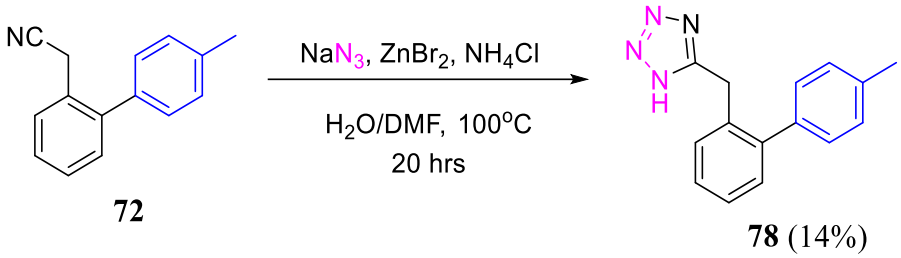


**Scheme 2.21:** Synthesis of compound **(78)**.

The desired product **(78)** was achieved following the structural elucidation of $^{1}$H NMR and $^{13}$C NMR spectra showing expected peaks that corresponded to the structure **(Figure 2.33 & 2.34)**.

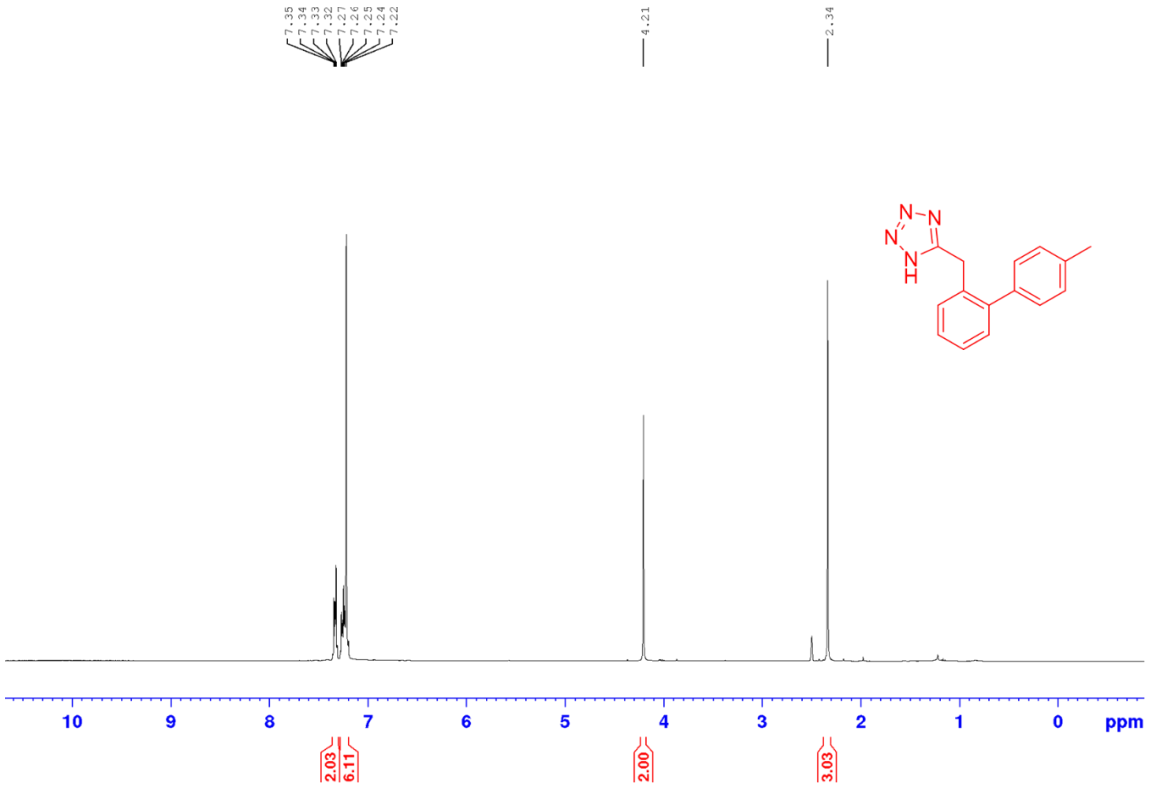


**Figure 2.33:** $^{1}$H NMR for 5-((4'-methyl[1, 1'-biphenyl]-2-yl)methyl)-1*H*-tetrazole **(78)**.

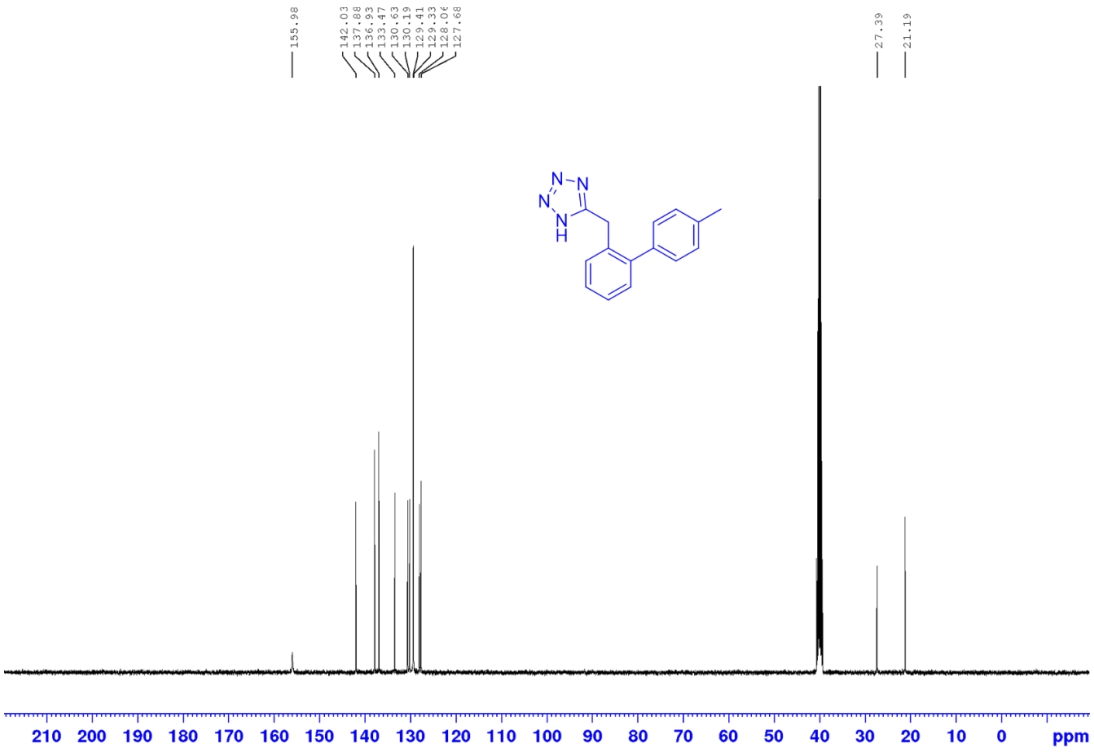


**Figure 2.34:** $^{13}$C NMR for 5-((4'-methyl[1, 1'-biphenyl]-2-yl)methyl)-1*H*-tetrazole **(78)**.

### 2.5.4 The synthesis of 5-((4'-fluoro-[1, 1'-biphenyl]-2-yl)methyl)-1*H*-tetrazole (79)

The titled compound **(79)** was synthesised in 29% yield as a white solid from the cyclisation of 2-(4'-fluoro-[1, 1'-biphenyl]-2-yl)acetonitrile **(73)** with sodium azide **(33)** following the procedure below **(Scheme 2.22)**.

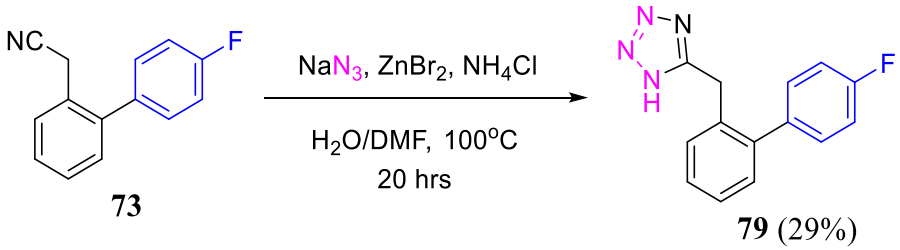


**Scheme 2.22:** Synthesis of compound **(79)**.

The structural elucidation of the furnished compound **(79)** was done and the signals in $^{1}$H NMR and $^{13}$C NMR spectra corresponded to the structure **(Appendix A1.18)**. The HRMS of the product showed the molecular peak [$M^+$ - $H^+$] resonating at *m/z* 253.0892 which agrees with the calculated *m/z* value for $C_{14}H_{10}N_4F$ of 253.26 **(Figure 2.35)**.

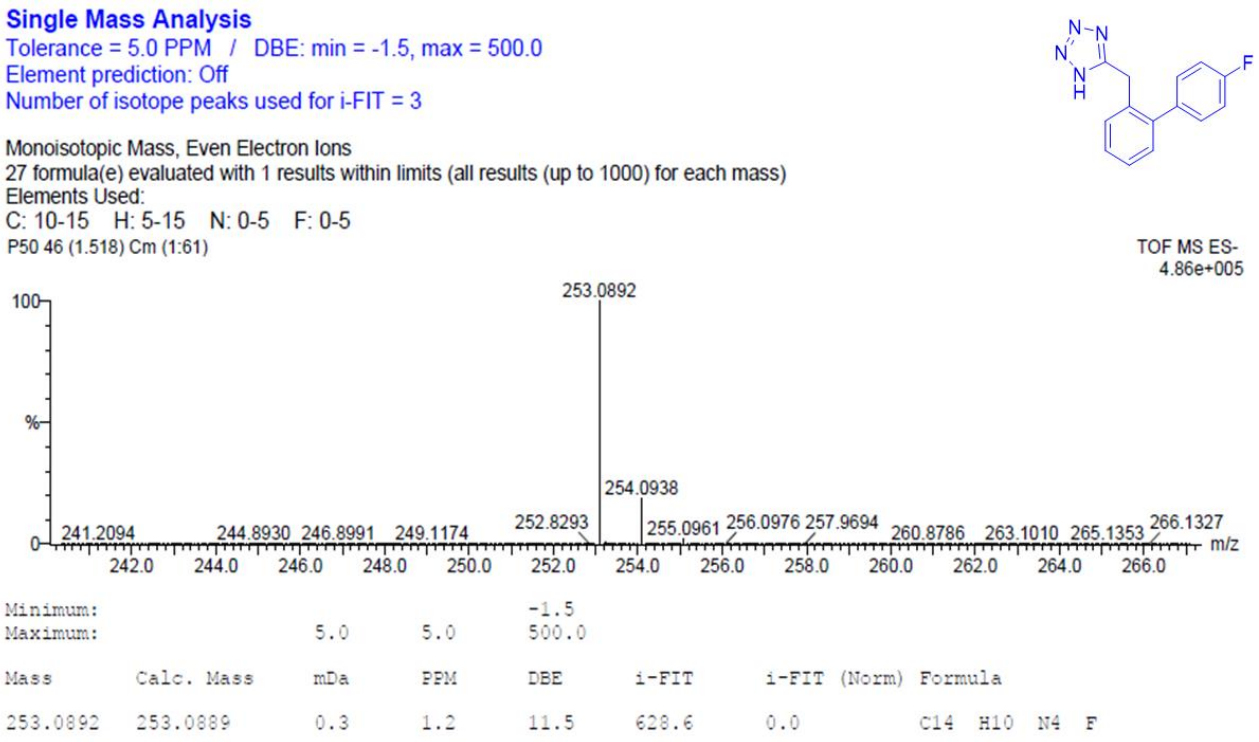


**Figure 2. 35:** HRMS for 5-((4'-fluoro-[1, 1'-biphenyl]-2-yl)methyl)-1*H*-tetrazole **(79)**.

**Table 2.4**: Cyclisation of the nitrile with sodium azide **(33)** [a].

| Entry | Organic nitrile | Product | Yield (%) |
|---|---|---|---|
| 1 | 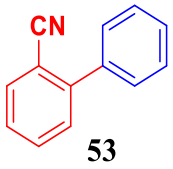 **53** | 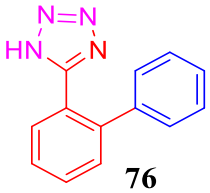 **76** | 33 |
| 2 | 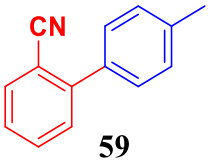 **59** | 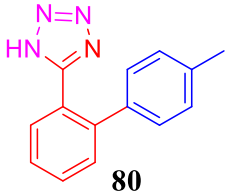 **80** | 15 |
| 3 | 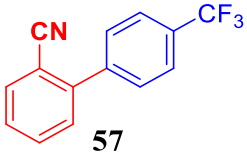 **57** | 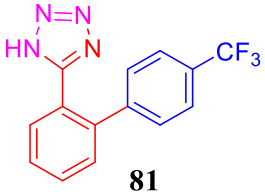 **81** | 24 |
| 4 | 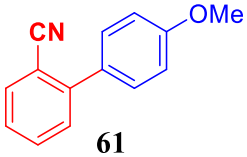 **61** | 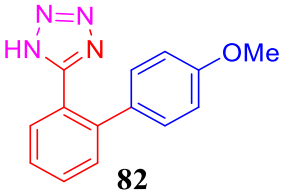 **82** | 21 |
| 5 | 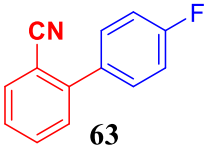 **63** | 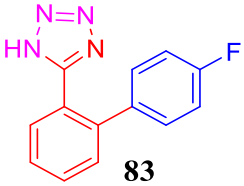 **83** | 42 |
| 6 | 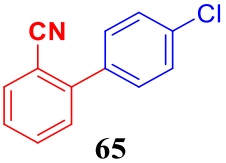 **65** | 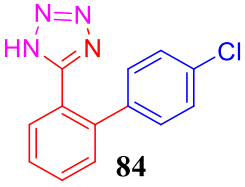 **84** | 56 |

| Entry | Organic nitrile | Product | Yield (%) |
|---|---|---|---|
| 7 | 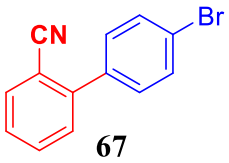 **67** | 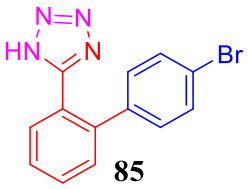 **85** | 21 |
| 8 | 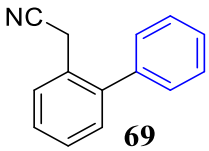 **69** | 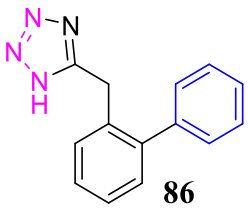 **86** | 14 |
| 9 | 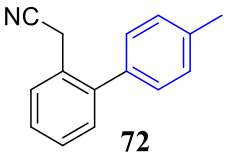 **72** | 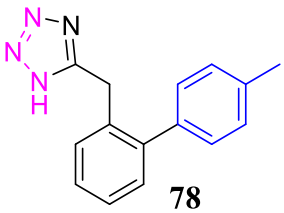 **78** | 59 |
| 10 | 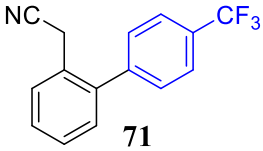 **71** | 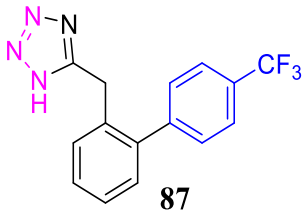 **87** | 16 |
| 11 | 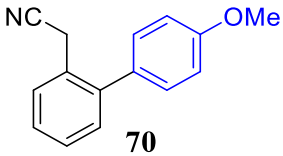 **70** | 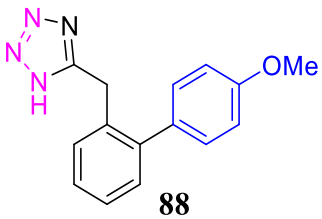 **88** | 17 |
| 12 | 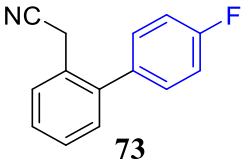 **73** | 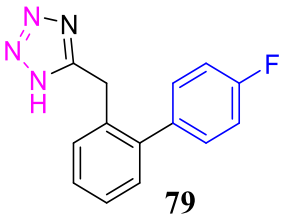 **79** | 29 |

| Entry | Organic nitrile | Product | Yield (%) |
|---|---|---|---|
| 13 | 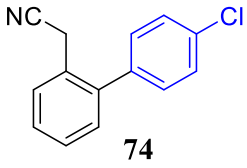 **74** | 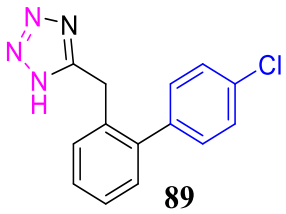 **89** | 15 |

[a]Reaction conditions: nitrile (1 eq.), $NaN_3$ (1 eq.), $ZnBr_2$ (2 eq.), $NH_4Cl$ (1 eq.), water (10 mL), DMF (1 mL). All reactions were heated at 100°C for 20 hours and the yields were isolated using the flash column chromatography.

# Chapter 3

## 3.1 Results of Biological Studies

After the successful synthesis of *ortho*-substituted phenyl tetrazoles displayed in **Figure 3.1**, they were submitted for protein-protein interaction (PPI) inhibition evaluation of HOP-HSP90 at Rhodes University in collaboration with Prof. Adriene Atkins. It has been mentioned in **Chapter 1** that the PPI is a promising drug target; however, the challenge is finding new PPI inhibitors. Vaaltyn and co-workers [108] reported the potential of targeting the HOP-HSP90 PPI using *ortho*-substituted biphenyl tetrazoles as an inhibitor that interacted with the TPR2A domain of HOP, inhibiting PPI. From the suggestion that was observed from the structural overlap of the fragments that they investigated, losartan **(26)** and valsartan **(27)** showed PPI inhibition activity. Drawing information from Vaaltyn's study, we hypothesised that valsartan derivatives would inhibit the PPI of HOP-HSP90.

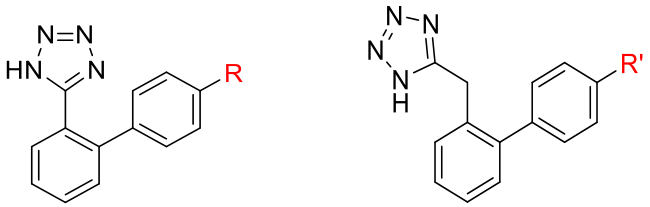


**27** - Valsartan

**76** R = H

**80** R = $CH_3$

**81** R = $CF_3$

**82** R = $OCH_3$

**83** R = F

**84** R = Cl

**85** R = Br

**78** R' = $CH_3$

**79** R' = F

**86** R' = H

**87** R' = $CF_3$

**88** R' = $OCH_3$

**89** R' = Cl

**Figure 3.1:** Synthesised and assayed compounds.

### 3.1.1 TPR2A and HSP90 CTD Solid phase binding PPI

Significantly, some of the assayed compounds displayed weak inhibitory PPI dose-dependent activity including **76**, **80**, **82**, **83** and **84 (Figure 3.2)**, where the electron-donating R-group ($OCH_3$ and $CH_3$) showed the highest activity compared to the electron-withdrawing group (Cl and F). The predictions of Vaaltyn and co-workers [108] about the fragments that would bound to the TPR2A

domain from studying MEEVD structure did not correlate especially the six-membered ring fragments since the MEEVD contains long glutamic acid chains residues and no aromatics. However, the features that they noted from their active fragments had aromatic moiety, mostly being a six-membered aromatic ring being either directly bonded through a benzylic carbon or to a tetrazole ring. In addition, *ortho*-substituents to the tetrazoles either halogen or an aromatic ring fragment were part of the active fragments. With the mentioned structural features from the literature, this project reports the active fragments that had the same features. Even though the aromatic ring was predicted not to be active, the above-mentioned authors suggested that the TPR2A aromatic residues including the hydrophobic Val4 binding site, two tyrosine residues (Tyr236 and Tyr248) whereas a third aromatic residue (Phe270) is positioned next to the Glu2 binding region interact with the aromatic fragments, hence facilitating the formation of the salt bridge.

From the results in **Figure 3.2** the addition of benzylic carbon to the tetrazole did not improve the activity even at a high concentration of 2 mM as Vaaltyn *et al*. [108] suggested. In his results, the halogen *ortho*-substituted to the benzylic position agreed with this prediction, but our fragments had a bulky *ortho*-substituted six-membered ring to the benzylic position imposing hindrance. Together these data suggest that the synthesised valsartan derivatives with a benzylic carbon tetrazole (**78**, **79**, **86**, **87**, **88** and **89**) were not inhibiting HOP-HSP90 PPI but they showed PPI stabiliser activity since they displayed higher PPI formation. This might be due to allosteric regulation by stabilizing the protein bound structure or by increasing PPI indirectly [151]. Since valsartan **(27)** showed higher PPI inhibitory activity compared to its derivatives presented in this report, the effect was induced by the R-group that contained a straight chain similarly to glutamic acids chains that are featured in the MEEVD region.

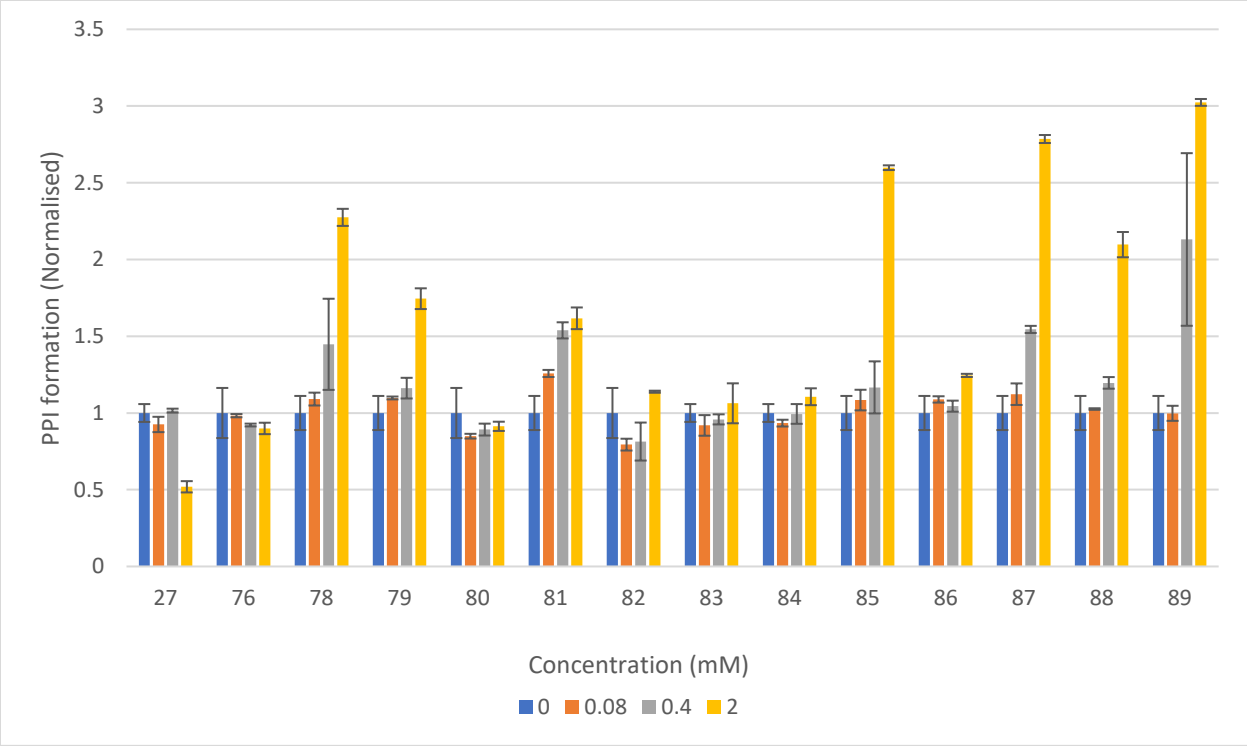


**Figure 3.2:** CTD Solid phase binding PPI assay, between the HPS90 C-terminal domain and HOP TPR2A domain in the presence of synthesised compounds. Compound **76**, **80**, **82**, **83** and **84** showed significant PPI inhibitory activity. * p <.05, ** p<.01, *** p<.001, **** p<.0001.

# Chapter 4

# Conclusion

The discovery of the PPI's potential to be a drug target has opened a new era in drug discovery that seems promising, with valsartan **(27)** being one of the hit compounds that were previously reported [108]. The challenges that were reported with drugging PPI are the unfavourable characteristics in the protein-protein interface of multiprotein assemblies resulting in difficulties in the development of the inhibitors [77]. Therefore, we envisioned the addition of benzyl tetrazole while varying the *ortho*-phenyl substrate would improve the PPI inhibitory activity using FBDD techniques **(Figure 2.1)**.

This study has successfully synthesised valsartan **(27)** and its analogues as hit compounds for HOP-HSP90 PPI inhibition for the treatment of TNBC using developed methods and well-modified procedures. Since the Suzuki-Miyaura cross-coupling reaction and [3 + 2] cycloaddition reaction were the main backbone reactions, functional group conversion was done to obtain a nitrile group for the cycloaddition reaction. Valsartan **(27)** synthesis had challenges with the purification of the intermediates, with two routes in hand in **Scheme 2.1**. **Route A** was shown to be superior as the cross-coupling reaction was done before acylation; this reduced the number of spots that had the same $R_f$ value to be isolated, therefore, better purification. The modified procedure for the synthesis of valsartan **(27)** brought a powerful shift in industrial application since it applied a mild Suzuki-Miyaura cross-coupling reaction for the synthesis of biphenyl moiety that accommodated sensitive functional groups.

Following the optimised methodologies as shown in **Chapter 2**, 13 valsartan analogues were synthesised and assayed for HOP-HSP90 PPI inhibition. The hypothesis was for these fragments to bind to the TPR2A domain of HOP, therefore inhibiting the interaction with the MEEVD C-terminal of HSP90. The findings were consistent with the hypothesis, *ortho*-biphenyl tetrazole fragments showed dose-dependent PPI inhibitory activity, namely, compound **76**, **80**, **82**, **83** and **84**. However, none of the fragments had higher PPI activity above valsartan **(27)**. Upon the introduction of benzylic tetrazole to our fragments, no PPI activity was observed, hence, higher PPI formation indicating that these fragments had high PPI stabiliser ability at high concentration. This study highlights the development of novel active fragments for the treatment of TNBC by

targeting one of the difficult drug targets, PPI. Further extensive structure-activity relationship (SAR) investigation is required and to further optimise the active fragments to increase their efficacy. We can conclude that the *ortho*-biphenyl tetrazole fragments displayed promising activity against the HOP-HSP90 PPI inhibition for new TNBC therapies and this study report their synthetic method that accommodate a wide range of functional groups.

# Chapter 5

# Experimental

## 5.1 General Experimental Procedures.

### 5.1.1 Chemical and instrumental

All reactions were carried out in oven-dried glassware with a magnetic stirrer bar on a hot plate. All reagents (including solvents) purchased from Sigma Aldrich and Honeywell were used without further purification. Moisture-sensitive reactions were carried out in dry solvents under a nitrogen or argon atmosphere. All products were confirmed with $^{1}H$ NMR (400 MHz) and $^{13}C$ NMR (100 MHz) spectra recorded on Bruker Avance III 400 MHz (9.4 T) using a normal NMR tube in deuterated solvent and are reported in part per million downfield from tetramethylsilane (TSM) as an internal standard. High-resolution mass spectrometry (HRMS) was used to determine the molecular mass of the products in a negative mode, obtained on a Waters Acquits LCT premier (TOF) mass-spectrometer and reported in *m/z*. Infrared spectra were recorded on Bruker Alpha II FTIR Base Spectrometer using Platinum ATR diamond 1 Bounce. Column chromatography was carried out using Fluka silica gel 60 cat No.70-230 mesh (0.063-0.2 mm) to purify products. Thin layer chromatography (TLC) was performed on aluminium-supported silica gel 60 TLC plates, coated with fluorescent indicator F254 and visualised under an ultraviolet (UV) light.

### 5.1.2 Protein expression and purification

*E. coli* BL21(DE3) cells were transformed with the pGEX-3X-1400 plasmid containing the coding region for the TPR2AB region (residues 208-543) from murine HOP (which shares 98% amino acid sequence identity with human HOP) [152, 153]. The production of GST-TPR2AB protein was induced by the addition of 1 mM isopropylthio-β-galactoside (IPTG) for 3 hours at 37℃ and GST-TPR2AB purified by native GSHaffinity chromatography [154]. The GST tag was removed to yield the untagged TPR2AB domain using the Factor Xa Cleavage Capture Kit (Merck Millipore) according to the manufacturer's instructions. The stages of protein purification and proteolytic cleavage of the GST tag were monitored by SDS-PAGE and Western blot analysis [154]. The average yield of TPR2AB was 0.70 ± 0.05 mg/L.

### 5.1.3 X-ray crystallography

X-ray diffraction data were recorded on a Bruker Apex Duo diffractometer equipped with an Oxford Instruments Cryojet operating at 100 (2) K and an Incoatec microsource operating at 30 W power. The data were collected with Cu Kα (λ = 1.54184 Å) radiation at a crystal-to-detector distance of 50 mm using omega and phi scans with exposures taken at 30 W X-ray power and 0.50° frame widths using APEX4 [155].

The data were reduced with the programme SAINT [155] using outlier rejection, scan speed scaling, and standard Lorentz and polarisation correction factors. A SADABS semi-empirical multi-scan absorption correction [155] was applied to the data. Intrinsic Phasing methods SHELXT-2014 [156] and Olex2-1.5 [157] were used to solve the structures. All non-hydrogen atoms in each of the structures were located in the difference density map and refined anisotropically with SHELXL-2014 [156]. All hydrogen atoms in each of the structures were included as idealised contributors in the least-squares process with standard SHELXL-2014 [156] parameters. All diagrams were rendered using Mercury 2023.2.0. The final ligand structure was validated using an IUCR checkcif.

**Table 5.1:** Crystal data for compound **77**.

| ***Crystal Data*** | |
|---|---|
| Chemical formula | $C_8H_7BrN_4$ |
| Formula weight | 239.09 |
| Crystal system | Orthorhombic |
| Space group | Pbca |
| Temperature (K) | 100 (02) |
| ***Unit cell dimension*** | |
| *a* (Å) | 4.89670(10) |
| *b* (Å) | 13.5160(4) |
| *c* (Å) | 26.7090(7) |
| α (Å) | 90 |
| *β* (Å) | 90 |
| *γ* (Å) | 90 |
| Crystal size (mm) | 0.225 × 0.105 × 0.035 |
| V ($Å^3$) | 1767.70 (8) |
| *Z* | 8 |
| Radiation type | Cu *K*α |
| μ ($mm^{-1}$) | 5.981 |
| ***Data collection*** | |
| Diffractometer | Bruker APEX-II Duo |

| | |
|---|---|
| Absorption correction | Multi-scan SADABS, Bruker 2010 |
| ***Refinement*** | |
| $R_{int}$ | 0.0488 |
| No. of reflections | 1666 |
| No. of parameters | 122 |
| No. of restraints | 0 |
| Final R indices, [I>2σ>(I)] | $R_1$ = 0.0285<br>$wR_2$ = 0.0648 |

## 5.2 Synthesis of Amide

### 5.2.1 Synthesis of 2-iodobenzamide (46)

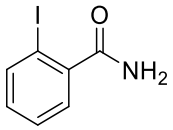


**2-Iodobenzamide (46):** In an oven-dried 100 mL round-bottomed flask, $SOCl_2$ (12.3 mmol) was added in 2-iodobenzoic acid **(45)** (8.81 mmol) dissolved in dry THF (20 mL). The mixture was heated to 50℃ for 1 hour then cooled to room temperature then to 0℃. The cooled mixture was added to ice cooled $NH_4OH$ (10 mL, 25%) and then stirred for 5 minutes at 0℃. Extraction was done using chloroform (75 mL X 3), the organic layer was dried with anhydrous magnesium sulphate and then concentrated under a vacuum. The crude was soaked in hexane and then filtered to obtain a pure product [137]. The compound was afforded as a white solid (76%). **$^1$H NMR** (400 MHz, $CDCl_3$) δ ppm: 7.10-7.14 (m, 1H), 7.37-7.41 (m, 1H), 7.47-7.49 (dd, *J* = 7.64, 1.33 Hz, 1H), 7.88-7.90 (d, *J* = 8.02 Hz, 1H).

## 5.3 Synthesis of Nitriles

### 5.3.1 General procedure A

In an oven-dried 50 mL round-bottomed flask with a magnetic stirrer bar $POCl_3$ (2 mmol) was added to dry DMF (8 mmol) then the mixture turned yellow under anhydrous condition. An amide (2 mmol) was dissolved in DMF (1 mL) then the mixture was added dropwise with a syringe in the flask at 0℃ and kept at this temperature stirred for 20 hours. The solution was quenched with ice then liquid extraction was done using dichloromethane (50 mL x 3), dried with magnesium sulphate, and dried over a vacuum. Column chromatography was used to obtain a pure product using hexane (90%): ethyl acetate (10%) [118].

### 5.3.2 Synthesis of benzonitrile (42)

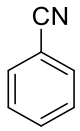


**Benzonitrile (42)**: Following the general procedure A, the compound **42** was produced as a white liquid (77%). **$^{1}$H NMR** (400 MHz, $CDCl_3$) δ ppm: 7.46-7.50 (t, *J* = 7.48 Hz, 2H), 7.60-7.64 (tt, 1H), 8.12-8.15 (dd, *J* = 8.45, 1.35 Hz, 2H). **$^{13}$C NMR** (100 MHz, $CDCl_3$) δ ppm: 112.4, 118.8, 129.1, 132.1, 132.8. IR ($\nu_{max}$ $cm^{-1}$): 1447, 1490, 2228, 3064.

### 5.3.3 Synthesis of 2-iodobenzonitrile (47)

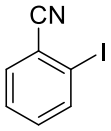


**2-Iodobenzonitrile (47):** Following the general procedure A, the compound **47** was synthesised as a cream solid (93%). **$^{1}$H NMR** (400 MHz, $CDCl_3$) δ ppm: 7.26-7.30 (td, *J* = 7.80, 1.64 Hz, 1H), 7.43-7.47 (td, *J* = 7.62, 1.03 Hz, 1H), 7.59-7.62 (dd, *J* = 7.77, 1.57 Hz, 1H), 7.91-7.93 (dd, *J* = 8.06, 0.77 Hz, 1H). **$^{13}$C NMR** (100 MHz, $CDCl_3$) δ ppm: 98.3, 119.3, 120.7, 128.3, 133.6, 134.2, 139.5.

## 5.4 Synthesis of Valsartan

### 5.4.1 Synthesis of methyl(4-bromobenzyl)-L-valinate (38)

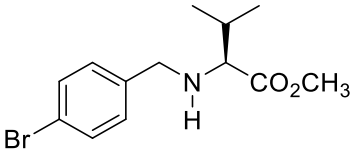


**Methyl(4-bromobenzyl)-*L*-valinate (38):** 1-Bromo-4-(bromomethyl)benzene **(40)** (1 mmol), L-valine methyl ester hydrochloride **(39)** (1 mmol), potassium carbonate (3 mmol) and DMF (5 mL) were added in a 100 mL round-bottomed flask with a magnetic stirrer bar, a rubber septum and the mixture was stirred at 80℃ for 3 hours. The residue was extracted with ethyl acetate and washed with ice-cooled water (50 mL x 2) and the organic layer was washed with brine, dried with magnesium sulphate then concentrated. The crude was purified with flash column chromatography

using hexane (90%): ethyl acetate (10%) and $R_f$ value = 0.36, colourless liquid was obtained with 93% yield. **$^1$H NMR** (400 MHz, $CDCl_3$) δ ppm: 0.89-0.93 (t, 6H), 1.81-1.94 (m, 1H), 2.94-2.96 (d, *J* = 6.91 Hz, 1H), 3.47-3.51 (d, *J* = 13.86 Hz, 1H), 3.69 (s, 3H), 3.74-3.77 (d, *J* = 13.39 Hz, 1H), 7.18-7.20 (d, *J* = 8.25 Hz, 2H), 7.38-7.40 (d, *J* = 8.25 Hz, 2H). **$^{13}$C NMR** (100 MHz, $CDCl_3$) δ ppm: 18.5, 19.3, 31.6, 51.2, 51.7, 66.3, 120.6, 129.8, 131.2, 139.1, 175.3.

### 5.4.2 Synthesis of methyl *N*-(4-bromobenzyl)-*N*-pentanoyl-*L*-valinate (37)

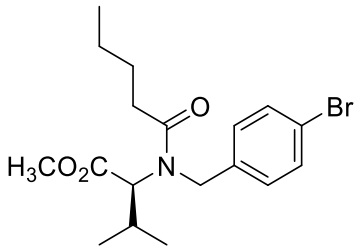


**Methyl *N*-(4-bromobenzyl)-*N*-pentanoyl-*L*-valinate (37):** methyl(4-bromobenzyl)-*L*-valinate **(38)** (0.9291 mmol) was dissolved in dichloromethane (20 mL) as triethylamine (1.9 mmol) was added dropwise at 0℃ in a 100 mL round-bottomed flask with a stirrer bar. As the mixture was stirred, valeryl chloride **(35)** (0.9291 mmol) was added then the mixture was stirred at 25℃ for 16 hours. The residue was washed with water (50 mL x 2), dried with magnesium sulphate then concentrated. Flash-column chromatography was used to purify the product using hexane (90%): ethyl acetate (10%) and the $R_f$ value = 0.4, the yellow liquid was obtained with a 73% yield. **$^1$H NMR** (400 MHz, $CDCl_3$) δ ppm: 0.78-0.88 (m, 9H), 0.99-1.09 (tt, 1H), 1.17-1.29 (m, 2H), 1.43-1.53 (m, 1H), 1.80-1.85 (m, 1H), 2.18-2.31 (tt, 1H), 2.89-2.90 (d, *J* = 6.18 Hz, 1H), 3.20-3.30 (m, 1H), 3.42-3.45 (d, *J* = 13.80 Hz, 1H), 3.61 (s, 3H), 3.67-3.71 (d, *J* = 13.32 Hz, 1H), 7.11-7.13 (d, *J* = 7.45 Hz, 2H), 7.30-7.32 (d, *J* = 8.45 Hz, 2H). **$^{13}$C NMR** (100 MHz, $CDCl_3$) δ ppm: 13.7 (d), 18.7, 19.1, 19.7, 22.2, 22.8, 25.8, 31.4, 51.2, 51.5, 66.2, 120.5, 129.8, 131.1, 138.8, 175.2. IR ($\nu_{max}$ $cm^{-1}$): 1195, 1487, 1651, 1732, 2959.

### 5.4.3 Synthesis of methyl ((2'-cyano-[1, 1'-biphenyl]-4-yl)methyl)-*L*-valinate (34)

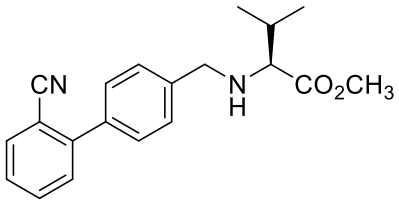

**Methyl ((2'-cyano-[1, 1'-biphenyl]-4-yl)methyl)-*L*-valinate (34)**: Following Procedure C, compound **34** was produced as a colourless liquid in 26% yield from the cross-coupling of 2-cyanophenylboronic acid **(36)** with methyl (4-bromobenzyl)-*D*-valinate **(38)**. **$^{1}$H NMR** (400 MHz, $CDCl_3$) δ ppm: 0.95-0.98 (d, *J* = 6.59 Hz, 6H), 1.92-197 (m, 1H), 3.05-3.07 (d, *J* = 5.91 Hz, 1H), 3.64-3.67 (d, *J* = 13.36 Hz, 1H), 3.73 (s, 3H), 3.88-3.91 (d, *J* = 13.36 Hz, 1H), 7.39-7.43 (td, *J* = 7.62, 0.88 Hz, 1H), 7.45-7.52 (m, 5H), 7.60-7.64 (td, *J* = 7.73, 1.10 Hz, 1H), 7.73-7.75 (dd, *J* = 7.79, 0.69 Hz, 1H). **$^{13}$C NMR** (100 MHz, $CDCl_3$) δ ppm: 18.7, 19.4, 31.8, 51.5, 52.2, 66.8, 111.3, 118.8, 127.5, 128.6, 128.7, 130.1, 133.8, 136.9, 140.8, 145.4, 175.7.

### 5.4.4 Synthesis of methyl N-((2'-cyano-[1, 1'-biphenyl]-4-yl)methyl)-N-pentanoyl-L-valinate (32)

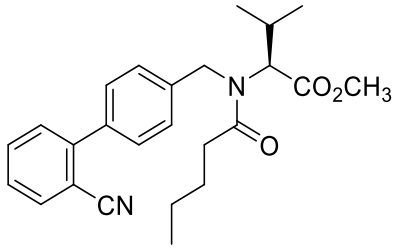


**Methyl *N*-((2'-cyano-[1, 1'-biphenyl]-4-yl)methyl)-*N*-pentanoyl-*L*-valinate (32):** Following general procedure B, methyl *N*-(4-bromobenzyl)-*N*-pentanoyl-*L*-valinate **(37)** (0.6784 mmol) and 2-cyanophenyl boronic acid **(36)** (0.8141 mmol) was reacted with the rest of the regents mentioned in the general procedure B. $R_f$ value = 0.3, hexane (80%): ethyl acetate (20%). A yellow liquid was produced with a yield of 11%. Following a different method to afford compound **32** in 86% yield, methyl ((2'-cyano-[1, 1'-biphenyl]-4-yl)methyl)-L-valinate **(34)** was dissolved in dichloromethane (20 mL) and triethylamine (1.9 mmol) was added dropwise at 0℃ in a 100 mL round-bottomed flask with a stirrer bar. As the mixture was stirred, valeryl chloride **(35)** (0.9291 mmol) was added then the mixture was stirred at 25℃ for 16 hours. The residue was washed with water (50 mL x 2), dried with magnesium sulphate then concentrated and flash-column chromatography was used to purify the product using hexane (90%): ethyl acetate (10%). **$^{1}$H NMR** (400 MHz, $CDCl_3$) δ ppm: 0.85-0.93 (m, 6H), 0.97-0.99 (m, 3H), 1.25-1.43 (m, 2H), 1.57-1.74 (m, 2H), 2.28-2.37 (m, 3H), 3.36 (s, 3H), 4.05-4.08 (d, *J* = 10.72 Hz, 0.4H), 4.25-4.28 (d, *J* = 15.66 Hz, 0.4H), 4.69 (s, 1H), 4.94-4.97 (d, *J* = 10.26 Hz, 0.5H), 5.05-5.09 (m, 0.5H), 7.28-7.31 (m, 2H), 7.40-7.54 (m, 4H), 7.61-7.63 (d, *J* = 8.54 Hz, 1H), 7.71-7.75 (m, 1H). **$^{13}$C NMR** (100 MHz, $CDCl_3$) δ ppm: 13.8, 13.9, 14.0, 18.8, 20.0, 22.0, 22.5, 22.6, 27.5, 27.6, 27.9, 33.4, 45.4, 48.2, 51.8, 52.1,

53.5, 61.8, 65.9, 111.4, 118.6, 126.4, 127.5, 127.7, 128.0, 128.6, 129.1, 130.0, 132.9, 133.9, 136.7, 137.3, 138.9, 141.7, 144.9, 145.4, 170.3, 171.2, 174.4, 174.7. IR ($\nu_{max}$ $cm^{-1}$): 1239, 1435, 1642, 1735, 2224, 2959.

### 5.4.5 Synthesis of methyl *N*-((2‘-(1*H*-tetrazol-5-yl)-[1, 1’-biphenyl]-4-yl)methyl)-*N*-pentanoyl-*L*-valinate (31)

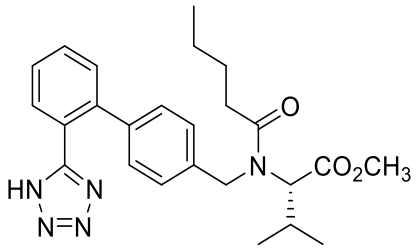


**Methyl *N*-((2‘-(1*H*-tetrazol-5-yl)-[1, 1’-biphenyl]-4-yl)methyl)-*N*-pentanoyl-*L*-valinate (31):** Following the general procedure D, methyl *N*-((2’-cyano-[1, 1’-biphenyl]-4-yl)methyl)-*N*-pentanoyl-*L*-valinate **(32)** (0.07894 mmol) was reacted affording a yellow liquid with 90 % yield. **$^{1}$H NMR** (400 MHz, DMSO/MeOD) δ ppm: 0.67-0.88 (m, 10H), 1.09-1.21 (m, 2H), 1.25-1.30 (m, 1H), 1.36-1.54 (m, 2H), 2.07-2.31 (m, 2H), 3.31 (s, 3H), 3.56 (s, 0.5H), 4.54-4.63 (m, 1H), 4.69-4.74 (d, *J* = 18.07 Hz, 0.5H), 4.84-4.97 (m, 0.5H), 7.14-7.16 (d, *J* = 8.80 Hz, 1H), 7.23-7.25 (d, *J* = 8.06 Hz, 1H), 7.35-7.37 (d, *J* = 8.80 Hz, 1H), 7.43-7.50 (m, 3H), 7.66-7.69 (m, 1H), 7.76-7.79 (m, 1H). **$^{13}$C NMR** (100 MHz, DMSO/MeOD) δ ppm: 13.7, 18.4, 19.9, 22.0, 27.2, 32.7, 51.6, 51.8, 62.2, 65.2, 110.5, 118.8, 126.6, 127.4, 128.4, 128.5, 129.0, 130.2, 131.5, 133.7, 133.9, 136.9, 138.6, 170.4, 170.8, 174.3. IR ($\nu_{max}$ $cm^{-1}$): 1087, 1459, 1629, 2852, 2921, 3415.

### 5.4.6 Synthesis of N-((2’(1*H*-tetrazol-5-yl)-[1, 1’-biphenyl]-4-yl)methyl)-*N*-pentanoyl-*L*-valine (27)

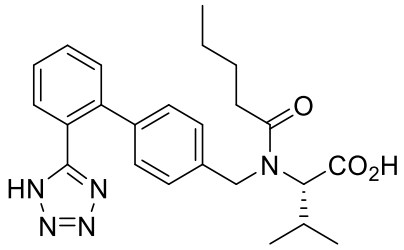


***N*-((2’(1*H*-tetrazol-5-yl)-[1, 1’-biphenyl]-4-yl)methyl)-*N*-pentanoyl-*L*-valine (27):** To a solution of compound **31** (0.07103 mmol) in methanol (5 mL), sodium hydroxide (1 M, 0.5 mL) was added in the round-bottomed flask then stirred under reflux for 21 hours. After cooling the

mixture, hydrochloric acid (3 M) was added dropwise until the pH was 4 then the aqueous solution was washed with ethyl acetate (30 mL x 3) and then concentrated under vacuum after drying with anhydrous magnesium sulphate. The pure desired product was obtained by recrystallisation using ethyl acetate affording a yellow solid with a 95% yield. **$^{1}$H NMR** (400 MHz, $CDCl_3$/MeOD) δ ppm: 0.73-0.99 (m, 9H), 1.16-1.23 (m, 1H), 1.33-1.39 (m, 1H), 1.51-1.65 (m, 1H), 2.07-2.29 (m, 2H), 2.49-2.64 (m, 0.6H), 3.93-3.96 (m, 0.7H), 4.52-4.65 (m, 1H), 4.83-4.92 (m, 0.7H), 5.05-5.11 (m, 0.6H), 7.35-7.50 (m, 6H), 7.60-7.66 (m, 1H), 7.70-7.75 (m, 1H). **$^{13}$C NMR** (100 MHz, $CDCl_3$/MeOD) δ ppm: 13.3, 18.9, 19.1, 19.2, 19.8, 22.2, 22.4, 22.8, 27.3, 27.4, 27.9, 28.5, 33.5, 33.9, 65.9, 67.0, 126.7, 127.6, 127.9, 128.2, 128.7, 128.9, 130.0, 133.1, 133.5, 133.6, 136.0, 136.9, 137.7, 138.9, 140.1, 156.9, 175.6, 176.3, 176.7. **HR-ESI-(-)-MS**, *m/z*: 434.2192 (calculated for $C_{24}H_{28}N_5O_3$, 434.2148).

## 5.5 Synthesis of Biaryls

### 5.5.1 General procedure B

In an oven-dried round-bottomed flask with a magnetic stirrer bar, iodo/bromobenzene (1 mmol), phenylboronic acid (1.2 mmol), potassium carbonate (3 mmol), palladium acetate (5 mol%), triphenylphosphate (10 mol%) were added. A condenser was placed with a rubber septum and then closed tight with a teflon and parafilm. The contents of the flask were kept under nitrogen then dry tetrahydrofuran (5 mL) was added then stirred at 80℃. After 24 hours, the residue was concentrated, and dichloromethane (0.3 mL) was added to dissolve the concentrate to be purified using flash-column chromatography using hexane (80%): ethyl acetate (20%) to afford a desired product.

### 5.5.2 General procedure C

In an oven-dried round-bottomed flask with a magnetic stirrer bar, 2-iodobenzonitrile **(47)** (1 mmol), boronic acid (1.2 mmol), potassium carbonate (3 mmol), $Pd(PPh_3)_4$ (5 mol%) were added. A condenser was placed with a rubber septum and then closed tight with a teflon and parafilm. The contents of the flask were kept under nitrogen then toluene (4 mL) and water (0.5 mL) were added and then stirred at 80℃. After 24 hours, the residue was concentrated, and dichloromethane (0.3 mL) was added to dissolve the concentrate to be purified using flash-column chromatography using hexane (80%): and ethyl acetate (20%) to obtain the desired product.

### 5.5.3 Synthesis of 4'-chloro-[1, 1'-biphenyl]-2-carbonitrile (65)

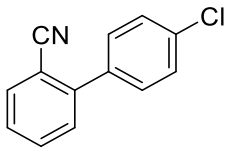


**4'-Chloro-[1, 1'-biphenyl]-2-carbonitrile (65):** Following the general procedure B, the compound **65** was successfully synthesised to afford a white solid in 44% yield. **$^{1}$H NMR** (400 MHz, $CDCl_3$) δ ppm: 7.43-7.50 (m, 6H), 7.62-7.67 (td, *J* = 1.30, 7.71 Hz, 1H), 7.75-7.77 (dd, *J* = 7.79, 0.87 Hz, 1H). **$^{13}$C NMR** (100 MHz, $CDCl_3$) δ ppm: 111.2, 118.4, 127.9, 129.0, 129.9, 130.0, 132.9, 133.8, 135.0, 136.5, 144.2.

### 5.5.4 Synthesis of 4'-methyl[1, 1'-biphenyl]-2-carbonitrile (59)

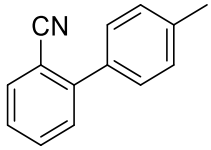


**4'-Methyl[1, 1'-biphenyl]-2-carbonitrile (59):** Following the general procedure B, the compound **59** was produced as a white solid (81%). **$^{1}$H NMR** (400 MHz, $CDCl_3$) δ ppm: 2.43 (s, 3H), 7.30-7.32 (d, *J* = 7.87 Hz, 2H), 7.39-7.43 (td, *J* = 7.63, 1.11 Hz, 1H), 7.46-7.48 (d, *J* = 8.02 Hz, 2H), 7.49-7.51 (d, *J* = 7.88 Hz, 1H), 7.59-7.66 (td, *J* = 7.63, 1.25 Hz, 1H), 7.73-7.76 (m, 1H). **$^{13}$C NMR** (100 MHz, $CDCl_3$) δ ppm: 21.2, 111.2, 118.9, 127.3, 128.3, 129.4, 130.0, 132.8, 133.7, 135.3, 138.7, 145.5.

### 5.5.5 Synthesis of [1, 1'-biphenyl]-2-carbonitrile (53)

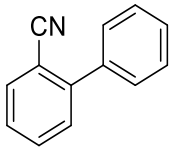


**[1, 1'-Biphenyl]-2-carbonitrile (53):** Following the general procedure B, [158] compound **53** was afforded as white solid yielding 86%. **$^{1}$H NMR** (400 MHz, CDCl3): δ ppm: 7.42-7.53 (m, 5H), 7.56-7.59 (m, 2H), 7.62-7.66 (m, 1H), 7.75-7.78 (dd, *J* = 7.70, 0.64 Hz, 1H). **$^{13}$C NMR** (100 MHz, $CDCl_3$) δ ppm: 111.3, 118.7, 127.6, 128.7, 128.7, 130.1, 132.8, 133.7, 138.2, 145.5.

### 5.5.6 Synthesis of 4'-bromo-[1, 1'-biphenyl]-2-carbonitrile (67).

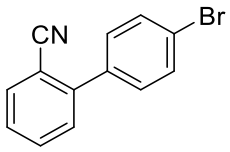


**4'-Bromo-[1, 1'-biphenyl]-2-carbonitrile (67):** Following the general procedure B, the compound **67** was afforded as white solid (79%). **$^{1}$H NMR** (400 MHz, CDCl3) δ ppm: 7.42-7.44 (d, *J* = 8.40 Hz, 2H), 7.46-7.49 (m, 2H), 7.61-7.67 (m, 3H), 7.75-7.77 (s, *J* = 7.74 Hz, 1H). **$^{13}$C NMR** (100 MHz, $CDCl_3$) δ ppm: 111.2, 118.4, 123.3, 127.9, 129.8, 130.3, 131.9, 132.9, 133.8, 137.0, 144.2.

### 5.5.7 Synthesis of 4'-fluoro-[1, 1'-biphenyl]-2-carbonitrile (63)

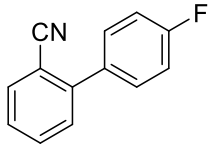


**4'-Fluoro-[1, 1'-biphenyl]-2-carbonitrile (63):** Following the general procedure C, 73% yield of the compound **63** was afforded as a white solid. **$^{1}$H NMR** (400 MHz, CDCl3) δ ppm: 7.15-7.19 (m, 2H), 7.41-7.48 (m, 2H), 7.51-7.54 (m, 2H), 7.61-7.65 (m, 1H), 7.73-7.76 (dd, *J* = 7.72, 0.90 Hz, 1H). **$^{13}$C NMR** (100 MHz, $CDCl_3$) δ ppm: 111.2, 115.6, 115.9, 118.6, 127.7, 130.0, 130.5, 130.6, 132.9, 133.7, 144.4, 161.8, 164.3.

### 5.5.8 Synthesis of 4'4-methoxy-[1, 1'-biphenyl]-2-carbonitrile (61)

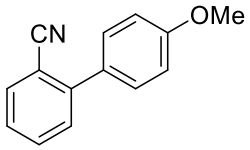


**4'4-Methoxy-[1, 1'-biphenyl]-2-carbonitrile (61):** Following the general procedure C, the compound **61** was afforded as white solid (28%). **$^{1}$H NMR** (400 MHz, $CDCl_3$) δ ppm: 3.86 (s, 3H), 7.01-7.03 (d, *J* = 8.89 Hz, 2H), 7.73-7.40 (m, 1H), 7.47-7.52 (m, 3H), 7.58-7.62 (m, 1H), 7.72-7.74 (d, *J* = 7.49 Hz, 1H). **$^{13}$C NMR** (100 MHz, $CDCl_3$) δ ppm: 55.3, 111.0, 114.2, 118.9, 127.0, 129.9, 130.0, 130.5, 132.8, 133.7, 145.2, 160.1.

### 5.5.9 Synthesis of 4'-(trifluoromethyl)-[1, 1'-biphenyl]-2-carbonitrile (57)

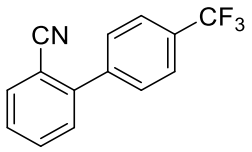


**4'-(Trifluoromethyl)-[1, 1'-biphenyl]-2-carbonitrile (57):** Following the general procedure C, the compound **57** was synthesised as a white solid (65%). **$^{1}$H NMR** (400 MHz, CDCl3) δ ppm: 7.48-7.53 (m, 2H), 7.67-7.71 (m, 3H), 7.74-7.80 (m, 3H). **$^{13}$C NMR** (100 MHz, $CDCl_3$) δ ppm: 111.3, 118.2, 122.6, 125.3, 125.7, 125.8, 128.4, 129.2, 130.0, 133.0, 133.8, 141.6, 143.9.

### 5.5.10 Synthesis of 2-(4'-(trifluoromethyl)-[1, 1'-biphenyl]-2-yl)acetonitrile (71)

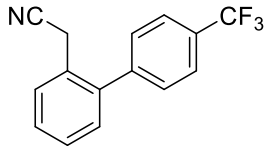


**2-(4'-(Trifluoromethyl)-[1, 1'-biphenyl]-2-yl)acetonitrile (71):** General procedure C was followed. Colourless liquid was produced with a yield of 64%. **$^{1}$H NMR** (400 MHz, $CDCl_3$) δ ppm: 3.61 (s, 2H), 7.28-7.30 (m, 1H), 7.43-7.46 (m, 4H), 7.56-7.59 (m, 1H), 7.73-7.75 (d, *J* = 8.10 Hz, 2H). **$^{13}$C NMR** (100 MHz, $CDCl_3$) δ ppm: 22.0, 117.9, 125.6, 125.7, 128.5, 128.9, 129.3, 129.4, 129.9, 130.2, 130.3, 140.4, 143.6.

### 5.5.11 Synthesis of 2-(4'-fluoro-[1, 1'biphenyl]-2-yl)acetonitrile (63)

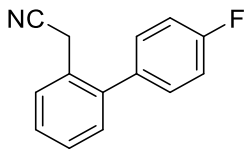


**2-(4'-Fluoro-[1, 1'biphenyl]-2-yl)acetonitrile (63):** General procedure C was followed. Colourless liquid was produced as a desired product, yielding 84%. **$^{1}$H NMR** (400 MHz, $CDCl_3$) δ ppm: 3.62 (s, 2H), 7.13-7.17 (t, *J* = 8.54 Hz, 2H), 7.26-7.30 (m, 3H), 7.39-7.42 (m, 2H), 7.53-7.56 (m, 1H). **$^{13}$C NMR** (100 MHz, $CDCl_3$) δ ppm: 22.0, 115.6, 115.8, 118.2, 128.0, 128.3, 128.4, 129.1, 130.6, 130.6, 130.7, 135.9, 140.8, 161.2, 163.6.

### 5.5.12 Synthesis of 2-(4'-methoxy-[1, 1'-biphenyl]-2-yl)acetonitrile (70)

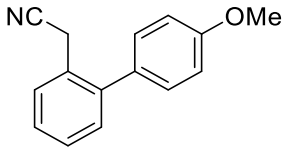


**2-(4'-Methoxy-[1, 1'-biphenyl]-2-yl)acetonitrile (70):** Following the procedure C, the compound **70** was produced as a yellow liquid (96%). **$^{1}$H NMR** (400 MHz, $CDCl_3$) δ ppm: 3.63 (s, 2H), 3.87 (s, 3H), 7.00- 7.02 (m, 2H), 7.23-7.25 (m, 2H), 7.28-7.30 (m, 1H), 7.37-7.39 (m, 2H), 7.53-7.56 (m, 1H). **$^{13}$C NMR** (100 MHz, $CDCl_3$) δ ppm: 22.1, 55.4, 114.2, 118.4, 128.0, 128.1, 128.2, 129.0, 130.1, 130.7, 132.2, 141.6, 159.3.

### 5.5.13 Synthesis of 2-([1, 1'-biphenyl]-2-yl)acetonitrile (69)

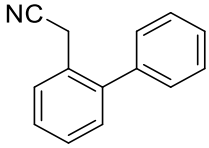


**2-([1, 1'-Biphenyl]-2-yl)acetonitrile (69):** General procedure C was used. Colourless liquid, with yield of 74% [159]. **$^{1}$H NMR** (400 MHz, $CDCl_3$) δ ppm: 3.63 (s, 2H), 7.31-7.33 (m, 3H), 7.41-7.50 (m, 5H), 7.57-7.59 (m, 1H). **$^{13}$C NMR** (100 MHz, $CDCl_3$) δ ppm: 22.1, 118.3, 127.8, 127.9, 128.3, 128.7, 129.0, 129.0, 130.5, 139.9, 141.9.

### 5.5.14 Synthesis of 2-(4'-chloro-[1, 1'-biphenyl]-2-yl)acetonitrile (74)

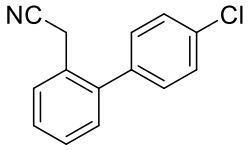


**2-(4'-Chloro-[1, 1'-biphenyl]-2-yl)acetonitrile (74):** Prepared following the general procedure C as a colourless liquid, yield 55%. **$^{1}$H NMR** (400 MHz, $CDCl_3$) δ ppm: 3.60 (s, 2H), 7.23-7.27 (m, 3H), 7.39-7.44 (m, 4H), 7.53-7.54 (d, $J$ = 6.57 Hz, 1H). **$^{13}$C NMR** (100 MHz, $CDCl_3$) δ ppm: 22.0, 118.0, 127.7, 128.4, 128.6, 128.9, 129.1, 130.3, 130.4, 134.0, 138.3, 140.6.

### 5.5.15 Synthesis of 2-(4'-methyl-[1, 1'-biphenyl]-2-yl)acetonitrile (72).

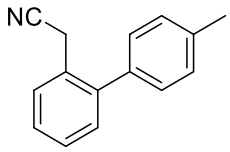


**2-(4'-Methyl-[1, 1'-biphenyl]-2-yl)acetonitrile (72):** Compound **72** was prepared following general procedure C as a colourless liquid, yielding 92%. **$^{1}$H NMR** (400 MHz, $CDCl_3$) δ ppm: 2.46 (s, 3H), 3.66 (s, 2H), 7.21-7.23 (d, *J* = 8.01 Hz, 2H), 7.29-7.32 (m, 3H), 7.40-7.42 (m, 2H), 7.56-7.59 (m, 1H). **$^{13}$C NMR** (100 MHz, $CDCl_3$) δ ppm: 21.2, 22.3, 118.4, 127.9, 128.0, 128.2, 128.8, 128.9, 129.4, 130.5, 137.0, 137.5, 141.9.

## 5.6 Synthesis of Tetrazole

### 5.6.1 General procedure D

Nitrile (1 mmol), sodium azide (1 mmol), zinc bromide (2 mmol), ammonium chloride (1 mmol), and water (5 mL) were added in a 50 mL round-bottomed flask with a magnetic stirrer bar then a condenser was placed with the rubber septum as the reaction was refluxed for 20 hours. After cooling the mixture, hydrochloric acid (3 M) was added dropwise until the pH was 4 then ethyl acetate (30 mL x 2) was added for extraction. Magnesium sulphate was used to dry the organic layer after brine wash filtered with gravitation filtration then concentrated under vacuum. Hexane (70%): ethyl acetate (30%) and ethyl acetate (100%) elute were used to purify the product.

### 5.6.2 Synthesis of 5-phenyl-1*H*-tetrazole (44)

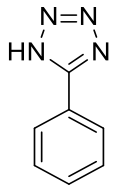


**5-Phenyl-1*H*-tetrazole (44):** Following the general procedure D, the compound was afforded as a 5-phenyl-1H-tetrazole white solid (61%). **$^{1}$H NMR** (400 MHz, DMSO) δ ppm: 7.60-7.61 (m, 3H), 8.03-8.05 (m, 2H). **$^{13}$C NMR** (100 MHz, DMSO) δ ppm: 124.7, 127.4, 129.8, 131.6, 155.8.

### 5.6.3 Synthesis of 5-(2-bromobenzyl)-1*H*-tetrazole (77)

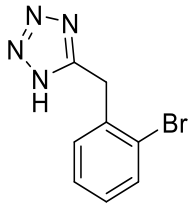


**5-(2-Bromobenzyl)-1*H*-tetrazole (77):** Following the General procedure D, the compound was produced as a white solid with 42% yield. **$^{1}$H NMR** (400 MHz, DMSO) δ ppm: 4.39 (s, 2H), 7.23-7.26 (m, 1H), 7.37-7.38 (d, *J* = 4.17 Hz, 2H), 7.62-7.64 (d, *J* = 7.84 Hz, 1H), **$^{13}$C NMR** (100 MHz, DMSO) δ ppm: 30.2, 124.3, 128.5, 129.8, 131.9, 133.2, 135.6, 154.9.

### 5.6.4 General procedure E

Nitrile (1 mmol), sodium azide (1 mmol), zinc bromide (2 mmol), ammonium chloride (1 mmol), DMF (0.5 mL), and water (5 mL) were added in a 50 mL round-bottomed flask with a magnetic stirrer bar then a condenser was placed with the rubber septum as the reaction was refluxed for 20 hours. After cooling the mixture, hydrochloric acid (3 M) was added dropwise until the pH was 4 then ethyl acetate (30 mL x 2) was added for extraction. Magnesium sulphate was used to dry the organic layer after brine wash filtered with gravitation filtration then concentrated under vacuum. Hexane (70%): ethyl acetate (30%) and ethyl acetate (100%) elute were used to purify the product.

### 5.6.5 Synthesis of 5-(4'-chloro-[1, 1'-biphenyl]-2-yl)-1*H*-tetrazole (84)

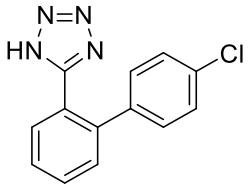


**5-(4'-Chloro-[1, 1'-biphenyl]-2-yl)-1*H*-tetrazole (84)**. Following general procedure E, the compound **84** was synthesised affording yellow liquid with 56% yield. **$^{1}$H NMR** (400 MHz, DMSO) δ ppm: 7.11-7.13 (d, *J* = 8.80 Hz, 2H), 7.37-7.39(d, *J* = 8.80 Hz, 2H), 7.54-7.62 (m, 2H), 7.68-7.71 (m, 2H). **$^{13}$C NMR** (100 MHz, DMSO) δ ppm: 123.8, 128.6, 128.7, 131.0, 131.0, 131.1, 131.6, 132.9, 138.6, 140.6, 162.7. **HR-ESI-(-)-MS**, *m/z*: 255.0432 (calculated for $C_{13}H_8N_4Cl$, 255.0437).

### 5.6.6 Synthesis of 5-(4'-methoxy-[1, 1'-biphenyl]-2-yl)-1*H*-tetrazole (82)

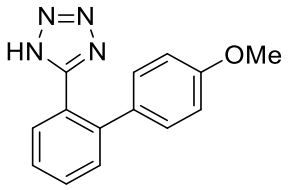


**5-(4'-Methoxy-[1, 1'-biphenyl]-2-yl)-1*H*-tetrazole (82)**: Following the general procedure E, [160] cream wax was afforded, yielding 21%. **$^{1}$H NMR** (400 MHz, DMSO) δ ppm: 3.74 (s, 3H), 6.85-6.88 (d, *J* = 8.87 Hz, 2H), 7.00-7.02 (m, 2H), 7.51-7.54 (m, 2H), 7.61-7.65 (m, 2H). **$^{13}$C NMR** (100 MHz, DMSO) δ ppm: 55.5, 114.2, 123.7, 127.7, 130.4, 130.9, 131.0, 131.5, 131.8, 141.6, 159.1. **HR-ESI-(-)-MS**, *m/z*: 251.0926 (calculated for $C_{14}H_{11}N_4O$, 251.0933).

### 5.6.7 Synthesis of 5-(4'-methyl-[1, 1'-biphenyl]-2-yl)-1*H*-tetrazole (80)

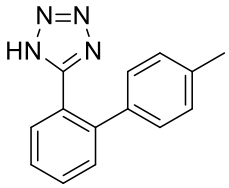


**5-(4'-Methyl-[1, 1'-biphenyl]-2-yl)-1*H*-tetrazole (80)**: Following general procedure E, [161] a white solid was produced, yielding 15%. **$^{1}$H NMR** (400 MHz, DMSO) δ ppm: 2.28 (s, 3H), 6.96-6.98 (d, *J* = 8.36 Hz, 2H), 7.10-7.12 (d, *J* = 7.84 Hz, 2H), 7.52-7.56 (m, 2H), 7.62-7.67 (m, 2H). **$^{13}$C NMR** (100 MHz, DMSO) δ ppm: 21.0, 123.8, 127.9, 129.1, 129.3, 130.9, 131.0, 131.5, 136.7, 137.2, 141.9. **HR-ESI-(-)-MS**, *m/z*: 235.0989 (calculated for $C_{14}H_{11}N_4$, 235.0984).

### 5.6.8 Synthesis of 5-([1, 1'-biphenyl]-2-yl)-1*H*-tetrazole (76)

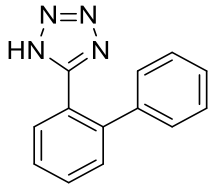


**5-([1, 1'-Biphenyl]-2-yl)-1*H*-tetrazole (76):** Following the general procedure E, [162] white solid (33%) was afforded. **$^{1}$H NMR** (400 MHz, DMSO) δ ppm: 7.08-7.10 (m, 2H), 7.29-7.31 (m, 3H), 7.54-7.59 (m, 2H), 7.65-7.68 (m, 2H). **$^{13}$C NMR** (100 MHz, DMSO) δ ppm: 123.4, 127.4, 128.2, 128.7, 130.5 (d), 131.0, 139.2, 141.5, 155.0. **HR-ESI-(-)-MS**, *m/z*: 221.0826 (calculated for $C_{13}H_9N_4$, 221.0827).

### 5.6.9 Synthesis of 5-(4'-fluoro-[1, 1'-biphenyl]-2-yl)-1*H*-tetrazole (83)

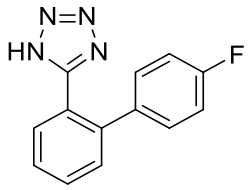


**5-(4'-Fluoro-[1, 1'-biphenyl]-2-yl)-1*H*-tetrazole (83):** Prepared following the general procedure E, yellow liquid, yield 42%. **$^{1}$H NMR** (400 MHz, DMSO) δ ppm: 7.13-7.15 (m, 4H), 7.53-7.56 (m, 2H), 7.58-7.60 (m, 2H), 7.66-7.70 (m, 2H). **$^{13}$C NMR** (100 MHz, DMSO) δ ppm: 115.4, 115.7, 124.0, 128.3, 131.0, 131.1, 131.2, 131.3, 131.5, 136.1 (d), 140.9, 160.9, 163.3. **HR-ESI-(-)-MS**, *m/z*: 239.0732 (calculated for $C_{13}H_8N_4F$, 239.0733).

### 5.6.10 Synthesis of 5-(4'-(trifluoromethyl)-[1, 1'-biphenyl]-2-yl)-1*H*-tetrazole (81)

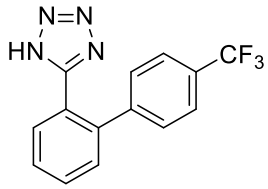


**5-(4'-(Trifluoromethyl)-[1, 1'-biphenyl]-2-yl)-1*H*-tetrazole (81):** Following the general procedure E, [163] compound **81** was afforded as a yellow liquid, yield 24%.**$^{1}$H NMR** (400 MHz, DMSO) δ ppm: 7.32-7.34 (d, *J* = 8.18 Hz, 2H), 7.58-7.60 (m, 1H), 7.62-7.72 (m, 4H), 7.74-7.76 (m, 1H). **$^{13}$C NMR** (100 MHz, DMSO) δ ppm: 123.4, 125.3 (d, CF), 126.1, 127.9, 128.7, 130.2, 130.8, 131.0, 140.2, 144.6. **HR-ESI-(-)-MS**, *m/z*: 289.0709 (calculated for $C_{14}H_8N_4F_3$, 289.0701).

### 5.6.11 Synthesis of 5-(4'-bromo-[1, 1'-biphenyl]-2-yl)-1*H*-tetrazole (85)

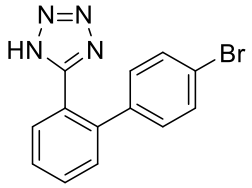


**5-(4'-Bromo-[1, 1'-biphenyl]-2-yl)-1*H*-tetrazole (85):** Compound **85** was produced following the general procedure E. White wax, yield 21%. **$^{1}$H NMR** (400 MHz, DMSO) δ ppm: 7.03-7.06 (d, *J* = 8.03 Hz, 2H), 7.49-7.52 (m, 2H), 7.53-7.62 (m, 2H), 7.67-7.71 (m, 2H). **$^{13}$C NMR** (100

MHz, DMSO) δ ppm: 121.5, 123.8, 128.6, 131.0, 131.0, 131.4, 131.6, 139.0, 140.6. **HR-ESI-(-)-MS**, *m/z*: 289.9930 (calculated for $C_{13}H_8N_4Br$, 298.9932).

### 5.6.12 Synthesis of 5-(1, 1'-biphenyl]-2-ylmethyl)-1*H*-tetrazole (86)

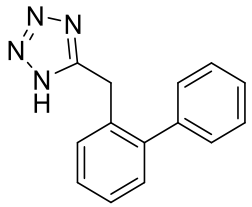

**5-(1, 1'-Biphenyl]-2-ylmethyl)-1H-tetrazole (85):** Following the general procedure E, a white solid was synthesised (14%). **$^1$H NMR** (400 MHz, DMSO) δ ppm: 4.20 (s, 2H), 7.25-7.27 (m, 2H), 7.30-7.33 (m, 2H), 7.34-7.38 (m, 3H), 7.40-7.44 (m, 2H). **$^{13}$C NMR** (100 MHz, DMSO) δ ppm: 27.4, 127.7, 128.2, 129.4, 130.2, 130.5, 133.4, 140.7, 142.0. **HR-ESI-(-)-MS**, *m/z*: 235.0978 (calculated for $C_{14}H_{11}N_4$, 235.0984).

### 5.6.13 Synthesis of 5-((4'-methyl-[1, 1'-biphenyl]-2-yl)methyl)-1*H*-tetrazole (78)

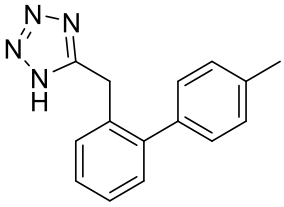

**5-((4'-Methyl-[1, 1'-biphenyl]-2-yl)methyl)-1*H*-tetrazole (78):** Prepared following the general procedure E. White solid, yield 59%. **$^1$H NMR** (400 MHz, DMSO) δ ppm: 2.33 (s, 3H), 4.20 (s, 2H), 7.22-7.27 (m, 6H), 7.32-7.34 (m, 2H). **$^{13}$C NMR** (100 MHz, DMSO) δ ppm: 21.2, 27.3, 127.6, 128.0, 129.3, 129.4, 130.1, 130.6, 133.4, 136.9, 137.8, 142.0, 155.0. **HR-ESI-(-)-MS**, *m/z*: 249.1135 (calculated for $C_{15}H_{13}N_4$, 249.1140).

### 5.6.14 Synthesis of 5-((4'-chloro-[1, 1'-biphenyl]-2-yl)methyl)-1*H*-tetrazole (89)

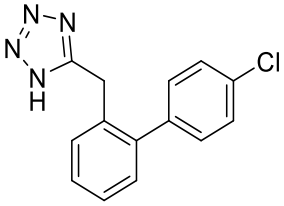

**5-((4'-Chloro-[1, 1'-biphenyl]-2-yl)methyl)-1*H*-tetrazole (88):** Following the general procedure E, the compound **88** was afforded as a white solid (15%). **$^{1}$H NMR** (400 MHz, DMSO) δ ppm: 4.19 (s, 2H), 7.24-7.30 (m, 2H), 7.32-7.39 (m, 4H), 7.45-7.48 (d, *J* = 8.52 Hz, 2H). **$^{13}$C NMR** (100 MHz, DMSO) δ ppm: 27.4, 127.8, 128.5, 128.8, 130.4, 130.5, 131.2, 132.6, 133.5, 139.5, 140.7. **HR-ESI-(-)-MS**, *m/z*: 269.0589 (calculated for $C_{14}H_{10}N_4Cl$, 269.0594), melting point: 199.4-200.1°C.

### 5.6.15 Synthesis of 5-((4'-fluoro-[1, 1'-biphenyl]-2-yl)methyl)-1*H*-tetrazole (79)

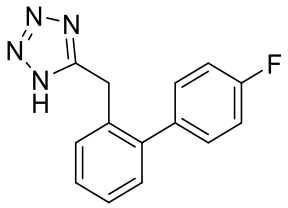

**5-((4'-Fluoro-[1, 1'-biphenyl]-2-yl)methyl)-1*H*-tetrazole (79):** Afforded following the general procedure E. White solid, yield 29%. **$^{1}$H NMR** (400 MHz, DMSO) δ ppm: 4.19 (s, 2H), 7.21-7.29 (m, 4H), 7.32-7.37 (m, 4H). **$^{13}$C NMR** (100 MHz, DMSO) δ ppm: 26.9, 115.0, 115.2, 127.2, 127.9, 129.8, 130.1, 130.7, 130.8, 130.9, 133.1, 136.5 (d), 410.5, 160.2, 162.6. **HR-ESI-(-)-MS**, *m/z*: 253.0892 (calculated for $C_{14}H_{10}N_4F$, 253.0889).

### 5.6.16 Synthesis of 5-((4'-trifluoromethyl-[1, 1'-biphenyl]-2-yl)methyl)-1H-tetrazole (87)

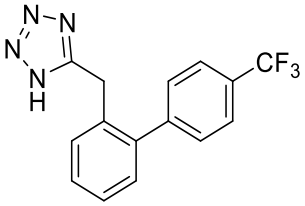

**5-((4'-Trifluoromethyl-[1, 1'-biphenyl]-2-yl)methyl)-1*H*-tetrazole (87):** Following the general procedure E, the compound **87** was afforded as a white solid (16%). **$^{1}$H NMR** (400 MHz, DMSO) δ ppm: 4.20 (s, 2H), 7.28-7.34 (m, 2H), 7.37-7.42 (m, 2H), 7.54-7.56 (d, *J* = 8.03 Hz, 2H), 7.76-7.78 (d, *J* = 8.03 Hz, 2H). **$^{13}$C NMR** (100 MHz, DMSO) δ ppm: 27.4, 125.6, 125.6, 125.7, 127.9, 128.1, 128.5, 128.9, 130.3, 130.4, 130.5 (d), 133.5, 140.6, 144.9. **HR-ESI-(-)-MS**, *m/z*: 303.0857 (calculated for $C_{15}H_{10}N_4F_3$, 303.0858).

### 5.6.17 Synthesis of 5-((4'-methoxy-[1, 1'-biphenyl]-2-yl)methyl)-1*H*-tetrazole (88)

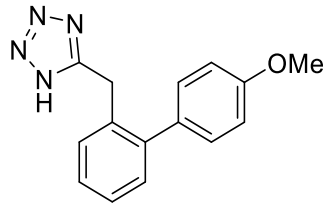


**5-((4'-Methoxy-[1, 1'-biphenyl]-2-yl)methyl)-1*H*-tetrazole (88):** Produced following the general procedure E. White solid, yield 17%. **$^{1}$H NMR** (400 MHz, DMSO) δ ppm: 3.77 (s, 3H), 4.19 (s, 2H), 6.95-6.98 (m, 2H), 7.21-7.25 (m, 4H), 7.30-7.32 (m, 2H). **$^{13}$C NMR** (100 MHz, DMSO) δ ppm: 27.4, 55.5, 114.2, 127.6, 130.1, 130.5, 130.7, 132.9, 133.5, 141.7, 158.9. **HR-ESI-(-)-MS**, *m/z*: 265.1081 (calculated for $C_{15}H_{14}N_4O$, 265.1089), melting points: 185.6-186.1°C.

# References


(1) Alharbi, F.; Vakanski, A. *J. Bioeng.* **2023**, *10* (2), 173.

(2) Miller, K. D.; Ortiz, A. P.; Pinheiro, P. S.; Bandi, P.; Minihan, A.; Fuchs, H. E.; Martinez Tyson, D.; Tortolero-Luna, G.; Fedewa, S. A.; Jemal, A. M. *CA Cancer J Clin* **2021**, *71* (6), 466-487.

(3) Chhikara, B. S.; Parang, K. *Chem. Biol. Lett.* **2023**, *10* (1), 451-451.

(4) Allison, K. H.; Hammond, M. E. H.; Dowsett, M.; McKernin, S. E.; Carey, L. A.; Fitzgibbons, P. L.; Hayes, D. F.; Lakhani, S. R.; Chavez-MacGregor, M.; Perlmutter, J. **2020**.

(5) Wolff, A. C.; Hammond, M. E. H.; Allison, K. H.; Harvey, B. E.; Mangu, P. B.; Bartlett, J. M.; Bilous, M.; Ellis, I. O.; Fitzgibbons, P.; Hanna, W. *Arch. Path. Lab.* **2018**, *142* (11), 1364-1382.

(6) Jordan, V. C. *Nat. Rev. Drug Discov.* **2003**, *2* (3), 205-213.

(7) Wynn, C. S.; Tang, S.-C. *Cancer Metastasis Rev.* **2022**, *41* (1), 193-209.

(8) da Silva, J. L.; Nunes, N. C. C.; Izetti, P.; de Mesquita, G. G.; de Melo, A. C. *Crit. Rev. Oncol. Hematol.* **2019**, 102855.

(9) Sung, H.; Ferlay, J.; Siegel, R. L.; Laversanne, M.; Soerjomataram, I.; Jemal, A.; Bray, F. *CA Cancer J Clin* **2021**, *71* (3), 209-249.

(10) Bray, F.; Parkin, D. M.; Gnangnon, F.; Tshisimogo, G.; Peko, J.-F.; Adoubi, I.; Assefa, M.; Bojang, L.; Awuah, B.; Koulibaly, M. *Lancet Oncol.* **2022**.

(11) Lehmann, B. D.; Jovanović, B.; Chen, X.; Estrada, M. V.; Johnson, K. N.; Shyr, Y.; Moses, H. L.; Sanders, M. E.; Pietenpol, J. A. *PloS one* **2016**, *11* (6).

(12) Fitzgerald, R. C.; Antoniou, A. C.; Fruk, L.; Rosenfeld, N. *Nat. Med.* **2022**, *28* (4), 666-677.

(13) Marsolier, J.; Prompsy, P.; Durand, A.; Lyne, A.-M.; Landragin, C.; Trouchet, A.; Bento, S. T.; Eisele, A.; Foulon, S.; Baudre, L. *Nat. Genet.* **2022**, *54* (4), 459-468.

(14) Smolarz, B.; Nowak, A. Z.; Romanowicz, H. *Cancers* **2022**, *14* (10), 2569.

(15) Lehmann, B. D.; Bauer, J. A.; Chen, X.; Sanders, M. E.; Chakravarthy, A. B.; Shyr, Y.; Pietenpol, J. A. *JCI* **2011**, *121* (7), 2750-2767.

(16) Burstein, M. D.; Tsimelzon, A.; Poage, G. M.; Covington, K. R.; Contreras, A.; Fuqua, S. A.; Savage, M. I.; Osborne, C. K.; Hilsenbeck, S. G.; Chang, J. C. *Clin. Cancer Investig. J.* **2015**, *21* (7), 1688-1698.

(17) Wahba, H. A.; El-Hadaad, H. A. *Cancer Biol. Med.* **2015**, *12* (2), 106.

(18) Gerratana, L.; Basile, D.; Buono, G.; De Placido, S.; Giuliano, M.; Minichillo, S.; Coinu, A.; Martorana, F.; De Santo, I.; Del Mastro, L. *Cancer Treat. Rev.* **2018**, *68*, 102-110.
(19) O'Meara, T. A.; Tolaney, S. M. *Oncotarget* **2021**, *12* (5), 394.
(20) Schmid, P.; Adams, S.; Rugo, H. S.; Schneeweiss, A.; Barrios, C. H.; Iwata, H.; Diéras, V.; Hegg, R.; Im, S.-A.; Shaw Wright, G. *NEJM.* **2018**, *379* (22), 2108-2121.
(21) Cortes, J.; Cescon, D. W.; Rugo, H. S.; Nowecki, Z.; Im, S.-A.; Yusof, M. M.; Gallardo, C.; Lipatov, O.; Barrios, C. H.; Holgado, E. *Lancet* **2020**, *396* (10265), 1817-1828.
(22) Liao, M.; Qin, R.; Huang, W.; Zhu, H.-P.; Peng, F.; Han, B.; Liu, B. *J. Hematol. Oncol.* **2022**, *15* (1), 1-44.
(23) Moghtaderi, H.; Sepehri, H.; Delphi, L.; Attari, F. *Bioimpacts* . **2018**, *8* (3), 185.
(24) Pirali, M.; Taheri, M.; Zarei, S.; Majidi, M.; Ghafouri, H. *Int. J. Biol. Macromol.* **2020**, *164*, 3369-3375.
(25) Mohs, R. C.; Greig, N. H. *Alzheimer's Dement.: Transl. Res. Clin. Interv.* **2017**, *3* (4), 651-657.
(26) Hughes, J. P.; Rees, S.; Kalindjian, S. B.; Philpott, K. L. *Br. J. Pharmacol.* **2011**, *162* (6), 1239-1249.
(27) Hoffmann, R. D.; Gohier, A.; Pospisil, P.; Wiley-VCH, **2013**.
(28) Gashaw, I.; Ellinghaus, P.; Sommer, A.; Asadullah, K. *Drug Discov. Today* **2011**, *16* (23-24), 1037-1043.
(29) Sieber, S. A.; Cravatt, B. F. *ChemComm* **2006**, (22), 2311-2319.
(30) Deng, H.; Lei, Q.; Wu, Y.; He, Y.; Li, W. *Eur. J. Med. Chem.* **2020**, 112151.
(31) Honore, P.; Kage, K.; Mikusa, J.; Watt, A. T.; Johnston, J. F.; Wyatt, J. R.; Faltynek, C. R.; Jarvis, M. F.; Lynch, K. *J Pain* **2002**, *99* (1-2), 11-19.
(32) Willett, P.; Barnard, J. M.; Downs, G. M. *J. Chem. Inf. Comput.* **1998**, *38* (6), 983-996.
(33) Sperandio, O.; Petitjean, M.; Tufféry, P. *Nucleic Acids Res.* **2009**, *37* (suppl_2), W504-W509.
(34) Kroemer, R. T. *Curr. Protein Pept. Sci.* **2007**, *8* (4), 312-328.
(35) Hajare, A. A.; Salunkhe, S. S.; Mali, S. S.; Gorde, S. S.; Nadaf, S. J.; Pishawikar, S. A. *Am. J. PharmTech. Res* **2013**, *4*, 112-129.
(36) Macarron, R.; Banks, M. N.; Bojanic, D.; Burns, D. J.; Cirovic, D. A.; Garyantes, T.; Green, D. V.; Hertzberg, R. P.; Janzen, W. P.; Paslay, J. W. *Nat. Rev. Drug Discov.* **2011**, *10* (3), 188-195.

(37) Cherry, M.; Mitchell, T.; John Wiley & Sons: Chichester, **2008**.

(38) Lipinski, C. A.; Lombardo, F.; Dominy, B. W.; Feeney, P. J. *Adv. Drug Deliv. Rev.* **1997**, *23* (1-3), 3-25.

(39) Kirsch, P.; Hartman, A. M.; Hirsch, A. K.; Empting, M. *Mol.* **2019**, *24* (23), 4309.

(40) Bon, M.; Bilsland, A.; Bower, J.; McAulay, K. *Mol. Oncol.* **2022**, *16* (21), 3761-3777.

(41) Kuntz, I.; Chen, K.; Sharp, K.; Kollman, P. *PNAS USA* **1999**, *96* (18), 9997-10002.

(42) Hopkins, A. L.; Groom, C. R.; Alex, A. *Drug Discov. Today* **2004**, *9* (10), 430-431.

(43) Congreve, M.; Carr, R.; Murray, C.; Jhoti, H. *Drug Discov. Today* **2003**, *19* (8), 876-877.

(44) Jacoby, E.; Davies, J.; Blommers, M. J. *Curr Top Med Chem* . **2003**, *3* (1), 11-23.

(45) Blundell, T. L. *IUCrJ* **2017**, *4* (4), 308-321.

(46) Veale, C. G.; Mateos-Jimenez, M.; Vaaltyn, M. C.; Müller, R.; Makhubu, M. P.; Alhassan, M.; Beatriz, G.; Albericio, F.; Mackay, C. L.; Edkins, A. L. *ChemComm* **2021**, *57* (83), 10919-10922.

(47) Erlanson, D. A. In *Fragment-based drug discovery and X-ray crystallography*, Springer, **2011**; pp 1-32.

(48) Price, A. J.; Howard, S.; Cons, B. D. *Essays Biochem.* **2017**, *61* (5), 475-484.

(49) Bollag, G.; Tsai, J.; Zhang, J.; Zhang, C.; Ibrahim, P.; Nolop, K.; Hirth, P. *Nat. Rev. Drug Discov.* **2012**, *11* (11), 873-886.

(50) Kim, A.; Cohen, M. S. *Expert Opin Drug Discov.* **2016**, *11* (9), 907-916. DOI: 10.1080/17460441.2016.1201057.

(51) Murray, C. W.; Newell, D. R.; Angibaud, P. *MedChemComm* **2019**, *10* (9), 1509-1511. DOI: 10.1039/c9md90044f.

(52) Schoepfer, J.; Jahnke, W.; Berellini, G.; Buonamici, S.; Cotesta, S.; Cowan-Jacob, S. W.; Dodd, S.; Drueckes, P.; Fabbro, D.; Gabriel, T.  ACS Publications: **2018**.

(53) Fairbrother, W. J.; Leverson, J. D.; Sampath, D.; Souers, A. J.; **2019**.

(54) Benner, B.; Good, L.; Quiroga, D.; Schultz, T. E.; Kassem, M.; Carson, W. E.; Cherian, M. A.; Sardesai, S.; Wesolowski, R. *Drug Des Devel Ther.* **2020**, *14*, 1693.

(55) Lanman, B. A.; Allen, J. R.; Allen, J. G.; Amegadzie, A. K.; Ashton, K. S.; Booker, S. K.; Chen, J. J.; Chen, N.; Frohn, M. J.; Goodman, G.; Kopecky, D. J.; Liu, L.; Lopez, P.; Low, J. D.; Ma, V.; Minatti, A. E.; Nguyen, T. T.; Nishimura, N.; Pickrell, A. J.; Reed, A. B.; Shin, Y.; Siegmund, A. C.; Tamayo, N. A.; Tegley, C. M.; Walton, M. C.; Wang, H.-L.; Wurz, R. P.; Xue,

M.; Yang, K. C.; Achanta, P.; Bartberger, M. D.; Canon, J.; Hollis, L. S.; McCarter, J. D.; Mohr, C.; Rex, K.; Saiki, A. Y.; San Miguel, T.; Volak, L. P.; Wang, K. H.; Whittington, D. A.; Zech, S. G.; Lipford, J. R.; Cee, V. J. *J. Med. Chem.* **2020**, *63* (1), 52-65. DOI: 10.1021/acs.jmedchem.9b01180.

(56) Beddell, C.; Goodford, P.; Norrington, F.; Wilkinson, S.; Wootton, R. *Br. J. Pharmacol.* **1976**, *57* (2), 201-209.

(57) Subramanian, E.; Swan, I.; Liu, M.; Davies, D.; Jenkins, J.; Tickle, I.; Blundell, T. *PNAS USA* **1977**, *74* (2), 556-559.

(58) Blundell, T.; Sibanda, B. L.; Pearl, L. *Nature* **1983**, *304* (5923), 273-275.

(59) Lapatto, R.; Blundell, T.; Hemmings, A.; Overington, J.; Wilderspin, A.; Wood, S.; Merson, J. R.; Whittle, P. J.; Danley, D. E.; Geoghegan, K. F. *Nature* **1989**, *342* (6247), 299-302.

(60) Wlodawer, A.; Miller, M.; Jaskolski, M.; Sathyanarayana, B. K.; Baldwin, E.; Weber, I. T.; Selk, L. M.; Clawson, L.; Schneider, J.; Kent, S. *Science* **1989**, *245* (4918), 616-621.

(61) Tsai, J.; Lee, J. T.; Wang, W.; Zhang, J.; Cho, H.; Mamo, S.; Bremer, R.; Gillette, S.; Kong, J.; Haass, N. K. *PNAS USA* **2008**, *105* (8), 3041-3046.

(62) Shoichet, B. K.; Stroud, R. M.; Santi, D. V.; Kuntz, I. D.; Perry, K. M. *Science* **1993**, *259* (5100), 1445-1450.

(63) Erickson, J. A.; Jalaie, M.; Robertson, D. H.; Lewis, R. A.; Vieth, M. *J. Med. Chem.* **2004**, *47* (1), 45-55.

(64) Chau, P.-L.; Dean, P. *J. Comput. Aided Mol. Des. J COMPUT AID MOL DES* **1992**, *6* (4), 385-396.

(65) Verlinde, C. L.; Rudenko, G.; Hol, W. G. *J. Comput. Aided Mol. Des. J COMPUT AID MOL DES* **1992**, *6* (2), 131-147.

(66) Stultz, C. M.; Karplus, M. *Proteins: Structure, Function, and Bioinformatics* **2000**, *40* (2), 258-289.

(67) Erlanson, D. A.; McDowell, R. S.; O'Brien, T. *J. Med. Chem.* **2004**, *47* (14), 3463-3482.

(68) Sheet, P. F.

(69) Shaukat, Z.; Aiman, S.; Li, C.-H. *WJV, World J Virol* **2021**, *10* (6), 288.

(70) Garland, W.; Benezra, R.; Chaudhary, J. *Annu Rep Med Chem* . **2013**, *48*, 227-245.

(71) Rao, V. S.; Srinivas, K.; Sujini, G.; Kumar, G. *J Proteomics J PROTEOMICS* **2014**, *2014*.

(72) Surade, S.; Blundell, T. L. *Chem. Biol.* **2012**, *19* (1), 42-50.

(73) Jeyachandran, S.; Chellapandian, H.; Park, K.; Kwak, I.-S. *J. Antioxid. Act.* **2023**, *12* (7), 1444.

(74) Braun, P.; Gingras, A. C. *J Proteomics* **2012**, *12* (10), 1478-1498.

(75) Edkins, A. L.; Boshoff, A. In *Heat Shock Proteins of Malaria*, Springer, **2021**; pp 11-73.

(76) Macario, A. J.; de Macario, E. C. *NEJM.* **2005**, *353* (14), 1489-1501.

(77) Powers, M. V.; Workman, P. *FEBS Lett.* **2007**, *581* (19), 3758-3769.

(78) Whitesell, L.; Lindquist, S. L. *Nat. Rev. Cancer.* **2005**, *5* (10), 761-772.

(79) Neckers, L.; Workman, P. *Clin. Cancer Investig. J.* **2012**, *18* (1), 64-76.

(80) Garcia-Carbonero, R.; Carnero, A.; Paz-Ares, L. *Lancet Oncol.* **2013**, *14* (9), e358-e369.

(81) Hartson, S. D.; Matts, R. L. *Biochim Biophys Acta Mol Cell Res BBA-MOL CELL RES* **2012**, *1823* (3), 656-667.

(82) Picard, D. *Biochim Biophys Acta Mol Cell Res BBA-MOL CELL RES* **2012**, *1823* (3), 605-606.

(83) Darby, J. F.; Vidler, L. R.; Simpson, P. J.; Al-Lazikani, B.; Matthews, S. J.; Sharp, S. Y.; Pearl, L. H.; Hoelder, S.; Workman, P. *Sci. Rep.* **2020**, *10* (1), 1-13.

(84) Samarasinghe, B.; Wales, C. T.; Taylor, F. R.; Jacobs, A. T. *Biochem. Pharmacol.* **2014**, *87* (3), 445-455.

(85) Zhang, H.; Burrows, F. *J. Mol. Med.* **2004**, *82* (8), 488-499.

(86) Drysdale, M. J.; Brough, P. A.; Massey, A.; Jensen, M. R.; Schoepfer, J. *Curr. opin. drug discov.* **2006**, *9* (4), 483-495.

(87) Whitesell, L.; Bagatell, R.; Falsey, R. *Curr. Cancer Drug Targets* **2003**, *3* (5), 349-358.

(88) Edkins, A. L. *Heat shock protein inhibitors* **2016**, 21-54.

(89) Seo, Y. H. *J. Cancer Prev.* **2015**, *20* (1), 5.

(90) Kubota, H.; Yamamoto, S.; Itoh, E.; Abe, Y.; Nakamura, A.; Izumi, Y.; Okada, H.; Iida, M.; Nanjo, H.; Itoh, H. *Cell Stress and Chaperones* **2010**, *15* (6), 1003-1011.

(91) Smith, M. C.; Gestwicki, J. E. *Expert Rev. Mol. Med.* **2012**, *14*.

(92) Onuoha, S.; Coulstock, E.; Grossmann, J.; Jackson, S. *J. Mol. Biol.* **2008**, *379* (4), 732-744.

(93) Brinker, A.; Scheufler, C.; Von Der Mülbe, F.; Fleckenstein, B.; Herrmann, C.; Jung, G.; Moarefi, I.; Hartl, F. U. *J. Biol. Chem.* **2002**, *277* (22), 19265-19275.

(94) Chen, S.; Smith, D. F. *J. Biol. Chem.* **1998**, *273* (52), 35194-35200.

(95) Morishima, Y.; Kanelakis, K. C.; Silverstein, A. M.; Dittmar, K. D.; Estrada, L.; Pratt, W. B. *J. Biol. Chem.* **2000**, *275* (10), 6894-6900.

(96) Bose, S.; Weikl, T.; Bügl, H.; Buchner, J. *Science* **1996**, *274* (5293), 1715-1717.

(97) Terasawa, K.; Minami, M.; Minami, Y. *J. Biochem.* **2005**, *137* (4), 443-447.

(98) Longshaw, V. M.; Baxter, M.; Prewitz, M.; Blatch, G. L. *Eur. J. Cell Biol.* **2009**, *88* (3), 153-166.

(99) Beraldo, F. H.; Soares, I. N.; Goncalves, D. F.; Fan, J.; Thomas, A. A.; Santos, T. G.; Mohammad, A. H.; Roffé, M.; Calder, M. D.; Nikolova, S. *FASEB J.* **2013**, *27* (9), 3594-3607.

(100) Ardi, V. C.; Alexander, L. D.; Johnson, V. A.; McAlpine, S. R. *ACS Chem. Biol* **2011**, *6* (12), 1357-1366.

(101) Horibe, T.; Kawamoto, M.; Kohno, M.; Kawakami, K. *J. Biosci. Bioeng. J BIOSCI BIOENG* **2012**, *114* (1), 96-103.

(102) Horibe, T.; Kohno, M.; Haramoto, M.; Ohara, K.; Kawakami, K. *J. Transl. Med.* **2011**, *9* (1), 1-12.

(103) Horibe, T.; Torisawa, A.; Kohno, M.; Kawakami, K. *Mol. Cancer* **2012**, *11* (1), 1-11.

(104) Pimienta, G.; Herbert, K. M.; Regan, L. *Mol. Pharmaceutics.* **2011**, *8* (6), 2252-2261.

(105) Rahimi, M. N.; McAlpine, S. R. *ChemComm* **2019**, *55* (6), 846-849.

(106) Wei, C. X.; Bian, M.; Gong, G. H. *Mol.* **2015**, *20* (4), 5528-5553. DOI: 10.3390/molecules20045528.

(107) Demko, Z. P.; Sharpless, K. B. *J. Org. Chem.* **2001**, *66* (24), 7945-7950. DOI: 10.1021/jo010635w.

(108) Vaaltyn, M. C.; Mateos-Jimenez, M.; Müller, R.; Mackay, C. L.; Edkins, A. L.; Clarke, D. J.; Veale, C. G. *ChemBioChem* **2022**, *23* (21), e202200322.

(109) Irvin Jr, W. J.; Carey, L. A. *Eur. J. Cancer* **2008**, *44* (18), 2799-2805.

(110) Liedtke, C.; Mazouni, C.; Hess, K. R.; André, F.; Tordai, A.; Mejia, J. A.; Symmans, W. F.; Gonzalez-Angulo, A. M.; Hennessy, B.; Green, M. *J. Clin. Oncol.* **2008**, *26* (8), 1275-1281.

(111) Tan, D. S.; Marchió, C.; Jones, R. L.; Savage, K.; Smith, I. E.; Dowsett, M.; Reis-Filho, J. S. *Breast cancer research and treatment* **2008**, *111*, 27-44.

(112) Foulkes, W. D.; Smith, I. E.; Reis-Filho, J. S. *NEJM.* **2010**, *363* (20), 1938-1948.

(113) Scheufler, C.; Brinker, A.; Bourenkov, G.; Pegoraro, S.; Moroder, L.; Bartunik, H.; Hartl, F. U.; Moarefi, I. *Cell J.* **2000**, *101* (2), 199-210.

(114) Reddy, S. B.; Sinha, B. K.; Mukkanti, K.; Dandala, R. *Org Process Res Dev* **2009**, *6* (13), 1185-1189.

(115) Frija, L. M.; Fausto, R.; Loureiro, R. M.; Cristiano, M. L. S. *J Mol Catal A Chem* **2009**, *305* (1-2), 142-146.

(116) Quinn, D. J.; Haun, G. J.; Moura-Letts, G. *Tetrahedron Lett.* **2016**, *57* (34), 3844-3847.

(117) Rickborn, B.; Jensen, F. R. *J. Org. Chem.* **1962**, *27* (12), 4608-4610.

(118) Kusurkar, R.; Goswami, S.; Vyas, S. **2003**.

(119) Fang, W.-Y.; Qin, H.-L. *J. Org. Chem.* **2019**, *84* (9), 5803-5812.

(120) Zou, Y.; Liu, L.; Liu, J.; Liu, G. Future Science: **2020**; Vol. 12, pp 91-93.

(121) Wei, C.-X.; Bian, M.; Gong, G.-H. *Mol.* **2015**, *20* (4), 5528-5553.

(122) Ostrovskii, V.; Trifonov, R.; Popova, E. *Russ. Chem. Bull.* **2012**, *61*, 768-780.

(123) Yapuri, U.; Palle, S.; Gudaparthi, O.; Narahari, S. R.; Rawat, D. K.; Mukkanti, K.; Vantikommu, J. *Tetrahedron Lett.* **2013**, *54* (35), 4732-4734.

(124) Herr, R. J. *Bioorg. Med. Chem. BIOORGAN MED CHEM* **2002**, *10* (11), 3379-3393.

(125) Roh, J.; Vávrová, K.; Hrabálek, A. *EurJOC* **2012**, *2012* (31), 6101-6118.

(126) Demko, Z. P.; Sharpless, K. B. *The Journal of organic chemistry* **2001**, *66* (24), 7945-7950.

(127) Zhang, J.; Wang, S.; Ba, Y.; Xu, Z. *Eur. J. Med. Chem.* **2019**, *178*, 341-351.

(128) Gao, F.; Xiao, J.; Huang, G. *Eur. J. Med. Chem.* **2019**, *184*, 111744.

(129) Gao, C.; Chang, L.; Xu, Z.; Yan, X.-F.; Ding, C.; Zhao, F.; Wu, X.; Feng, L.-S. *Eur. J. Med. Chem.* **2019**, *163*, 404-412.

(130) Wang, S.-Q.; Wang, Y.-F.; Xu, Z. *Eur. J. Med. Chem.* **2019**, *170*, 225-234.

(131) Roh, J.; Karabanovich, G.; Vlčková, H.; Carazo, A.; Němeček, J.; Sychra, P.; Valášková, L.; Pavliš, O.; Stolaříková, J.; Klimešová, V. *Bioorg. Med. Chem. BIOORGAN MED CHEM* **2017**, *25* (20), 5468-5476.

(132) Zhan, P.; Li, Z.; Liu, X.; De Clercq, E. *Mini Rev Med Chem MINI-REV MED CHEM* **2009**, *9* (8), 1014-1023.

(133) Kushwaha, P.; Fatima, S.; Upadhyay, A.; Gupta, S.; Bhagwati, S.; Baghel, T.; Siddiqi, M.; Nazir, A.; Sashidhara, K. V. *Bioorganic Med. Chem. Lett. BIOORG MED CHEM LETT* **2019**, *29* (1), 66-72.

(134) Li, Y.; Pasunooti, K. K.; Li, R.-J.; Liu, W.; Head, S. A.; Shi, W. Q.; Liu, J. O. *J. Med. Chem.* **2018**, *61* (24), 11158-11168.

(135) Zhu, Y.; Ren, Y.; Cai, C. *Helv. Chim. Acta* **2009**, *92* (1), 171-175.
(136) Amantini, D.; Beleggia, R.; Fringuelli, F.; Pizzo, F.; Vaccaro, L. *J. Org. Chem.* **2004**, *69* (8), 2896-2898.
(137) Al-Huniti, M. H.; Rivera-Chávez, J.; Colón, K. L.; Stanley, J. L.; Burdette, J. E.; Pearce, C. J.; Oberlies, N. H.; Croatt, M. P. *Org. Lett.* **2018**, *20* (19), 6046-6050.
(138) Du, B.; Jiang, X.; Sun, P. *J. Org. Chem.* **2013**, *78* (6), 2786-2791.
(139) Li, Z.-L.; Wu, P.-Y.; Cai, C. *New J Chem* **2019**, *43* (8), 3462-3468.
(140) Pavia, D. L.; Lampman, G. M.; Kriz, G. S.; Vyvyan, J. A.; Cengage learning, **2014**.
(141) Hussain, I.; Capricho, J.; Yawer, M. A. *Adv. Synth. Catal. ADV SYNTH CATAL* **2016**, *358* (21), 3320-3349.
(142) Li, X.; Teng, Y.; Feng, F.; Hu, Q.; Yuan, Z. *ChemistrySelect* **2018**, *3* (21), 6022-6027.
(143) Zhang, C. X.; Zheng, G. J.; Bi, F. Q.; Li, Y. L. *Chin Chem Lett .* **2008**, *19* (7), 759-761.
(144) Ghosh, S.; Kumar, A. S.; Mehta, G. *Beilstein Journal of Organic Chemistry* **2010**, *6* (1), 27.
(145) Gorlova, O.; Colvin, S. M.; Brathwaite, A.; Menges, F. S.; Craig, S. M.; Miller, S. J.; Johnson, M. A. *Journal of The American Society for Mass Spectrometry* **2017**, *28* (11), 2414-2422.
(146) Liu, C.; Ni, Q.; Bao, F.; Qiu, J. *Green chemistry* **2011**, *13* (5), 1260-1266.
(147) Zhang, L.; Ang, G. Y.; Chiba, S. *Org. Lett.* **2010**, *12* (16), 3682-3685.
(148) Wolfe, J. P.; Singer, R. A.; Yang, B. H.; Buchwald, S. L. *J. Am. Chem. Soc.* **1999**, *121* (41), 9550-9561.
(149) Wang, H.; Wang, Y.; Han, Y.; Zhao, W.; Wang, X. *RSC advances* **2020**, *10* (2), 784-789.
(150) Zamani, L.; Mirjailli, B.; Zomorodian, K.; Zomorodian, S. *South African Journal of Chemistry* **2015**, *68*, 133-137.
(151) Chen, S.-Y.; Zacharias, M. *ACS Central Science* **2023**, *9* (5), 969-979.
(152) Van Der Spuy, J.; Kana, B. D.; Dirr, H. W.; Blatch, G. L. *Biochem. J. BIOCHEM J* **2000**, *345* (3), 645-651.
(153) Makumire, S.; Zininga, T.; Vahokoski, J.; Kursula, I.; Shonhai, A. *PloS one* **2020**, *15* (4), e0226657.
(154) Beckley, S. J.; Hunter, M. C.; Kituyi, S. N.; Wingate, I.; Chakraborty, A.; Schwarz, K.; Makhubu, M. P.; Rousseau, R. P.; Ruck, D. K.; de la Mare, J.-A. *Int. J. Mol. Sci.* **2020**, *21* (9), 3152.
(155) Bruker, A. *Search in*.

(156) Spek, A. L. *Acta Crystallogr. C Struct. Chem. ACTA CRYSTALLOGR C* **2015**, *71* (1), 9-18.
(157) Dolomanov, O. V.; Bourhis, L. J.; Gildea, R. J.; Howard, J. A.; Puschmann, H. *J. Appl. Crystallogr.* **2009**, *42* (2), 339-341.
(158) West, M. J.; Watson, A. J. *Org. Biomol. Chem.* **2019**, *17* (20), 5055-5059.
(159) Jaiswal, Y.; Kumar, Y.; Thakur, R.; Pal, J.; Subramanian, R.; Kumar, A. *J. Org. Chem.* **2016**, *81* (24), 12499-12505.
(160) Cousaert, N.; Willand, N.; Gesquière, J.-C.; Tartar, A.; Déprez, B.; Deprez-Poulain, R. *Tetrahedron Lett.* **2008**, *49* (17), 2743-2747.
(161) Behloul, C.; Bouchelouche, K.; Hadji, Y.; Benseghir, S.; Guijarro, D.; Najera, C.; Yus, M. *Synth.* **2016**, *48* (15), 2455-2460.
(162) Wang, H.; Zhao, W.; Du, J.; Wei, F.; Chen, Q.; Wang, X. *Appl. Organomet. Chem.* **2019**, *33* (10), e5132.
(163) Cousaert, N.; Toto, P.; Willand, N.; Deprez, B. *Tetrahedron Lett.* **2005**, *46* (38), 6529-6532.

# Appendix

**Appendix A1.1**: IR spectrum for 2-iodobenzonitrile **(47)**.

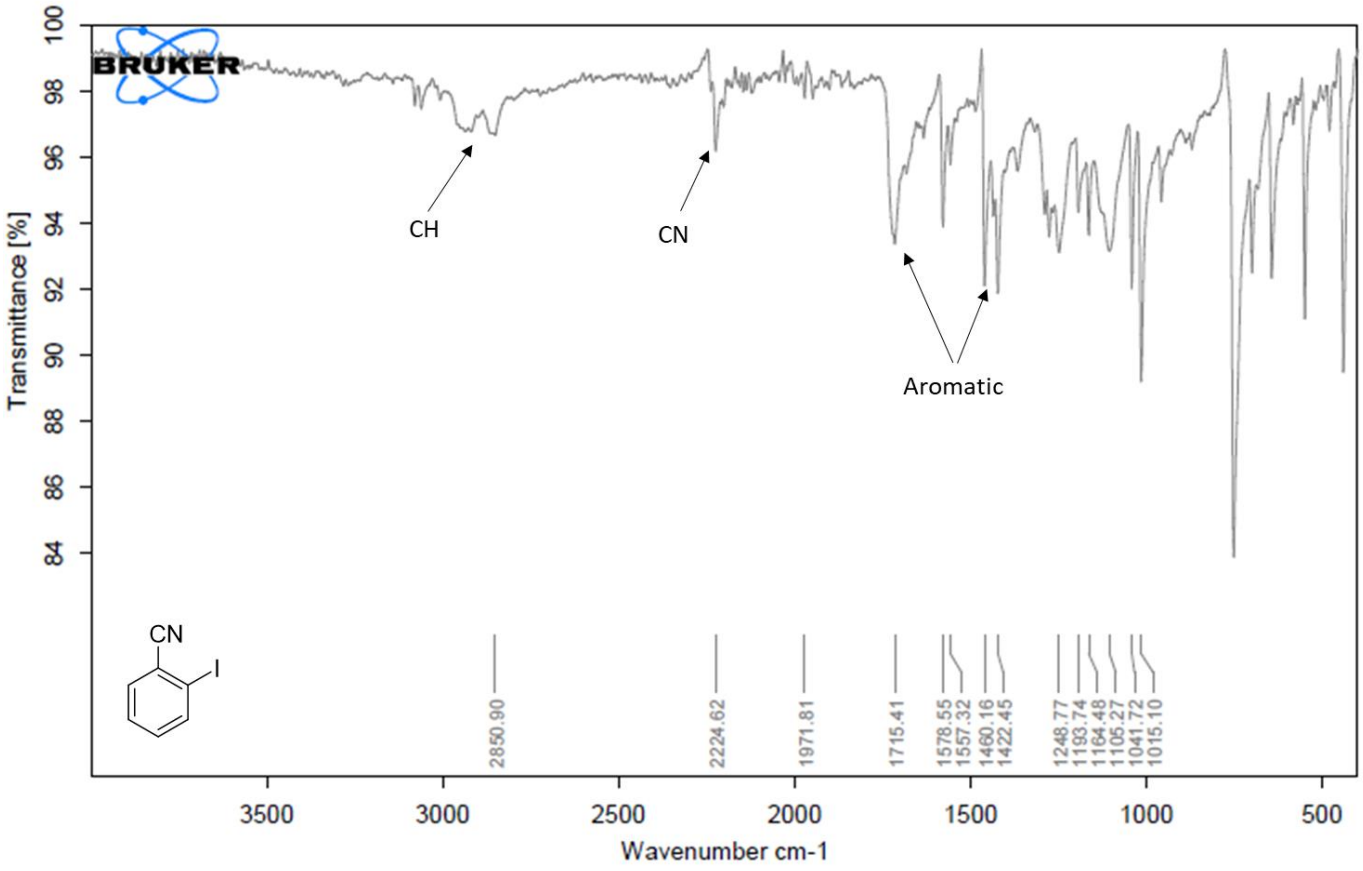

**Appendix A1.2:** $^{13}C$ NMR for spectrum for methyl N-(4-bromobenzyl)-N-pentanoyl-L-valinate **(37)**.

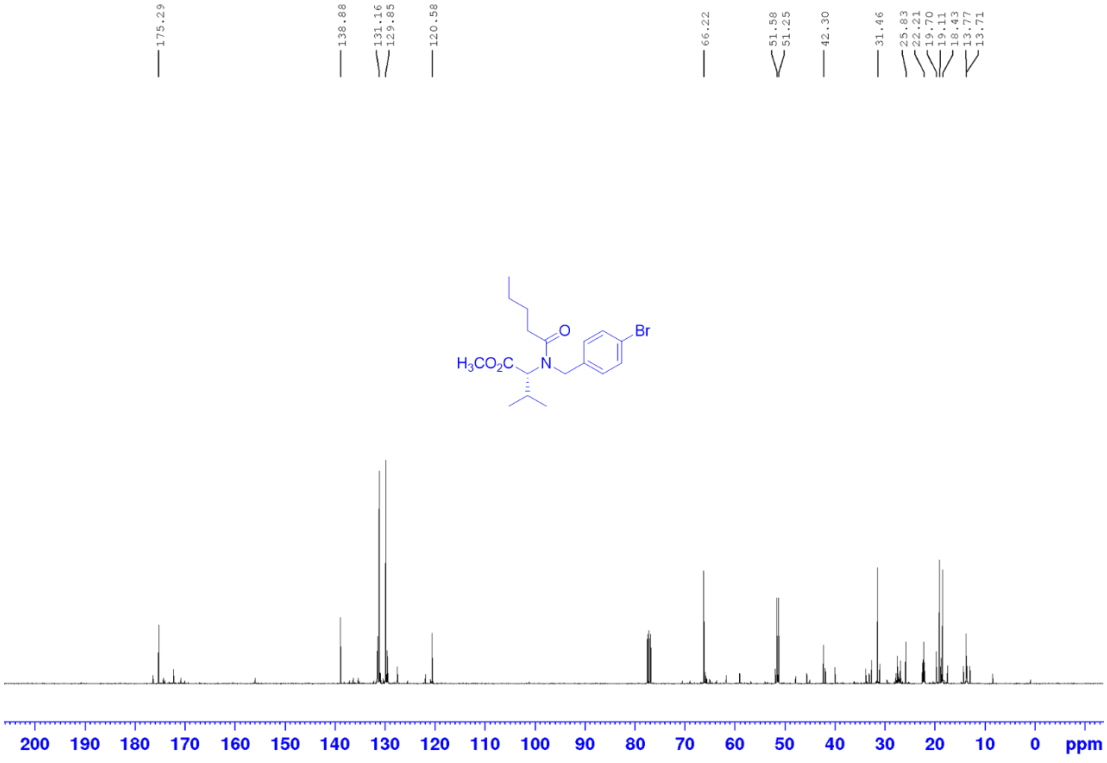

**Appendix A1.3**: $^{1}H$ NMR and $^{13}C$ NMR spectra for methyl N-((2'-cyano-[1, 1'-biphenyl]-4-yl)methyl)-N-pentanoyl-L-valinate **(32)**.

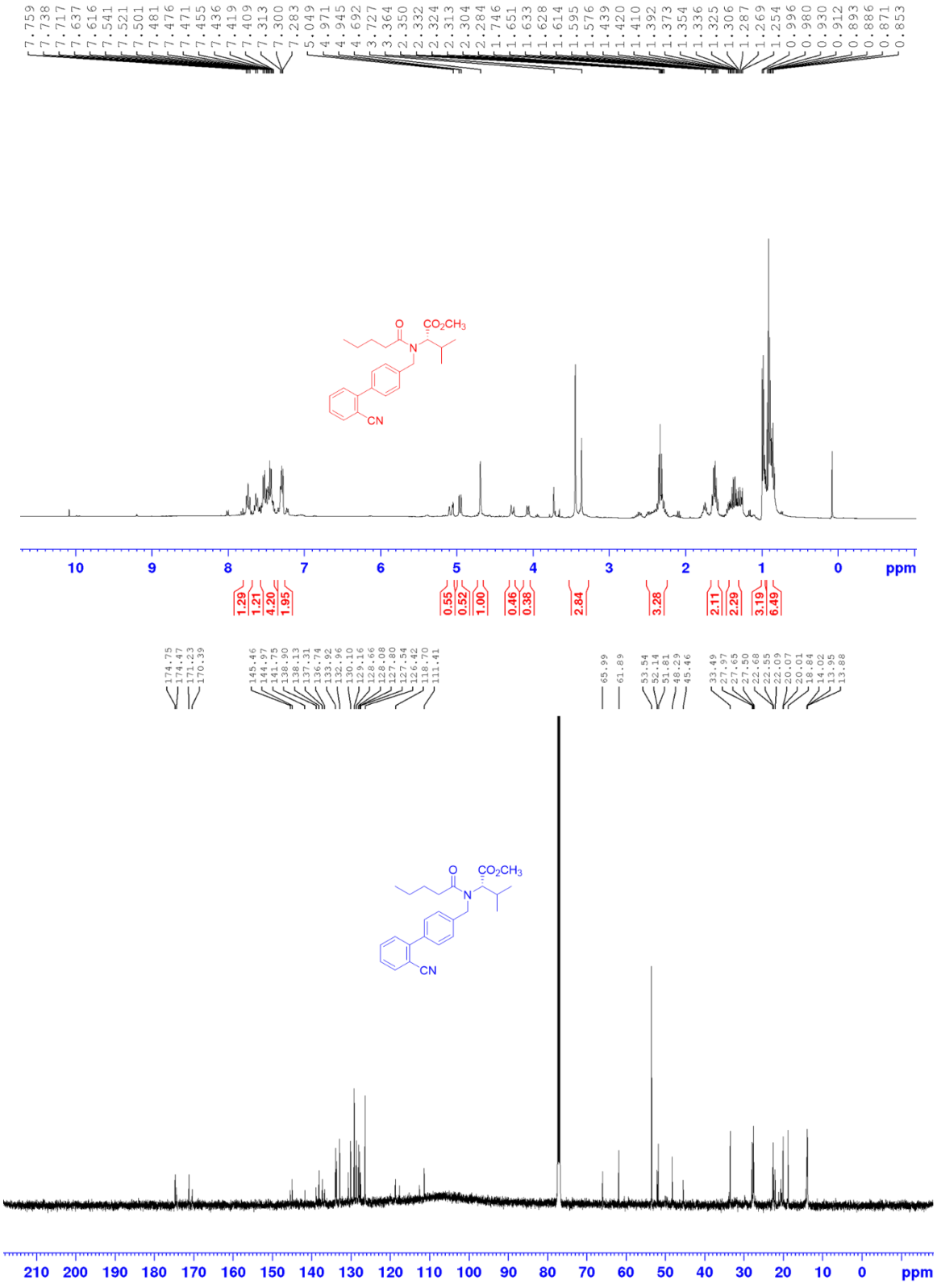

**Appendix A1.4**: $^{1}H$ NMR and $^{13}C$ NMR spectra for methyl N-((2'-(1H-tetrazol-5-yl)-[1, 1'-biphenyl]-4-yl)methyl)-N-pentanoyl-D-valinate **(31)**.

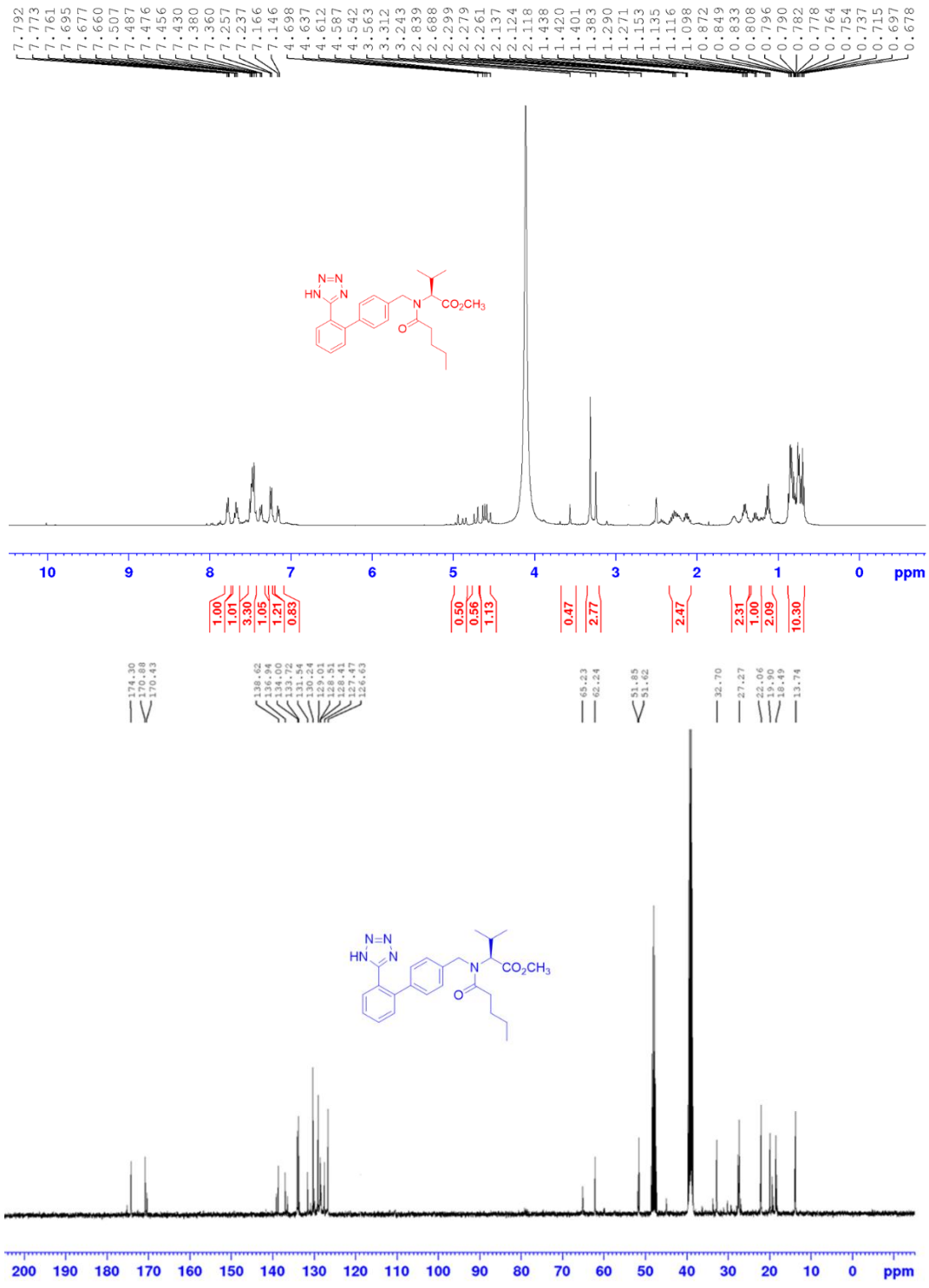

**Appendix A1.5:** $^{13}$C NMR spectrum for *N*-((2'-(1*H*-tetrazol-5-yl)-[1, 1'-biphenyl]-4-yl)-*N*-pentanoyl-*L*-valine **(27)**.

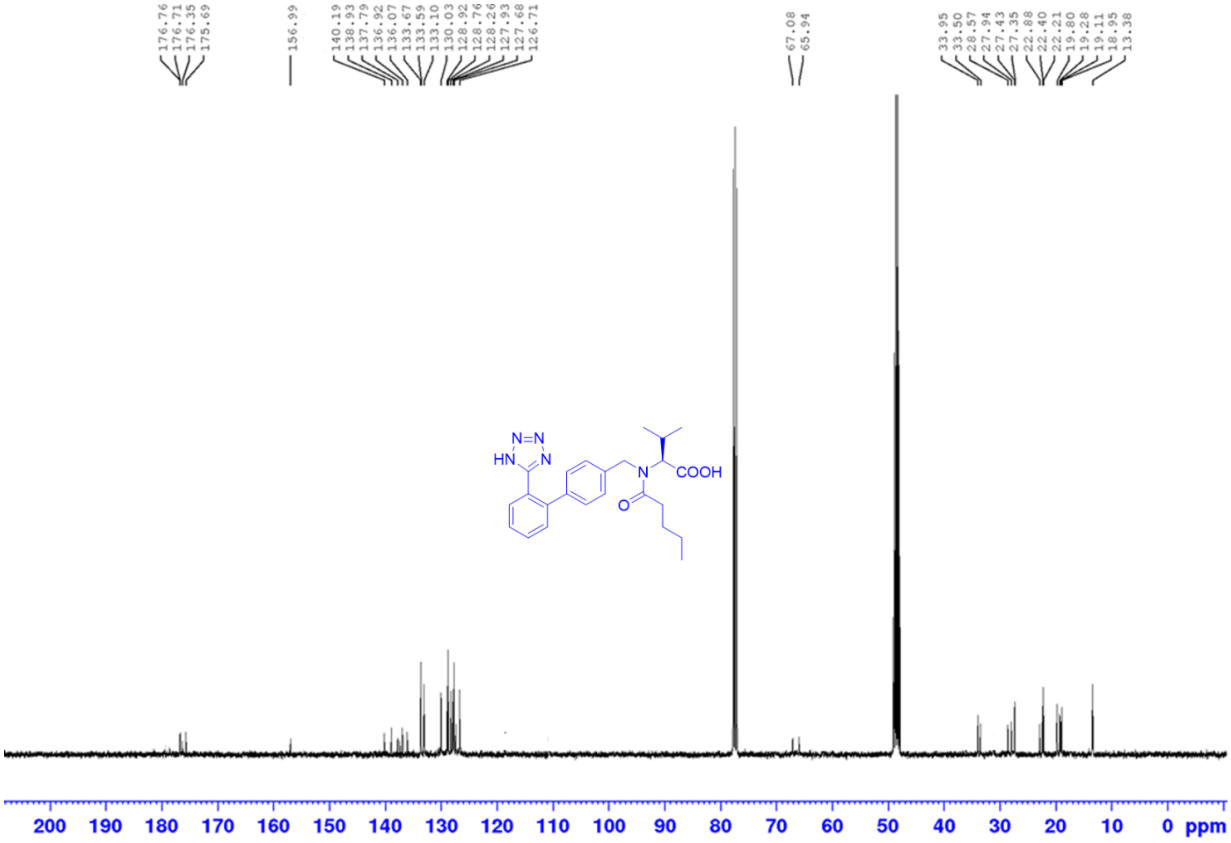

**Appendix A1.6:** $^{1}$H NMR and $^{13}$C NMR spectra for 4'-methyl[1, 1'-biphenyl]-2-carbonitrile **(59)**.

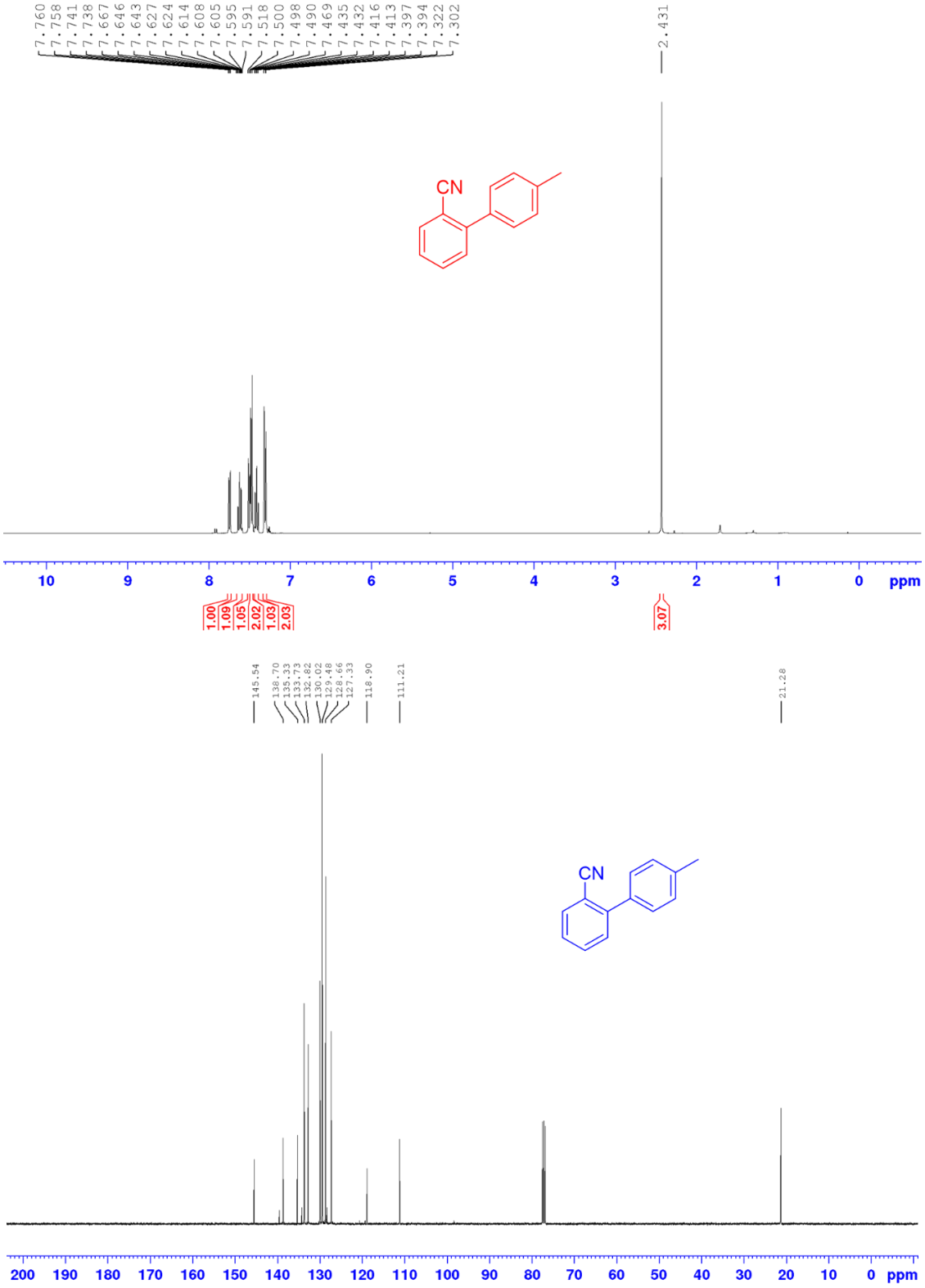

**Appendix A1.7:** $^{1}$H NMR and $^{13}$C NMR spectra for 4'4-methoxy-[1, 1'-biphenyl]-2-carbonitrile **(61)**.

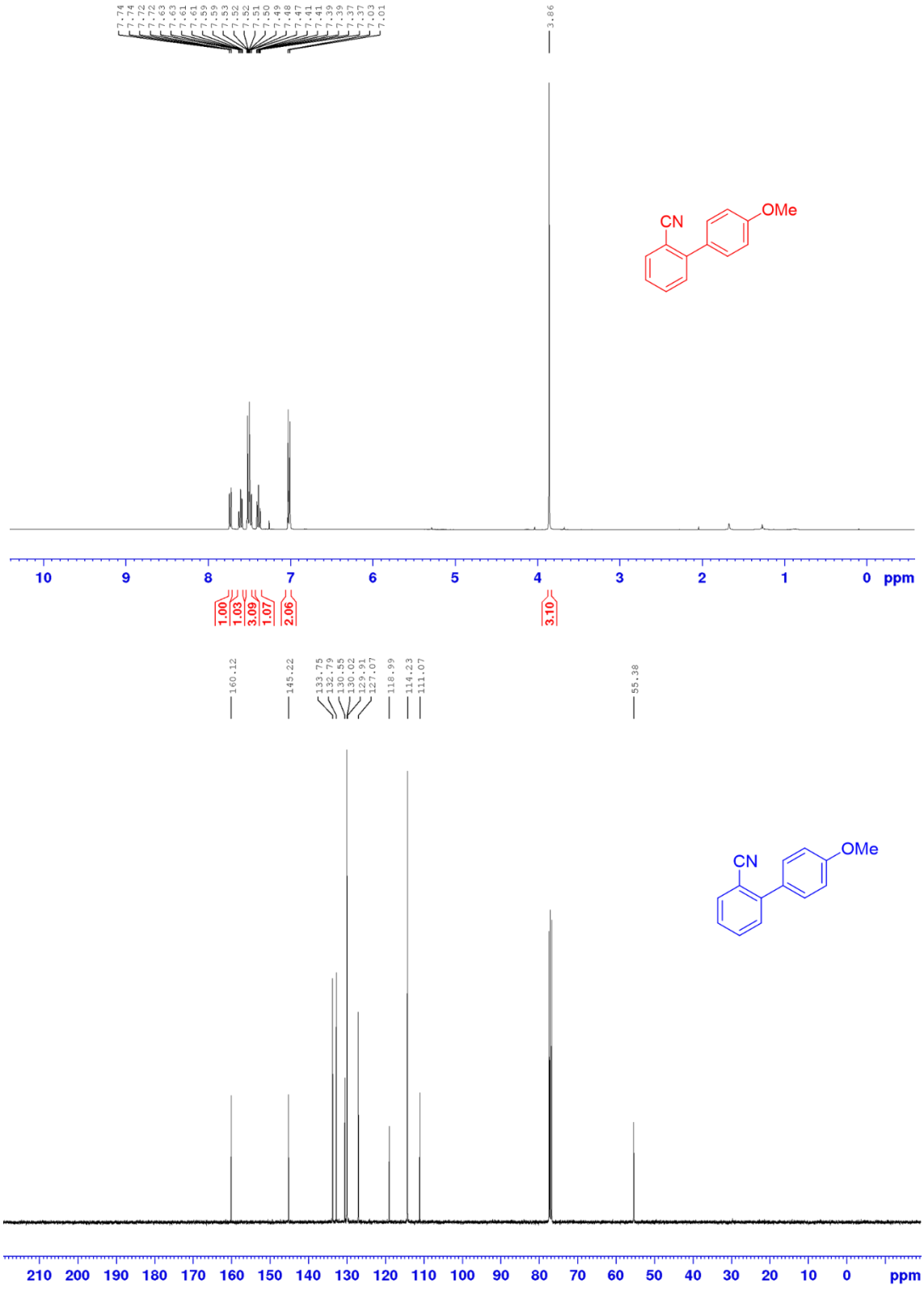

**Appendix A1.8:** $^{1}$H NMR and $^{13}$C NMR spectra for 4'-fluoro-[1, 1'-biphenyl]-2-carbonitrile **(63)**.

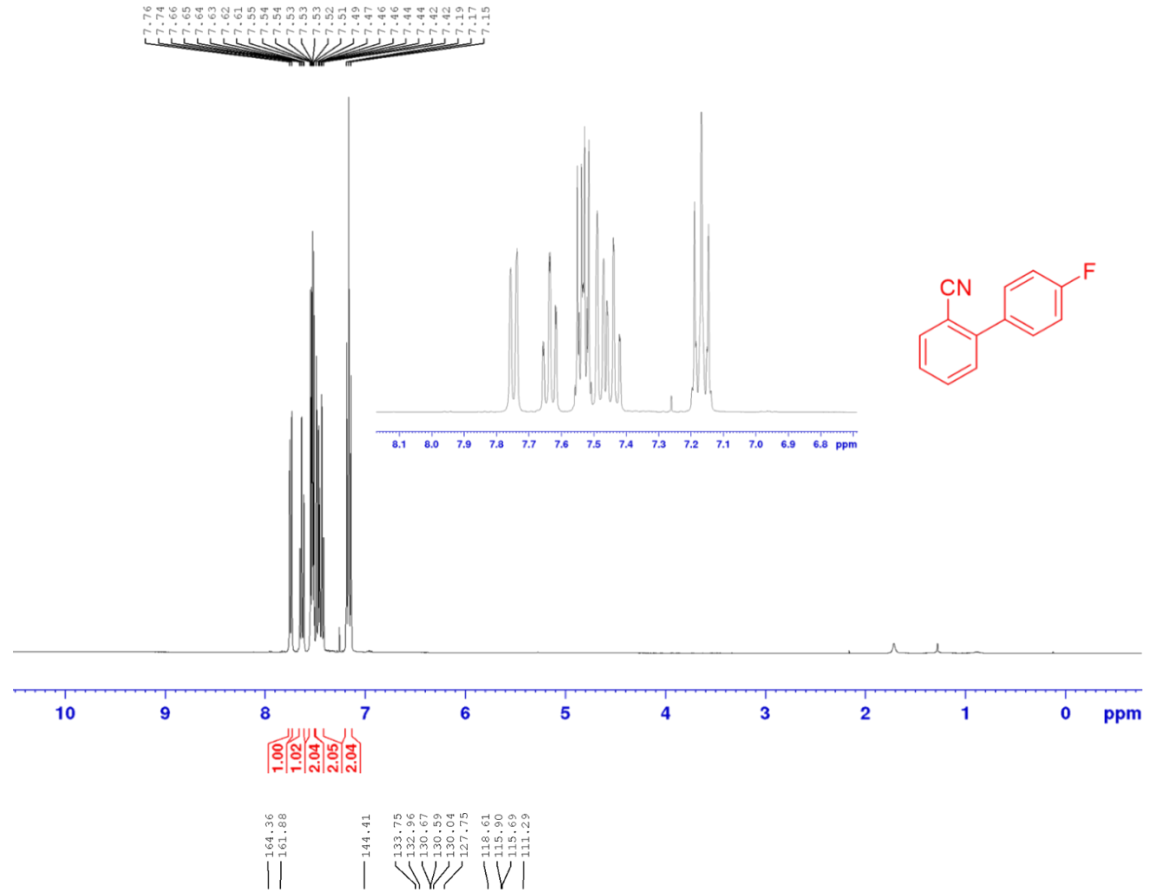


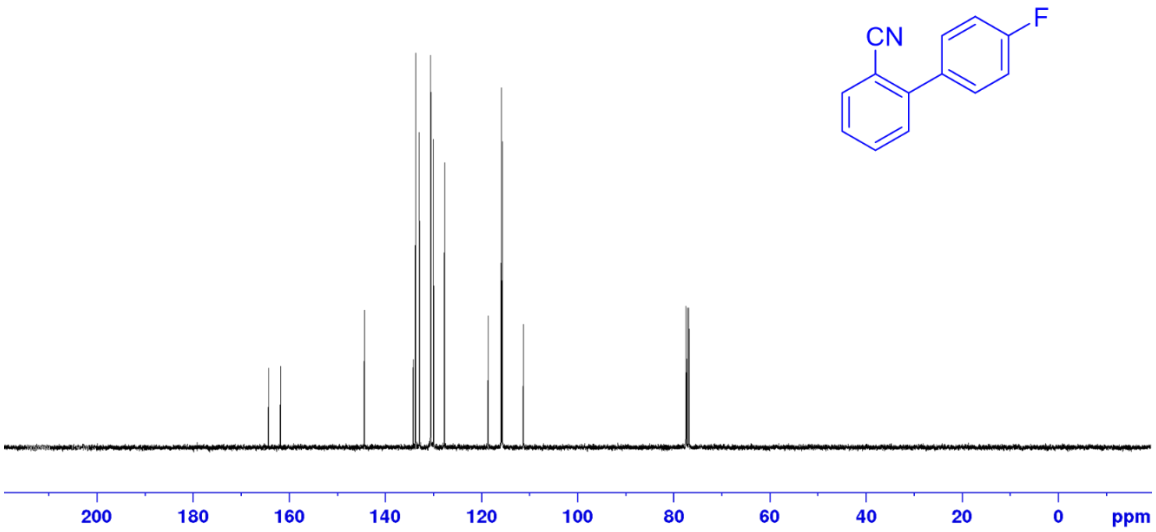

**Appendix A1.9:** $^{1}$H NMR and $^{13}$C NMR spectra for 4'-chloro-[1, 1'-biphenyl]-2-carbonitrile **(65)**.

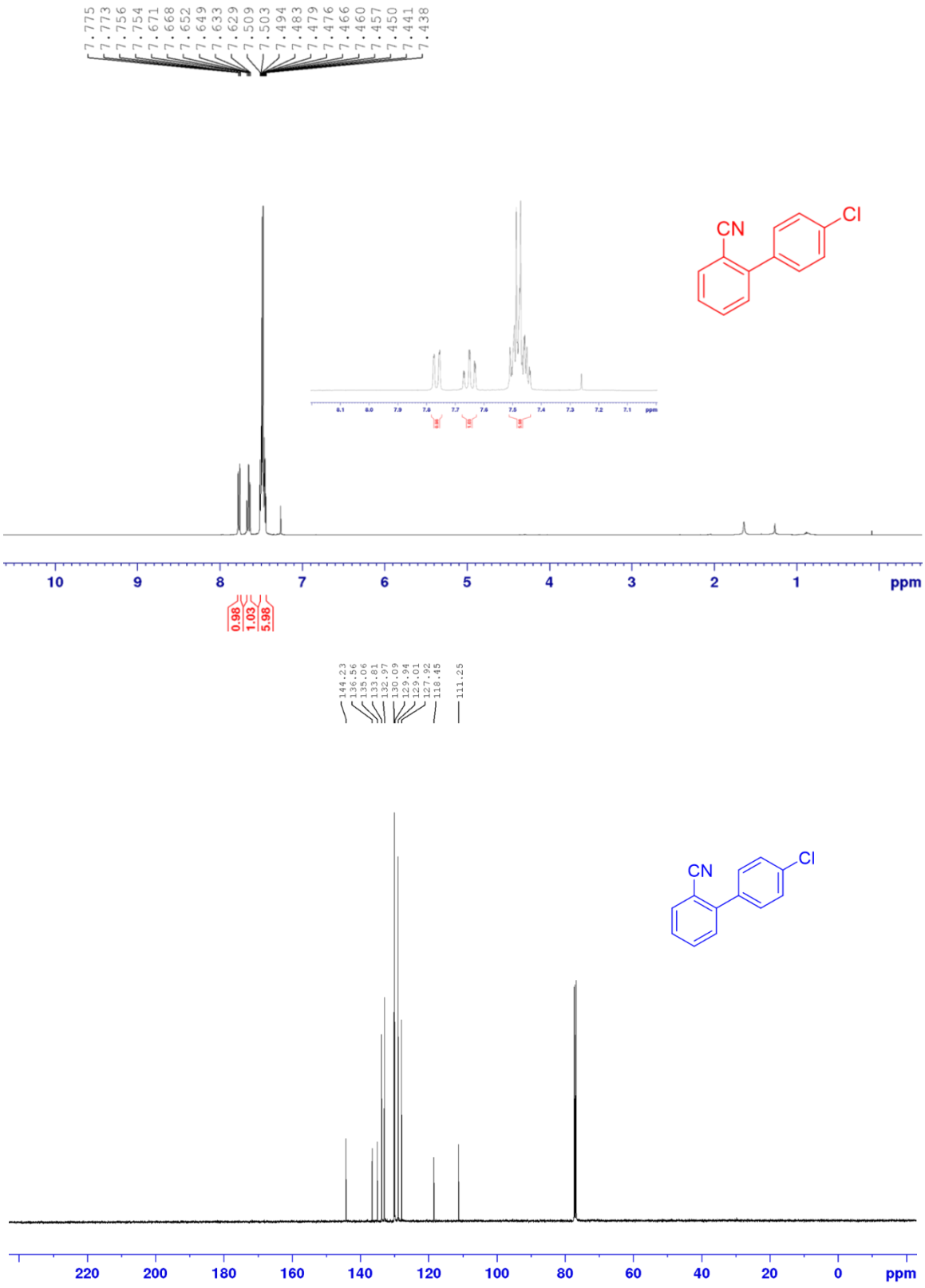

**Appendix A1.10:** $^{1}$H NMR and $^{13}$C NMR spectra for 4'-(bromo)-[1, 1'-biphenyl]-2-carbonitrile **(67)**.

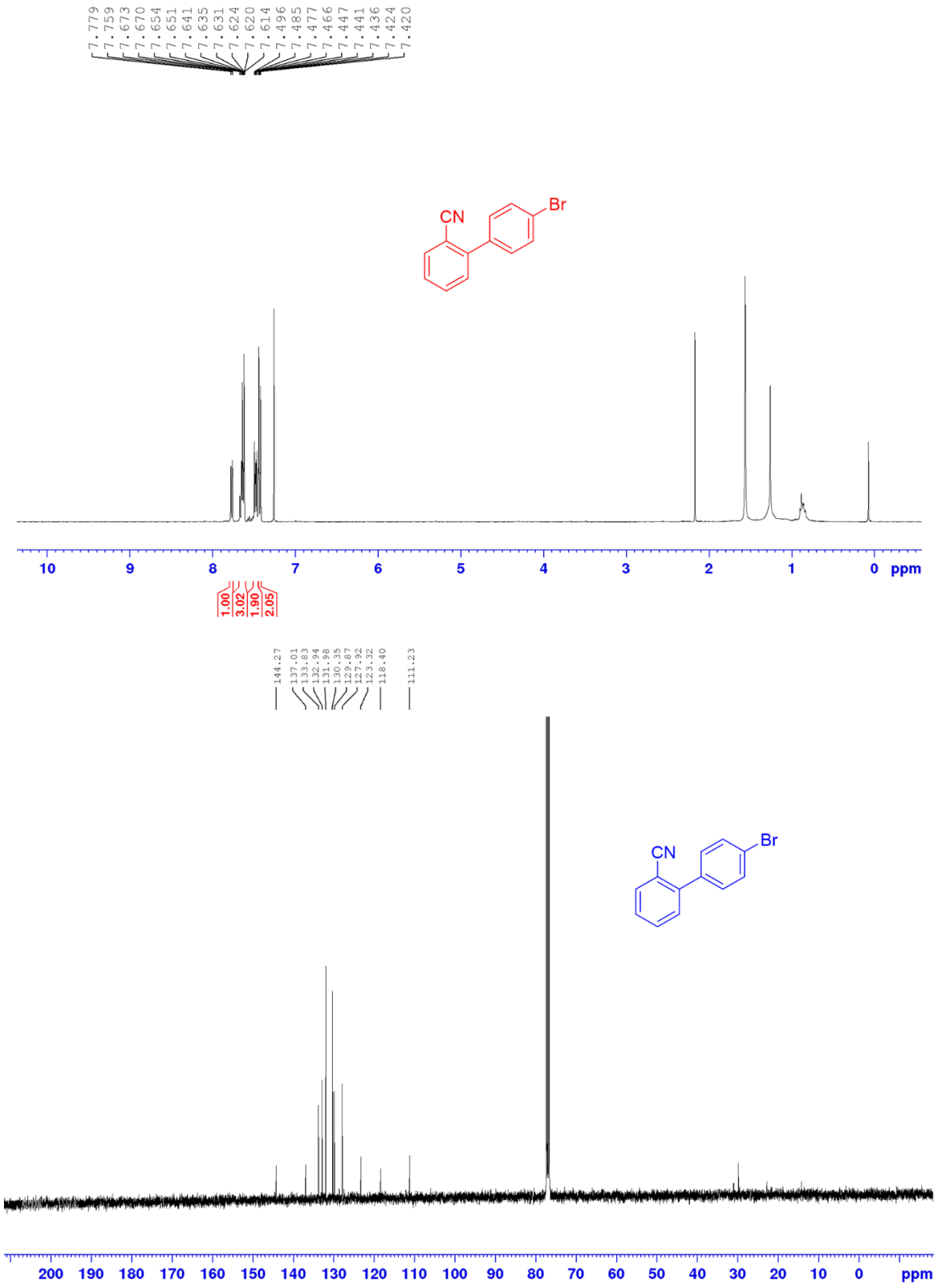

**Appendix A1.11:** $^{1}$H NMR and $^{13}$C NMR spectra for 2-(4'-methyl-[1, 1'-biphenyl]-2-yl)acetonitrile **(72)**.

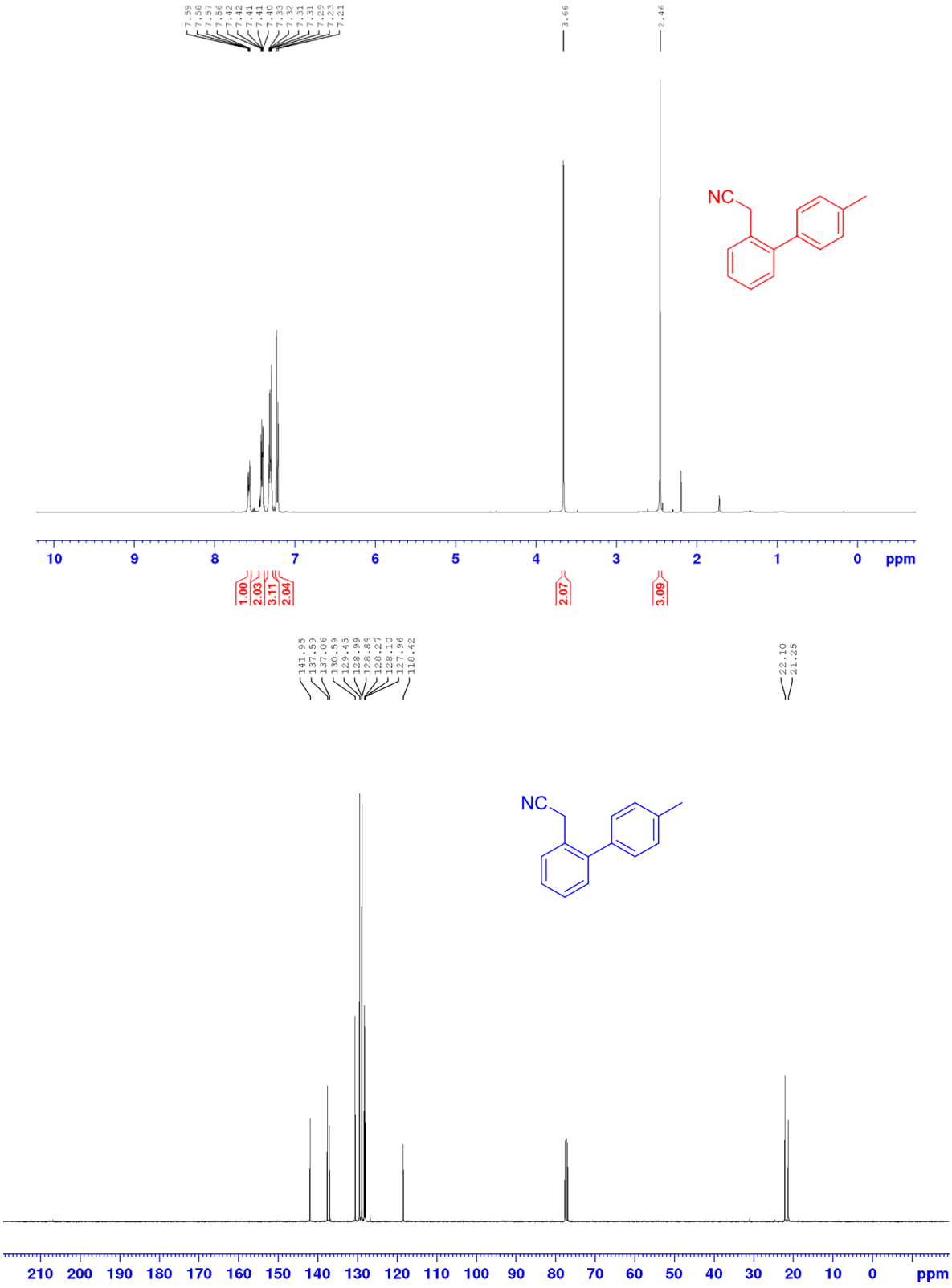

**Appendix A1.12:** $^{1}$H NMR and $^{13}$C NMR spectra for 2-(4'-trifluoromethyl-[1, 1'-biphenyl]-2-yl)acetonitrile **(71)**.

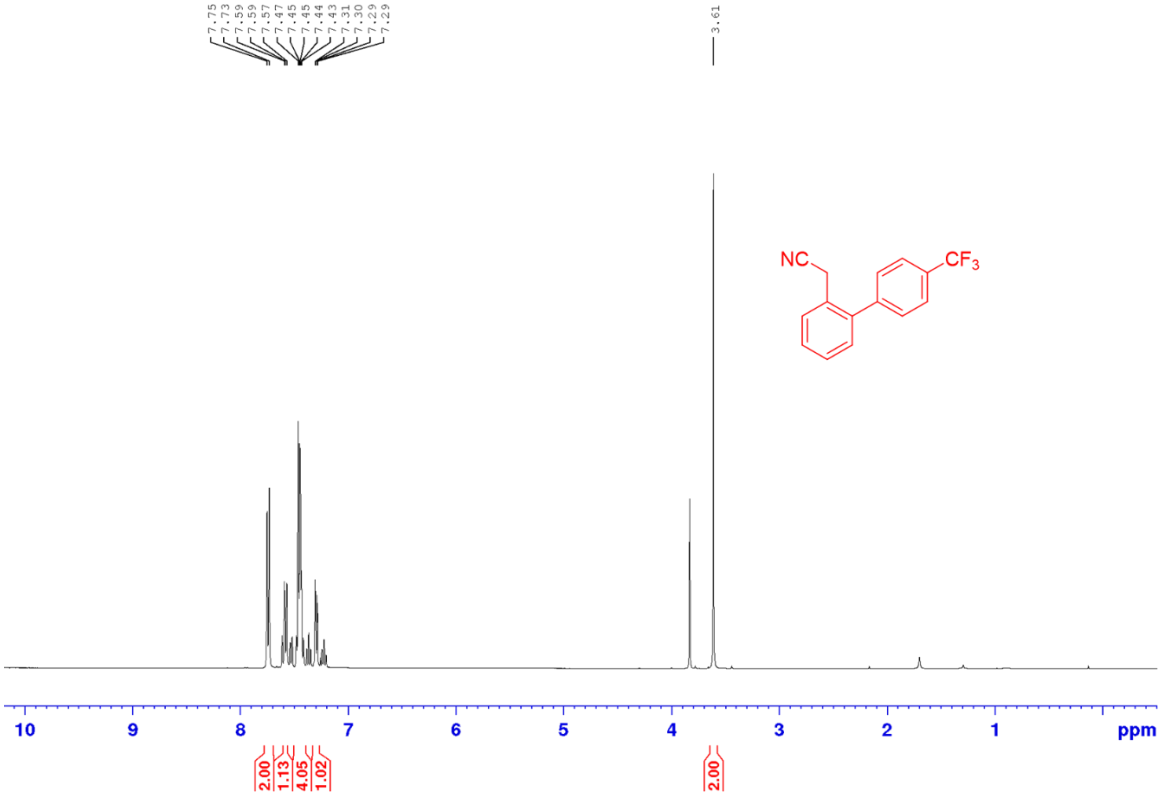


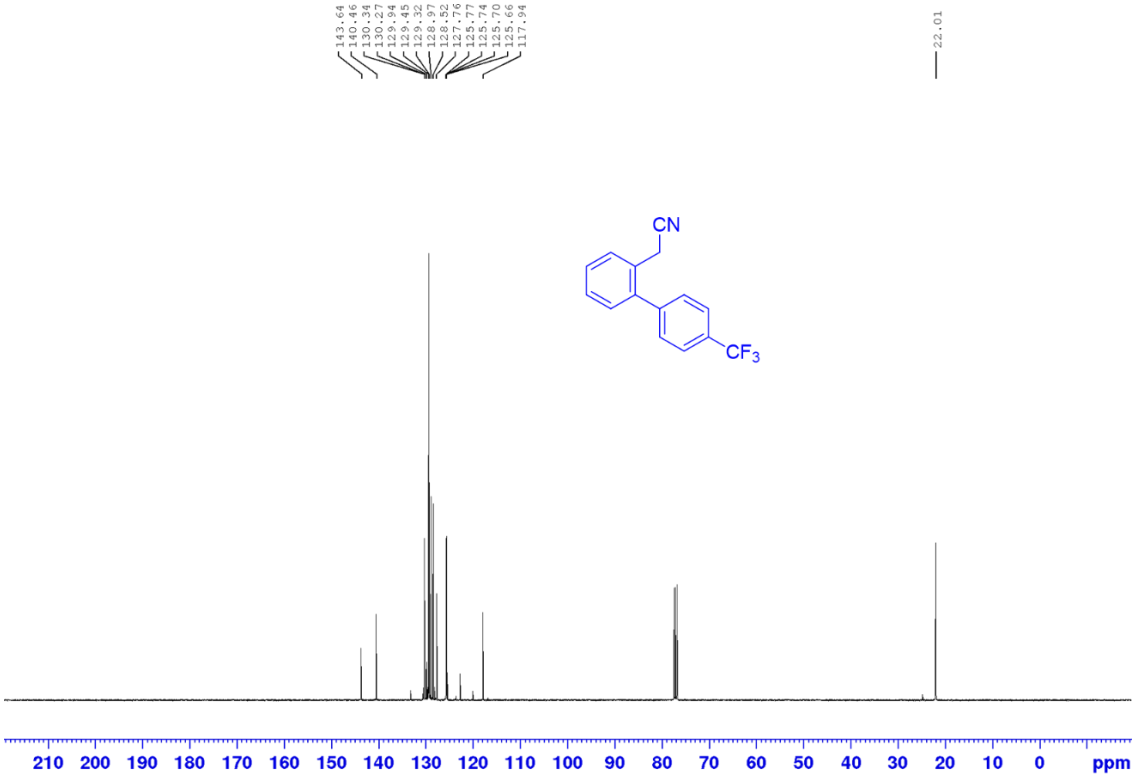

**Appendix A1.13:** $^{1}H$ NMR and $^{13}C$ NMR spectra for 2-(4'-fluoro-[1, 1'-biphenyl]-2-yl)acetonitrile **(73)**.

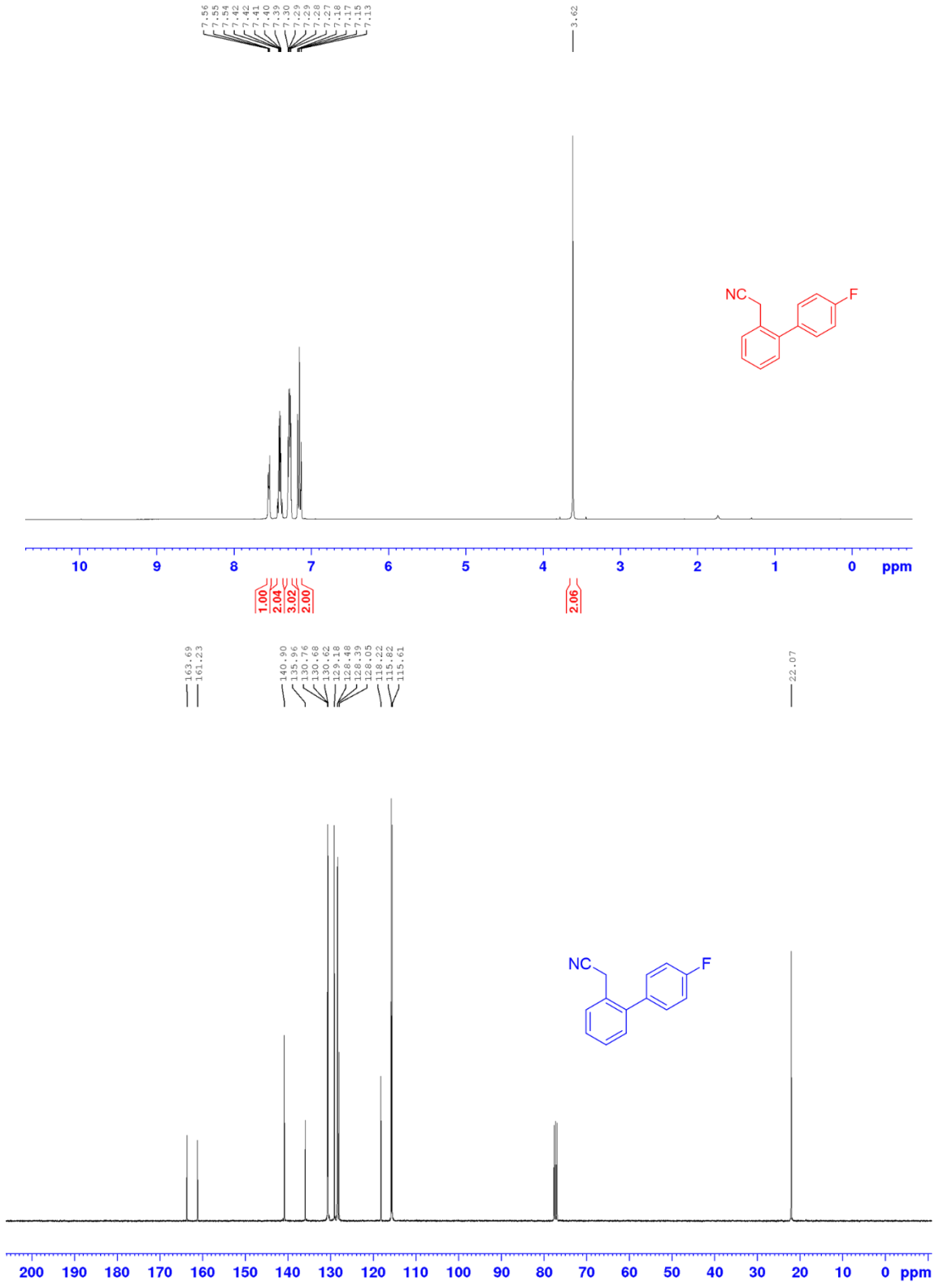

**Appendix A1.14:** $^{1}$H NMR and $^{13}$C NMR spectra for 2-(4'-chloro-[1, 1'-biphenyl]-2-yl)acetonitrile **(74)**.

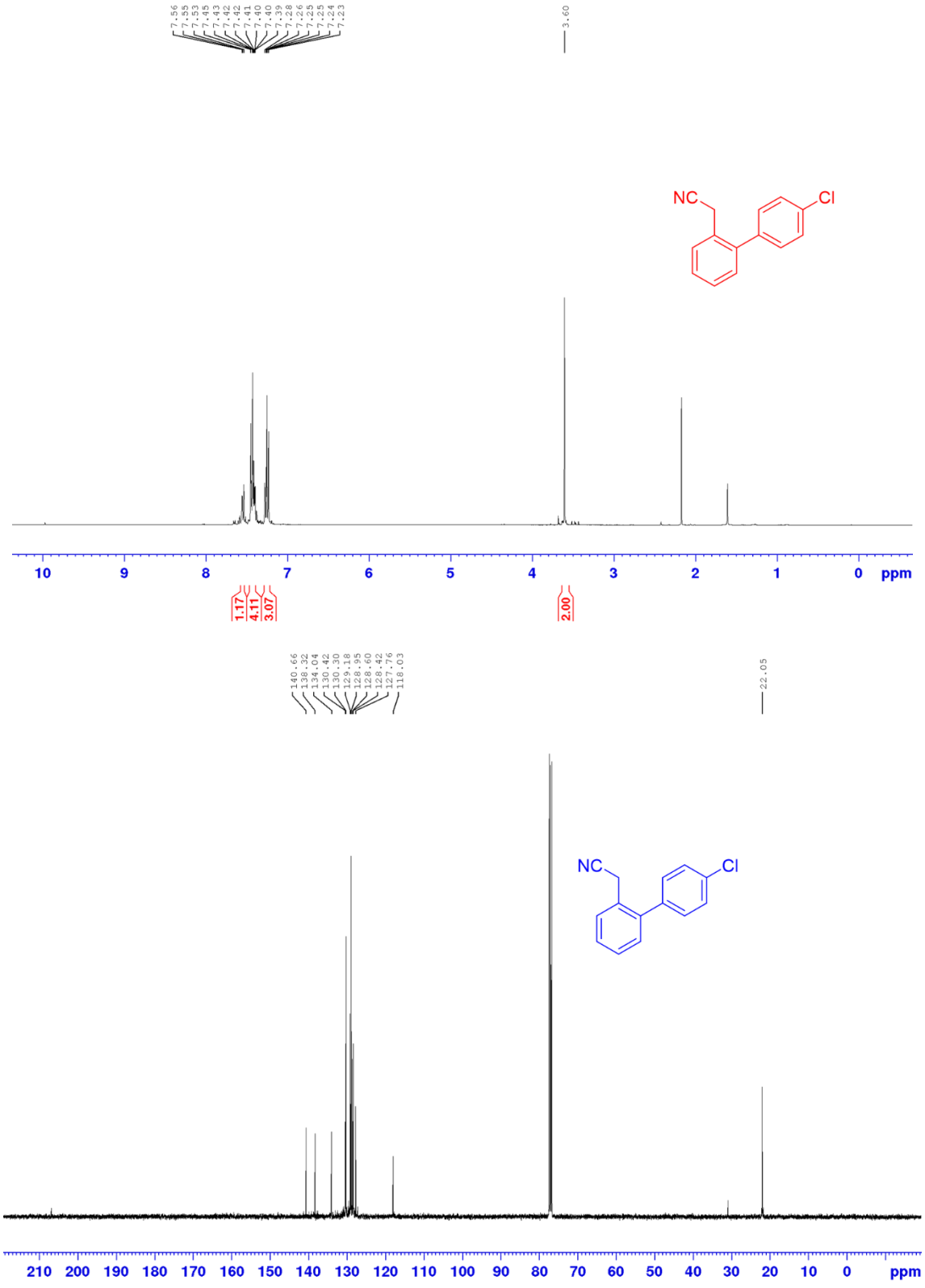

**Appendix A1.15:** HRMS for 5-([1, 1'-biphenyl]-2-yl)-1*H*-tetrazole **(76)**.

**Single Mass Analysis**
Tolerance = 5.0 PPM / DBE: min = -1.5, max = 500.0
Element prediction: Off
Number of isotope peaks used for i-FIT = 3

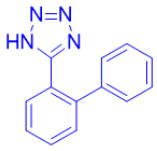


Monoisotopic Mass, Even Electron Ions
2 formula(e) evaluated with 1 results within limits (all results (up to 1000) for each mass)
Elements Used:
C: 10-15 H: 5-10 N: 0-5
P28 19 (0.607) Cm (1:61)

TOF MS ES-
5.43e+005

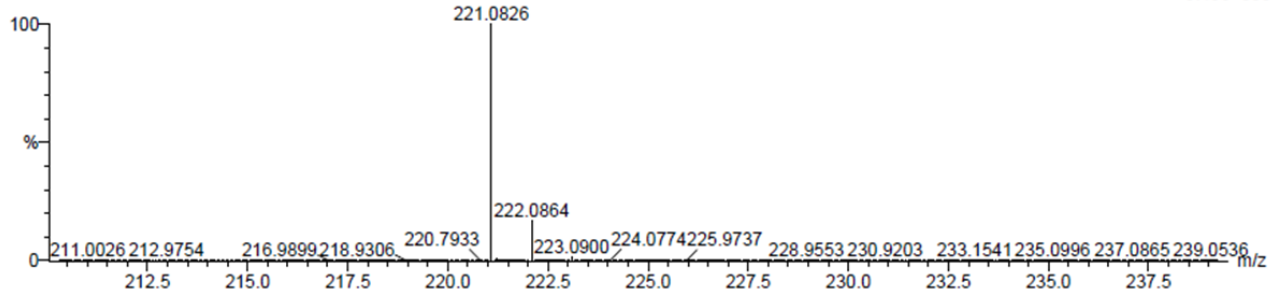


| | | | | | | | |
|---|---|---|---|---|---|---|---|
| Minimum: | | | | -1.5 | | | |
| Maximum: | | 5.0 | 5.0 | 500.0 | | | |
| Mass | Calc. Mass | mDa | PPM | DBE | i-FIT | i-FIT (Norm) | Formula |
| 221.0826 | 221.0827 | -0.1 | -0.5 | 11.5 | 676.1 | 0.0 | C13 H9 N4 |

**Appendix A1.16:** $^{1}$H NMR and $^{13}$C NMR for spectra for 5-(bromobenzyl)-1*H*-tetrazole **(77)**.

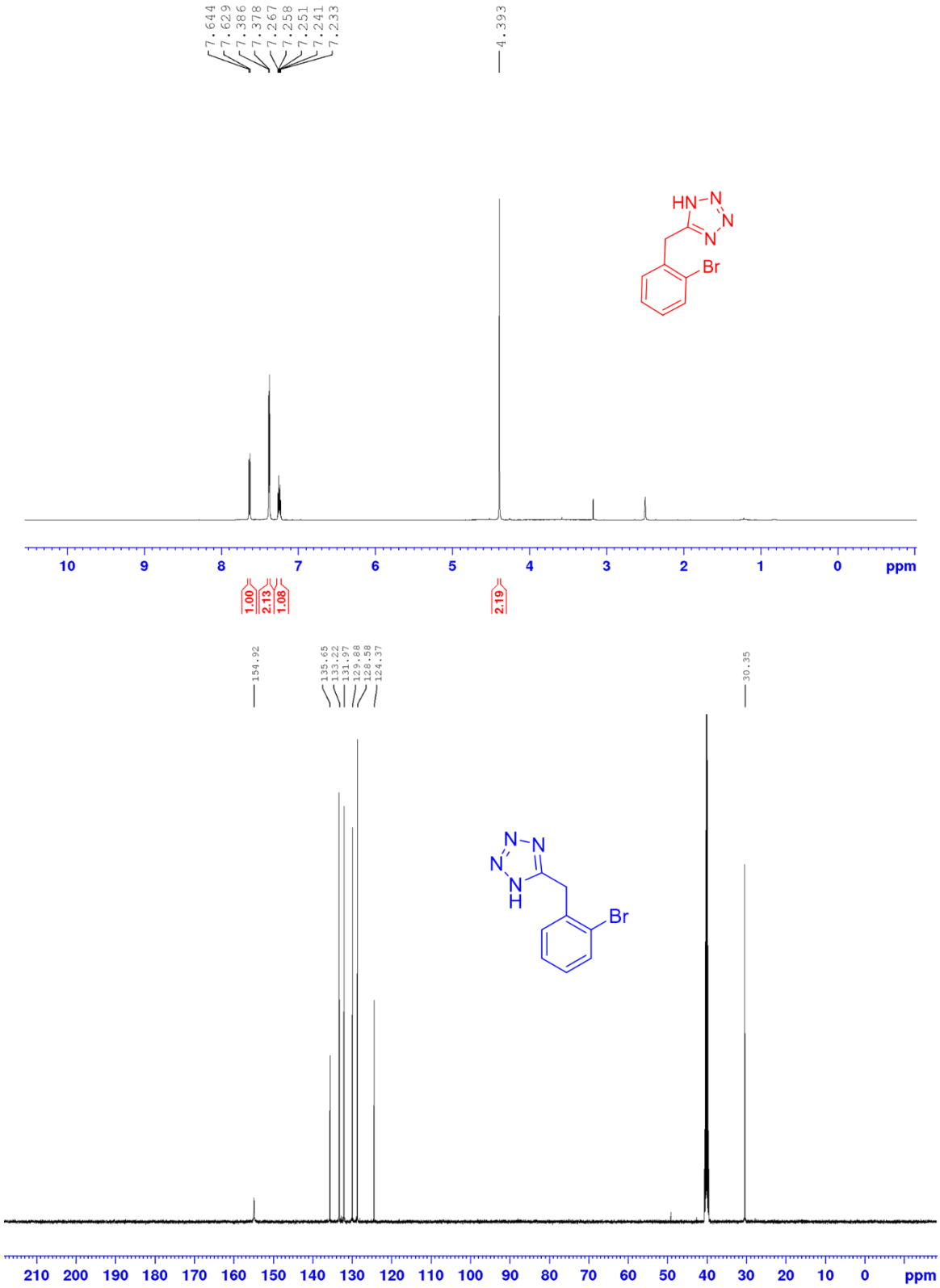

**Appendix A1.17:** HRMS for 5-((4'-methyl[1, 1'-biphenyl]-2-yl)methyl)-1*H*-tetrazole **(78)**.

**Single Mass Analysis**
Tolerance = 50.0 PPM / DBE: min = -1.5, max = 500.0
Element prediction: Off
Number of isotope peaks used for i-FIT = 3

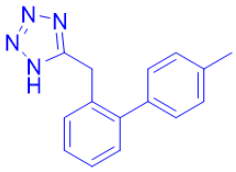

Monoisotopic Mass, Even Electron Ions
4 formula(e) evaluated with 1 results within limits (all results (up to 1000) for each mass)
Elements Used:
C: 10-15 H: 5-15 N: 0-5
P55 53 (1.754) Cm (1:61)

TOF MS ES-
5.01e+005

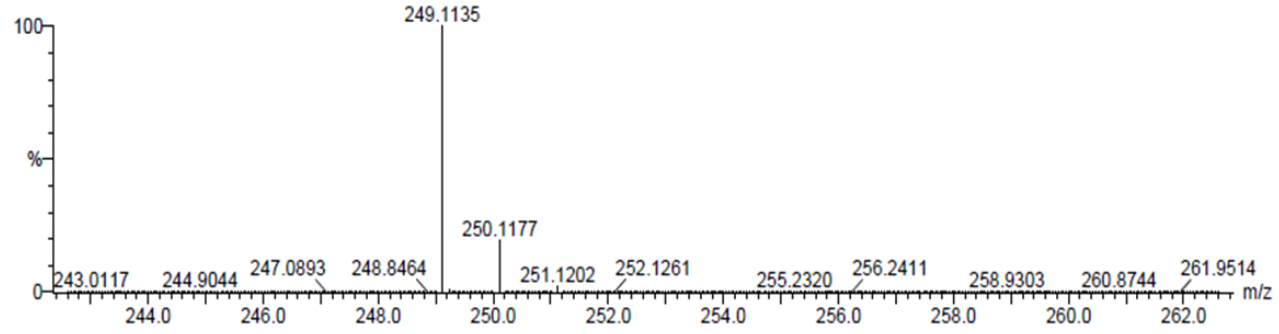


| | | | | | | | |
|---|---|---|---|---|---|---|---|
| Minimum: | | | | -1.5 | | | |
| Maximum: | | 5.0 | 50.0 | 500.0 | | | |
| Mass | Calc. Mass | mDa | PPM | DBE | i-FIT | i-FIT (Norm) | Formula |
| 249.1135 | 249.1140 | -0.5 | -2.0 | 11.5 | 619.0 | 0.0 | C15 H13 N4 |

**Appendix A1.18:** $^{1}$H NMR and $^{13}$C NMR for spectra for 5-((4'-fluoro[1, 1'-biphenyl]-2-yl)methyl)-1*H*-tetrazole **(79)**.

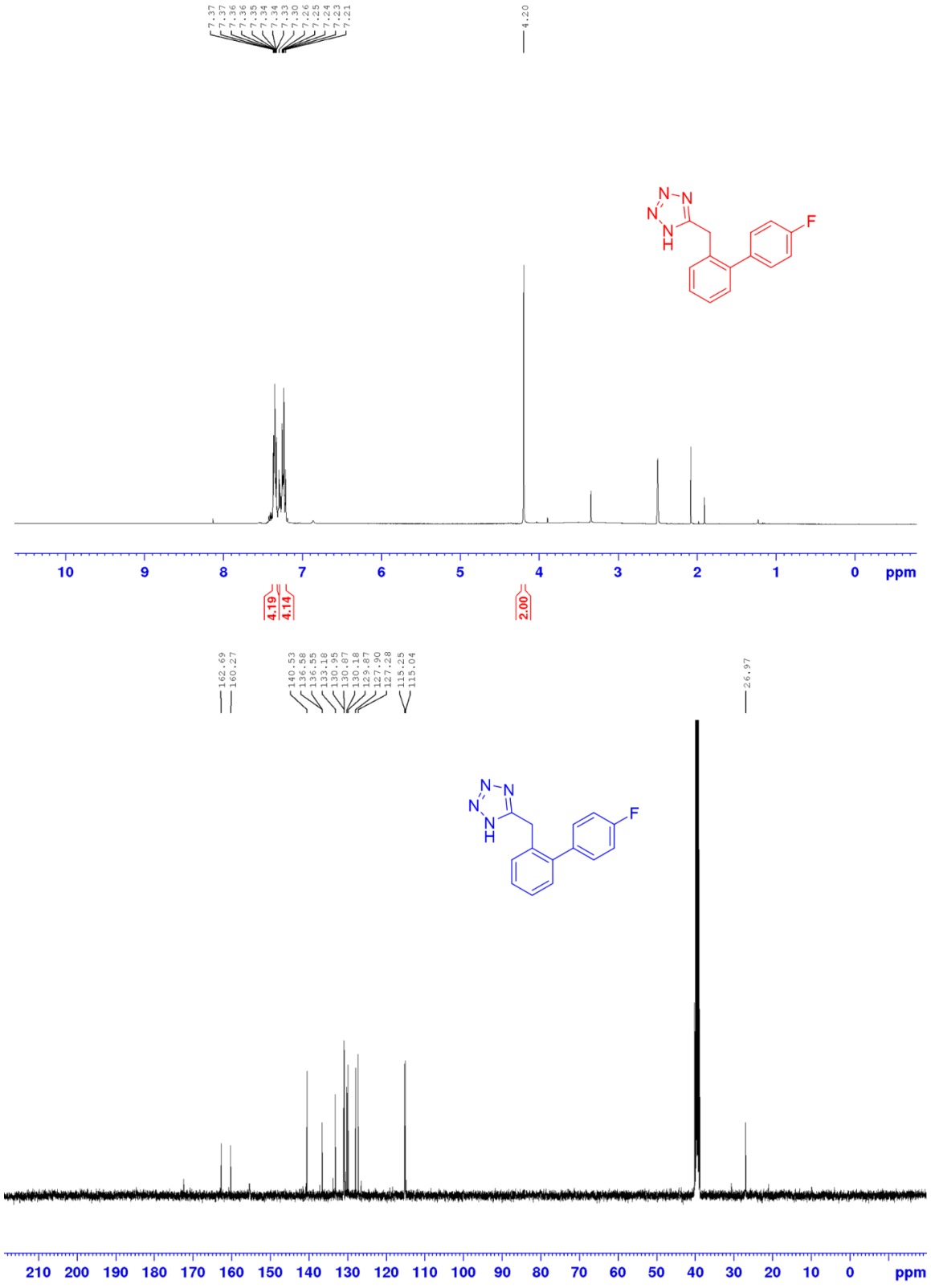

**Appendix A1.19**: $^{1}$H NMR, $^{13}$C NMR and HRMS for 5-(4'-methyl-[1, 1'-biphenyl]-2-yl)-1*H*-tetrazole **(80)**.

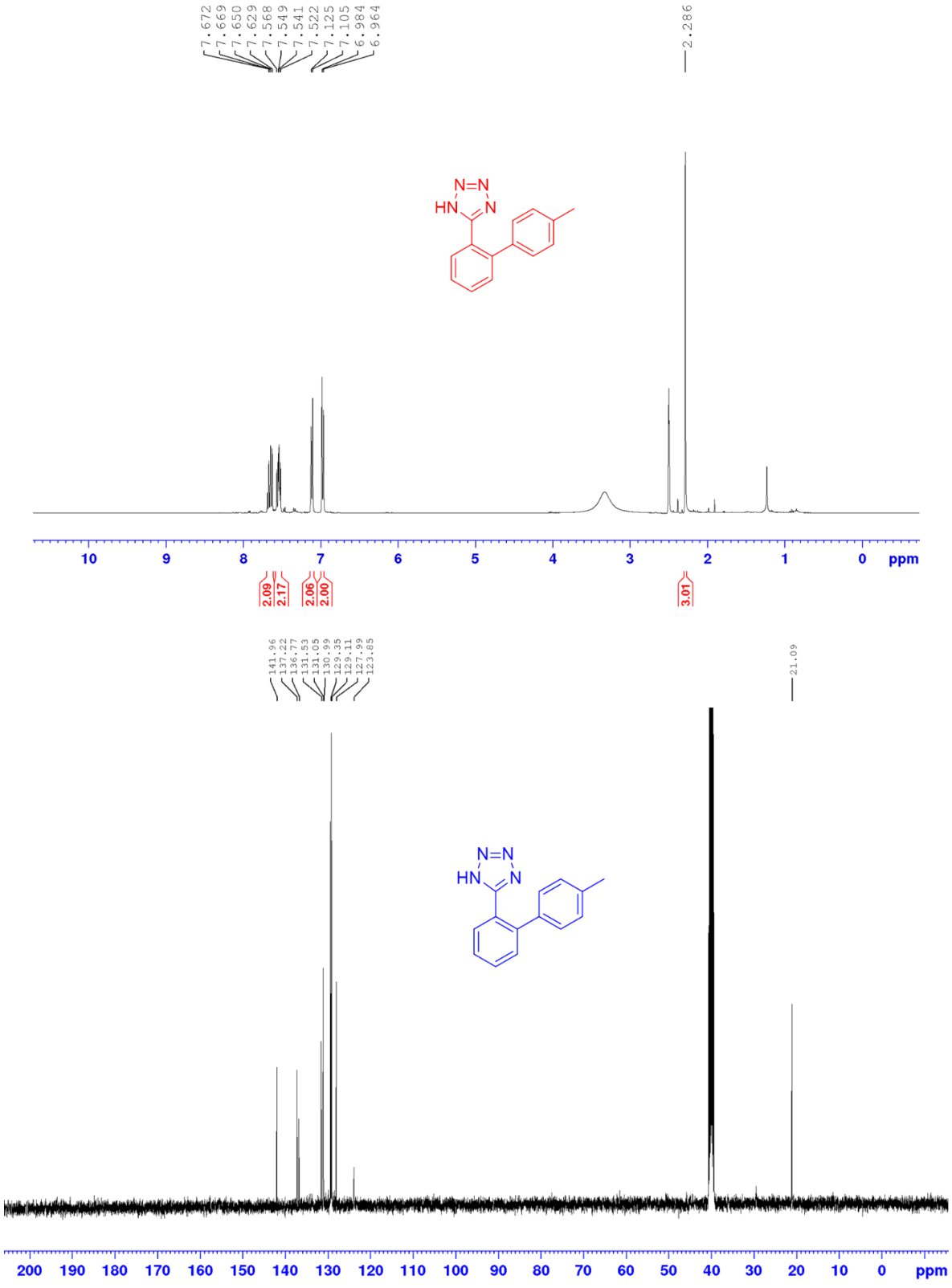

**Single Mass Analysis**
Tolerance = 5.0 PPM / DBE: min = -1.5, max = 500.0
Element prediction: Off
Number of isotope peaks used for i-FIT = 3

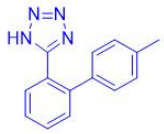


Monoisotopic Mass, Even Electron Ions
3 formula(e) evaluated with 1 results within limits (all results (up to 1000) for each mass)
Elements Used:
C: 10-15 H: 10-15 N: 0-5
P3B 2 (0.034) Cm (1:61)

TOF MS ES-
1.01e+006

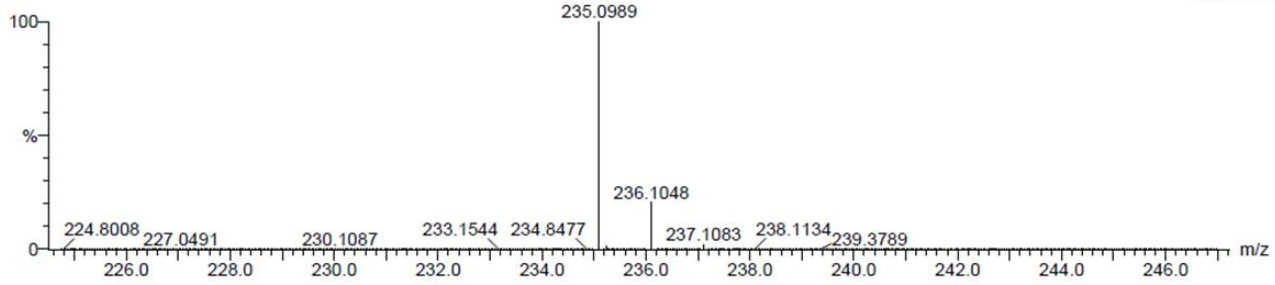


| | | | | | | | |
|---|---|---|---|---|---|---|---|
| Minimum: | | | | -1.5 | | | |
| Maximum: | | 5.0 | 5.0 | 500.0 | | | |
| Mass | Calc. Mass | mDa | PPM | DBE | i-FIT | i-FIT (Norm) | Formula |
| 235.0989 | 235.0984 | 0.5 | 2.1 | 11.5 | 693.7 | 0.0 | C14 H11 N4 |

**Appendix A1.20:** $^{1}$H NMR, $^{13}$C NMR and HRMS for 5-(4'-trifluoromethyl-[1, 1'-biphenyl]-2-yl)-1*H*-tetrazole **(81)**.

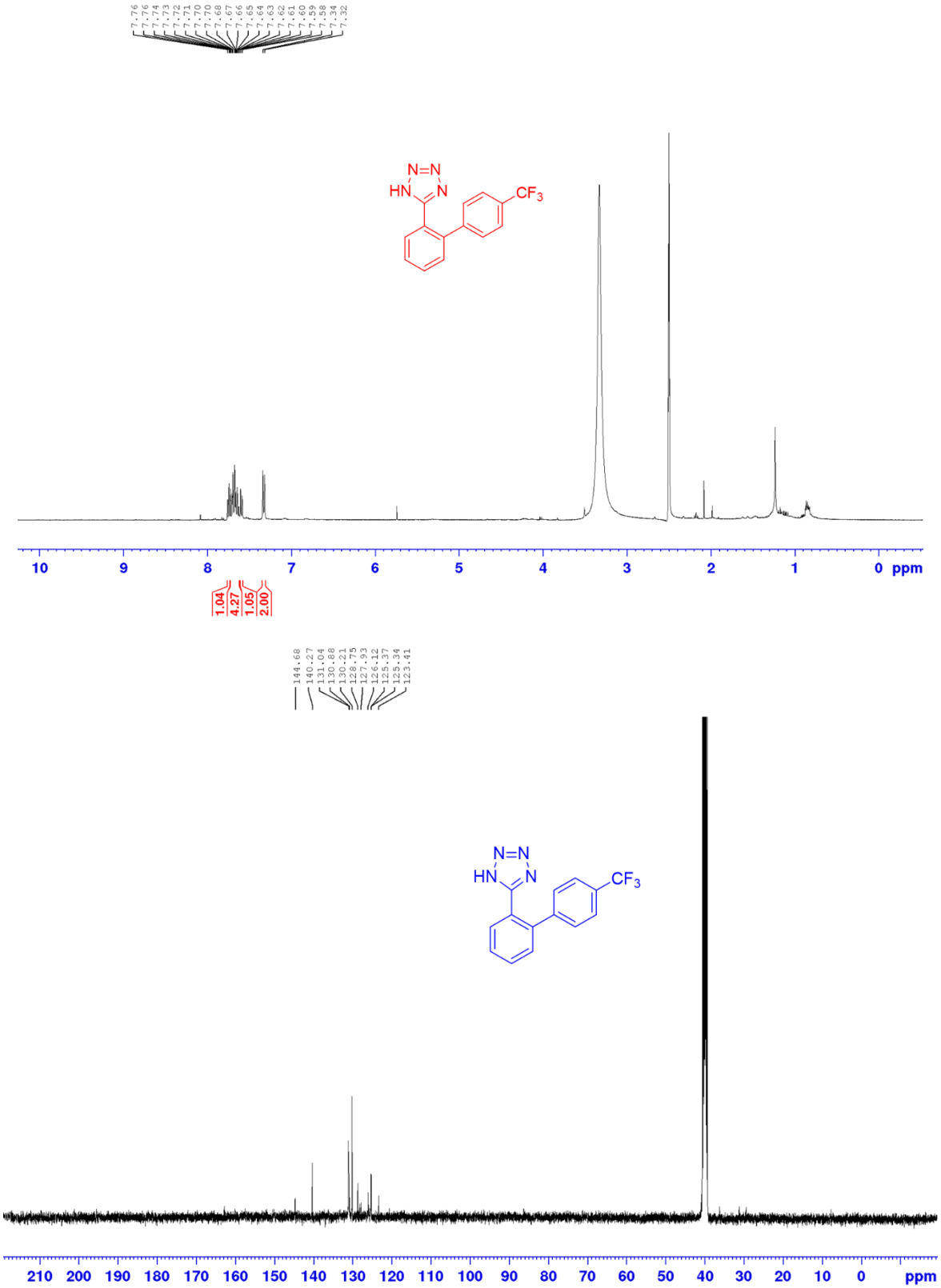

**Single Mass Analysis**

Tolerance = 5.0 PPM / DBE: min = -1.5, max = 500.0

Element prediction: Off

Number of isotope peaks used for i-FIT = 3

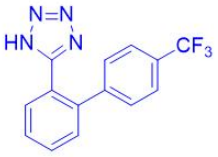


Monoisotopic Mass, Even Electron Ions

27 formula(e) evaluated with 1 results within limits (all results (up to 1000) for each mass)

Elements Used:

C: 10-15 H: 5-15 N: 0-5 F: 0-5

P18 7 (0.203) Cm (1:61)

TOF MS ES-
7.37e+004

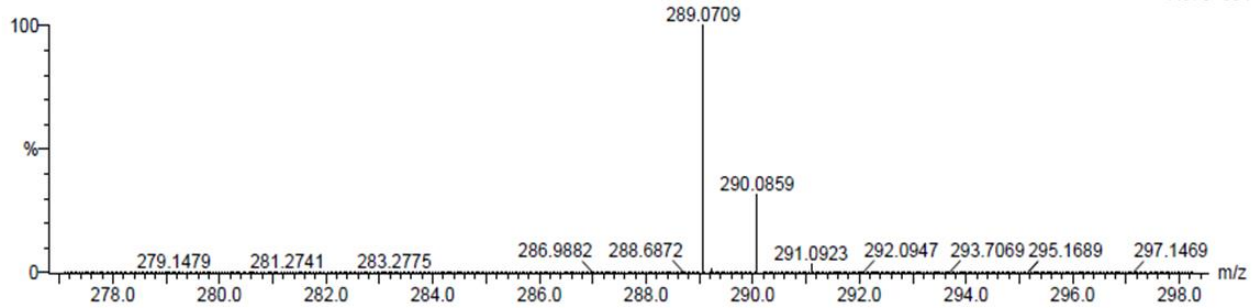


| | | | | | | | |
|---|---|---|---|---|---|---|---|
| Minimum: | | | | -1.5 | | | |
| Maximum: | | 5.0 | 5.0 | 500.0 | | | |
| Mass | Calc. Mass | mDa | PPM | DBE | i-FIT | i-FIT (Norm) | Formula |
| 289.0709 | 289.0701 | 0.8 | 2.8 | 11.5 | 445.3 | 0.0 | C14 H8 N4 F3 |

**Appendix A1.21:** $^{1}$H NMR, $^{13}$C NMR and HRMS for 5-(4'-methoxy-[1, 1'-biphenyl]-2-yl)-1*H*-tetrazole **(82)**.

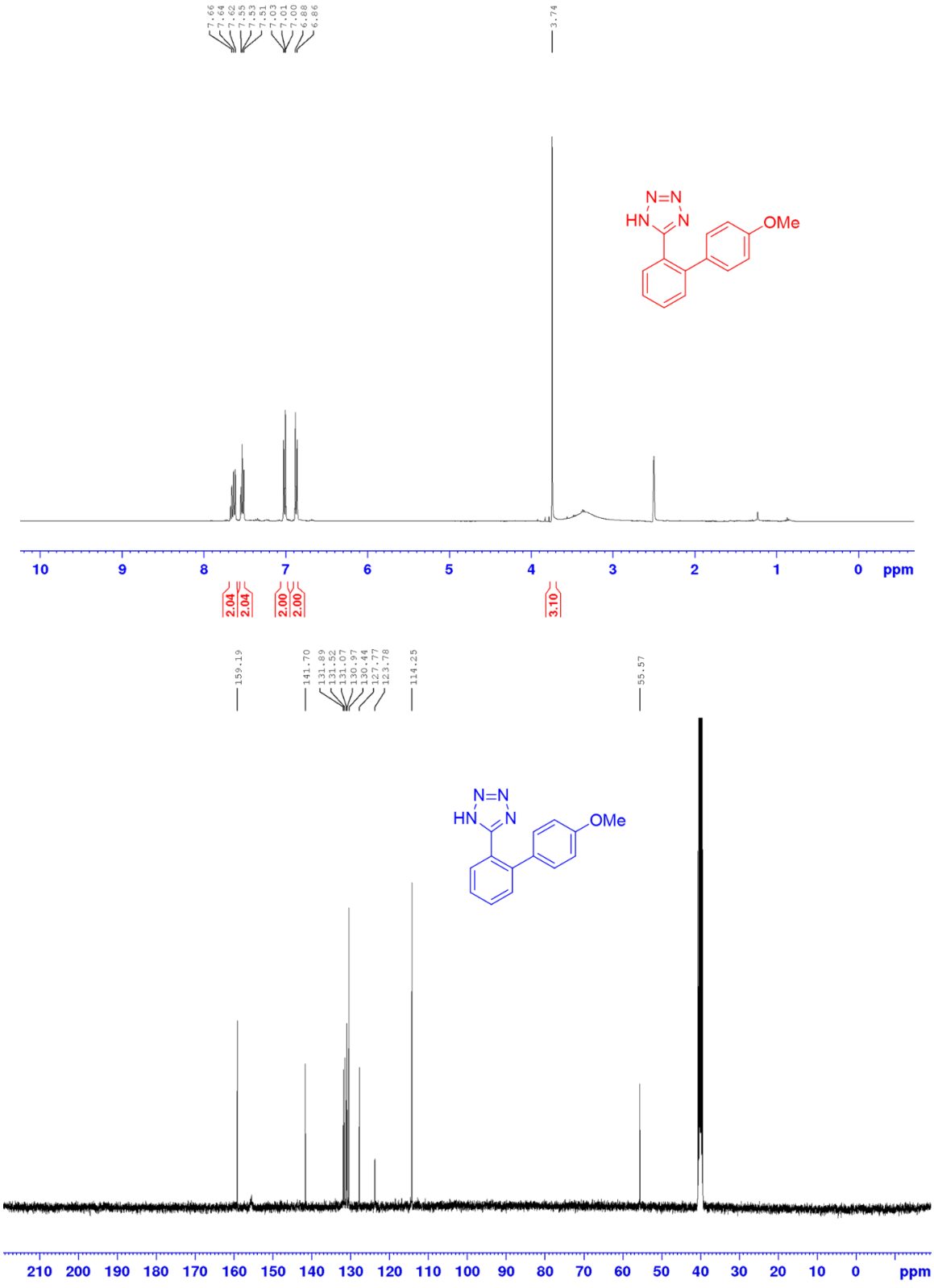

**Single Mass Analysis**

Tolerance = 5.0 PPM / DBE: min = -1.5, max = 500.0

Element prediction: Off

Number of isotope peaks used for i-FIT = 3

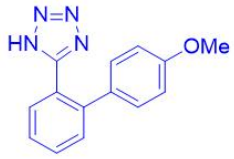


Monoisotopic Mass, Even Electron Ions

8 formula(e) evaluated with 1 results within limits (all results (up to 1000) for each mass)

Elements Used:

C: 10-15 H: 5-15 N: 0-5 O: 0-1

P26 2 (0.034) Cm (1:61)

TOF MS ES-
2.83e+005

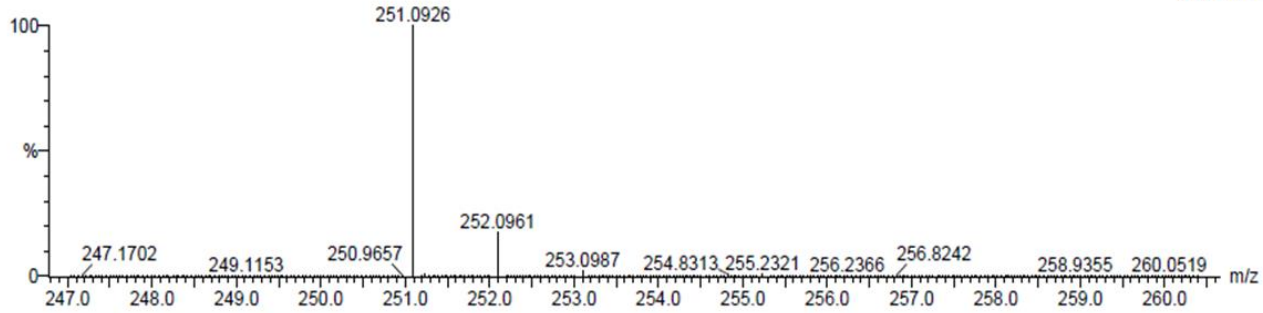


| | | | | | | | |
|---|---|---|---|---|---|---|---|
| Minimum: | | | | -1.5 | | | |
| Maximum: | | 5.0 | 5.0 | 500.0 | | | |
| Mass | Calc. Mass | mDa | PPM | DBE | i-FIT | i-FIT (Norm) | Formula |
| 251.0926 | 251.0933 | -0.7 | -2.8 | 11.5 | 568.7 | 0.0 | C14 H11 N4 O |

**Appendix A1.22:** $^{1}$H NMR, $^{13}$C NMR and HRMS for 5-(4'-fluoro-[1, 1'-biphenyl]-2-yl)-1*H*-tetrazole **(83)**.

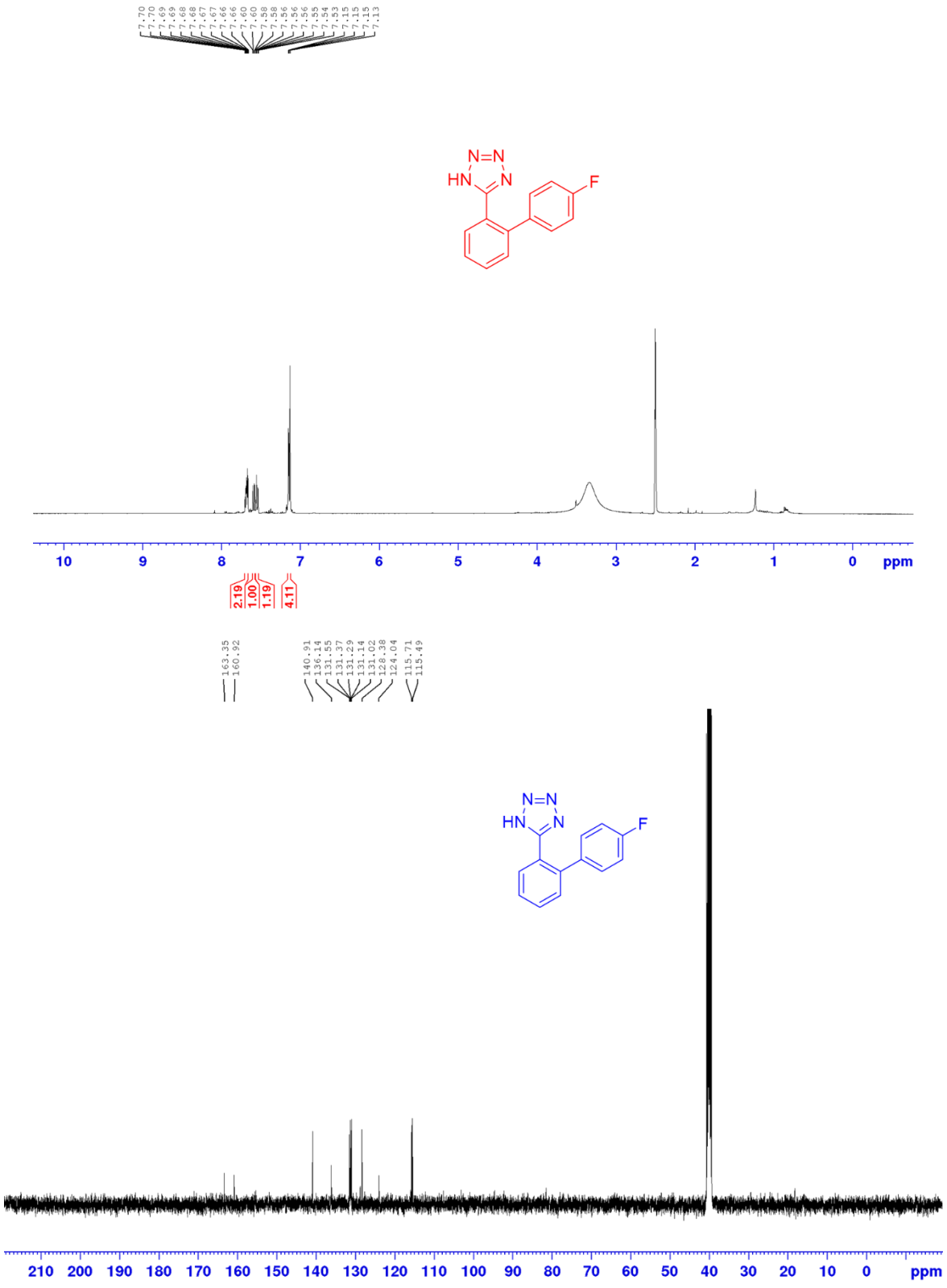

**Single Mass Analysis**

Tolerance = 5.0 PPM / DBE: min = -1.5, max = 500.0
Element prediction: Off
Number of isotope peaks used for i-FIT = 3


Monoisotopic Mass, Even Electron Ions
8 formula(e) evaluated with 1 results within limits (all results (up to 1000) for each mass)
Elements Used:
C: 10-15 H: 5-15 N: 0-5 F: 0-1

P27 6 (0.169) Cm (1:61)

TOF MS ES-
4.63e+005

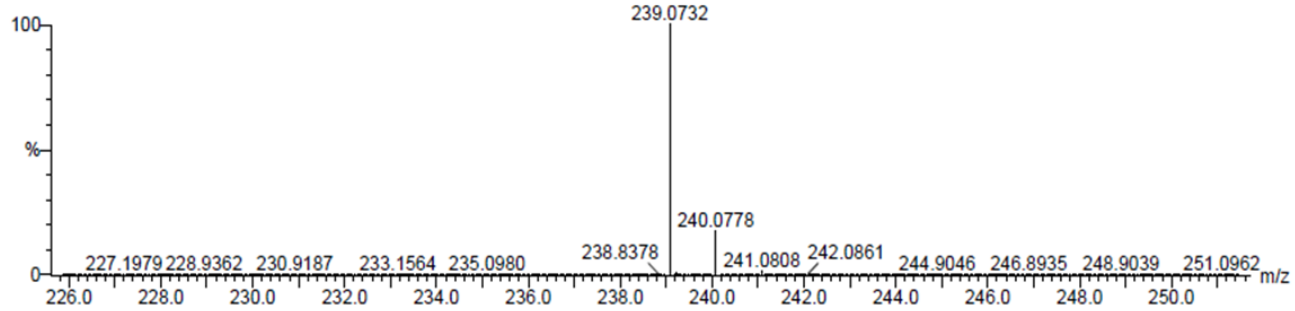


| | | | | | | | |
|---|---|---|---|---|---|---|---|
| Minimum: | | | | -1.5 | | | |
| Maximum: | | 5.0 | 5.0 | 500.0 | | | |
| Mass | Calc. Mass | mDa | PPM | DBE | i-FIT | i-FIT (Norm) | Formula |
| 239.0732 | 239.0733 | -0.1 | -0.4 | 11.5 | 626.1 | 0.0 | C13 H8 N4 F |

**Appendix A1.23:** $^{1}$H NMR, $^{13}$C NMR and HRMS for 5-(4'-chloro-[1, 1'-biphenyl]-2-yl)-1*H*-tetrazole **(84)**.

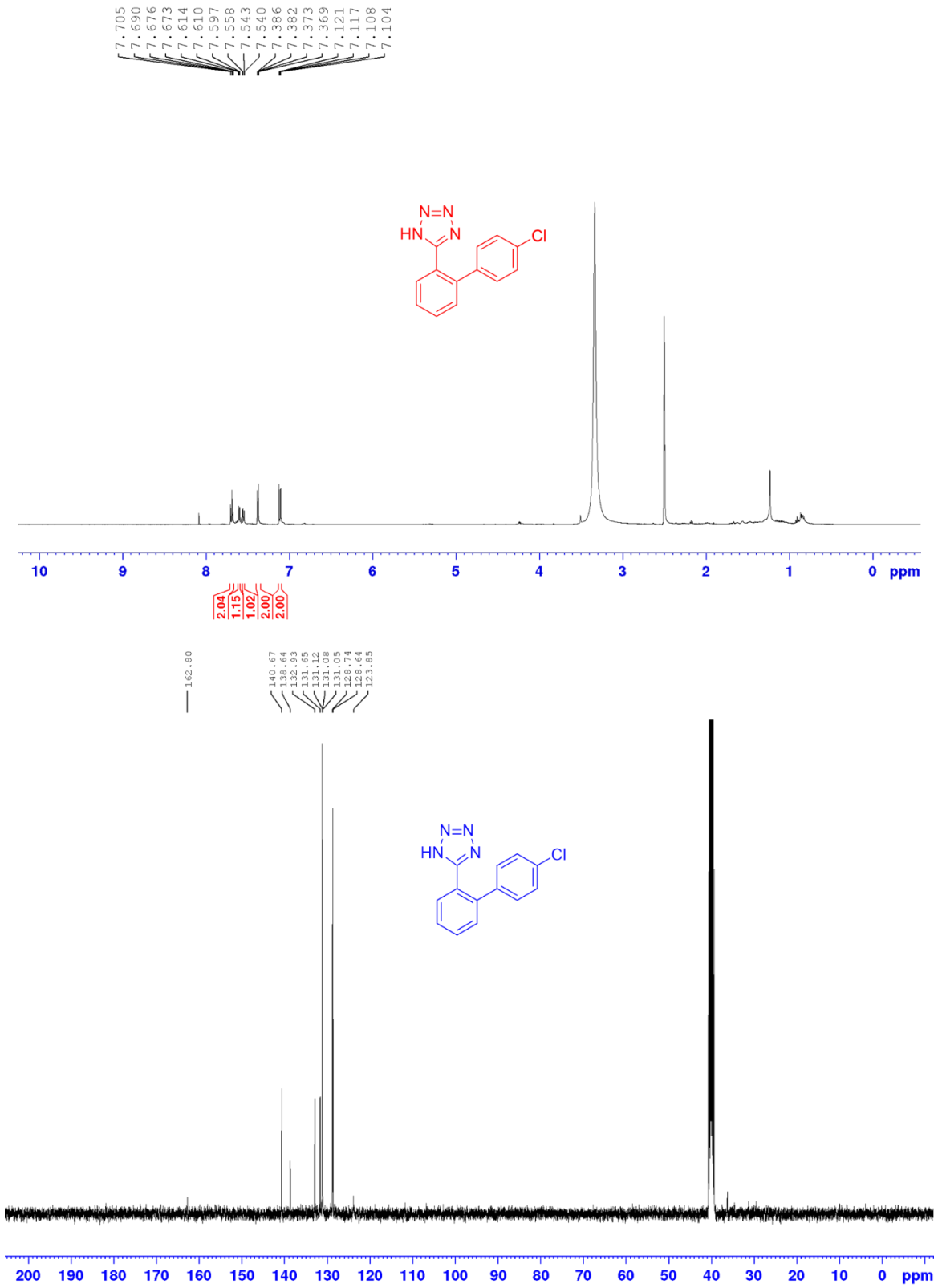

## Single Mass Analysis

Tolerance = 5.0 PPM / DBE: min = -1.5, max = 500.0
Element prediction: Off
Number of isotope peaks used for i-FIT = 3

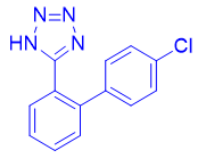


Monoisotopic Mass, Even Electron Ions
8 formula(e) evaluated with 1 results within limits (all results (up to 1000) for each mass)
Elements Used:
C: 10-15 H: 5-15 N: 0-5 Cl: 0-1
P2B 9 (0.270) Cm (1:61)

TOF MS ES-
4.71e+005

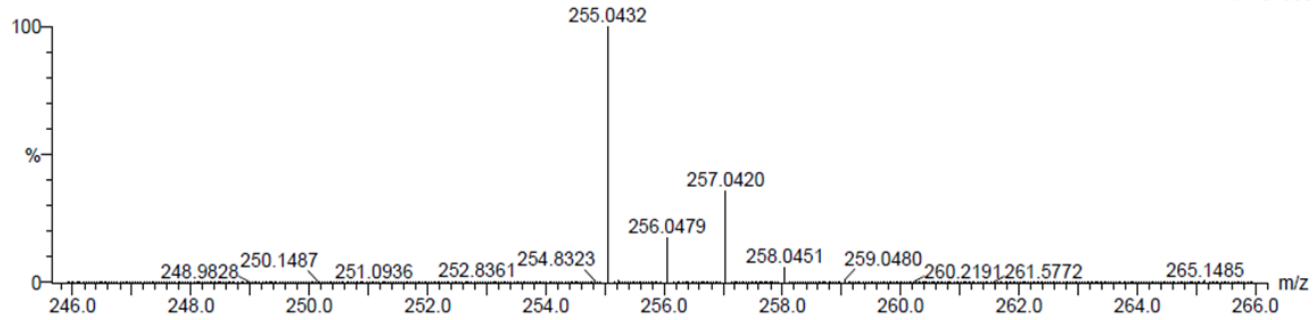


| | | | | | | | |
|---|---|---|---|---|---|---|---|
| Minimum: | | | | -1.5 | | | |
| Maximum: | | 5.0 | 5.0 | 500.0 | | | |
| Mass | Calc. Mass | mDa | PPM | DBE | i-FIT | i-FIT (Norm) | Formula |
| 255.0432 | 255.0437 | -0.5 | -2.0 | 11.5 | 629.0 | 0.0 | C13 H8 N4 Cl |

**Appendix A1.24:** $^{1}$H NMR, $^{13}$C NMR and HRMS for 5-(4'-bromo-[1, 1'-biphenyl]-2-yl)-1*H*-tetrazole **(85)**.

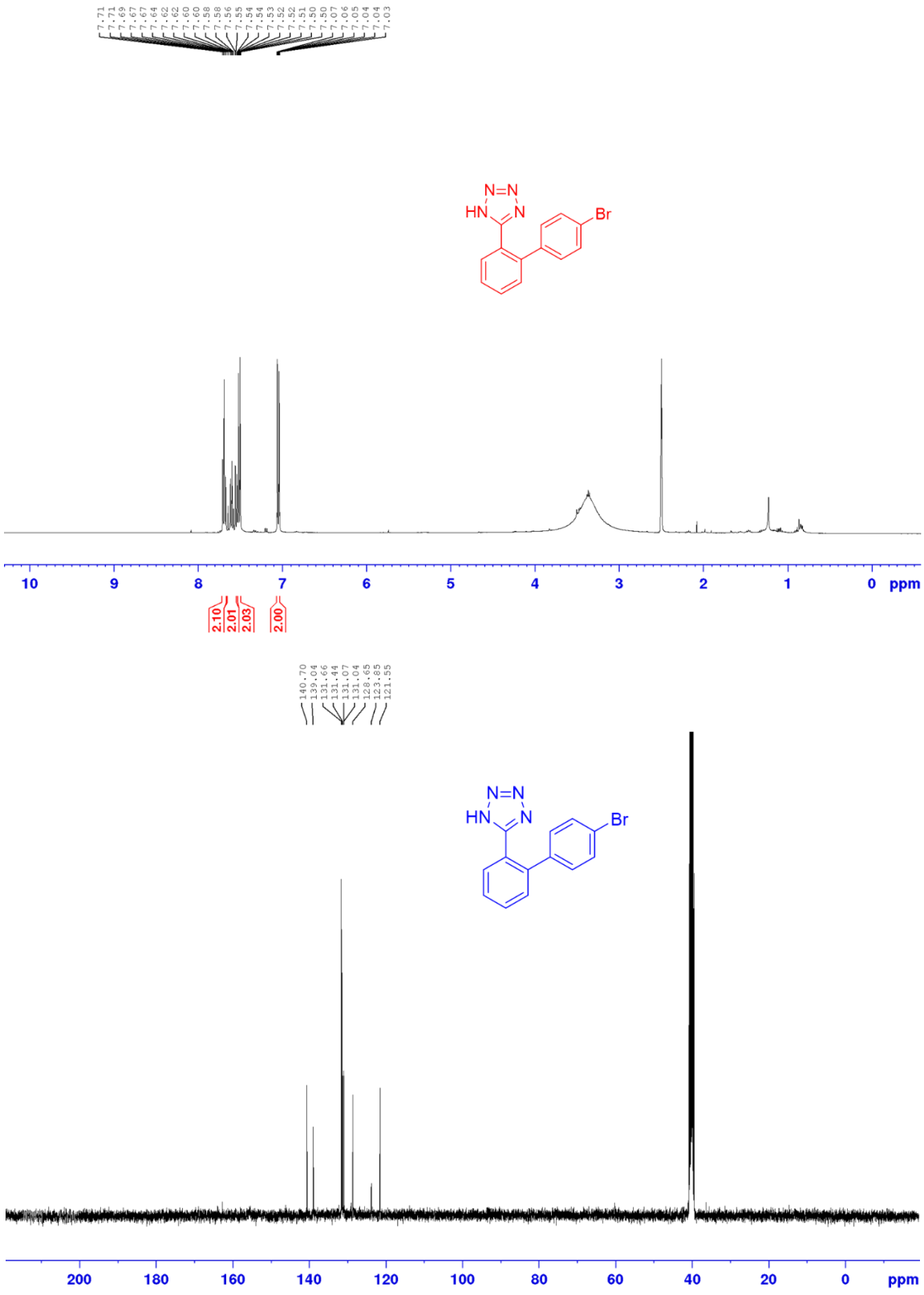

**Single Mass Analysis**
Tolerance = 5.0 PPM / DBE: min = -1.5, max = 500.0
Element prediction: Off
Number of isotope peaks used for i-FIT = 3

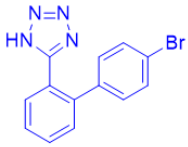


Monoisotopic Mass, Even Electron Ions
10 formula(e) evaluated with 1 results within limits (all results (up to 1000) for each mass)
Elements Used:
C: 10-15 H: 5-15 N: 0-5 Br: 0-1

P19 20 (0.640) Cm (1:61)

TOF MS ES-
2.55e+005

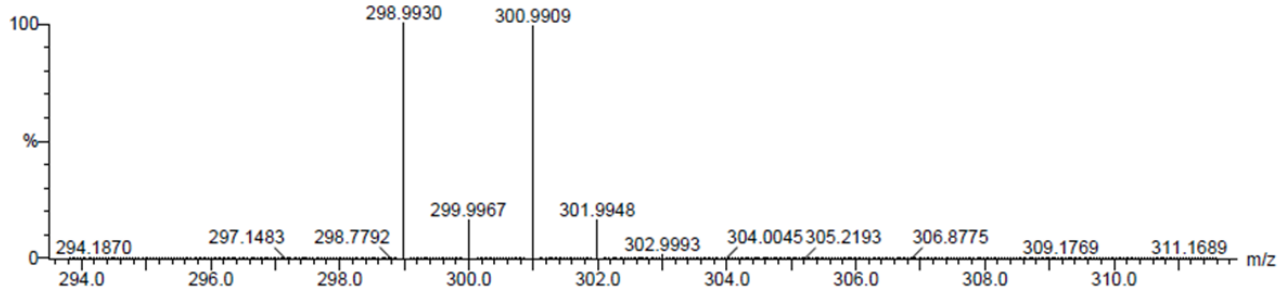


| | | | | | | | |
|---|---|---|---|---|---|---|---|
| Minimum: | | | | -1.5 | | | |
| Maximum: | | 5.0 | 5.0 | 500.0 | | | |
| Mass | Calc. Mass | mDa | PPM | DBE | i-FIT | i-FIT (Norm) | Formula |
| 298.9930 | 298.9932 | -0.2 | -0.7 | 11.5 | 539.7 | 0.0 | C13 H8 N4 Br |

**Appendix A1.25:** $^{1}$H NMR, $^{13}$C NMR and HRMS for spectra for 5-(([1, 1'-biphenyl]-2-yl)methyl)-1*H*-tetrazole **(86)**.

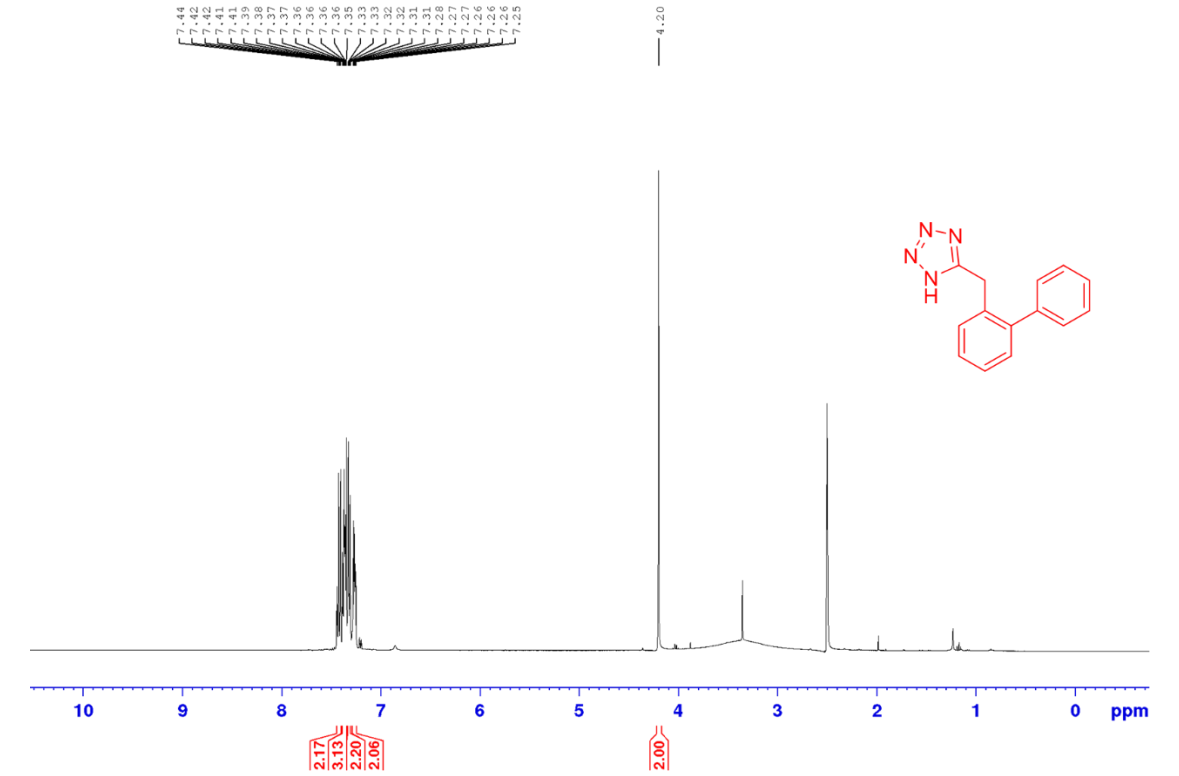


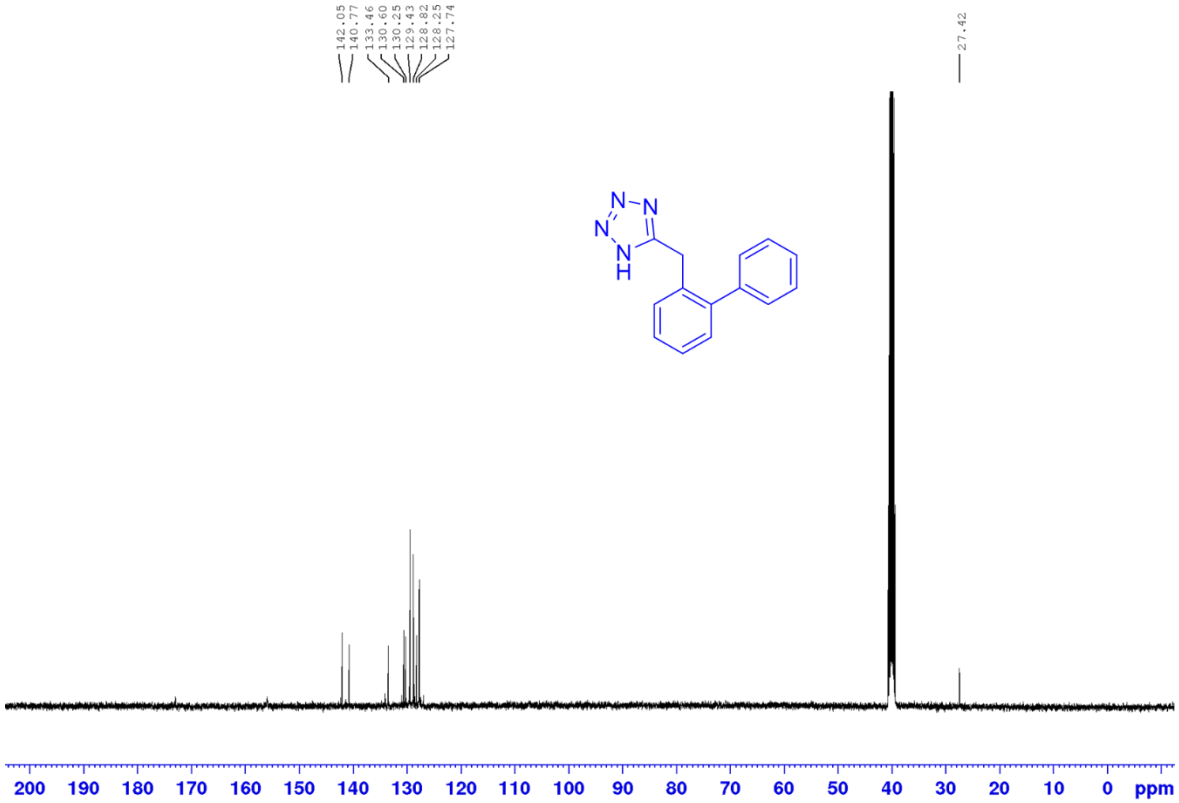

**Single Mass Analysis**
Tolerance = 5.0 PPM / DBE: min = -1.5, max = 500.0
Element prediction: Off
Number of isotope peaks used for i-FIT = 3

Monoisotopic Mass, Even Electron Ions
4 formula(e) evaluated with 1 results within limits (all results (up to 1000) for each mass)
Elements Used:
C: 10-15 H: 5-15 N: 0-5
P52 2 (0.034) Cm (1:61)

TOF MS ES-
8.72e+005

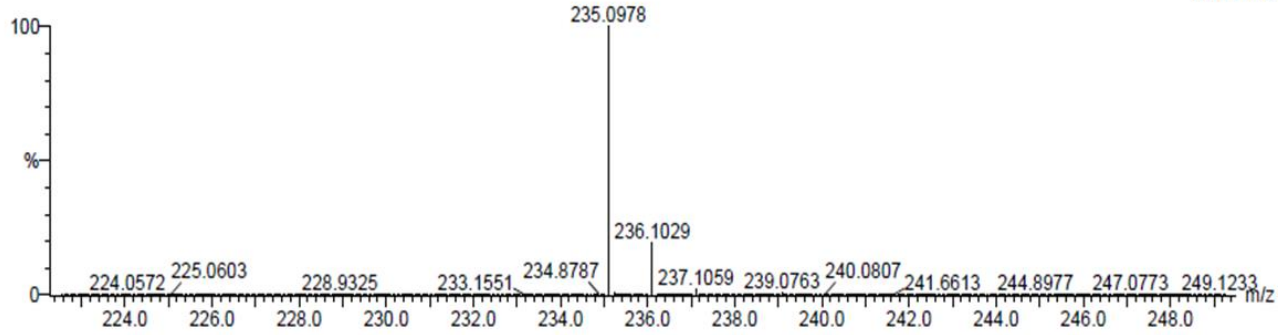


| | | | | | | | |
|---|---|---|---|---|---|---|---|
| Minimum: | | | | -1.5 | | | |
| Maximum: | | 5.0 | 5.0 | 500.0 | | | |
| Mass | Calc. Mass | mDa | PPM | DBE | i-FIT | i-FIT (Norm) | Formula |
| 235.0978 | 235.0984 | -0.6 | -2.6 | 11.5 | 710.3 | 0.0 | C14 H11 N4 |

**Appendix A1.26:** $^{1}$H NMR, $^{13}$C NMR and HRMS for spectra for 5-((trifluoromethyl[1, 1'-biphenyl]-2-yl)methyl)-1*H*-tetrazole **(87)**.

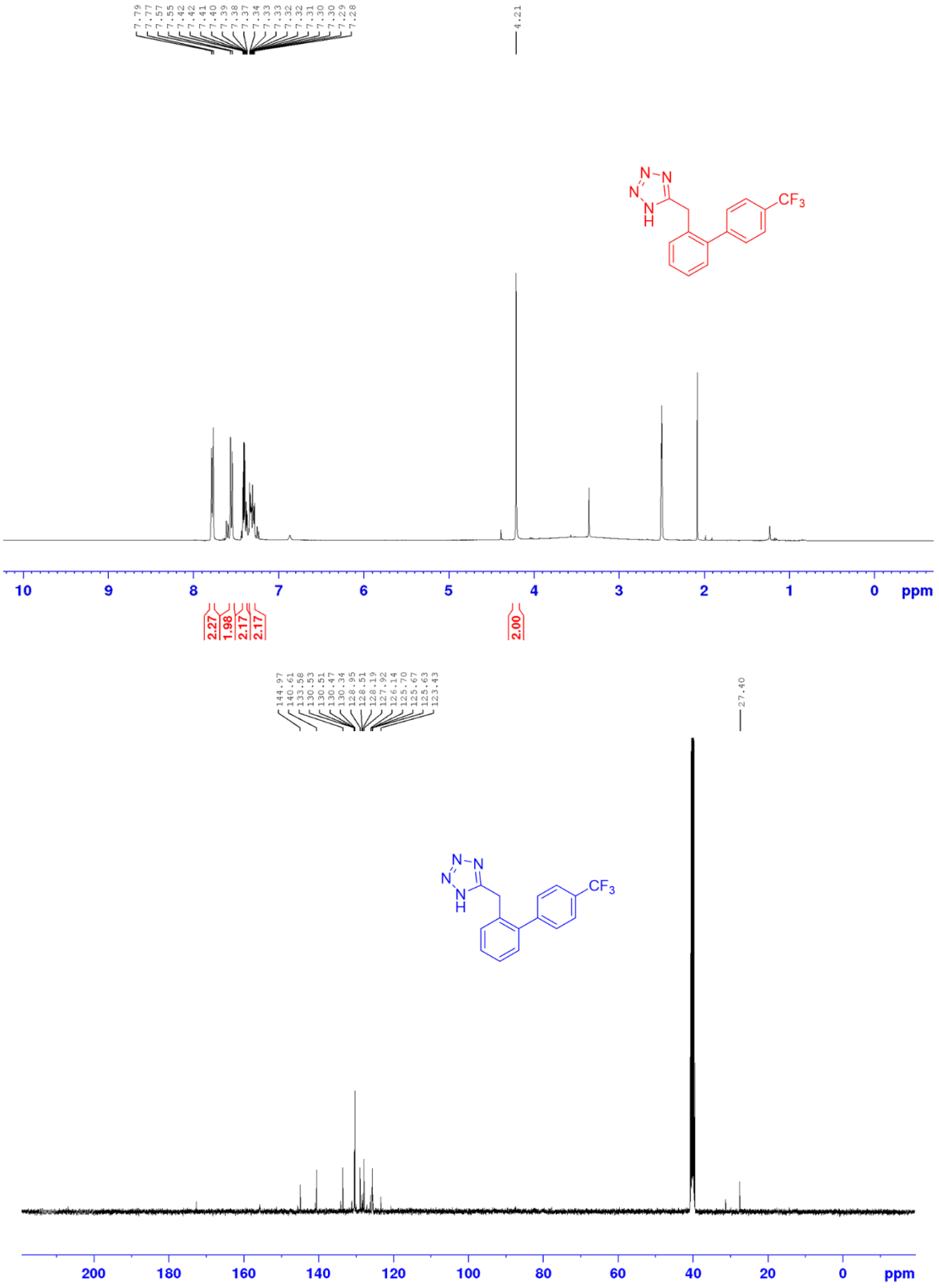

**Single Mass Analysis**

Tolerance = 5.0 PPM / DBE: min = -1.5, max = 500.0
Element prediction: Off
Number of isotope peaks used for i-FIT = 3

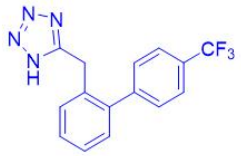


Monoisotopic Mass, Even Electron Ions
28 formula(e) evaluated with 1 results within limits (all results (up to 1000) for each mass)
Elements Used:
C: 10-15 H: 5-15 N: 0-5 F: 0-5

P49 39 (1.281) Cm (1:61)

TOF MS ES-
9.16e+005

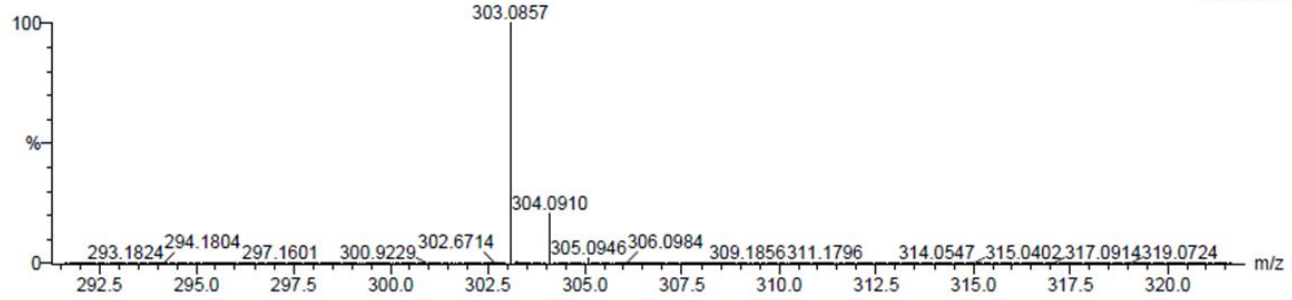


| | | | | | | | |
|---|---|---|---|---|---|---|---|
| Minimum: | | | | -1.5 | | | |
| Maximum: | | 5.0 | 5.0 | 500.0 | | | |
| Mass | Calc. Mass | mDa | PPM | DBE | i-FIT | i-FIT (Norm) | Formula |
| 303.0857 | 303.0858 | -0.1 | -0.3 | 11.5 | 618.6 | 0.0 | C15 H10 N4 F3 |

**Appendix A1.27:** $^{1}$H NMR, $^{13}$C NMR and HRMS for spectra for 5-((methoxy[1, 1'-biphenyl]-2-yl)methyl)-1*H*-tetrazole **(88)**.

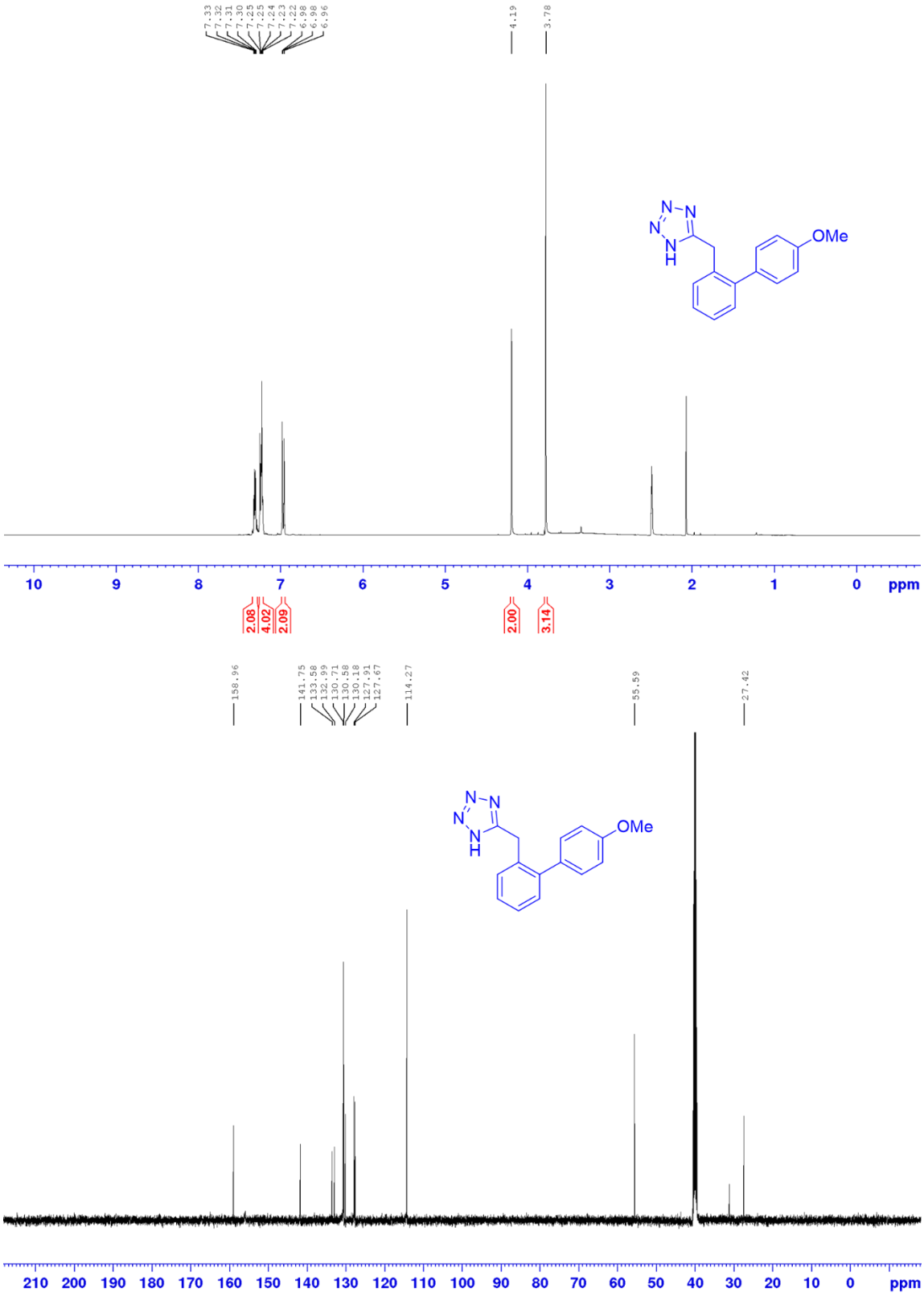

**Single Mass Analysis**

Tolerance = 50.0 PPM / DBE: min = -1.5, max = 500.0

Element prediction: Off

Number of isotope peaks used for i-FIT = 3

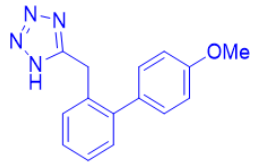


Monoisotopic Mass, Even Electron Ions

8 formula(e) evaluated with 1 results within limits (all results (up to 1000) for each mass)

Elements Used:

C: 10-15 H: 5-15 N: 0-5 O: 0-1

P51 27 (0.877) Cm (1:61)

TOF MS ES-
4.46e+005

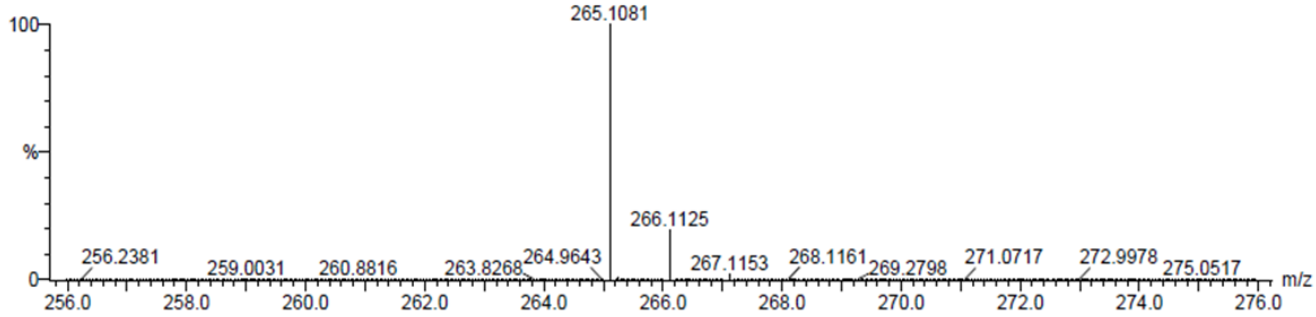


| | | | | | | | |
|---|---|---|---|---|---|---|---|
| Minimum: | | | | -1.5 | | | |
| Maximum: | | 5.0 | 50.0 | 500.0 | | | |
| Mass | Calc. Mass | mDa | PPM | DBE | i-FIT | i-FIT (Norm) | Formula |
| 265.1081 | 265.1089 | -0.8 | -3.0 | 11.5 | 592.0 | 0.0 | C15 H13 N4 O |

**Appendix A1.28:** $^{1}$H NMR, $^{13}$C NMR and HRMS for 5-((4'-chloro[1, 1'-biphenyl]-2-yl)methyl)-1*H*-tetrazole **(89)**.

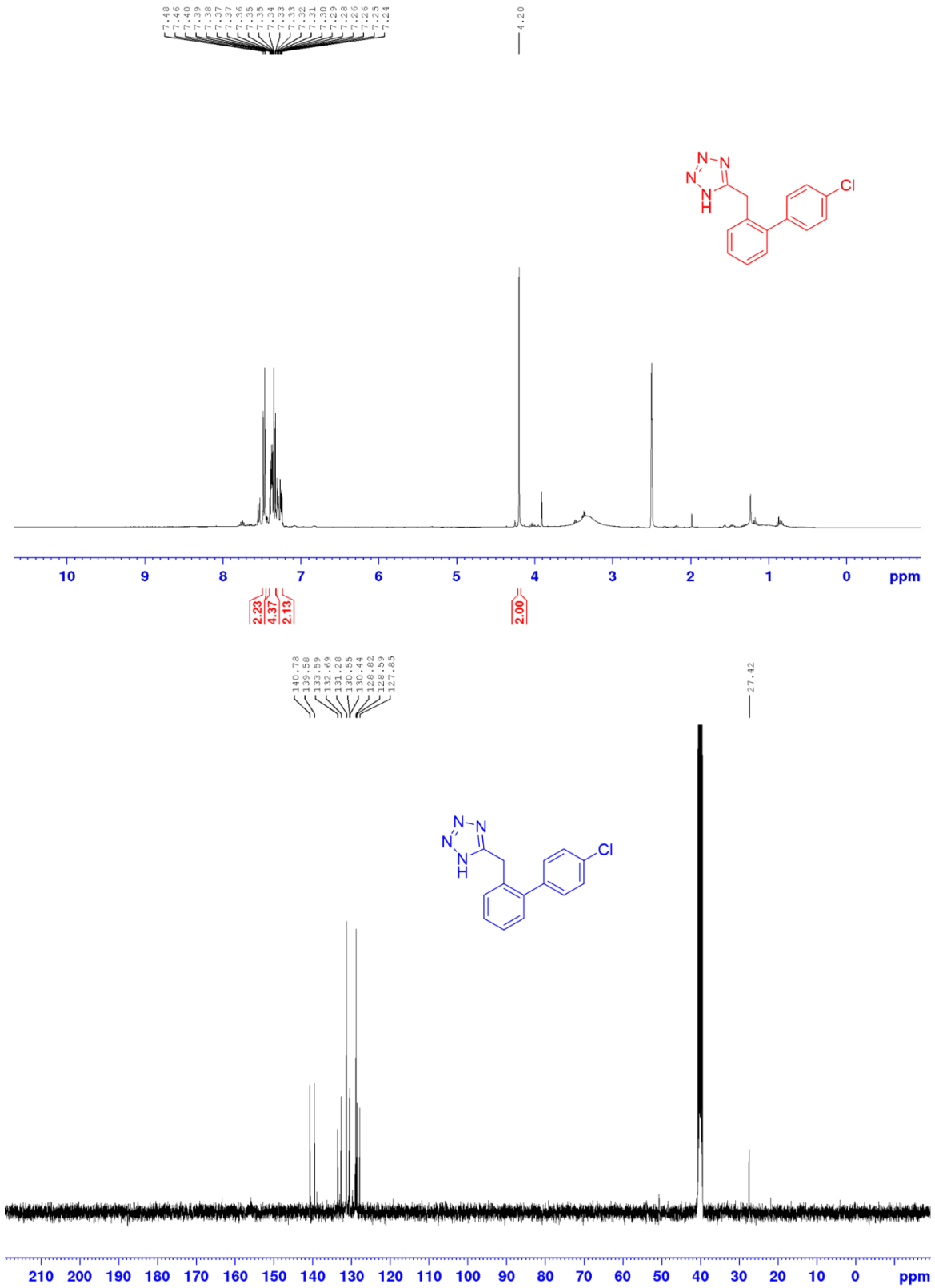

**Single Mass Analysis**

Tolerance = 50.0 PPM / DBE: min = -1.5, max = 500.0

Element prediction: Off

Number of isotope peaks used for i-FIT = 3

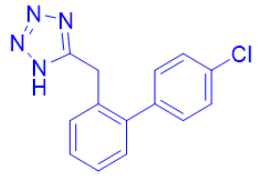


Monoisotopic Mass, Even Electron Ions

8 formula(e) evaluated with 1 results within limits (all results (up to 1000) for each mass)

Elements Used:

C: 10-15 H: 5-15 N: 0-5 Cl: 0-1

P54 59 (1.956) Cm (1:61)

TOF MS ES-
2.95e+005

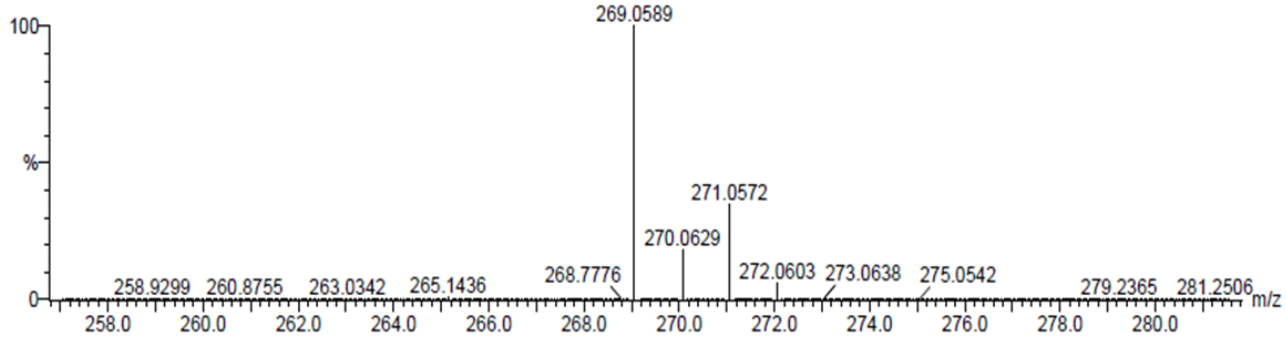


| | | | | | | | |
|---|---|---|---|---|---|---|---|
| Minimum: | | | | -1.5 | | | |
| Maximum: | | 5.0 | 50.0 | 500.0 | | | |
| Mass | Calc. Mass | mDa | PPM | DBE | i-FIT | i-FIT (Norm) | Formula |
| 269.0589 | 269.0594 | -0.5 | -1.9 | 11.5 | 569.7 | 0.0 | C14 H10 N4 Cl |